Active tectonics in the NW-German Basin: Evidence from correlations between the modern landscape and deep geological structures (Lower Saxony, river Hunte)

Dissertation
zur Erlangung des Grades
"Doktor der Naturwissenschaften"

am Fachbereich Geowissenschaften
der Johannes Gutenberg-Universität
in Mainz

Thore Szeder
geboren in Bremen

Mainz, Januar 2003

1. Gutachter:
2. Gutachter:
Tag der mündlichen Prüfung: 21.02.2003

Erklärung

Ich versichere, diese Dissertation nur unter Zuhilfenahme der angegebenen Mittel und ohne unzulässige Hilfe verfasst zu haben. Alle Quellen und von Dritten durchgeführte Arbeiten sind als solche kenntlich gemacht und vollständig aufgeführt.

Diese Arbeit liegt an keiner anderen Hochschule vor.

Thore Szeder

Contents

Zusammenfassung

Im Einzugsgebiet der Hunte (NW-Deutsches Becken, Niedersachsen) wurde über eine Länge von ~90 km untersucht, ob die Landschaftsgenese durch tektonische Bewegungen der Oberkruste beeinflußt ist. Hierzu wurden folgende Arbeitstechniken und Daten verwendet:

(1) Georadar und Reflektionsseismik wurden eingesetzt, Bohrungen niedergebracht und Aufschlüsse aufgenommen, um die Genese der weichselzeitlichen Niederterrasse zu untersuchen;

(2) absolute Datierungen: Optisch Stimulierte Lumineszenz [OSL] und AMS ^{14}C-Radiokarbon Datierungen wurden an weichselzeitlichen Niederterrassensedimenten durchgeführt, um Sedimentationraten und das Alter der Terrassenoberfläche zu bestimmen;

(3) in einem Geo Informationssystem (GIS) wurde untersucht, ob der tiefere geologische Untergrund die heutige Landschaft beeinflußt (Auswertung von strukturgeologischen, geologischen und topographischen Karteninhalten);

(4) Wiederholungsmessungen im Nivellementnetz wurden ausgewertet, um den Betrag rezenter Höhenänderungen zu bestimmen.

Krustenbewegungen führten im Bereich einer Hauptschollengrenze des NW-Deutschen Beckens (Niedersächsisches Becken/Pompeckj´scher Block) zu einer Hebung der weichselzeitlichen Niederterrasse mit einer durchschnittlichen Hebungssrate von ~0,5 mm/a über die letzten 12000 Jahre und zu einer Verjüngung der Niederterrasse und des Einzugsgebietes der Hunte. Tektonischer Einfluß auf die holozäne Aue ist über einem permischen Salzkissen zu verzeichnen, das in Form einer Aufwölbung des Untergrundes über eine vertikale Distanz von ~4000 m bis in das höhere Tertiär (-100 m NN) nachzuweisbar ist. Über der Aufwölbung verjüngt sich die holozäne Aue und das Gefälle kehrt sich um (negativer Gradient). Anomalien des Flußsystems, die sich mit Anomalien des geologischen Untergrundes decken, zeigen, daß rezente Krustenbewegungen an die strukturgeologische Situation des Beckens gebunden sind und Einfluß auf die Flußdynamik nehmen.

Krustenbewegungen haben mit großer Wahrscheinlichkeit Vorzugsrichtungen verursacht, die an der Tertiärbasis (Orientierung der Isolinien) und in der heutigen Landschaft nachweisbar sind. An der Tertiärbasis zeigen sich zwei Vorzugsrichtungen E-W, N-S (0-5° und 90-95°), die sich auch an der Oberfläche (Steilhänge, Seen und Senken, Topographie, Flußsystem) nachweisen lassen. Die Orientierung der Tertiärbasis korreliert mit der Orientierung von Landschaftselementen, wobei Seen und Senken die höchste Korrelation mit der Tertiärbasis aufweisen (r^2=0,78). Es zeigen sich außerdem hohe Korrelationen zwischen den einzelnen Landschaftselementen, mit der höchsten Korrelation zwischen Steilhängen und Seen/Senken (r^2=0,90).

Eine vergleichende Studie zwischen zwei unterschiedlich großen Arbeitsgebieten zeigt, daß Landschaftselemente hinsichtlich ihrer Orientierung deutlich miteinander korrelieren (z.B. Seen und Senken, r^2=0,94). Diese Ähnlichkeiten lassen sich nicht allein durch fluviatile Erosion erklären, da Seen und Senken, die unabhängig von fluviatiler Erosion sind (=geschlossene Hohlformen), ebenfalls die Vorzugsrichtungen zeigen. Glaziale Prozesse können als Verursacher der Vorzugsrichtungen ausgeschlossen werden, da das skandinavische Inlandeis das Untersuchungsgebiet zuletzt vor etwa 135000 Jahren bedeckt hat und sich seitdem die Landschaft durch erosive und akkumulative Prozesse stetig veränderte. Der Prozess, der die Vorzugsrichtungen verursacht hat ist noch unbekannt, aber tektonische Prozesse haben das Potential sowohl lokal als auch regional zu wirken und hierdurch gleiche Orientierungen in der heutigen Landschaft zu verursachen.

Das Abfließen der Hunte nach Norden scheint durch eine aktive, nordwärts gerichtete Kippung des NW-Deutschen Beckens verursacht zu sein, hervorgerufen durch eine Hebung des Hinterlandes (Wiehengebirge,

Rheinische Masse) und eine Senkung des Nordseebeckens. Hohe lineare Korrelationskoeffizienten zwischen der Tiefenlage der Tertiärbasis und der Höhenlage der heutigen Landoberfläche (Einzugsgebiet der Hunte r^2=0,87, weichselzeitliche Niederterrasse r^2=0,95, holozäne Alluvione r^2=0,95), weisen auf eine tektonische Einflußnahme (Kippung des Beckens) auf die heutige Topographie hin.

Beckensubsidenz hat möglicherweise die Akkumulation der weichselzeitlichen Niederterrasse gesteuert. Es konnte eine Übereinstimmung zwischen der rezenten Beckensubsidenz (~-0,21 mm/a), (ermittelt aus Wiederholungsmessungen im Nivellementnetz) und der durchschnittlichen Sedimentationsrate des Niederterrassenkörpers (~0,2 - 0,4 mm/a) nachgewiesen werden. Es zeigt sich außerdem, daß die Sedimentationsrate der weichselzeitlichen Niederterrasse über einen Zeitraum von etwa 35 ka nahezu konstant blieb (~47-12 ka BP). Während dieser Zeitspanne unterlag Nordeuropa hochvariablen Klimawechseln (Dansgaard-Oeschger Zyklen), die Flußmorphologie, Hydrologie und Sedimenttransport beeinflußt haben. Die Beobachtung, daß nahezu keine Veränderung der durchschnittlichen Niederterrassen-Sedimentationsrate zu verzeichnen ist, spricht für eine langanhaltende Beckensubsidenz. Diese hat, unabhängig von kurzzeitigen Klimafluktuationen, zur Akkumulation von längeren fluviatilen Sequenzen geführt.

Eine geschlossene Hohlform wurde mit Hilfe von Georadar, Reflektionsseismik, Bohrungen und absoluten Altersdatierungen untersucht. Die Hohlform ist kein saalezeitliches Toteisloch, da sie sich auf der weichselzeitlichen Niederterrasse befindet, wie eine OSL-Datierung außerhalb der untersuchten Struktur belegt. Es existieren ebenso keine geologisch/morphologischen Hinweise, daß es sich bei der Hohlform um ein Pingorelikt handelt. Geophysikalische Untersuchungen hingegen deuten auf eine aktive Sackungsstruktur hin, da sich Anomalien des geologischen Untergrundes mit der topographischen Lage der Struktur decken.

Summary

The catchment basin of the river Hunte (NW-German Basin, Lower Saxony) was studied on a mesoscale (length of ~90 km) by using the following techniques and data to investigate if tectonic movements in the upper crust influence modern landscape formation.

(1) Ground Penetrating Radar and Reflection-Seismics came into operation, corings were taken and several outcrops were studied to investigate Lower Weichselian Terrace formation;

(2) absolute datings (Optically Stimulated Luminescene [OSL] and Accelerator Mass Spectroscopy [AMS ^{14}C]) have been used to determine the age of the terrace surface and sedimentation rates and of Lower Weichselian Terrace sediments;

(3) a Geo Information System (GIS) was used to investigate the influence of the geological subground on modern morphology by integrating topographical, structural and geological maps and

(4) repeated precise levelling data to calculate the rate of recent horizontal movements.

Crustal movements led to upwarping of the Lower Weichselian Terrace above the transition zone of a major crustal boundery of the NW-German Basin (Lower Saxony Basin/Pompeckj Block) with an average vertical velocity of about 0,5 mm/a over the last 12 ka. The Lower Weichselian Terrace and the Hunte catchment basin are smallest at the same position. Even the Holocene Alluvial Plain is affected by active tectonics. The Holocene Alluvial Plain is narrower and shows a negative gradient directly above a deep seated Permian salt pillow which can be traced over a vertical distance of about 4000 m as an anticline structure to the uppermost Tertiary (100 m b.s.l.). The spatial similarity of fluvial anomalies with anomalies of the geological subground

indicates that crustal movements still exercise control on fluvial dynamics and are coupled to the geological predesign.

Active tectonic movements in the upper crust have most probably caused the formation of distinct orientations which are visible in both at the Base of Tertiary (orientation of iso-contour lines) and the modern morphology. The Base of Tertiary shows two preferred orientations E-W and N-S (0-5°, 90-95°). The same preferred orientations can be found in all of the investigated elements of the modern landscape (steep slopes, lakes and depressions, topography and the fluvial system). The orientation of the modern landscape correlates with the orientation of the Base of Tertiary basin geometry. Lakes and depressions show the highest correlation with the Base of Tertiary (r^2=0,78) and there is a high correlation between the orientation of the different elements of the modern landscape. The highest correlation can be found between the steep slopes and the lakes and depressions (r^2=0,90) and there is a high correlation between spatially different investigated areas regarding the orientation of morphological elements of the modern landscape (e.g. lakes and depression, r^2=0,94). These similarities are unlikely to have been caused by fluvial erosion alone, because the same high correlations are shown by the lakes and depressions which are closed structures and independent of fluvial erosion. Exogenic processes like an imprint of the landscape due to glacial processes could be excluded for the formation of the favoured orientations because ice did not reach the investigated area since ~135 ka and the morphology has changed continuously due to erosional and depositional processes. However, the exact mechanism which has caused the similar orientations is as yet unknown but tectonic processes have the potential to cause nearly identical orientations on local and regional scale and to influence modern topography.

Most likely northward tilting of the NW-German Basin forces the river Hunte to flow in a northerly direction by relative uplift of the hinterland (Wiehengebirge, Rhenish Massif) and subsidence of the North Sea area. High linear correlation coefficients between the Base of Tertiary and the height of the modern topography (catchmentbasin [r^2=0,87], Lower Weichselian Terrace [r^2=0,95] and Holocene Alluvial Plain [r^2=0,95]) indicate a control of the modern topography by the depth of the geological subsurface via tilting of the entire basin.

Basin subsidence is thought to have triggered primarily the aggradation of the Lower Weichselian Terrace, because there is an accordance between the mean recent velocity of basin subsidence (~-0,21 mm/a), calculated from repeated geodetic fine levelling and the mean sedimentation rate of the Lower Weichselian Terrace (~0,2-0,4 mm/a). In addition, sedimentation rates of the Lower Weichselian Terrace were nearly constant over a time span of about 35 ka (~47-12 ka BP). During these times the climate has changed rapidly over Northern Europe (Dansgaard-Oeschger Cycles) which affected river morphology, hydrology and sediment supply. However, the observation that no change of the mean sedimentation rate is observable indicates a long term subsiding tendency which enables accumulation of longer fluvial sequences independent of short scale climatic fluctuations.

A small scaled depression which was investigated by Georadar, Reflection Seismic, drilling and dating of sediments is not a Saalian dead ice hole, because it is positioned on the Lower Weichselian Terrace of the river Hunte as evident by an OSL dating from outside the structure and there is no morphological and geological indication that the depression represents a pingo remnant. The geophysical investigations show that the depression most likely represents an active subsiding structure, as evident by anomalies of the geological subground which correlate with the topographical position of the structure.

A) Introduction

A.1. Geographical position of the study area

Fig. 1 shows the geographical position of the study area (black rectangle). The investigated part of the river Hunte catchment basin is given in yellow. The river Hunte is the northerly left positioned tributary of the river Weser. The area of the total catchment basin is about 2640 km^2. The well is on the southern slope of the German Middle Mountain range (“Wiehengebirge") at 150 m a.s.l..

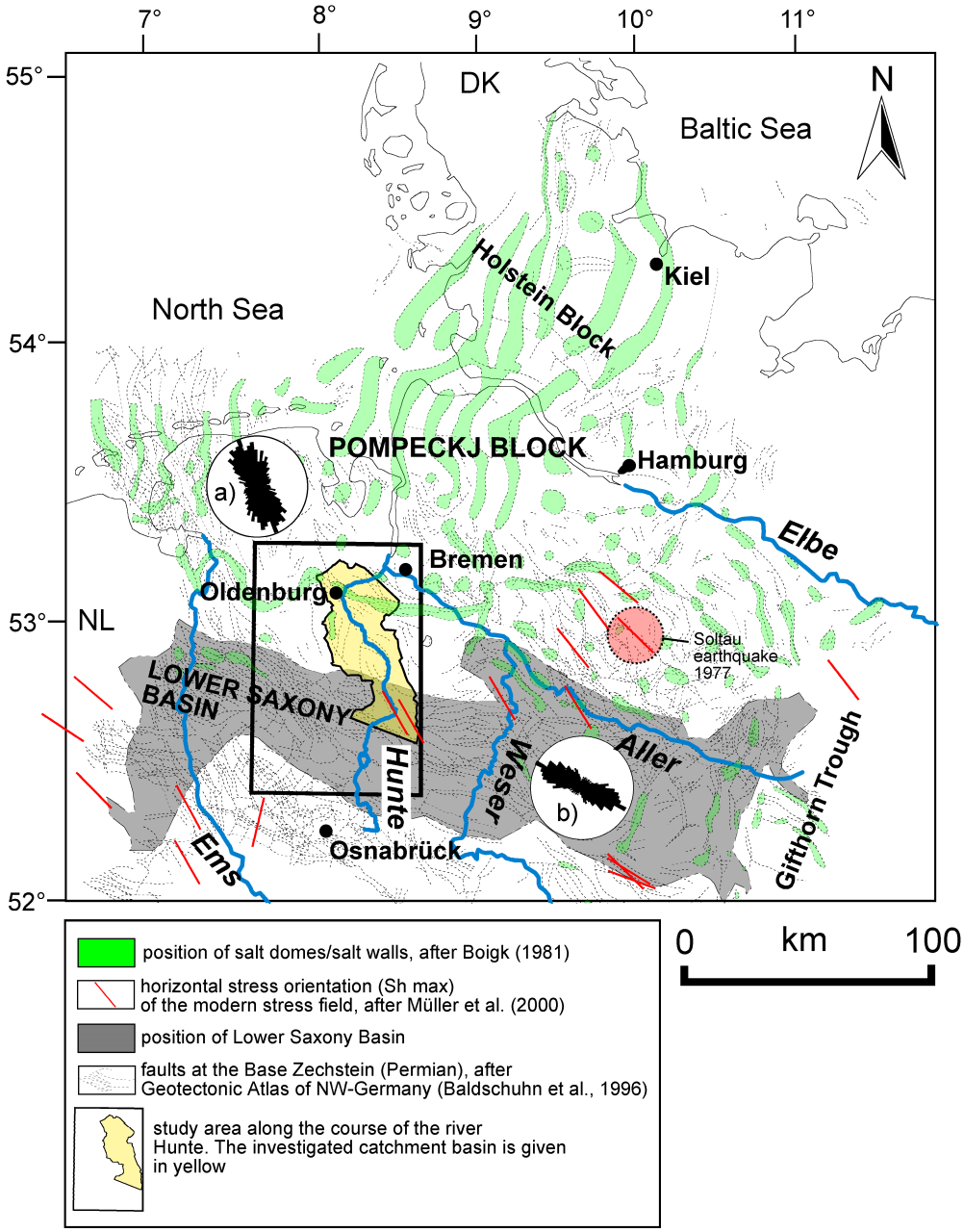

Fig. 1: Structural situation of the NW-German Basin. The position of salt domes and salt walls is given in green (after Boigk, 1981). The faults at the Base Zechstein (Permian) are shown in black (dashed lines), (after Baldschuhn et al., 1996). The position of the Lower Saxony Basin is presented in gray, (after Boigk, 1981; Betz et al., 1987). The position of modern horizontal stress orientation measurements (Sh max) are presented in red lines, after World Stress Map Data Base (Müller et al., 2000). The position of the Soltau, 1977 tectonic earth quake with the orientation of the striking fault plane (red line) is marked by the red circle, (after Leydecker et al., 1980). The rose diagrams show the orientation of the faults at the Base of Zechstein for a) the Pompeckj Block and b) the Lower Saxony Basin, plotted by length with a pedal width of 5°.

The river Hunte reaches the North German plain after ~8 km distance at a height level of about 50 m a.s.l.. After 37 km distance the river reaches the lake Dümmer. Lake Dümmer is a flat lake with max. 1,2 m water depth and about 12,3 km^2 in area (Dahms, 1974; Liedke, 1980; Pfaffenberg, 1939; Pfaffenberg and Dienemann, 1964). Near the town Barnstorf (Fig. 2) the river Hunte enters the hilly and undulating area of the "Cloppenburger and Wildeshauser Geest", formed by the glacial deposits of the Saalian glaciation. North of the town Oldenburg the river Hunte reaches the marshy area of the river Weser. Here, the river is already under tidal influences of the North Sea. The Hunte flows into the river Weser after a total length of ~110 km near the town Bremen at a height of about 0 m a.s.l. (Ness, 1994).

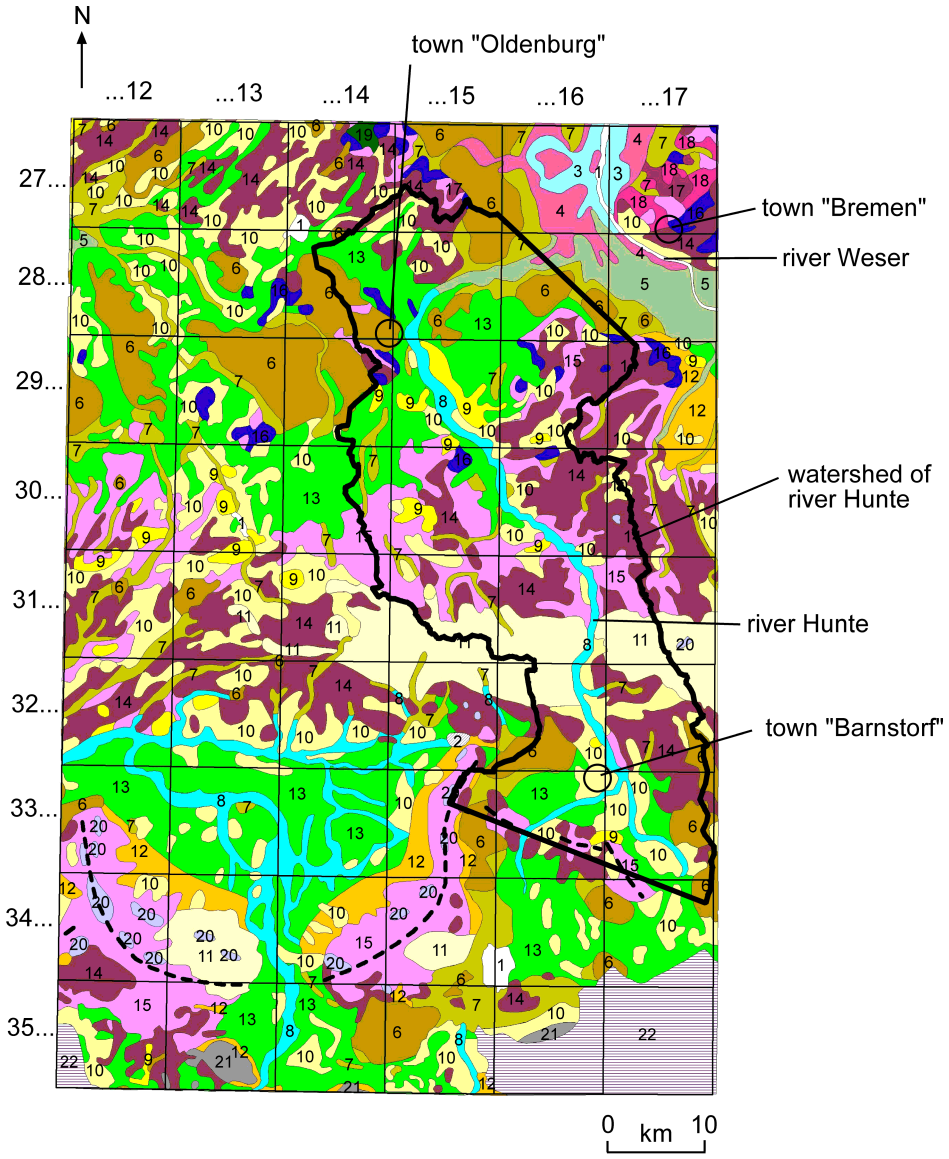

Fig. 2: Geological map; the grid shows the name (numbers) and position of the topographic maps. The black field shows the investigated part of the river Hunte catchment basin.
Holocene 1: water, 2: anthropogenic replenishment, 3: mudflat deposits, 4: brackish water deposits, 5: tidal deposits, 6: highmoor deposits, 7: lowmoor deposits, 8: alluvial-plain deposits, 9: dune sands; **Pleistocene** *Weichselian* 10: cover sands, 11: sandy loess, 12: sediments of solifluction, 13: lower terrace, *Saalian* 14: morainic deposits, 15: meltwater sands, - - - push-end-morain (dashed line), *Elsterian* 16: deposits of glacial meal "Lauenburger Ton", 17: morainic deposits, 18: meltwater sands, *Pre-Elsterian* 19: fluvial deposits of the oldest terraces, **Pre-Quaternary:** 20: Tertiary **(**transported by glacials), 21: mesocoic sediments, 22: unmapped area. (After NLfB, 1993).

A.2. Geological situation and evolution of the NW-German Basin

The NW German Basin is part of the Central European Basin, which extends from the North Sea through NW-Germany to the Polish lowland. Intensive exploration of the Oil Industry over the last decades led to a dense net of drillings and seismic data. Most of the structural and geological knowledge on the NW-German Basin is based on this data (Boigk, 1981).

The evolution of the basin must be seen in the context of the megatectonic evolution of Europe (Ziegler, 1990). The main orogenic/tectonic phases of Europe and the development of NW Germany from Devonian to Quaternary times are shown in Tab. 1. Multiple deformation phases occurred since the initial basin formation in the Early Permian around 290 Ma ago with continuously and sometimes rapid change in stress regime. Basement faults, already initiated during the pre-Permian Variscan Orogenese, became reactivated during later rifting and inversial times. The NW-German Basin was completely reorganised structurally during the Upper Cretaceous inversion. The tectonic evolution (stress regime) triggered the basin geometry and therefore the distribution of sediments (Ziegler et al., 1995). Even the distribution and orientation of salt structures is connected with deep fault zones/lineaments of the deeper crust (Baldschuhn et al., 2001).

Tab. 1: Geological timetable with main orogenetic/tectonic phases in Europe and structural, geological events for NW-Germany, (after Baldschuhn et al., 2001; Betz et al., 1987; ICS, 2000; Walter, 1995; Ziegler, 1990).

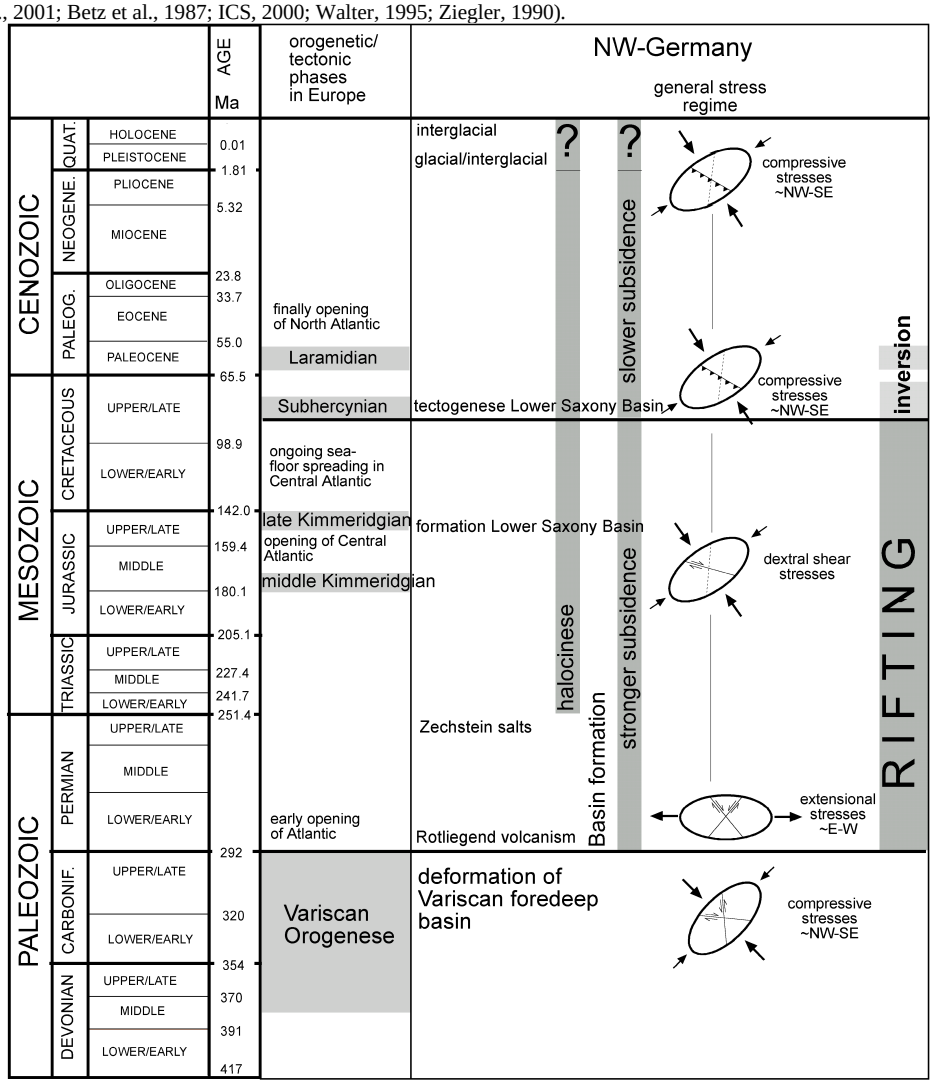

2.1. Deeper basement (pre-Permian)

Depth of the Mohorovicic discontinuity, Lower and Middle Crust

The Mohorovicic discontinuity (Moho) can be found in northern Germany at a mean depth of 30-32 km (Bachmann and Grosse, 1989; Ziegler, 1990). Two distinctive Moho highs are visible. One in Schleswig-Holstein (25-23 km) and a second in Mecklenburg (26-24 km). The Moho high of Schleswig-Holstein coincides with a sedimentary depocenter. Here, the thickness of Permian to Quaternary sediments increases from 5 to 9 km with a Precambrian crystallin crustal thickness of about 12 km. The normal thickness of the crystallin crust in adjacent areas is 20-25 km (Bachmann and Grosse, 1989). A local high of the Moho is also visible in the northern part of the study area (area of Oldenburg, the so called “Oldenburg high”). This high (proven by deep reflection/refraction seismic data and gravity data) is elevated by 3-4 km to a level of 28-29 (Brink et al., 1992). Deep seated faults seem to reach down to the Moho and penetrate it (offsets of the Moho) as visible in deep reflection seismic profiles of southern Lower Saxony (Dohr, 1989). Gravitational data lead one to believe that deep seated plutonites exist in the Lower Saxony Basin (Bachmann and Grosse, 1989). The existence of different crustal units in the depth of the Central European Basin can be explained by a thermo-rheological model of Caledonian and Variscan terrane accretion (Meissner, 1999).

Pre-Devonian (>417 Ma)

Lithofacies and tectonic information of the pre-Devonian exist only from few exposures on the southern and northern margin of the basin. Thus, there are considerable uncertainties about the regional distribution of the pre-Permian of the basin´s deeper parts (Franke, 1990).

Devonian (417-354 Ma)

Thick Devonian carbonates and clastics (deposited when northern Germany was located in tropical regions) are the deepest and oldest stratigraphic unit of NW-Germany, which can be geophysically defined and calibrated by wells (Brink et al., 1992). East Avalonia was part of the collision between Baltica and Laurentia. Due to this collision the new united continent Laurussia was formed at about 400 Ma, corresponding with the closure of the Iapetus and the Tornquist Ocean. This onset of collision/orogenese concluded the Caledonian development. East Avalonia forms amongst others North Germany and the Rhenohercynian (Meissner, 1999).

Carboniferous (354-292 Ma)

The middle and southern section of the North German Depression was filled with up to 1000 m thick clay- and siltstones and graywackes during the **Lower Carboniferous** (Walter, 1995). The best investigated pre-Permian stratigraphic unit is the **Upper Carboniferous**. Gaps in knowledge exist in the regions of depth greater than 6-7 km. Synsedimentary deep fractures are obviously partly responsible for variations in the general basin configuration, the thickness development, the coal content and the marine influences (Franke, 1990). During the late phases of the **Variscan orogeny** the southern part of the Variscan foredeep basin became deformed by NW-SE orientated compressive stresses (Tab. 1). At the end of the Variscan Orogeny **(Stephanian and Early Permian)** a fundamental alteration of the regional stress plan took place. Dextral wrenching along NW-SE orientated fault systems was accompanied by divergent sinistral wrench movements along N-S directed fractures. This induced the differential subsidence of grabens in the Early Rotliegend (Betz et al., 1987).

2.2. Permian to Quaternary

Permian (292-251 Ma)

During the **Early Permian** thick Rotliegend volcanics were deposited. The center of volcanic activity was in the eastern part of the North German Basin. Areas of higher volcanic deposits corresponded with mean fault systems (Ziegler, 1990). These fault zones are part of a system of conjugating sliding fractures, which were formed after the Variscan Orogenese. The reason for this is a E-W orientated extensional stress field (Tab. 1), which was caused by an eastward drift of the Eurasian Continental Plate relative to the African Plate (Ziegler, 1990). The overthickened Variscan mountain belts collapsed under this extensional stress regime (Meissner, 1999). NW striking sliding fractures had a dextral, NE striking fractures a sinistral direction of motion. The resulting strike-slipe faults reached deep and were used by the subsequent Magma as an ascent path.

During the **Upper Rotliegend** N-S running horst and graben structures were formed in Lower Saxony (Gast, 1988). The grabensystems strike perpendicular to the axis of maximum extension. This rift system can be traced southward into the Hessian Depression. In the Younger Saxon, fractureless subsidence dominated in Lower Saxony. Thermal subsidence was possibly the reason for the sinking of the basin (Bachmann and Grosse, 1989; Meissner, 1999). In the N-S oriented graben structures subsidence led to an enlargement of the sedimentation area. The Permian Basin reached from the British Isles to Poland. In northern Germany coloured clastic sediments (Sabkha-sediments, aeolian dune sands) were deposited with maximum thicknesses of up to 2000 m. There is a remarkable accordance between the position of the Rotliegend basin depocenter in Schleswig-Holstein and the position of the Moho high (Bachmann and Grosse, 1989).

At the end of the Saxon the **marine Zechstein** transgraded into NW-Germany. Cyclic evaporation lead to the deposition of thick carbonate/evaporite series. Later halocinetic processes are based on these salt deposits (starting with Triassic times).

Triassic (251-205 Ma)

Triassic subsidence was caused by thermal subsidence and a mechanical streching of the crust. There is a good accordance between the Basin depocenter and the Moho high at Schleswig Holstein (Bachmann and Grosse, 1989). In northern Germany a NNE-SSW trending system of grabens and troughs was established (Glückstadt Graben, the Emsland trough and the Weser depression). The area of the future Lower Saxony Basin was apparently affected by extensional stresses but these stress conditions were unable to reactivate the pre-existing NW-SE oriented fracture system of Hercynian trend (Betz et al., 1987). After the complete evaporation of the marine Zechstein, the **Buntsandstein** starts with a continental phase. Red coloured sandstones/mudstones were deposited with a maximal thickness of about 1500 m (Boigk, 1981; Walter, 1995). In the Upper Buntsandstein (Röt), occasionally marine transgressions occurred with evaporation of halite and anhydrite. During the **Muschelkalk** 250-300 m of chalk and marlstones were deposited under marine conditions. During the Keuper the sea became flatter and fine red clastic sediments were deposited. In local troughs up to 300 m of Keuper salt was deposited.

Jurassic (205-142 Ma)

A world-wide transgression occurred on the boundery to Jurassic (**Lias, Lower Jurassic**). This led to deposition of dark mudstones with a local thickness of about 1400 m in parts of the NW-German Basin. During the Upper Lias locally sapropelites (Posidonia shale) were accumulated and rhenish (NNE-SSW) orientated troughs were

formed by halocinetic movements of the Permian salt. Marine conditions continued during **the Dogger (Middle Jurassic)** with deposition of mudstones but with more frequent intercalations of clastic series than during Liassic times. At the boundary Dogger/**Malm (Upper Jurassic)** a new phase of tectonic movements led to a reorganisation of the sedimentation **(late Kimmeridgian)**. The mainland areas extended and confine the marine basins which led to brackish conditions and the deposition of sand and chalk (Boigk, 1981). The Lower Saxony Basin developed during the Malm (a WNW-ESE striking basin with a length of about 300 km and a width of 60-70 km), (Fig. 1). This basin is limited in the south by the German Middle Mountain range and to the north by the Pompeckj Block. While the Lower Saxony Basin was subsiding, the Pompeckj Block was uplifted above the erosional level. The marine connection between the South German Platform and the NW-German Basin was interrupted. After Betz et al. (1987) the Lower Saxony Basin is a pull-apart basin caused by dextral shear. Reactivation of Late Carboniferous WNW-ESE striking fracture systems was coupled with the subsidence of the Lower Saxony Basin. The Lower Saxony Basin consists of several rhomboid shaped sub-basins, separated by NNW-SSE trending sinistral translation zones. The origin of the Lower Saxony Basin is not linked with any observable crustal thinning (Bachmann and Grosse, 1989).

Cretaceous (142-65,5 Ma)

Lower Cretaceous

The connection of the Lower Saxony Basin to the open sea was almost completely interrupted during the **Early Berriasian (German Wealden)**. This caused changes in the depositional environment from restricted and evaporitic marine conditions in the Upper Malm to fresh water conditions. Lacustrine claystones, laminated bituminious shales, coal-bearing deltaic and coastal plain deposits containing barrier sands and channel sandstones were deposited with a thickness of up to 500 m. The onset of the **Valangin** is marked by a marine ingression into the area of the Lower Saxony Basin. The Pompeckj Block was transgressed by the sea in the area of the Ems estuary and Ostfriesland. Shallow water shales were deposited in the basin parts and along the marginal parts deltaic and shoreline sands (e.g. “Bentheimer Sandstein”). During the successional **Hauterive, Barreme and Early Aptian** no major changes occur regarding the position of the coastal zone in the Lower Saxony Basin.

A new chapter in the palaeogeographical development of the NW-German Basin is marked by the **Alb**. The mainlands which border the Lower Saxony Basin were flooded. Most of the synsedimentary basins had completed their embryonal stage and were covered by the marine clays of the Alb. The Early Cretaceous subsidence of the Lower Saxony Basin is contemporaneous with major rift pulses in the North Sea (Betz et al., 1987; Boigk, 1981; Walter, 1995).

Upper Cretaceous (Sub-Hercynian phase)

The convergence of Africa/Arabia with Eurasia resulted finally in the collision of the Alpine orogene with the southern passive margin of Europe. Collisional coupling of the Alpine orogen with its foreland is thought to be responsible for the onset of intra-plate compressional deformation of Western and Central Europe (Ziegler et al., 1995; Ziegler, 1990). This Senonium Sub-Hercynian phase of foreland compression led to the inversion of the Lower Saxony Basin. The Lower Saxony Basin was transformed to the **Lower Saxony Tectogene** by this process. Faults became reactivated and sediment fill was thrust over the northerly adjacent stable Pompeckj Block. Faults at the Base of Zechstein became reversed at this time. This inversion tectonism led to a substantial

uplift of the pre-Permian layers (Betz et al., 1987). Late Permian salts served as detachment planes (Baldschuhn et al., 2001). While the Lower Saxony Block was uplifted, the northerly Pompeckj Block subsided. This led to accumulation of up to 2000 m of sediments (marlstones, light chalkstones ["Schreibkreide"]) in the area of the Pompeckj Block. Inversion structures are not only restricted to the Lower Saxony Basin. They can also be found on the Pompeckj Block. Most of the inversion structures are coupled to basement faults. During the phase of inversion (Coniacian – Campanian) the sedimentary fill of the grabens was thrust over the graben shoulders. Salt domes were tectonically superimposed and subsequent movements of halocinetic structures led to local variation of thickness, hiatus and facies changes (Baldschuhn et al., 1985; Boigk, 1968). The intrusion of deep seated laccolithes (e.g. Bramscher Massiv at the southern border of the Lower Saxony Basin) is though to be coupled to this process of inversion.

Tertiary (65,5-1,8 Ma)

During the **Upper Paleocene** a first transgression of the Tertiary shallow epicontinental sea reached the south of Lower Saxony (Hinsch and Ortlam, 1974). During the Eocene the sea expanded again and reached its greatest size in the Oligocene. A connection from the North Sea via the Hessian Depression to the Mainz Basin and the Rhenish Graben existed during the Middle Oligocene (Gramann, 1966). During the Upper Oligocene the sea regressed and the connection to the Mainz Basin closed up. Isolated transgression phases with permanently changing shallow sea, brackish to terrestrial conditions occurred during the Miocene, when flat islands or depressions were formed by salt domes. In the Pliocene the sea retreated to the westerly part of Schleswig-Holstein and the Ems estuary. Limnic and fluviatile sediments were deposited. The sediment thickness of the Tertiary sediments varies strongly, because it is influenced by halocinetic processes. In the rim synclines of the salt structures, more than 3000 m of Tertiary sediments were deposited locally.

The stress field which affected NW-Europe changed during Cenocoic times because of repeated changes in (1) the convergence pattern between Africa-Arabia, (2) changes in sea-floor spreading rates in the different segments of the North-Atlantic and (3) plate boundary reorganisation (Bergerat, 1987; Ziegler et al., 1995). There is an observed systematic westward shift of the compressional foreland deformation. This is partly the expression of an increasingly important dextral translation component during the late Eocene to Pliocene convergence of Africa-Arabia to Europe. There was probably an interference of stresses related to the collision of Iberia with Europe and stresses transmitted from the Alpine collisions zone (Ziegler, 1990).

During the mid-**Paleocene** a second phase of basin inversion occurred (**Laramide-phase**), (Tab. 1), which is evident in the Lower Saxony Basin, the West Netherland Basin and the Central Graben of the North Sea (Betz et al., 1987). The most distal inversion structures can be observed in the Central North Sea, which is about 1400 km far from the Alpine thrust front. The compressional deformation was interrupted at the end of the Paleocene but resumed during the late Eocene and Early Oligocene. The evolution of the European Cenocoic rift system at **Eocene and younger times** is mostly synchronous with the compressional intra-plate deformations of the nortwestern Alpine foreland. These rift systems which can be traced from the western Mediterranean to the coastal area of the North Sea became evidental during the Middle Eocene to Early Oligocene (Ziegler et al., 1995). The last inversion moments in the Lower Saxony Basin could be observed in the Early Oligocene. The Lower Saxony Basin was smoothly uplifted during the **Mio-Pliocene**. This trend is coupled with the thermal doming of the Rhenish Massif, which was related to the evolution of the Rhine Graben System (Betz et al., 1987). Contemporaneously the Leine Graben was uplifted. The **present day stress field** was established

during the **Mio-Pliocene transition**, which is characterised by NW directed trajectories of maximum horizontal compression (Müller et al., 1992). Broad scale negative deflection of the North-Sea basin lithosphere is indicated by **Plio-Pleistocene** subsidence rates (Cloetingh et al., 1990; Cloetingh and Kooi, 1992; Ziegler et al., 1995; Ziegler, 1990).

Quaternary (1,8-0 Ma)

Sediments documenting **Lower Pleistocene** times are rarely known in Lower Saxony. Müller (1986) describes Lower Pleistocene sediments of the Menap-complex from a well on top of the salt dome Gorleben. A research borehole reached **Middle Pleistocene** interglacial sediments of the Cromer complex (Hunteburg-Interglacial**)** near the town Osnabrück in Lower Saxony (Hahne et al., 1994). The area of Lower Saxony was reached for the first time by Scandinavian inland glaciers during the **Elsterian** (~350 ka). The glacials overstepped possibly in some cases the border of the German Middle Mountains (Kaltwang, 1992). A net of Elsterian glacial tunnel valleys is detectable from Poland to the Netherlands (Schwab, 1996). These channels cut up to 500 m into the ground by hydrostatic pressure which was built up by the overlying glaciers and eroded strongly the pre-Quaternary strata (Kuster and Meyer, 1979; Ortlam and Vierhuff, 1978). The Elsterian was followed by the **Holsteinian Interglacial** with a duration of about 15-16 ka (Meyer, 1974). The **Saalian Glacial deposits** form most of the modern Lower Saxony topography. The oscillating ice margins formed high push end moraine walls of up to 150 m (e.g."Dammer Berge"). The push end moraine wall of the Rehburger-Phase can be traced between Hannover and the Netherlands. The duration of the **Eemian interglacial** for northern Germany was about 11 ka after counts on annually laminated Kieselgur sediments (Müller, 1974). The limit of the Eemain coastline was quite similar to that of today (Höfle et al., 1985). There are alterations of the Eemian palaeocoastal line in the North Sea area in the order of max. 20,5 m, which can only be explained by tectonism (Streif, 1991). The author assumes that glacial rebound triggers these neotectonic movements. After (Zagwijn, 1983) the Netherlands region shows a long term subsidence of about 0,14 mm/a since the Eemian in relation to the Channel area. According to (Streif, 1991), the Eemian coastal line of the southern North Sea is found 7 m below present sea level. After (Zagwijn, 1983) the Eemian coastal line of the Netherlands is found 8 m below present.

The Scandinavian inland glaciers did not pass the river Elbe during the **Weichselian (115-10 ka BP)**. Consequently, Lower Saxony was under periglacial permafrost conditions (Böse, 1995; Liedtke, 1981; Mol et al., 2000; Vaikmäe et al., 1995; Vandenberghe, 1993; Vandenberghe and Pissart, 1993). Aeolian transported sandy loess and coversands can be found there (Meier, 1996; Pyritz, 1972; Schwan, 1988; Vierhuff, 1967). The spare vegetation and the thaw of the active permafrost layer led to solifluction processes (Caspers and Freund, 2001; Caspers et al., 1995). The river valleys were filled with sandy deposits ("Talsande") from the adjacent higher areas and the Lower Weichselian Terrace was aggregated (Vandenberghe, 1992b). It is known from the Greenland ice-cores and marine cores from the North Atlantic that the Weichselian Glacial climate of northern Europe oscillated rapidly between **stadial** (colder and drier) and **interstadial** (warmer and more humid conditions with a total of 24 interglacials (Bond et al., 1992; Dansgaard et al., 1993). Terrestrial interstadial deposits could be proven in NW-Germany at Oerel near the town of Hamburg by (Behre and Lade, 1986). However, in Oerel only 4 of the 24 Weichselian interstadials of the Greenland ice cores are shown. The **Late Glacial (13-10 ka BP)** marks a transitional time for the NW-European rivers from a braided to meandering pattern due to the change in climate and associated change in vegetation. The rivers started to incise into the previously deposited Lower Weichselian Terrace (Huisink, 1998; Vandenberghe, 1993; Vandenberghe, 1995a;

Vandenberghe, 1995b; Vandenberghe et al., 1994). The climatic change during the late glacial also caused the formation of some North German lakes (Dahms, 1974; Grahle, 1968; Grahle and Müller, 1967; Merkt, 1979; Pfaffenberg and Dienemann, 1964). The Aeolian Phase of the Younger Dryas continued until the **Holocene Preboreal**. The climatic optimum of the **Boreal** led to the growing of moors.

2.3. Development of salt structures

Most of the NW-German salt structures were already developed during the Lower Triassic as **salt pillows**. The **diapiric stage** was reached by most of them during the Upper Triassic (Keuper), (Jaritz, 1992). The difference in the structure geological development of the Lower Saxony Basin and the tectonically more stable Pompeckj Block is also reflected in the development of the salt structures. Whilst the climax of diapirism on the Pompeckj Block was during the Triassic, the phase of diapirism in the Lower Saxony Basin was linked to the inversional phase during the Upper Cretaceous (Jaritz, 1973). The genesis of the Lower Saxonian Tectogene led to the formation of **salt wedges**. Permian salts intruded and filled extensional joints of the overlying strata during the pre-Upper Cretaceous tensional rifting phases. During the compressive phase of basin inversion these salts were pressed into the adjacent strata, diapirs and salt pillows were squashed and transformed and pre-Permian basement blocks were uplifted (Baldschuhn et al., 1998).

The **average uplift rate** of the NW-German **salt domes** in the diapiric stage varied between 0,1-0,5 mm/a, in the later stages only several hundredths of a millimeter were reached (Jaritz, 1980). After the halocinetic concept of (Trusheim, 1957) no tectonic impulse is necessary for the development of salt structures. Salt movement was thought to be a phenomena of gravitational forces, whereas buoyancy is controlled by the overburden. After (Trusheim, 1957) most of the North German salt structures are the result of **halocinese**. More recent works favour a tectonically induced or even triggered diapirism (**tectogenese**). A possible reason for this paradigm shift is the rapidly increasing knowledge about the structural situation of the deepest parts of the basin (Permian/pre-Permian strata) due to the exploration activities of the German oil industry over the last decades (Baldschuhn et al., 2001; Brink et al., 1992). After Jaritz (1992) about two-thirds of the three hundred NW-German salt structures were induced by tectonics and numerous diapirs were affected in their structural evolution by tectonism. Numerical models which simulated the process of salt diapirism came to the conclusion that buoyancy alone is not sufficient to break a brittle overburden. Necking and faulting induced by extension promotes and drives salt diapirism (Daudre and Cloetingh, 1994).

2.4. Modern stress field, fault reactivation and seismicity

It could be shown by the **World Stress Map Project** of the International Lithosphere Program that **horizontal stress orientation** and magnitude are uniform over broad regions of the Earth crust (Zoback et al., 1989). Most midplate regions are under compressive stress regimes (thrust or a combination of thrust and strike/slip deformation) with a striking correlation between Sh max orientation and azimuth of absolute plate motion.

Nearly 1500 stress orientation data are available for Europe (earthquake focal meachanism, overcoring measurements, well bore breakouts, hydraulic fracturing, young slip studies). **Western Europe** (between 45°N and 55°N and 10°W and 17°E) **shows a uniform NW-NNW Shmax orientation of N145°E +-26°** (Müller et al., 1992). The stress data indicate that western and northern Europe is subject to strike slip regime, characterised by NW-NNW compression and NE –ENE extension. The orientation of maximum stress is subparallel to the direction of relative plate motion between Africa and Europe and is rotated 17° clockwise to the direction of

absolute plate motion. Western Europe is stressed by ridge-push forces from the west and north and by collision forces in the south generated by the continent-continent collision of Africa and Eurasia. The results of the World Stress Map Project agree well with premilinary works on local stress orientation in Western Europe (Ahorner, 1975; Illies and Greiner, 1979). However, there are short scale variations of the tectonic regimes in the western European stress province (Müller et al., 1997; Müller et al., 1992). Müller et al. (1997) developed a tectonic model to explain these short scale lateral variations of Sh max by lateral plate boundery forces which cause upper crustal fragments to move independently of each other on the lithospheric mantle. Results of numerical models which simulated the European regional stress field are compatible with the observed regional stress pattern. Main **driving forces** for the observed and modelled stress field are thought to be **the North Atlantic seafloor spreading** and the **northward motion of the African and the Arabian plate** (Gölke and Coblentz, 1996; Grünthal and Stromeyer, 1992).

The style of fault deformation depends strongly upon lithology, temperature and strain rate. In the upper crust with temperatures below 300°C lithology is the dominating factor and strength is mainly controlled by pressure. Ridgid rocks deform by brittle processes whereas fluids are linked to faulting processes (Meissner, 1996). Analogue sand box experiments simulating thrust tectonics have shown that pre-existing faults lower the friction angle by about 10-20% (Sassi et al., 1993). The existence of fluids has major impact on the style of the formed thrust wedge during compression. Pore pressure effects of fluids reduce the pressure dependence in the brittle crust. It could be shown by the work of Nalpas et al. (1995) that a reactivation of normal faults occurs when the angle between the trajectory of horizontal stress and the strike direction of the normal fault is smaller than 45°. Ductile layers (clayish sediments or evaporites) deform in a plastic manner and can act as a detachment plane during compression. The Zechstein salt acted as a decollement layer for the overlying Mesocoic strata during both extensional and compressional phases as shown for a part of the Broad Fourteen Basin (offshore Netherlands), (Nalpas et al., 1995). Compressional faults are generally flatter in the upper crust than normal faults (Meissner, 1996). In the lower crust the role of temperature becomes important, because rocks tend to deform ductile. This change from the brittle domain of the upper crust to the dislocation by creep of the lower crust is documented by the fact that earthquakes are rare below 15-20 km (Meissner and Strehlau, 1982). In the lower crust faults are rare and extensional faults have yet not been observed (Meissner, 1996). Ziegler (1990) suggested that lithospheric strength reduction, caused by pre-existing faults, controls deformation of a large number of intra-plate basins in Europe and that sliding on pre-existing faults is favoured over formation of new ones.

Northern Germany is an area of low seismicity (Leydecker, 2002b; Leydecker and Kopera, 1999). A historical earthquake occurred anno 1770 about 25 km north of Osnabrück at the southern margin of the Lower Saxony Basin, probably the strongest earthquake in Northern Germany over the last 1000 years (Leydecker et al., 1980). Since the times of instrumental earthquake recording two **tectonic earthquakes** were detected for Northern Germany. The first in the year 1977 near the town Soltau about 50 km south of Hamburg (9°56,7 E +/-9,0 km; 52°56,9 N +/- 5,5 km) with a magnitude of ML=4,0. The focal depth was between 4-13 km, probably near the bottom of the Zechstein or pre-Zechstein sequence. A NNW-SSE striking fault plane is favoured because of local geological conditions (Leydecker et al., 1980), (Fig. 1, red circle). The second one occurred in the year 2000 at Zarrentin/Wittenburg 20 km SW of Schwerin near the river Elbe with a magnitude of ML=3,2 (Leydecker, 2002a).

2.5. Structural situation of the study area

Fig. 1 shows the position of the study area (black rectangle) in relation to the main structural units of the NW-German Basin. The southernmost part of the investigated part of the river Hunte catchment basin (yellow field) is located above the Lower Saxony Basin (gray field) and most of the northern area above the northerly adjacent tectonically more stable Pompeckj block. The black dashed lines mark the faults at the Base of Zechstein after the Geotectonic Atlas of NW-Germany (Baldschuhn et al., 1996) and the green areas the position of salt domes and salt walls after (Boigk, 1981). The rose diagrams show the strike direction for the faults at the Base of Zechstein for a) the Pompeckj Block and b) for the Lower Saxony Basin. The roses were plotted after length with a pedal width of 5°. The geographical orientation of the Lower Saxony Basin is WNW. This direction is also shown by the orientation of the faults at the Base of Zechstein. Most of the Zechstein faults on the Pompeckj Block are striking with NNW (Fig. 1 a). Salt walls and a salt dome can be found only in the northernmost part of the study area. The red lines show the orientation of stress measurements (Sh max) after the World Stress Map (Müller et al., 2000). Two measurements were available from the southern part of the study area, showing a stress orientation of 150°. Nearly the same orientation can be found westerly of the study area between the river Weser and Elbe.

Fig. 3 shows the pattern of basement blocks after the Geotectonic Atlas of NW-Germany (Baldschuhn et al., 2001). The red lines show the position of lineaments and faults at the basal Zechstein or below. These lineaments/faults separate the basement blocks. The faults at the Base of Zechstein are given in black dashed lines after the Geotectonic Atlas of NW-Germany (Baldschuhn et al., 1996). The gray circled letters A to I give the names of basement blocks, the watershed of the river Hunte is shown in black. Rivers are given in blue, the Holocene Alluvial Plain of the river Hunte in yellow. The Goldenstedt Blenhorst Lineament (number 3) in the east and the Rheder Moor Oythe Lineament (number 4) in the west separate the Lower Saxony Basin in the south from the Pompeckj Block in the north. The basement block **E (Bockstedt Graben Lessen-Staffhorst-Block)** is the northernmost block of the study area between the Lower Saxony Basin and the Pompeckj Block. It is part of a 70-80 km extending NNE vergent overthrust block (Baldschuhn et al., 2001). The Leer-Bremen-Lineament (number 1) which can be found on the Pompeckj Block separates the Ostfriesland Block in the north (A, B) from the Südoldenburg Block in the south (C, D). The NNW orientated Berdum-Jaderberg-Sagermeer-Fault (number 2) partitions the Ostfriesland Block into the westward Ostfriesland West-Block (A) and the eastward Ostfriesland East Block (B) and the Südoldenburg Block into the Südoldenburg Block East (C) and the Südoldenburg Block West (D).

In the following, important structural elements of the study area will be explained. Fig. 4 shows the structural situation at the Base of Upper Cretaceous with the position of structural elements. The depth is given from white (-100) to black (-3300 m a.s.l.). The faults are shown in red, salt structures (salt domes and salt pillows [dashed line] in blue) and outcrop of the Upper Cretaceous is shown in pink. The position of the investigated section of the river Hunte catchment basin is given in yellow and the Holocene Alluvial Plain of the river Hunte in green. The main structural elements which can be found in the study area are from north to south the SW-NE striking **salt dome "Zwischenahn"**. The salt dome is visible at the pre-Cretaceous level (Appendix, Fig.9: Base Upper Jurassic and "Wealden"). The salt dome is positioned above a SW-NE striking basement fault at the Base of Zechstein (Appendix, Fig.15: Base Zechstein). The salt dome "Zwischenahn" is part of the Leer-Bremen-Lineament (Fig. 3, number 1). A salt pillow formed during the Triassic above the basement faults; the diapiric stage started at the Upper Jurassic. As a result of the inversion tectonic during the Upper Cretaceous the

SE flank of the diapir was uplifted and thrust to the southeast. The uplift phase of the salt dome is detectable until the Miocene (Baldschuhn et al., 2001).

The structure **"Oldenburg-Delmenhorst"** is an inverted graben (bipolar inversion structure) modified by injection of salt. Like the structure "Zwischenahn" it is part of the Leer-Bremen-Lineament (Fig. 3, number 1). A graben structure was formed due to movements at the basement during the Middle Jurassic and Zechstein salts rised up. During the inversional phase in the Upper Cretaceous (Coniac-Santon) the graben fill was squeezed on the former graben shoulder. This bulge process lasted until the Younger Tertiary as documented by outcrops on top of the structure. Due to this bulge and stretching during the Tertiary a graben was formed on top (Appendix, Fig. 6: Base Tertiary). It is remarkable that in the deeper geological strata the single structural elements are in accordance with the basement pattern. Firstly in the Tertiary the structural connection between "Oldenburg-Delmenhorst" and "Zwischenahn" was formed by keystone faulting (Appendix, Fig. 6: Base Tertiary), (Baldschuhn et al., 2001).

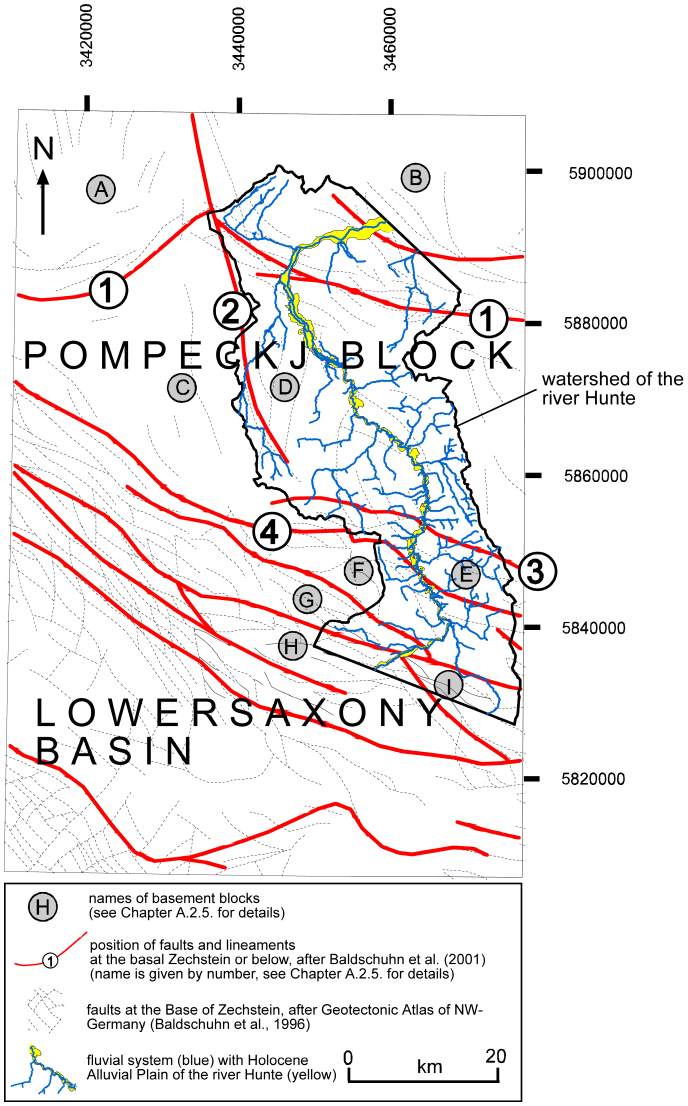

Fig. 3: Structural situation (pattern of basement blocks) of the study area (after Baldschuhn et al., 2001). The red lines show the position of faults, structure zones and lineaments at the basal Zechstein or below. Number 1 =„Leer-Bremen-Lineament“, number 2 = „Berdum-Jaderberg-Sagermeer-Fault”, number 3 =“ Goldenstedt Blenhorst Lineament” and number 4 = “ Rheder Moor Oythe Lineament”. The gray circled letters (A) to (I) stand for the names of basement blocks. The blocks (A)-(D) are positioned on the Pompeckj Block, (E)-(I) on the Lower Saxony Basin. (A) = Ostfriesland West-Block, (B) = Ostfriesland East-Block, (C) = Südoldenburg Block West, (D) = Südoldenburg Block East, (E) = Bockstedt Graben Lessen-Staffhorst-Block, (F) = Oythe-Düste-Wehrbleck-Block, (G) = Dersum-Börger-Hemmelte-Bokern-Block, (H) = Kroge-Diepholz-Neufeld-Block, (I) = Rheden-Bahrenborstel-Block. The dashed black lines show the faults at the Base of Zechstein after the Geotectonic Atlas of NW-Germany (Baldschuhn et al., 1996). The position of the investigated part of the river Hunte watershed is given by the bold black line, rivers are shown in blue and the Holocene Alluvial Plain of the river Hunte in yellow.

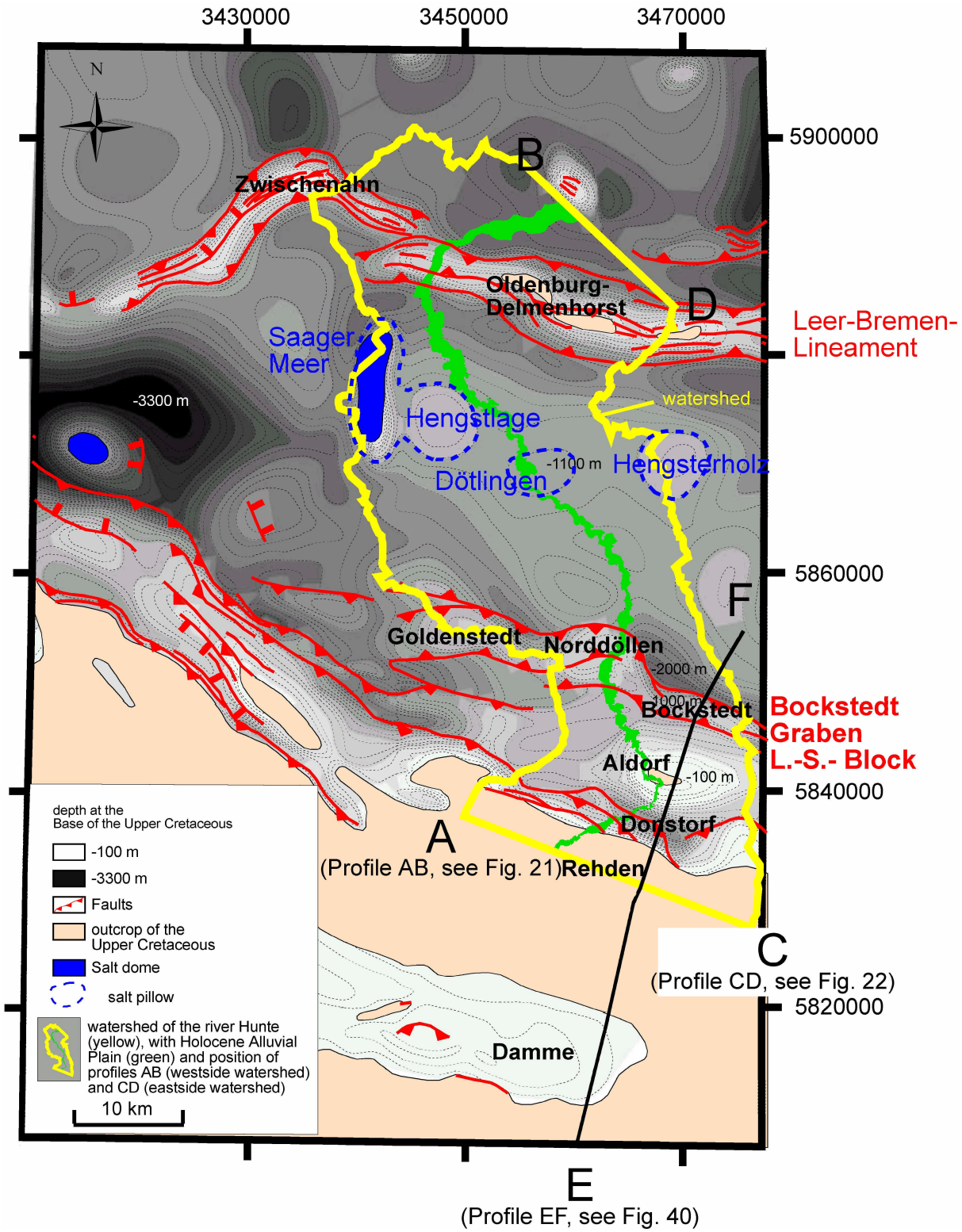

Fig. 4: Section of the river Hunte catchment basin with position of the watershed (yellow), Holocene Alluvial plain (green), depth at the Base of Upper Cretaceous from -100 (white) to -3300 m (black), faults (red), outcrop (pink), salt domes (blue), salt pillows (dashed blue), with structural names of tectonic blocks, salt structures and major lineaments, (after Baldschuhn et al., 2001; Baldschuhn et al., 1996). Position of profile AB (westerly watershed) is shown in Fig. 21, profile CD (easterly watershed) in Fig. 22 and profile EF in Fig. 40.

The genesis of the **salt dome "Saager Meer"** is caused by tectonics (Jaritz, 1992). There is a great spatial accordance between the N-S elongated salt dome and the NNW orientated Berdum-Jaderberg-Sagermeer deep seated fault and the NNE to NNW striking faults at the Base of Zechstein (Fig. 3, number 2).

Doming of the geological depth above the **salt pillow "Dötlingen"** are visible from the Base of Lower and Middle Buntsandstein to the Base Middle Oligocene to Upper Oligocene (Appendix, Fig. 14 to Fig. 4). The structure is framed by a half graben system at the Base of Zechstein (Appendix, Fig.15: Base Zechstein) striking NW-SE. A doming of the underground above the **salt pillow "Hengsterholz"** is visible from the Base of Lower and Middle Buntsandstein (Appendix, Fig. 14) to the Base of Tertiary (visible in the contour map of the Base Tertiary, based on 3D Seismic Data, (BEB, 2002), not shown). The graben structures **"Goldenstedt, Norddöllen, Bockstedt"** are part of the Bockstedt Graben Lessen-Staffhorst-Block" (Fig. 3, letter E). These Graben structures formed during Triassic to Jurassic times. During the inversional phase of the Upper Cretaceous (Coniac-Santon) the graben structures were uplifted and the former peripheral faults transformed to gently dipping NE-vergent thrust zones. At this inversional phase Zechstein salt penetrated into the overthrust sheets (Triassic, Bundsandstein, Röt) and formed salt wedges. The salt wedges amplified the process of anticlinal formation (Baldschuhn et al., 2001).

The inversional, anticlinal structure **"Aldorf"** is positioned on the Oythe-Düste-Wehrbleck-Block (Fig. 3, letter F). The W-E striking anticlinal structure is visible from the Base Upper Buntsandstein and Muschelkalk to the Base of Tertiary (Appendix, Fig. 13 - Fig. 6). The weak inversion (during Upper Cretaceous [Coniac/Santon]) of the structure was founded by the thrusting of the basement and the Triassic stata and the intrusion of Zechstein salts into the Upper Buntsandstein (Rötsalinar) and the linked doming of the overlying strata (Baldschuhn et al., 2001). The counterpart of these anticline structures like “Aldorf” is the formation of marginal troughs like the Upper Cretaceous trough **"Donstorf**".

2.6. Geological situation of the study area (Quaternary)

Fig. 2 shows the geological map of the study area after the Quaternary Overview Map of Lower Saxony and Bremen (NLfB, 1993). The grid gives the numbers and position of the topographical maps. The small numbers (1-21) present the lithological units of the Holocene (1-9), the Pleistocene (10-19) with the Weichselian (10-13), the Saalian (14-15), the Elsterian (16-18) and pre-Elsterian (19) and the pre-Quaternary (20-21). The investigated part of the river Hunte catchment basin is shown in black.

It is evident that the study area is dominated by Saalian deposits (meltwatersands [15] and morainic deposits [14]). The glacial Saalian deposits have been the sediment source for the geologically younger Lower Weichselian Terrace [13]. An E-W striking sandy loess cover [11] is visible at the river Hunte catchment basin. This aeolian coversand is disconnected by the ~NS striking river Hunte. The geological map 1:200.000 (BGR, 1982) shows that this sandy loess superimposes Saalian morainic deposits. The river Hunte breaks through the higher elevated Saalian deposits (called “Geest”) in the south above the anticline structure “Aldorf” and leaves it above the saltpillow “Hengstlage” (Fig. 4). The Digital Elevation Model of the river Hunte catchment basin (Fig. 5) illustrates this breakthrough of the river Hunte. South and north of the “Geest” a wider Lower Weichselian Terrace than inside the “Geest” area is visible (Fig. 6).

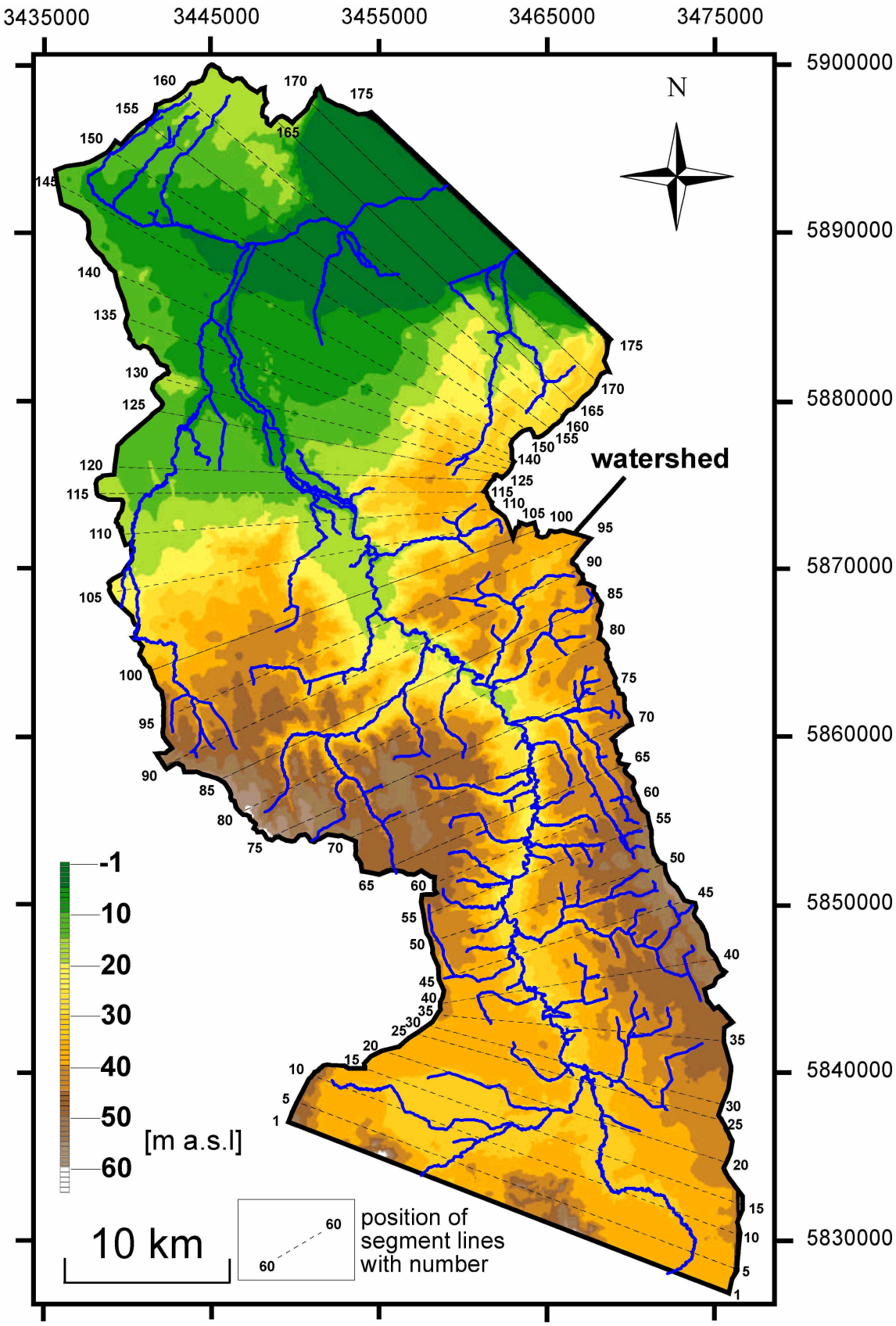

Fig. 5: Digital Elevation Model (DEM) for a section of the river Hunte catchment basin. Range of altitude is +65,0 to -0,69 m a.s.l. Database: Topographical Maps (LGN, 1898; LGN, 1994).
The numbered dashed lines give the position of segment lines. The fluvial system is shown in blue.

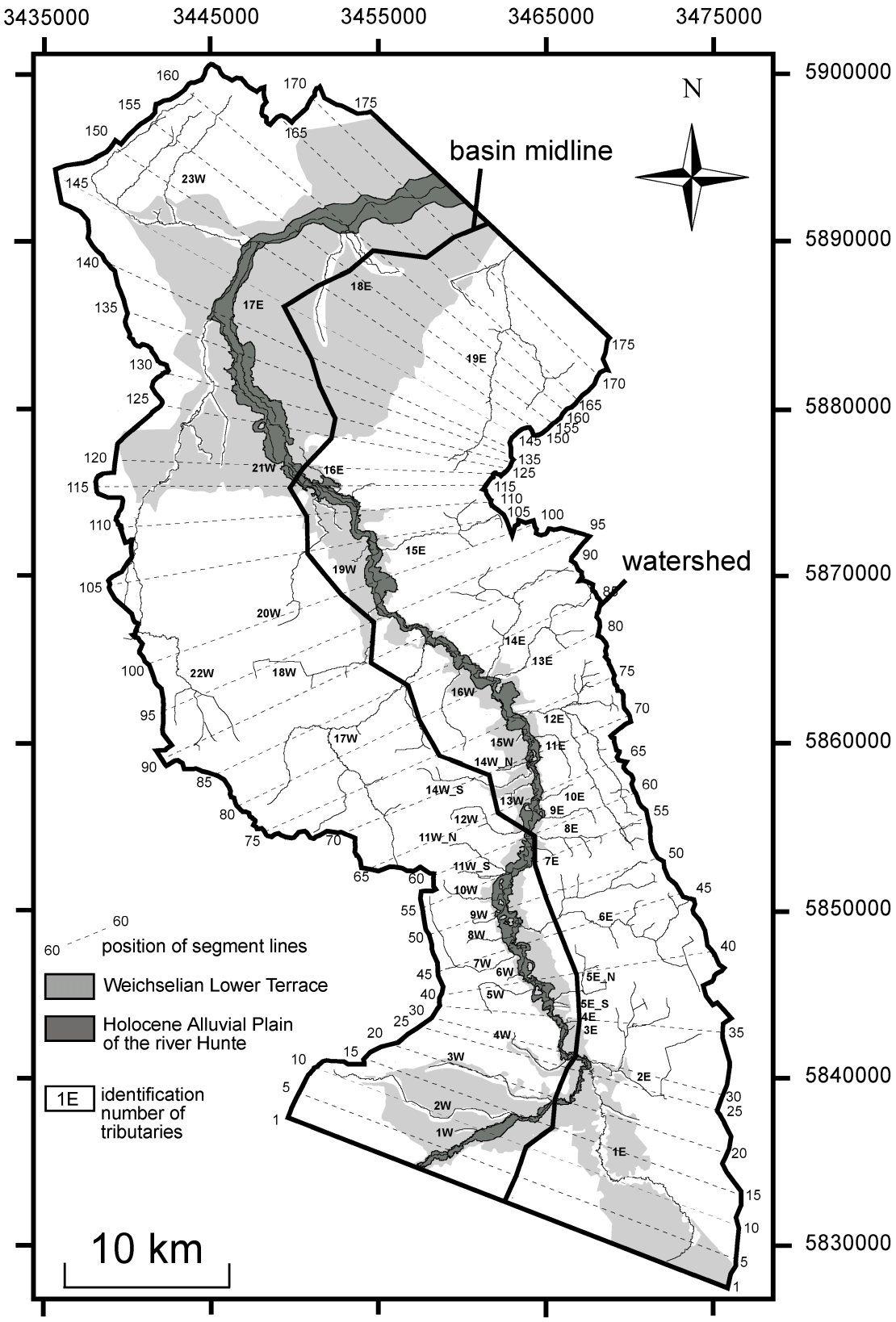

Fig. 6: Section of the river Hunte catchment basin with position of the Holocene Alluvial Plain, Weichselian Lower Terrace, tributaries (with identification number), basin midline, watershed and segment lines with identification numbers.
Holocene Alluvial Plain and the Lower Weichselian Terrace after field work, topographical- and geological maps (BGR, 1982; LGN, 1898; LGN, 1994). The fluvial system is based on the historical topographical maps and the position of the watershed on the modern and historical topographical maps (LGN, 1898; LGN, 1994).

2.7. Terminology of neotectonics and active tectonics

The neotectonic period is the youngest period of the tectonic evolution of a specific region. However, there is no consensus in the literature to define the exact beginning of a neotectonic period, because the tectonic evolution and thus the exact timing for the onset of the youngest period of tectonic evolution differs from region to region (Becker, 1993). For this reason, the terminology will be introduced in the following.

The neotectonic period is the time from the Oligocene/Miocene boundery at about 23,8 Ma until the Pleistocene/Holocene boundery at 0,01 Ma and the term active tectonic will be used for the time 0,01 Ma until present (Tab. 1).

2.8. Objective

The aim of this study is to investigate if neotectonic/active tectonic movements in the upper crust influence modern landscape formation. The study area is covered by Quaternary sediments. Sediments have the potential to record the youngest tectonic movements (Sirocko et al., in press; Vanneste et al., 1999) but are on the other hand easily erodable, which could lead to the destruction of "neotectonic/active tectonic fingerprints" during times of lower tectonic activity or even quiescence. However, there is no indication for tectonic quiescence in northern Europe during the Quaternary as shown by studies dealing with fluvial terrace warping (e.g. Houtgast et al., 2002; Maddy et al., 2000), subsidence analyses (e.g. Geluk et al., 1994; Houtgast and van Balen, 2000), recent seismicity (e.g. Camelbeeck and Meghraoui, 1996; Leydecker and Kopera, 1999; Leydecker et al., 1980), lineament analyses (e.g. Dulce and Gronemeier, 1982; Kronberg, 1991; Krull et al., 1985; Krull and Wegner, 1988; Sesören, 1976) and geodetic relevelling data (e.g. Bankwitz, 1976; DGK-Arbeitskreis, 1979; Ihde et al., 1987; Kooi et al., 1998; Leonhard, 1988; Schwab, 1981; Schwab et al., 1973; Wübbelmann, 1993). In contrast, there is evidence for a tectonic intensification starting with Pliocene/Pleistocene times as evident by an increament of subsidence (Geluk et al., 1994; Houtgast and van Balen, 2000; Kooi et al., 1989; Kooi et al., 1991; Thorne and Watts, 1989; Zagwijn, 1989) which is thought to be caused by a process of plate reorganisation (Cloetingh et al., 1990). An abruptly accelerated uplift of the Rhenish Massif is evident since about 800 000 years ago (Meyer and Stets, 1998), whereas the North Sea basin strongly subsided during the Quaternary as evident by local sediment thicknesses of up to 1000 m in the area of the southern Central Graben (Caston, 1977).

The following investigations have been carried out in the NW-German Basin (Lower Saxony) to evaluate a possible neotectonic/active tectonic influence on modern morphology.

- The Hunte catchment basin is studied to investigate the depth to height relationship between the geological subground and the modern topography (Chapter C.1.1.1., C.1.1.2., C.1.1.3., C.1.1.5.1.).
- The orientation of morphological elements [topography, fluvial system, lakes and depressions, steep slopes] is analysed and compared with the orienation of the geological subground, because neotectonic/active tectonic movements are able to cause distinct orientations in the landscape (Chapter C.1.1.4.).
- The Hunte valley and the fluvial system is investigated. If the NW-German Basin is tectonically active, anomalies of the fluvial system/morphology and the geological subsurface [fault zones, anticline/syncline structures] should spatially coincide (Chapter C.1.1.).
- The Lower Weichselian Terrace of the Hunte is studied to ascertain possible terrace warping (Chapter C.1.1.11.).

- λ A small scaled depression positioned on the Lower Weichselian Terrace is investigated by Georadar, Reflection Seismic, drilling and dating of sediments to evaluate a possible tectonic influence on formation of the structure (Chapter C.1.1.12.).
- λ Unpublished data from a repeated geodetic fine-levelling of NW-Germany are used for the calculation of recent vertical movement rates (Chapter C.1.2.).
- λ Lower Weichselian Terrace sediments have been dated by OSL and AMS ^{14}C to calculate sedimentation rates. Terrace aggradation could be related to basin subsidence. Thus, the velocity of terrace aggradation should be equal to the velocity of basin subsidence (Chapter C.2.).

B) Material and Methods

B.1. Geo Information System (GIS) and Geostatistics

Geo Information Systems (GIS) have become a powerful tool in Earth Sciences over the last years. The capability of computer systems and software solutions have increased rapidly. Even personal computers allow today the calculation of extensive mathematical operations and processing of data. Beside the aspect of graphical presentation (map production by combining different thematic maps) GIS enables the possibility of spatial data management and geostatistical calculations (Vitek et al., 1996).

1.1. Software and maps

The program Erdas Imagine 8.5 was used for the process of georeferencing. Redrawn and digitised maps were transformed into an orthogonal coordinate system (German National System, Gauss Krueger, system of ninth longitude). Map informations were vectorised from the georeferenced maps with the program ArcView GIS 3.2. The program was used for the construction of Digital Spatial and Digital Elevation Models, spatial data requests and the final map production (graphical presentation of results). The program Rockworks 98/99 was used for geostatistics (realisation of orientation analyses [calculation of rose diagrams]). The programs Excel and Microcal Origin 6.0 were used for the production of plots and for statistics.

Topographical maps

A total of 54 historical topographic maps (LGN, 1898) and 54 modern topographic maps (LGN, 1994) were used for geomorphological analyses. The maps cover the whole study area (Fig. 2). At this point I would like to thank the LGN (Landesvermessung + Geobasisinformation Niedersachsen) for permission to use their maps (Verfielfältigungsvermerk -52-1051/00). The historical maps were used because the courses of the rivers were straightened, natural slopes and depressions were smoothed due to land clearance projects about 40 years ago (Ness, 1994). The topographical maps (historical and modern) have a contour interval of 1,25 m.

Geological maps

Geological Maps on the scale 1:200.000 (CC3910, CC3110), (BGR, 1982) were used to support the mapping of the Holocene Alluvial Plain and the Lower Weichselian Terrace. The Geological Map (NLfB, 1993), was used for the presentation of the Quaternary-Geological situation of the study area (Fig. 2) and the depth of the Base Quaternary (Appendix, Fig. 1: Base of Quaternary).

Structural geological maps

Structural-geological informations about the subsurface were taken from the Geotectonic Atlas of NW-Germany. This atlas was recently published as a paper map (Baldschuhn et al., 1996) and in electronical mode on CD (Baldschuhn et al., 2001). It gives a synthesis of geological and geophysical data (from about 75000 deep wells and about 1000000 km of reflection seismic lines) made available from the German oil industry. Structural contour maps of fourteen geological horizons with a contour interval of 100 m on the scale of 1:300000 from Base Zechstein to Base Middle Miocene to Pliocene (Tertiary) are presented. The presentation of the structural situation of the study area is based on this data (Appendix, Fig. 2-15).

A map of the Base Tertiary based on 3D Seismic Data was available for a part of the study area (BEB, 2002). At this point I would like to thank the BEB, Hannover for permission to use their map. A graphical presentation of the map is not possible. Consequently, only derived data were shown (profiles, statistical analyses). The depth information from this high resolutioned map (contour interval of 25 m) were combined with the data from the Base Tertiary of the Geotectonic Atlas of NW-Germany. The geographical position of the map is shown in the Appendix (Fig. 6: Base Tertiary).

1.2. Data collection and spatial analyses

Morphological elements of the modern landscape (fluvial system, steep slopes, lakes and depressions, topography) were **vectorised** from the historical and modern topographical maps (LGN, 1898; LGN, 1994). Fig. 7 shows the fluvial system of the study area. The total length of the fluvial system is 2901074 km. It was vectorised from the historical maps. Fig. 8 shows the steep slopes (a total of 14911 steep slopes with a total length of 2094 km). The steep slopes have been vectorised from the historical maps. Fig. 9 shows the lakes and depressions. A total of 2101 lakes and 1442 depressions were vectorised from both historical and modern maps, with a total length of 1191 km (total of perimeters). Lakes and depressions were combined to a single layer for further geostatistical investigations. The ground level elevation was mainly vectorised from the modern topographical maps. The historical maps were only used for the reconstruction of artificial modified landscapes during the 20th century (e.g. high density areas). The ground level elevation of the investigated part of the river Hunte catchment basin (Fig. 5) was mapped with a contour interval of 1,25 m and the whole study area with a 10 m contour interval (Fig. 10). Bench marks were vectorisied from the topographical maps and integrated into the process of Digital Elevation Model generation. The structural informations (depth informations of the geological strata, faults, salt structures, outcrops) were vectorised from the Geotectonic Atlas of NW-Germany (Baldschuhn et al., 1996).

The vectorised contour lines from the structural- and topographical maps form the basis for **Digital Spatial Models (DSM)** and the **Digital Elevation Models (DEM)**. All DEMs and DSMs were calculated with the program Arc View 3.2 with a grid cell size of 30 m. These Digital Models form the basis for later spatial data requests (depth/height requests). All presented **orientation analyses** are based on the raw vector data**.** The presented **rose diagrams** were plotted by length with a pedal width of 5°.

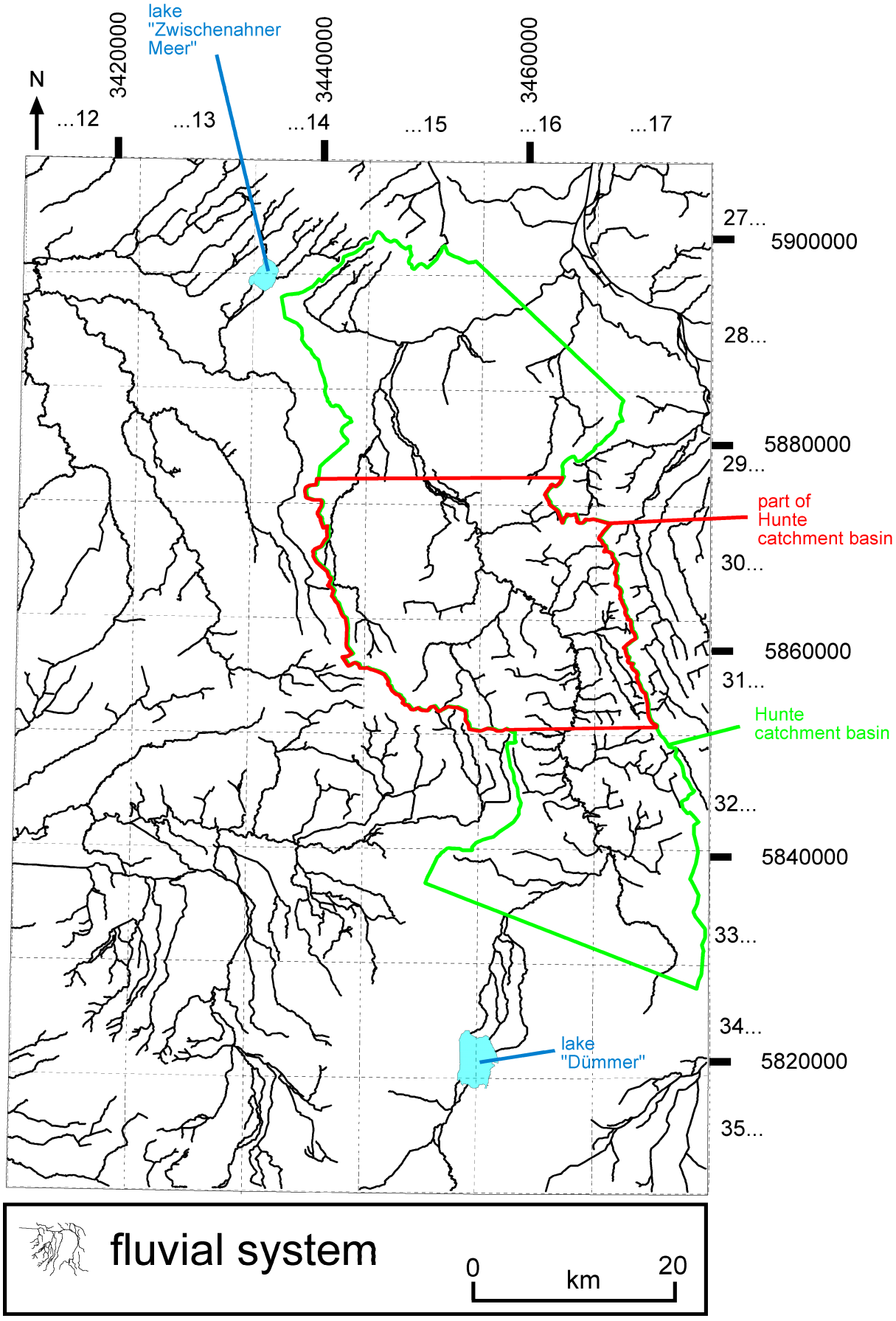

Fig. 7: Fluvial system (black lines) of the study area, after historical topographical maps (LGN, 1898). The dashed squares show the position of the topographical maps with map number. The investigated part of the river Hunte watershed is given in green. The red field shows the investigated part for the orientation analyses described in Chapter C. 1.1.4..

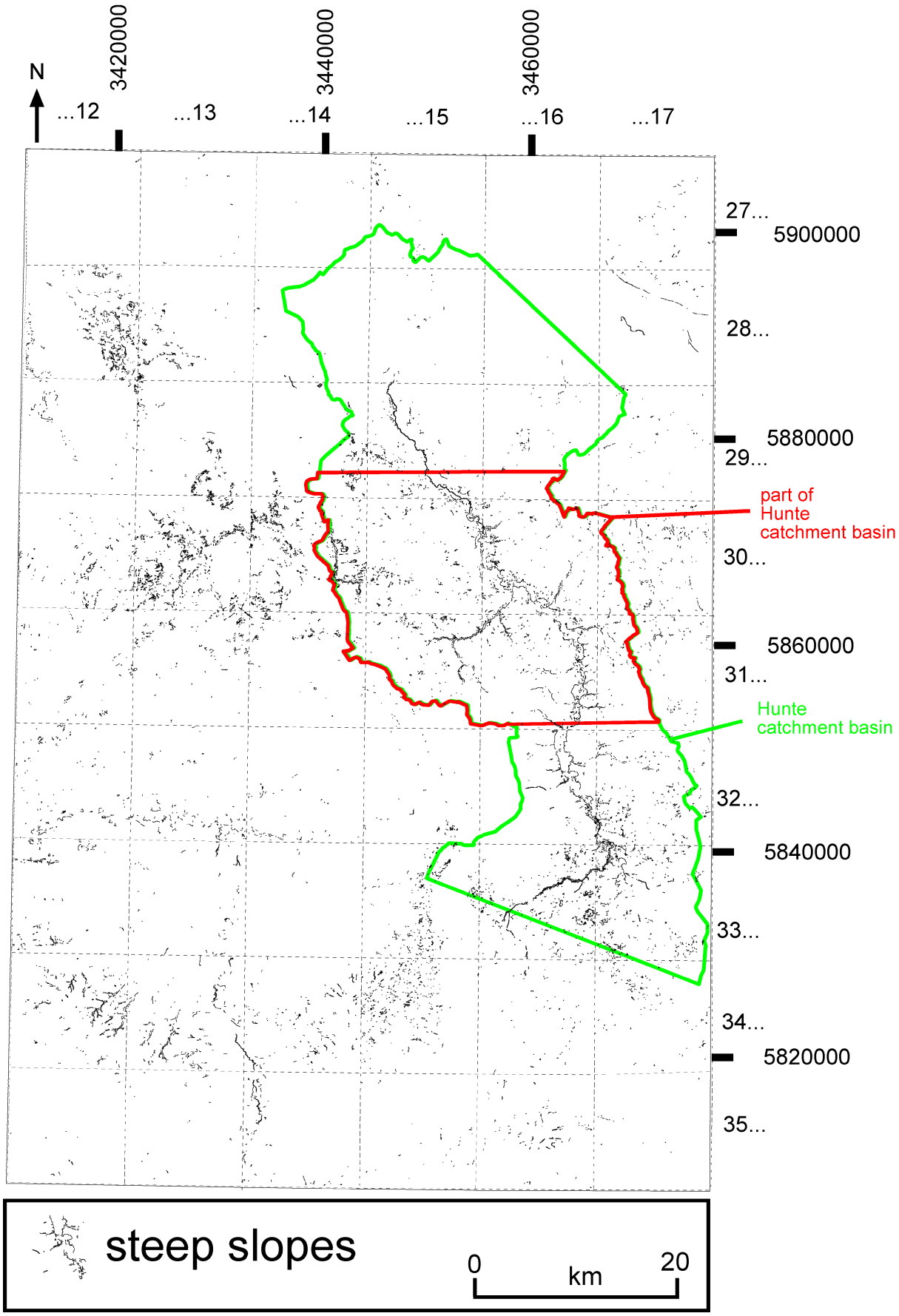

Fig. 8: Steep slopes (black lines) of the study area, after historical topographical maps (LGN, 1898). The dashed squares show the position of the topographical maps with map number. The investigated part of the river Hunte watershed is given in green. The red field shows the investigated part for the orientation analyses described in Chapter C. 1.1.4..

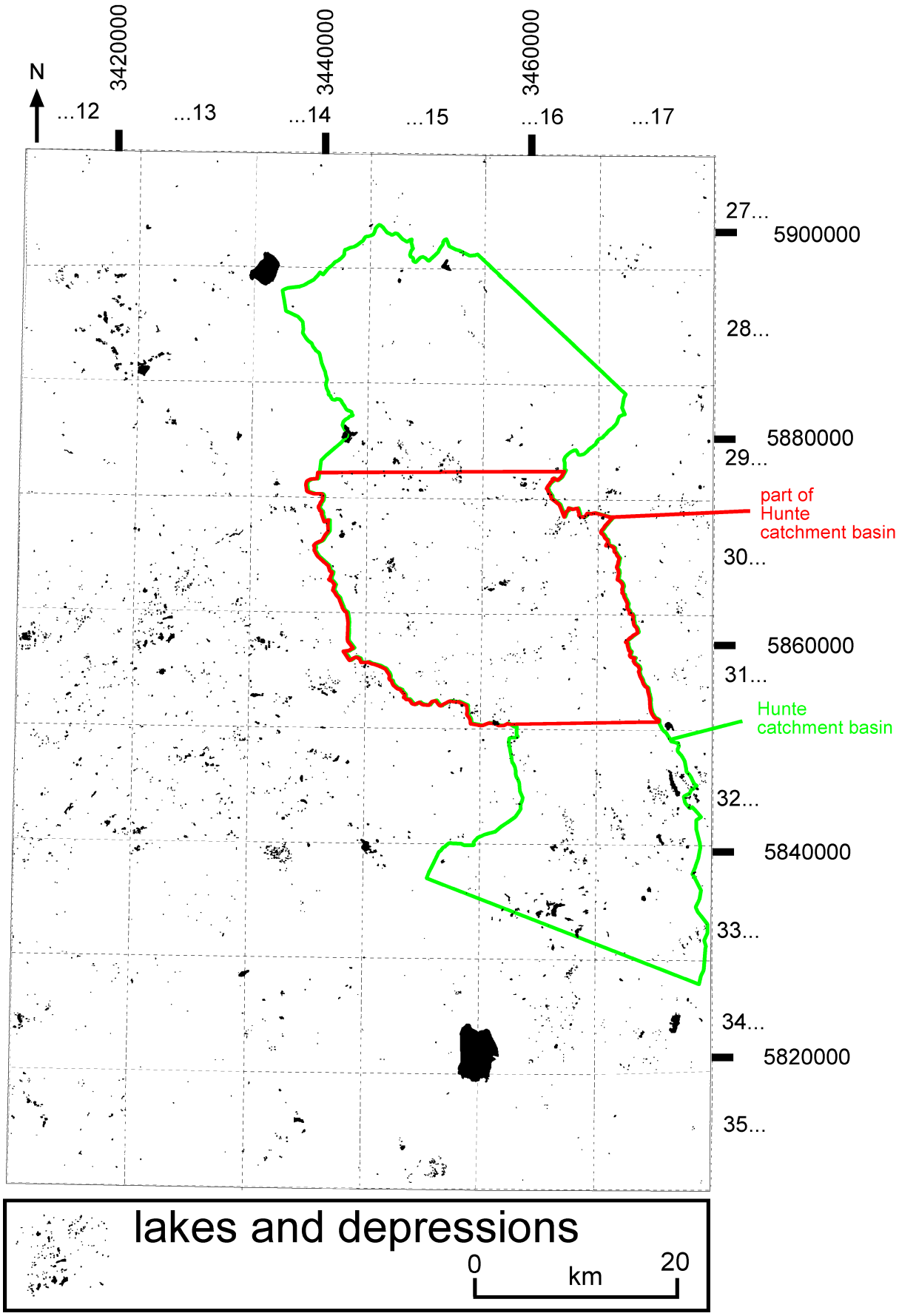

Fig. 9: Lakes and depressions (black) of the study area, after historical and modern topographical maps (LGN, 1898; LGN, 1994). The dashed squares show the position of the topographical maps with map number. The investigated part of the river Hunte watershed is given in green. The red field shows the investigated part for the orientation analyses described in Chapter C. 1.1.4..

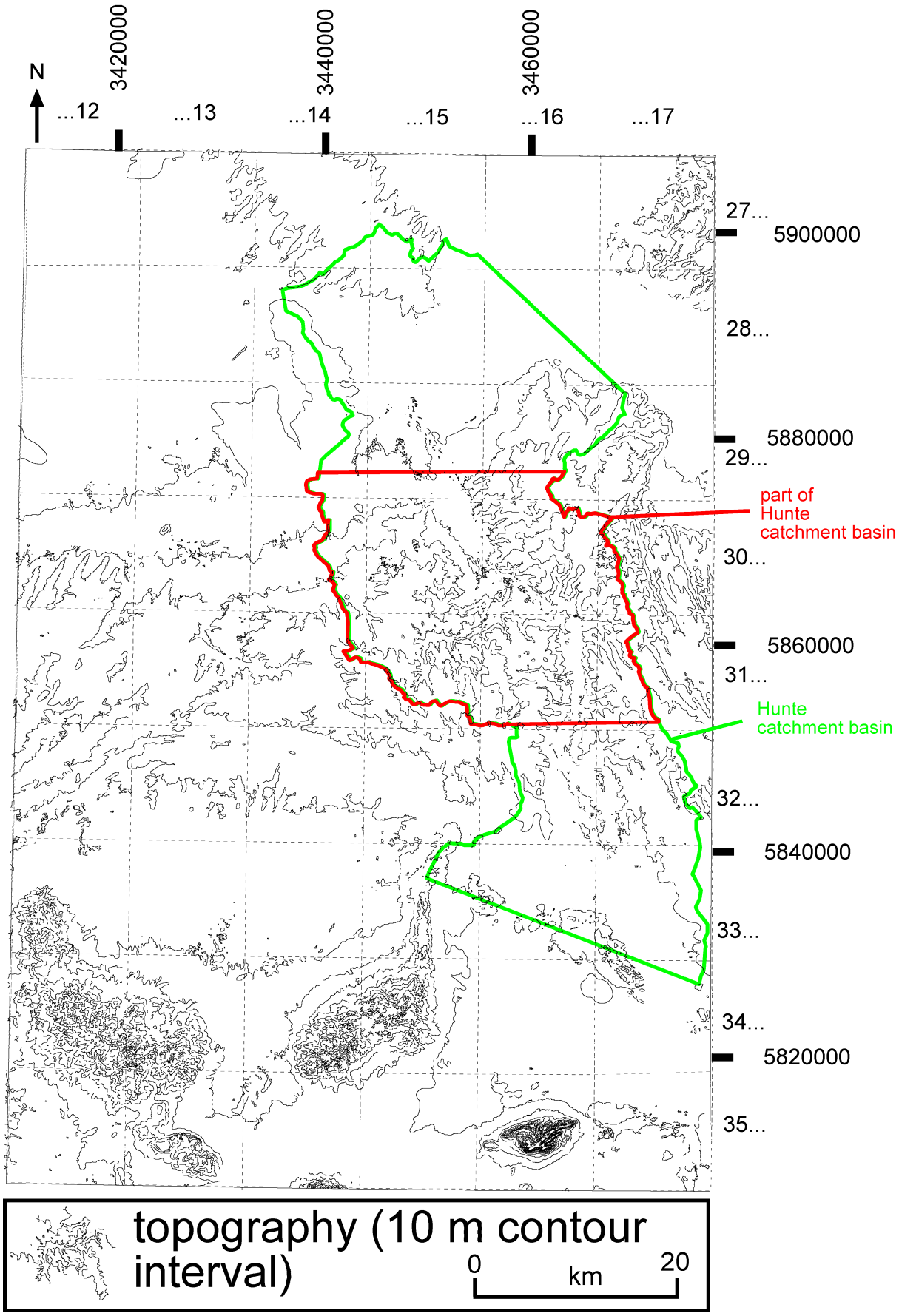

Fig. 10: Topography, 10 m contour interval (black line) of the study area, after historical and modern topographical maps (LGN, 1898; LGN, 1994). The dashed squares show the position of the topographical maps with map number. The investigated part of the river Hunte watershed is given in green. The red field shows the investigated part for the orientation analyses described in Chapter C. 1.1.4..

B.2. Sample preparation and measurements

2.1. Dating techniques

2.1.1. AMS ^{14}C

AMS (**A**ccelerator **M**ass **S**pectroscopy) ^{14}C measurements were carried out at the Leibnitz Labor für Altersbestimmung und Isotopenforschung at the Christian-Albrechts-Universität Kiel, Germany. The samples were wet-sieved to enrich datable material. Calcerous particles were removed with hydrochloric acid [10%] and clastic particles with the Atterberg method. The organic fraction >125 µm was used for dating. Only distilled water was used and samples were dried at 50°. Tab. 2 shows the dating results of the ^{14}C samples.

Tab. 2: Dating results of AMS ^{14}C samples. Calibration of ^{14}C ages after the data set CALPAL 2001 which is incooperated into the radiocarbon age conversion program (CALPAL, 2001).

internal sample code	lab code of Leibnitz Labor at Kiel Germany	material	measured on	sample size [mg C]	14C age BP [a]	calibrated age [calendar years BP]	shown in Figure
Ess_3, 450-480 cm	KIA 8819	plant detritus	lauge residue	2,1	28130 +220/-210	32000 +220/-210	38 b)
Ess_3, 450-480 cm	KIA 8819	plant detritus	humic acid	2,3	27700 +200/-200	31700 +200/-200	
Ess_3, 864-900 cm	KIA 8820	plant detritus	lauge residue	3	40940 +780/-710	42800 +780/-710	38 b)
Gla_1 P83, 685-695 cm	KIA 15399	plant detritus	lauge residue	1,6	28020 +330/-320	31900 +330/-320	32 c)
Gla_1 P83, 685-695 cm	KIA 15399	plant detritus	humic acid	3,2	27940 +210/-200	31900 +210/-200	
Ess_4, 421-424 cm	KIA 16634	plant detritus	lauge residue	2,2	29160 +270/-260	32800 +270/-260	38 c)
Ess_4, 852-858 cm	KIA 16635	plant detritus	lauge residue	2,7	45770 +1860/-1510	47000 +1860/-1510	38 c)
Ess_4, 974-975 cm	KIA 16636	plant detritus	lauge residue	1,9	>50960		38 c)
Ess_1, 24,5 m	KIA 2944	plant detritus	lauge residue	>1,0	34030 +1260/-1090		
Ess_1, 24,5 m	KIA 2945	seeds of "crowfoot"	lauge residue	>1,0	34310 +510/-480	39500 +1500/-1500	37 a)
Col_3 29,05 m	KIA 372	single fossil root	lauge residue	0,17	11010 +450/-430	12900 +450/-430	37 b)

2.1.2. Optically Stimulated Luminescence (OSL)

The OSL sample preparation was carried out at the OSL-preparation laboratory of the Institute for Geosciences, University of Mainz, following the methods described by (Aitken, 1998). The standard technique for extraction of potassium feldspar was expanded by a feldspar flotation procedure. The OSL measurements were carried out at the luminescence dating laboratory of the Saxon Academy of Sciences in Leipzig (Quaternary Geochronology Section at the Institute of Applied Physics, TU Freiberg) by Dr. M. Krbetschek. IR stimulation (IRSL) on potassium feldspar grains (100-160 µm) was applied to evaluate the paleodose using the multiple aliquote additive dose protocol. The sediment dose rate was calculated based on the radioisotope concentration (U, Th, K-40) determined by low-level high resolution gamma-spectrometry at the Freiberg laboratory. Tab. 3 shows the IRSL dating results of the measured samples.

Tab. 3: Dating results of OSL samples.

internal sample code	age [calendar years BP]	shown in Figure
Ess_1; 27,8 m	28900 +/-2600	37 a)
Ess_1; 27,0 m	30000 +/-3200	37 a)
Ess_1; 24,7 m	32100 +/-4300	37 a)
Col_3; 27,9 m	23000 +/-3700	37 b)
Gla_P33; 1,0 m	22800 +/-1700	32 c)

B.3. Field Work

3.1. Ground Penetrating Radar

A digital Ground Penetrating Radar System (model RAMAC/GPR, owned by the Institute for Geosciences, University of Mainz) was used to record the uppermost geological strata (~ 0-15 m). The system is shown in Fig. 11 a. Data processing was carried out with the program Reflexw Version 2.5 of the company Sandmeier Scientific Software. Basics and applications of the used Ground Penetrating Radar System are described in detail by (Diehl, 2002).

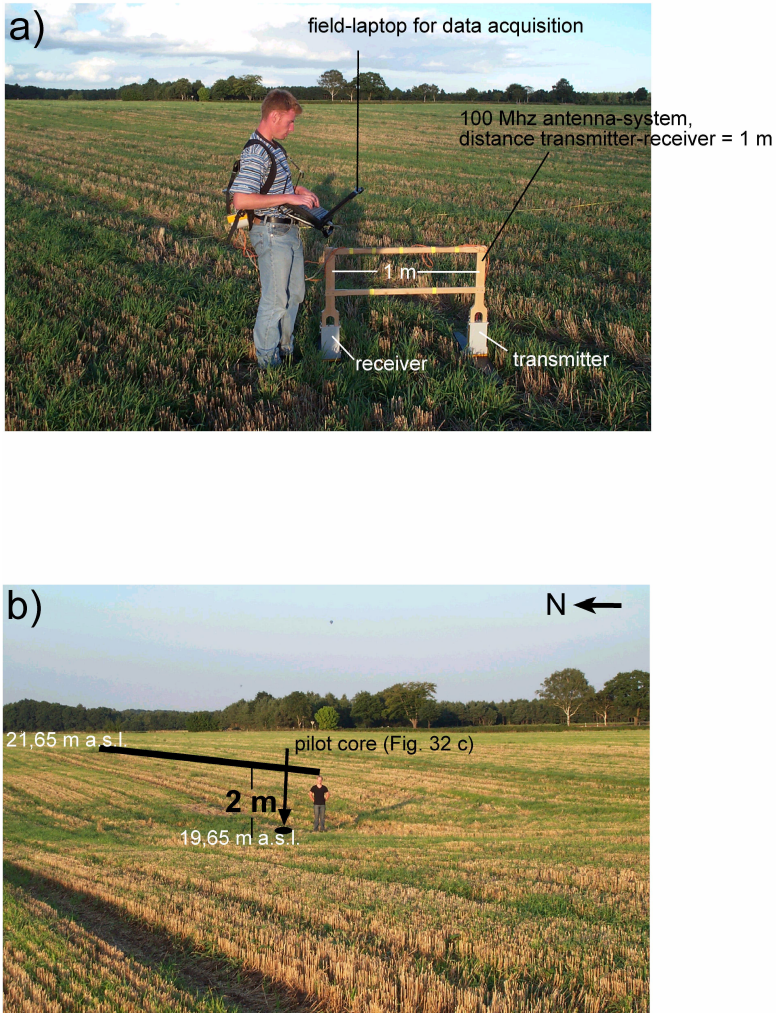

Fig. 11 a) used georadar (modell RAMAC/GPR with 100 MHz antenna). Distance receiver-transmitter = 1m;
b) investigated depression Glane 1 (Gla_ 1), positioned on Lower Weichselian Terrace, view to the east; height difference between depression deepest point and surrounding area is two meters; position of pilote core Gla_1 P83 (Fig. 32 c).

3.2. Reflection-Seismics

A 48 channel-digital reflection seismics apparature of the company Geometrics was used (owned by the Institute for Geosciences, University of Mainz). The energy source was a portable seismic impulse source for shallow reflection seismics (SISSY of the company Dynamit Nobel, cartridge with blasting powder), (Buness et al., 2000; Wiederhold et al., 1998). The shots were moved through a fixed spread with a geophone spacing of 2 m and a number of 48 geophones (Oyo Geospace 14Hz-geophones). The software Reflexw 2.5.4 (company Sandmeier Scientific Software) was used for data processing (CMP-stacking).

3.3. Corings and outcrops

Four cores were taken with a motor driven percussion penetrating method and three undisturbed sediment cores in a plastic tube liner by a cable tool coring technique (Tab. 4). A total of eighteen outcrops were studied and several excavations made to investigate Lower Weichselian Terrace formation along the course of the river Hunte (Tab. 4, Fig. 12).

Tab. 4: Outcrops, excavations and corings of the study area. The position of the locations is given in Gauss Krueger coordinates (R, H) and the height in m a.s.l.. The segment numbers give the position of the locations along the course of the river Hunte. Dated locations (AMS ^{14}C, OSL) are marked with a cross. The depth of corings (sediment cores, pilot cores) are given in [m] below surface. The geographical position of the locations is shown in Fig. 12.

													geographical	
river Hunte								absolute datings					coordinates [GK]	
W-side	acronym of location	figure	location	segment number	outcrop	sediment core, depth	pilot core with depth	AMS 14C	OSL	excavation	topographical map	height [m a.s.l.]	R	H
	Wes_1		Westrittrum_1	102						x	3015	17,50	3454736	5870591
	Hei_N1		Heinfelder Bäke N_1	97						x	3015	18,75	3455108	5867904
	Hei_S1		Heinfelder Bäke S_1	97						x	3015	20,00	3455158	5867775
	Dul_1		Dulshorn_1	77						x	3116	28,75	3462876	5861595
	PeM_1		Pestruper Moor_1	76						x	3116	27,50	3463248	5861314
	Gla_1	29-34	Glane_1	93			0-14 m	x	x	x	3016	21,25	3456524	5866221
	Ros_1		Rosengarten_1	74						x	3116	27,50	3463575	5860638
	Pes_2		Pestrup_2	70	x						3116	26,25	3464312	5858951
	Pes_1		Pestrup_1	69	x						3116	25,00	3464534	5858290
	Büh_1		Bühren_1	64	x						3116	25,00	3464537	5856269
	Gar_1		Garmhausen_1	63	x						3116	27,50	3464122	5855927
	Den_1		Denghausen_1	60	x						3116	28,75	3464234	5854122
	Sie_1		Siedlung Einen_1	59	x		0-8 m				3116	28,75	3464241	5853435
	Ein_1		Einen_1	55	x						3116	28,75	3462743	5852247
	Var_1		Varenesch_1	47	x	0-2 m	0-6 m				3216	32,50	3462775	5848160
	Lah_3		Lahrheide_3	42	x						3216	31,25	3463888	5846015
	Bar_1		Barnstorf_Schule_1	33						x	3217	35,00	3466500	5842703
E-side														
	Alt_1		Altona_1	82	x						3016	23,75	3461578	5864076
	Kat_1		Katenbäker Heide_1	76	x						3116	28,00	3465138	5861891
	Kat_2		Katenbäker Heide_2	76						x	3116	27,50	3463750	5861829
	Kat_3		Katenbäker Heide_3	76	x						3116	23,75	3463828	5861619
	Bec_1		Beckstedt_1	64	x						3116	26,25	3465108	5856118
	Col_3	37 b)	Colnrade_3	63	x	0-5 m		x	x		3116	30,00	3465160	5855663
	Ess_1	37 a)	Essemühle_1	48	x			x	x		3216	30,00	3464103	5848841
	Ess_2-4	38	Essemühle_2	48	x	0-38 m	0-9 m	x	x		3216	31,25	3464789	5848361
	Bro_1		Brocklage_1	44	x						3216	30,00	3464310	5847208
	Hol_1		Holzort_1	26							3317	30,00	3468122	5840236
	Hel_1		Helmsmühle_1	23						x	3317	32,50	3467647	5839134
	Dan_1		Danhollen_1		x						3317	33,75	3469187	5835625

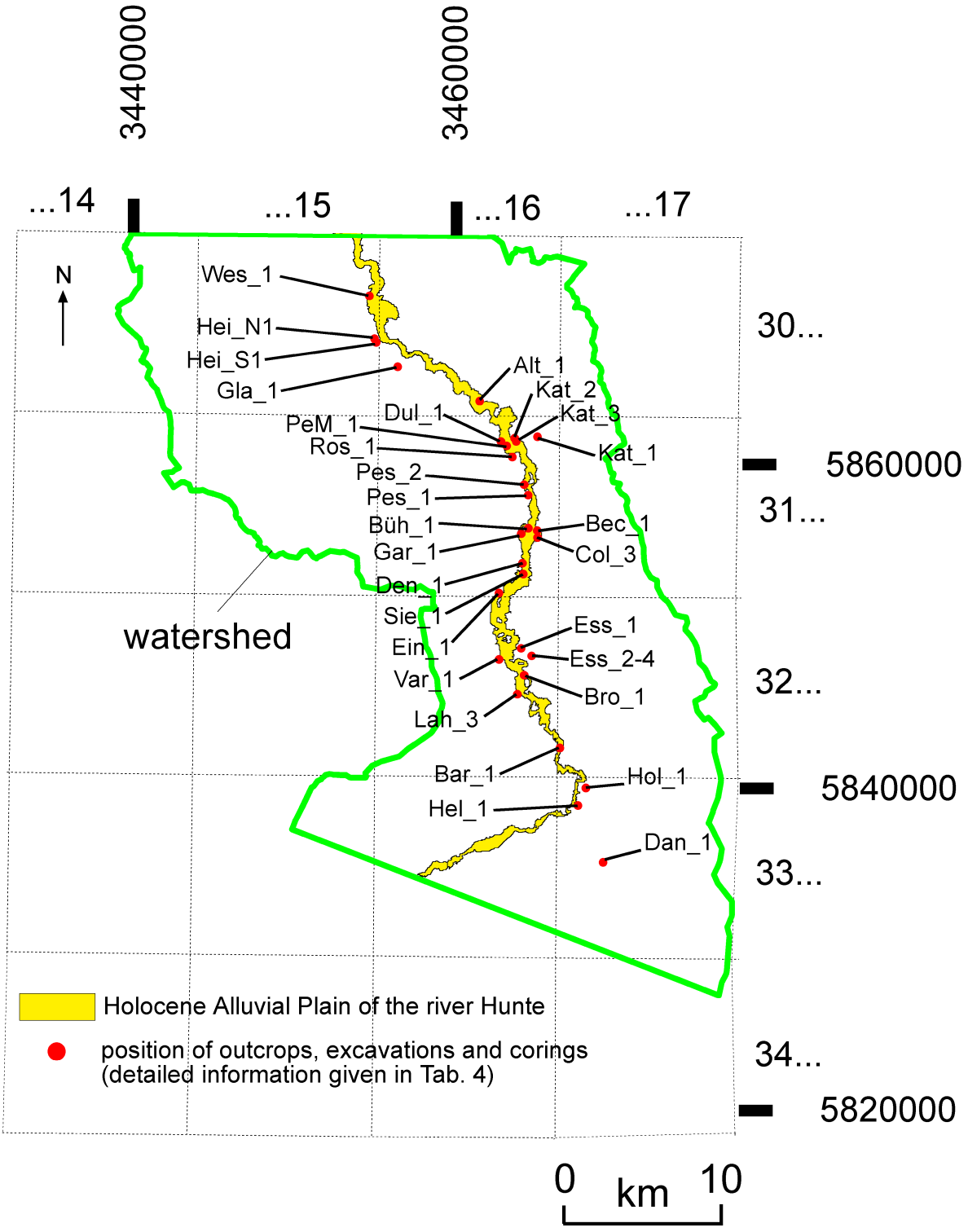

Fig. 12: Position of outcrops, excavations and corings (red point with acronym of locations). Detailed information about the locations is given in Tab. 4.

C) Results

C.1. Spatial connection between geological structures and the modern landscape

1.1. Catchment basin of the river Hunte

Two different tectonic blocks are crossed by the river Hunte (the Lower Saxony Basin and the more stable Pompeckj Block), (Fig. 1). Morphological features within the Hunte catchment basin in respect to the geological subsurface are described in following.

1.1.1. Correlations between the depth of the geological subsurface and the height of the Holocene Alluvial Plain/Lower Weichselian Terrace

Linear correlation coefficients between the geological underground and the morphology of the Holocene Alluvial Plain/Lower Weichselian Terrace for the Hunte catchment basin have been calculated (Fig. 6). This was done to investigate the depth/height relationship between the geological subground and the modern river. The Holocene Alluvial Plain of the river Hunte was cut into 177 segments of nearly equal length ~500 m. The mean depth of the geological subsurface was calculated for each of the 177 segments by the GIS from the Spatial Geological Models constructed from the Geotectonic Atlas of NW-Germany (Baldschuhn et al., 1996). The data were used for the construction of a longitudinal profile by plotting the depth of the geological strata against the segment numbers. The resulting longitudinal profile is shown in Fig. 13 c. Linear correlation coefficients were calculated between the different depth data and are summarized in Tab. 5. Not all of the fourteen geological layers available from the Geotectonic Atlas of NW-Germany (Baldschuhn et al., 1996) were used for the calculation of the linear correlation coefficients, because outcrops cover wide areas of the Base Middle Jurassic, Base Upper Jurassic and the Base Lower Miocene to Pliocene (Appendix, Fig. 3, 9, 10). Thus, no depth information is available from those outcrop parts. Consequently, those three layers were not taken into account for this study. Linear correlation coefficients between the remaining eleven layers of the geological subsurface are shown in the blue coloured cells „A-N“ (Tab. 5). Linear correlation coefficients calculated between the depth at the Base of Quaternary and the depth of the geological subsurface are shown in the green cells “O” (Tab. 5). Linear correlation coefficients calculated between the height of the Holocene Alluvial Plain and the depth of the geological subsurface are shown in the yellow cells “P” (Tab. 5). Correlation coefficients of ≥0,60 are given in red. The mean linear correlation coefficient for the whole blue field (cells A to N) is 0,74 (Tab. 5). Adjacent geological units are connected by a dashed line. The mean linear correlation coefficient for the adjacent geological units is 0,92, showing that the structural situation from the deeper geological basement up to the shallower strata is very similar. A linear correlation coefficient of 0,95 is visible between the height of the Holocene Alluvial Plain and the depth at the Base of Tertiary (Tab. 5, cell JP, black arrow). Fig. 14 c shows the corresponding XY-plot.

The green column “O” (Tab. 5) shows the linear correlation coefficients between the Base of Quaternary and the depth of the geological subsurface. All linear correlation coefficients are below 0,35. Consequently, there is no significant correlation between the depth of the Base Quaternary and the geological subsurface. The reason for these low correlation coefficients is the post-depositional erosion of the Elsterian glacial channels into the top of Tertiary (Fig. 13 b, black arrows). These glacial channels have cut up to a depth of –200 m a.s.l. into the subground. Thus, the top of the Tertiary sediments is controlled by the incision of the Elsterian glacial channels. Sediments of deeper than –200 m a.s.l. are unaffected by this glacial erosion because these are the deepest

detectable Elsterian subglacial channels in the study area (Appendix, Fig. 1: Base of Quaternary). This fact applies only to the this particular research area. Glacial channels more than 400 m in depth have been described (Kuster and Meyer, 1979; Ortlam and Vierhuff, 1978). A glacial erosion influence for the Base of Tertiary could therefore be excluded for the study area. The linear correlation coefficients are clearly below 0,6 between the height of the Holocene Alluvial Plain and the depth at the Base Upper Buntsandstein (Tab. 5, cell "CP", r^2= 0,48), the Base Keuper (Tab. 5, cell "DP", r^2=0,41) and the Base Lower Jurassic (Tab. 5, cell "EP", r^2=0,15). However, there is a higher linear correlation coefficient of 0,78 between the depth at the Base Zechstein and the height of the Holocene Alluvial Plain (Tab. 5, cell "AP") and a linear correlation coefficient of 0,66 between the depth at the Base of Lower and Middle Buntsandstein (Tab. 5, cell "BP"). Consequently, there is a high correlation between the deepest geological basement (Base Zechstein and Base Lower and Middle Buntsandstein), the uppermost geological strata (the depth of the entire Tertiary) and the modern landscape (height of the Holocene Alluvial Plain). It is evident by Fig. 14 b that the linear correlation between the height of the Lower Weichselian Terrace and the depth at the Base of Tertiary is 0,95. An explanation for these correlations will be discussed in Chapter D.1..

1.1.2. Correlations between the depth of the geological subsurface and the height of the catchment basin topography

The investigated Hunte catchment basin was cut into 35 segments. The position of the segments is shown in Fig. 6 (segment number 1 is given by the area between segment line1-5, number 2 by the area between segment line 5-10 ..., segment number 35 by the area between segment line 170-175). The mean depth of the geological subsurface and the mean topographical height was calculated for each of the 35 segments by the method already described in Chapter C. 1.1.1.. Linear correlation coefficients have been calculated based on the depth/height data (Tab. 6). Similarities and differences between Tab. 6 and 5 will be dealt with. There is the same high mean linear correlation coefficient (r^2=0,93) between adjacent geological units as shown for the segments of the Holocene Alluvial Plain (Tab. 5, r^2=0,92), indicating that the structural situation from the deeper geological basement up to the shallower strata is very similar. There are high linear correlation coefficients between the depth at the Base of Quaternary and the depth of Tertiary (Tab. 6, cell "JO", r^2=0,63; cell "KO", r^2=0,86; cell "LO", r^2=0,92; cell "NO", r^2=0,92) and the height of the modern catchment basin topography (Tab. 6, cell "OP", r^2=0,84, black arrow). This high linear correlation coefficient is not shown between the height of the Holocene Alluvial Plain and the Base of Quaternary (Tab. 5, cell "OP", r^2=0,33). The reason for this can be found in the size of the catchment basin segments. The area of these segments is much bigger than the Holocene Alluvial Plain segments; consequently, local changes of the Base Quaternary induced by Elsterian subglacial channel erosion are minimized by averaging. There are high linear correlation coefficients between the height of the catchment basin topography, the depth at the Base Zechstein (Tab. 6, cell "AP", r^2=0,67) and the depth at the Base Lower and Middle Buntsandstein (Tab. 6, cell "BP", r^2=0,69) and the depth of the Tertiary (Tab. 6, cell "JP" r^2=0,87, cell "KP" r^2=0,95, cell "LP" r^2=0,97, cell "NP" r^2=0,95). The XY-plot of Fig. 14 a shows that the correlation between the depth at the Base of Tertiary and the height of the catchment basin topography is r^2=0,87. Thus, the modern topography is clearly related to the morphology of the deep geological structures.

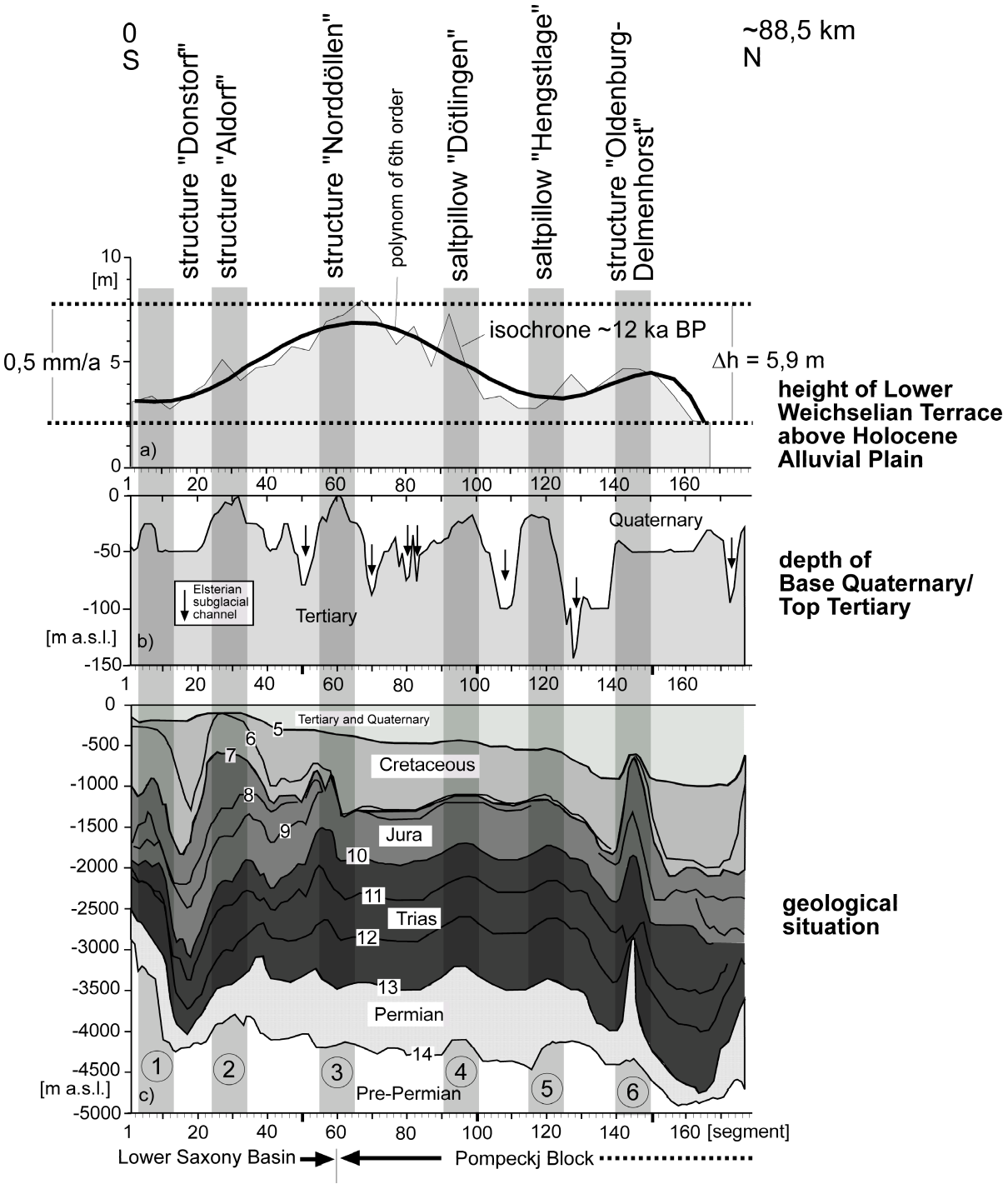

Fig. 13: Longitudinal profile for a part of the river Hunte from south to north with
a) height position of the Lower Weichselian Terrace above the Holocene Alluvial Plain in [m], after historical and modern topographical maps (LGN, 1898; LGN, 1994).
b) depth at the Base of Quaternary in [m a.s.l.], the black arrows show the position of Elsterian tunnel valleys, after Quaternary Geological Map (NLfB, 1993),
c) geological situation, depth at the Base of Zechstein (number 14) to the Base of Tertiary (number 5), after Geotectonic Atlas of NW-Germany (Baldschuhn et al., 1996). The depth at the Base of Tertiary is based on a 3D-seismic data contour map between segment 58-129 and 158-177 (BEB, 2002).
Gray markers 1 to 6 show the position of anticlines crossed by the river Hunte with the names of the geological structures (names are given in Fig. 4).

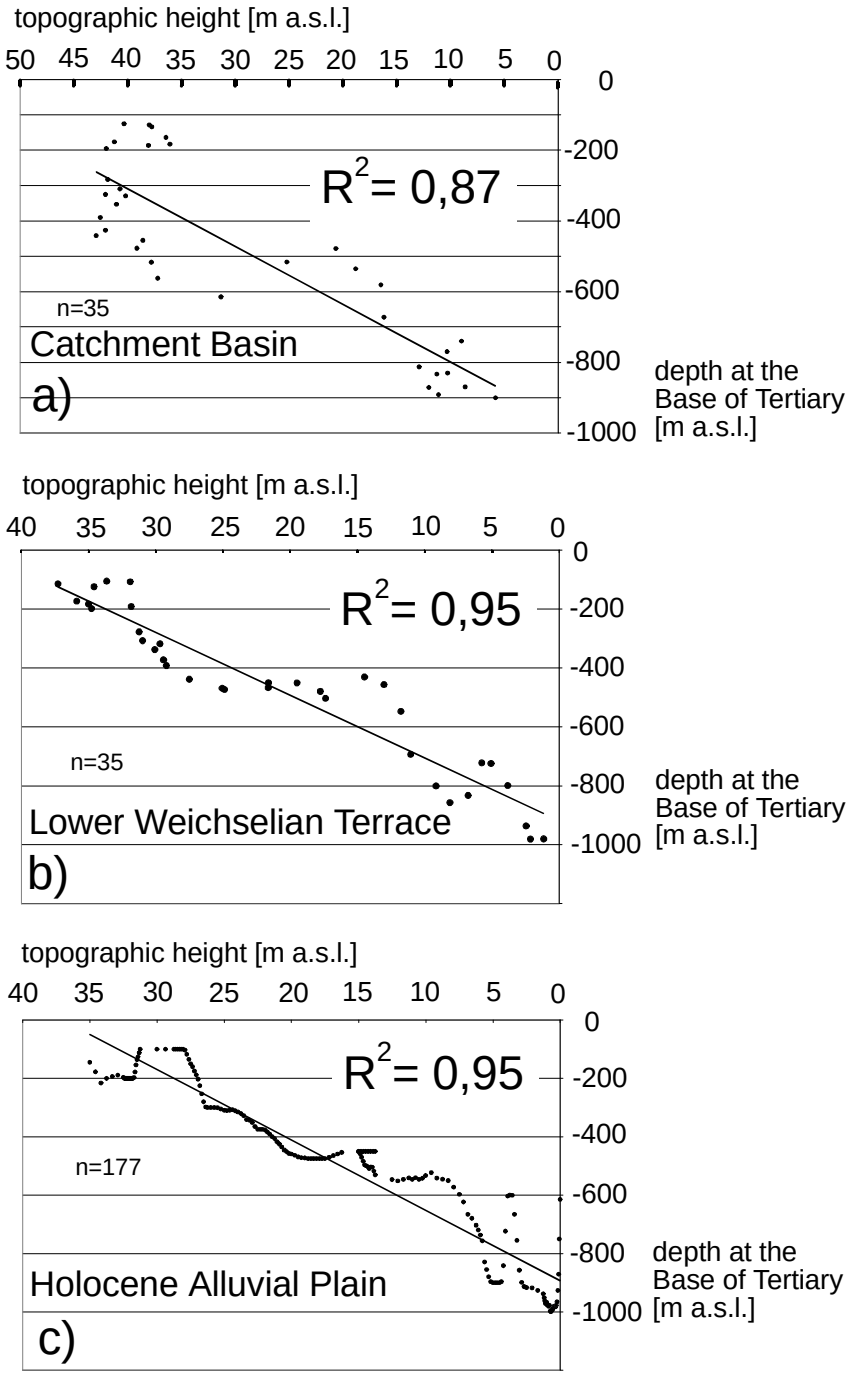

Fig. 14: XY-plots for a part of the river Hunte catchment basin. Depth at the Base of Tertiary against the topographic height of a) the catchment basin, b) the Lower Weichselian Terrace and c) the Holocene Alluvial Plain. Regression line and linear correlation coefficient are presented for all diagrams. The geographical position of the investigated catchment basin is shown in Fig. 6. For more explanation see Chapter C. 1.1.1.. After historical and modern topographical maps (LGN, 1898; LGN, 1994), Tectonic Atlas of NW-Germany (Baldschuhn et al., 1996) and 3D Seismic contour map of Base Tertiary (BEB, 2002).

Tab. 5: Linear correlation coefficients calculated between the height of the Holocene Alluvial Plain and the geological subsurface. The geographical position of the investigated area is shown in Fig. 6.. The blue field (cells “A-N”) after Geotectonic Atlas of NW-Germany (Baldschuhn et al., 1996) and 3D Seismic contour map of the Base Tertiary (BEB, 2002). The green field Base of Quaternary (cells “O”) after the Map of Base Quaternary for Lower Saxony (NLfB, 1993). The yellow field Holocene Alluvial Plain (cell “P”) after modern and historical topographical maps (LGN, 1898; LGN, 1994). For detailed explanation see Chapter C. 1.1.1..

		A	B	C	D	E	F	G	H	I	J	K	L	M	N	O	P
		Base Zechstein	B. L. + Middle Buntsandstein	B. U. Buntsandstein+Muschelk.	Base Keuper	B. L. Jurassic	Base Middle Jurassic*	Base Upper Jurassic*	Base marine Lower Cretaceous	Base Upper Cretaceous	Base Tertiary	B. M. Eocene to Lower Oligo.	B. M. Oligocene to Upper Oligo.	B. Lower Miocene to Pliocene	B. Middle Miocene to Pliocene	Base of Quaternary	Holocene Alluvial Plain
A	Base Zechstein		0,85	0,75	0,65	0,43			0,69	0,79	0,78	0,77	0,69		0,61	0,19	0,78
B	B. L. + Middle Buntsandstein			0,96	0,90	0,78			0,76	0,70	0,75	0,85	0,79		0,74	0,16	0,66
C	B. U. Buntsandstein+Muschelkalk				0,94	0,88			0,70	0,57	0,58	0,78	0,72		0,68	0,09	0,48
D	Base Keuper					0,93			0,72	0,52	0,53	0,74	0,72		0,71	0,05	0,41
E	Base Lower Jurassic								0,64	0,36	0,30	0,63	0,68		0,69	0,06	0,15
F	Base Middle Jurassic*																
G	Base Upper Jurassic*																
H	Base marine Lower Cretaceous									0,86	0,76	0,69	0,68		0,68	0,34	0,61
I	Base Upper Cretaceous										0,85	0,76	0,67		0,64	0,33	0,73
J	Base Tertiary											0,97	0,93		0,90	0,38	0,95
K	B. M. Eocene to Lower Oligocene												0,96		0,94	0,23	0,92
L	B. M. Oligocene to Upper Oligocene														0,97	0,33	0,92
M	Base Lower Miocene to Pliocene																
N	Base Middle Miocene to Pliocene															0,34	0,91
O	Base of Quaternary																0,33
P	Holocene Alluvial Plain																

mean of blue field (A-N) = 0,74 — *Base Upper Jurassic and *Base Middle Jurassic not shown, for explanation see Chapter C.1.1.1.

mean of adjacent geological units (dashed line) = 0,92 — red numbers = linear correlation coefficient >=0,6

blue field (cells "A-N") after Baldschuhn et al. (1996) and BEB (2000)

green field, cell "O", (Base of Quaternary) after (NLfB, 1993)

yellow field, cell "P", (Modern Holocene Alluvial Plain), after LGN (1898 and 1994)

Tab. 6: Linear correlation coefficients calculated between the modern topography and the geological subsurface for segments of the Hunte catchment basin. The geographical position of the investigated area is shown in Fig. 6.. The blue field (cells “A-N”) after Geotectonic Atlas of NW-Germany (Baldschuhn et al., 1996) and 3D Seismic contour map of the Base Tertiary (BEB, 2002). The green field Base of Quaternary (cells “O”) after the Map of Base Quaternary for Lower Saxony (NLfB, 1993). The yellow field Holocene Alluvial Plain (cells “P”) after modern and historical topographical maps (LGN, 1898; LGN, 1994). For detailed explanation see Chapter C. 1.1.2..

		A	B	C	D	E	F	G	H	I	J	K	L	M	N	O	P
		Base Zechstein	B. L. + Middle Buntsandstein	B. U. Buntsandstein+Muschelk.	Base Keuper	B. L. Jurassic	Base Middle Jurassic*	Base Upper Jurassic*	Base marine Lower Cretaceous	Base Upper Cretaceous	Base Tertiary	B. M. Eocene to Lower Oligo.	B. M. Oligocene to Upper Oligo.	B. Lower Miocene to Pliocene	B. Middle Miocene to Pliocene	Base of Quaternary	Modern Topography
A	Base Zechstein		0,94	0,87	0,76	0,56			0,79	0,66	0,75	0,73	0,63		0,62	0,34	0,67
B	B. L. + Middle Buntsandstein			0,97	0,92	0,77			0,79	0,51	0,71	0,76	0,63		0,60	0,39	0,69
C	B. U. Buntsandstein+Muschelkalk				0,96	0,87			0,72	0,34	0,55	0,68	0,54		0,51	0,30	0,58
D	Base Keuper					0,93			0,63	0,25	0,49	0,71	0,56		0,53	0,35	0,57
E	Base Lower Jurassic								0,51	0,08	0,25	0,66	0,51		0,48	0,26	0,39
F	Base Middle Jurassic*																
G	Base Upper Jurassic*																
H	Base marine Lower Cretaceous									0,84	0,76	0,59	0,46		0,47	0,33	0,58
I	Base Upper Cretaceous										0,85	0,63	0,53		0,55	0,34	0,56
J	Base Tertiary											0,97	0,91		0,91	0,83	0,87
K	B. M. Eocene to Lower Oligocene												0,96		0,95	0,86	0,95
L	B. M. Oligocene to Upper Oligocene														0,99	0,92	0,97
M	Base Lower Miocene to Pliocene																
N	Base Middle Miocene to Pliocene															0,92	0,95
O	Base of Quaternary																0,84
P	Modern Topography																

mean of blue field (A-N) = 0,67 — *Base Upper Jurassic and *Base Middle Jurassic not shown, for expl. see Chap. C.1.1.1.

mean of adjacent geological units (dashed line) = 0,93 — red numbers = linear correlation coefficient >=0,6

blue field (cells "A-N") after Baldschuhn et al. (1996) and BEB (2000)

green field, cell "O", (Base of Quaternary) after (NLfB, 1993)

yellow field, cell "P", (Modern Holocene Alluvial Plain), after LGN (1898 and 1994)

Summary of Chapter 1.1.1. and 1.1.2.

The high linear correlation coefficients between the different layer of the geological strata indicate a very similar tectonic style of the basin geometry from the deeper basement up to the higher strata (Tab. 5+6). The high linear correlation coefficients between the height of the modern topography (catchment basin, Lower Weichselian Terrace and Holocene Alluvial Plain) and the geological basement indicate a control of the modern topography by the depth of the geological subsurface.

1.1.3. Correlations between the depth of basement blocks and the height of topography

Fig. 15 shows the pattern of basement blocks for a part of the river Hunte catchment basin. Eight basement blocks are signed with the letters B, C, D, E, F, G, H, I, shown also in Fig. 3. Basement blocks C and D were combined to a single block. The mean topographical height for these seven blocks was determined with the GIS. The resulting mean heights are given in m a.s.l.. The gray tones of the individual blocks correspond to the mean topographic from white (E)=43,4 m to black (B)=8,2 m (Fig. 15). The basement block **E (Bockstedt Graben Lessen-Staffhorst-Block)** shows the highest average topographical height of 43,4 m. This block is 5,4 m higher than the southerly positioned Oythe-Düste-Wehrbleck-Block (F) and 14,5 m higher than the northerly adjacent Südoldenburg Block (C, D). Basement block E separates the Lower Saxony Basin in the south from the northerly adjacent Pompeckj Block. Fig. 16 a-h shows XY-plots between the average topographical height of the basement blocks and the average depth of the geological basement. The highest correlation of r^2=0,92 is visible between the topography and the depth at the Base of Tertiary (Fig. 16 a). The lowest correlation of r^2=0,55 is presented by the Base of Lower Jurassic (Fig. 16 d). All linear correlation coefficients for the Basin deepest parts are higher than r^2=0,72 (between the Base of Keuper [Fig. 16 e] and the Base of Zechstein [Fig. 16 h]). The Base of Lower and Middle Buntsandstein (Fig. 16 g) shows with r^2=0,81 the highest linear correlation coefficient.

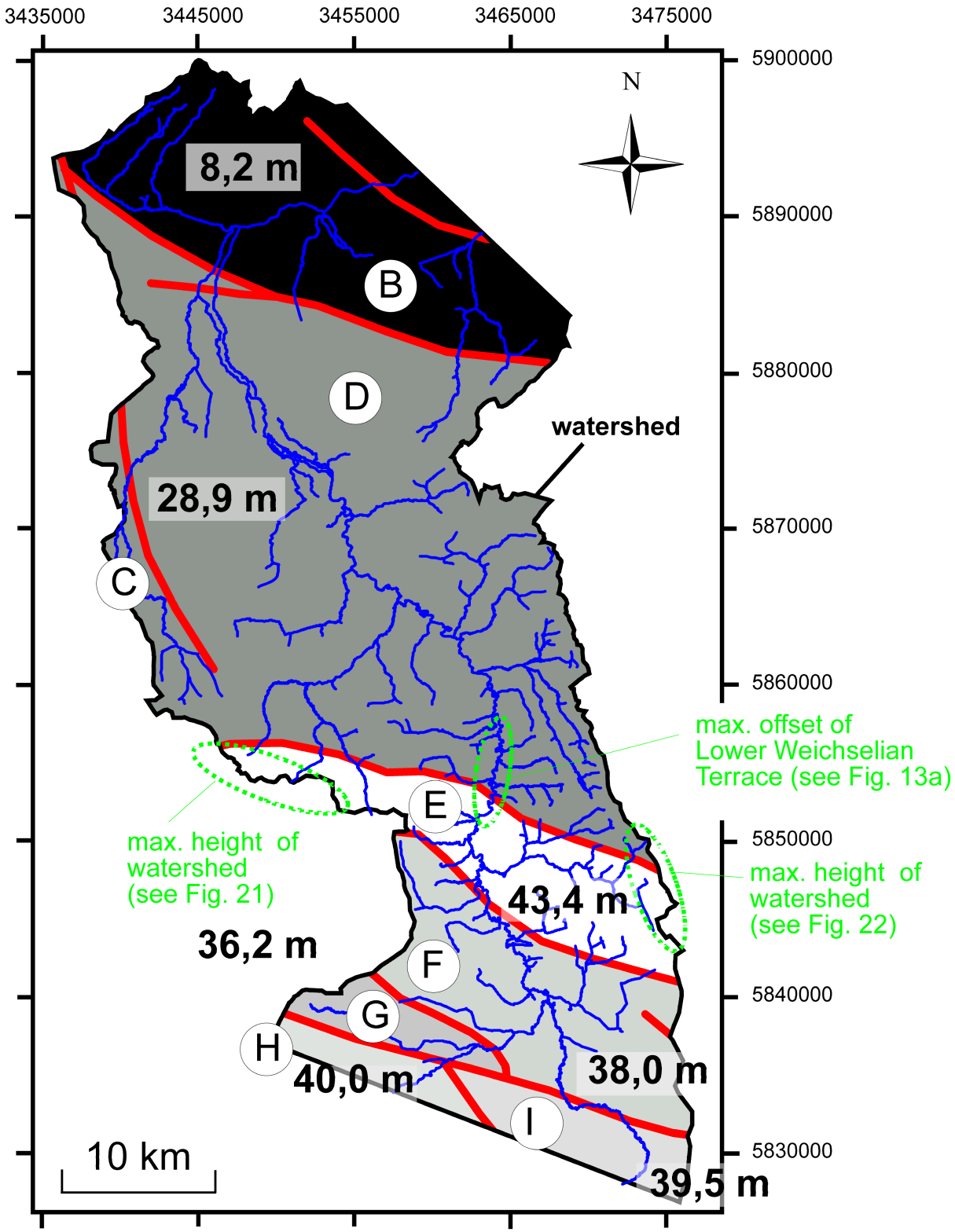

Fig. 15: Pattern of basement blocks for the investigated part of the river Hunte catchment basin, after Tectonic Atlas of NW-Germany (Baldschuhn et al., 2001). The letters (B) to (I) indicate the names of the basement blocks. The names are given in Fig. 3. The fluvial system is shown in blue, after historical topographical map (LGN, 1898).

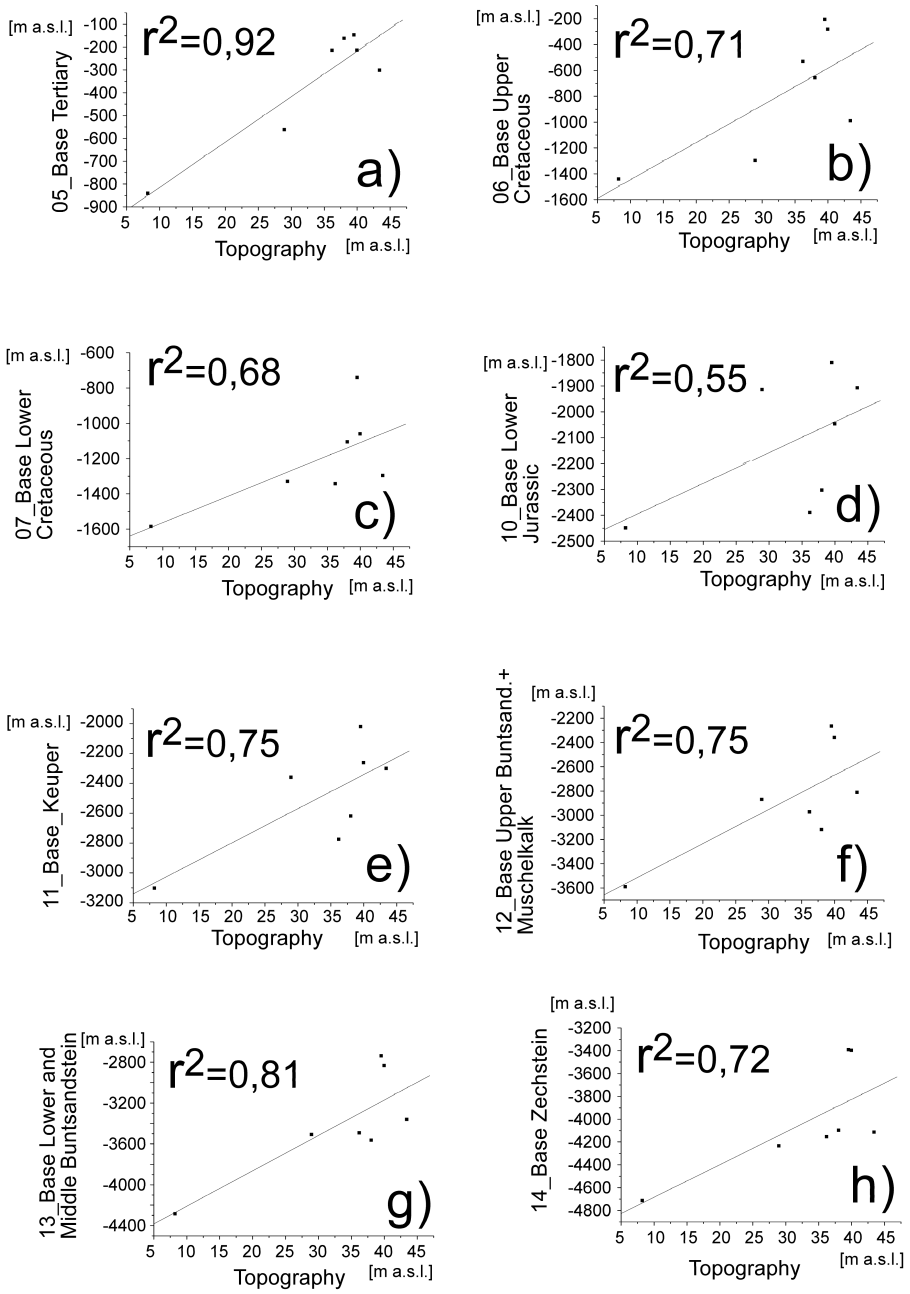

Fig. 16: XY-plots. Mean topographical height of basement blocks (Fig. 15) against the a) Base of Tertiary, b) Base Upper Cretaceous, c) Base Lower Cretaceous, d) Base Lower Jurassic, e) Base Keuper, f) Base Upper Bundsandstein + Muschelkalk, g) Base Lower and Middle Buntsandstein and h) Base Zechstein (Permian) with regression lines and linear correlation coefficients (r^2).

Summary of Chapter 1.1.3.

The basement block “Bockstedt Graben Lessen-Staffhorst-Block” (Fig. 3+15, letter E) which separates the Lower Saxony Basin in the south from the northerly adjacent Pompeckj Block shows the highest topographical elevation of all investigated basement blocks. There are high linear correlations between topography and the depth of the geological basement for entire structural blocks. The highest correlation of 0,92 is visible between the Base of Tertiary and the topography (Fig. 16 a).

1.1.4. Correlations between the orientation of the modern landscape and the orientation of the Base of Tertiary

A direction analysis was carried out for a part of the river Hunte catchment basin (Fig. 7, red section of river Hunte catchment basin), between elements of the modern landscape (steep slopes, lakes and depressions, topography [10 m contour interval], fluvial system) and the Base of Tertiary. This part was chosen, because a contour map from the Base of Tertiary which is based on 3D-Seismic Data was available for this section (BEB, 2002). This study was only possible due to the high contour interval of 25 m. Rose diagrams (weighted by length [%] with a pedal width of five degrees) have been calculated (Fig. 17 a-e).

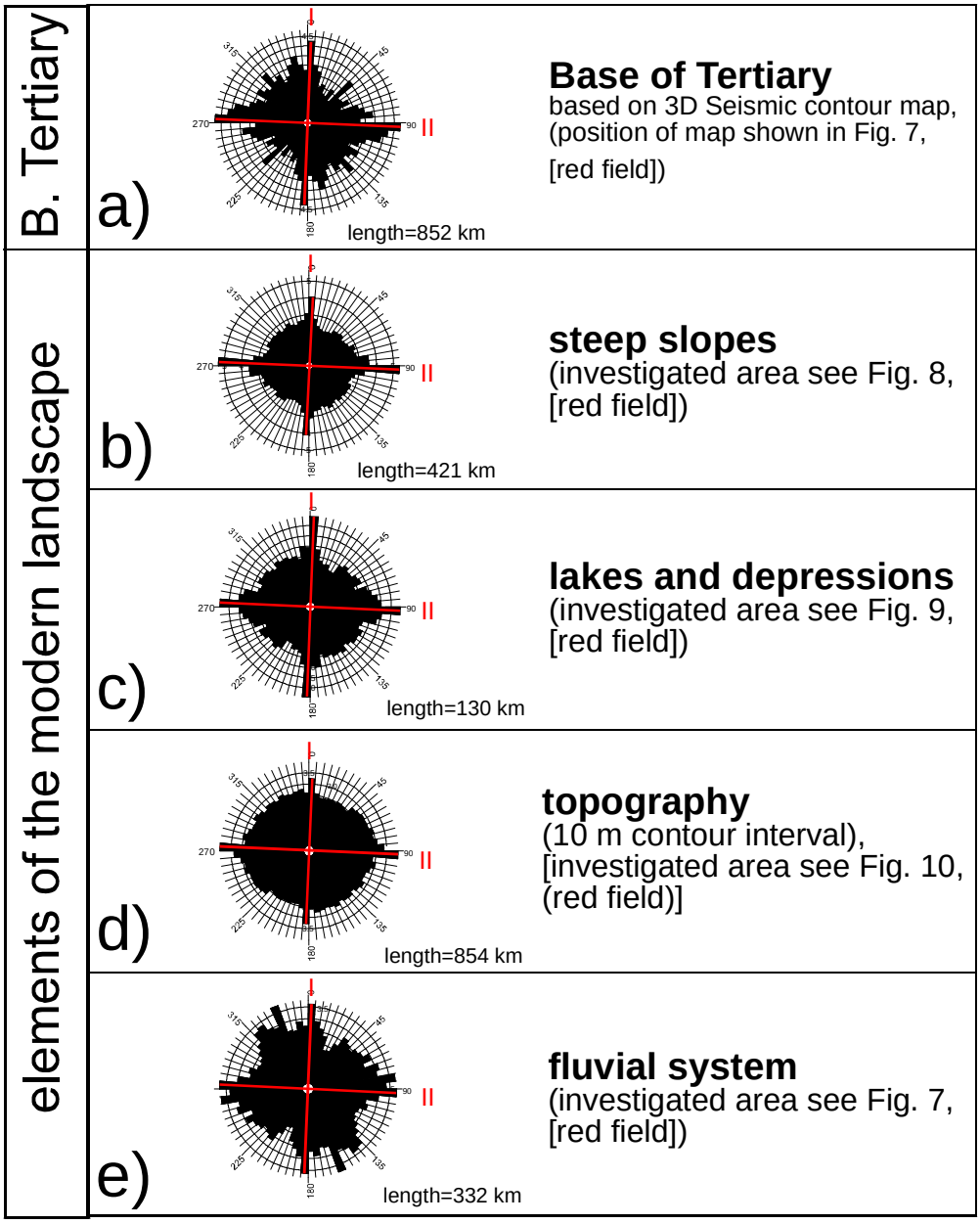

Fig. 17: Orientation analyses for a part of the river Hunte catchment basin (the position of investigated area is shown in Fig. 7, [red field]). All presented rose diagrams were plotted by length [%] with a pedal width of 5°, with orientation of the a) Base Tertiary contour lines, after 3D Seismic contour map (BEB, 2002), b) steep slopes, after historical topographical map (LGN, 1898), c) lakes and depressions, after historical and modern topographical map (LGN, 1898; LGN, 1994), d) topography, 10 m contour interval, after historical and modern topographical map (LGN, 1898; LGN, 1994) and e) fluvial system, after historical topographical map (LGN, 1898). The total vector length is given in [km] for each rose diagram.
The red cross shows the two directions common in all presented rose diagrams (I) 0-5° and (II) 90-95°.

Only „raw-data“ were used for the calculation of the rose diagrams. The contour lines have been directly vectorised from the Base of Tertiary map (BEB, 2002). The same data collection principle applied for the elements of the modern landscape (steep slopes, lakes and depressions, topography [10 m contourinterval], fluvial system). All morphological elements were directly vectorised from the topographical maps (LGN, 1898; LGN, 1994), (Fig. 7-10), therefore a “human interpretation factor” in the data collection can be excluded. The results of this study must be regarded as a reflection of the geology/morphology. Pronounced N-S (I = 0-5°) and E-W (II = 90-95°) peaks are visible in all data (Fig. 17 a-e), clearly separated from the background (marked by the red cross).

The rose diagrams were used for the calculation of linear correlation coefficients. For each rose diagram the percentages have been determined between 0°-180° (resulting in a total of 36 datapoints, by the chosen pedal width of 5°). XY-plots have been produced based on this data (Fig. 18 a-f).

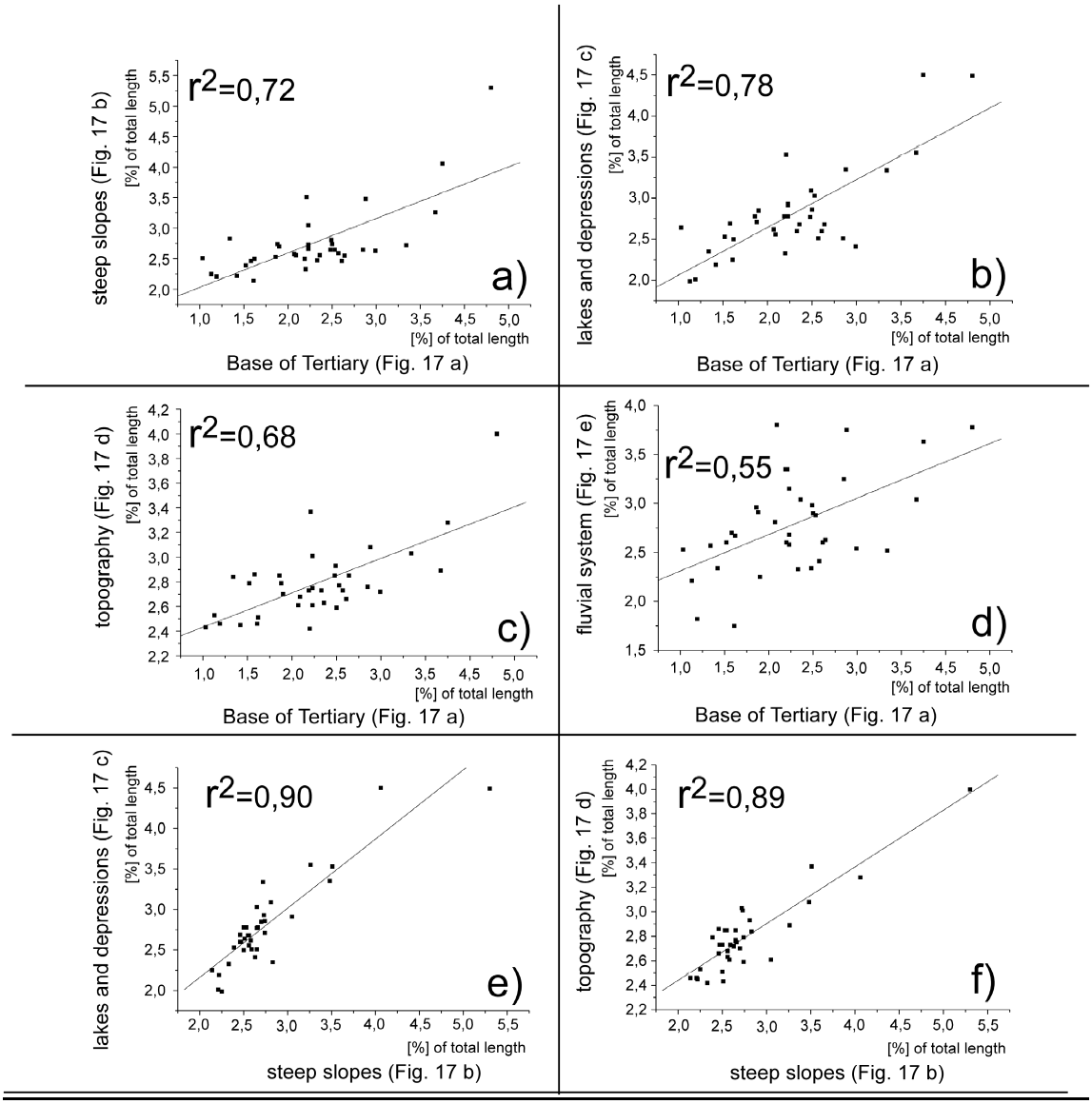

Fig. 18 a-f: XY-plots based on the rose diagrams shown in Fig. 17 a-e. The percentages for each pedal (0-5°, 5-10°,..., 175-180°) of the rose diagrams have been determined. Afterwards the pedal percentages have been used for the production of the XY-plots with Base of Tertiary [Fig. 17 a] against a) the steep slopes [Fig. 17 b], b) the lakes and depressions [Fig. 17 c], c) the topography [Fig. 17 d], d) the fluvial system [Fig. 17 e] and the e) steep slopes [Fig. 17 b] against the lakes and depressions [Fig. 17 c], f) steep slopes [Fig. 17 b] against the topography [Fig. 17 d]. The linear regression line and the linear correlation coefficient (r^2) is presented for all XY-plots.

The size of the linear correlation coefficients is therefore a direct measure of the similarity between both roses. Tab. 7 shows the summarized linear correlation coefficients.

Tab. 7: Linear correlation coefficients calculated between the orientation of Base Tertiary contour lines [blue field, cell A] and the orientation of elements of the modern landscape [yellow field, cells B-E], (steep slopes [cell B], lakes and depression [cell C], topography [cell D], fluvial system [cell E]). Database: rose diagrams shown in Fig. 17 a-e. For detailed explanation see Chapter C. 1.1.4..

		A	B	C	D	E
		Base of Tertiary	steep slopes	lakes + depressions	topography	fluvial system
A	Base of Tertiary		0,72	0,78	0,68	0,55
B	steep slopes			0,90	0,89	0,66
C	lakes + depressions				0,85	0,68
D	topography					0,63
E	fluvial system					
	red numbers =	linear correlation coefficient >=0,6				
	mean of morphological elements (yellow field)=	0,77				
	mean of Base Tertiary (blue field)=	0,68				
	Base of Tertiary after 3D Seismic contour map (BEB, 2002)					
	morphological elements after topo. maps (LGN, 1898 and 1994)					

The linear correlation coefficient between the Base of Tertiary and the steep slopes is r^2=0,72 (Tab. 7 cell AB; Fig. 18 a), for the lakes and depressions r^2=0,78 (Tab. 7 cell AC; Fig. 18 b), for the topography r^2=0,68 (Tab. 7 cell AD; Fig. 18 c) and for the fluvial system r^2=0,55 (Tab. 7 cell AE; Fig. 18 d). The mean linear correlation coefficient between the Base of Tertiary and the elements of the modern landscape is r^2=0,68. Consequently, there is a general connection between the basin geometry (orientation of the Base of Tertiary contour lines) and the orientation of the modern landscape, in particular the orientation of steep slopes along the rivers, the orientation of lakes and also closed depressions, independent of the fluvial system.

The highest linear correlation of r^2=0,90 is visible between the steep slopes and the lakes and depression (Tab. 7 cell BC, Fig. 18 e), followed by the steep slopes/topography of r^2=0,89 (Tab. 7 cell BD, Fig. 18 f), i.e. the orientation of morphological surface structures are also high connected (Tab. 7, r^2=0,77).

The whole study area was investigated in the same way as already shown before for the part of the Hunte catchment basin in order to analyse the orientation of the steep slopes, lakes and depressions, the topography and the fluvial system. In Fig. 19 the rose diagrams of the whole study area and the part of the Hunte catchment basin are compared with each other.

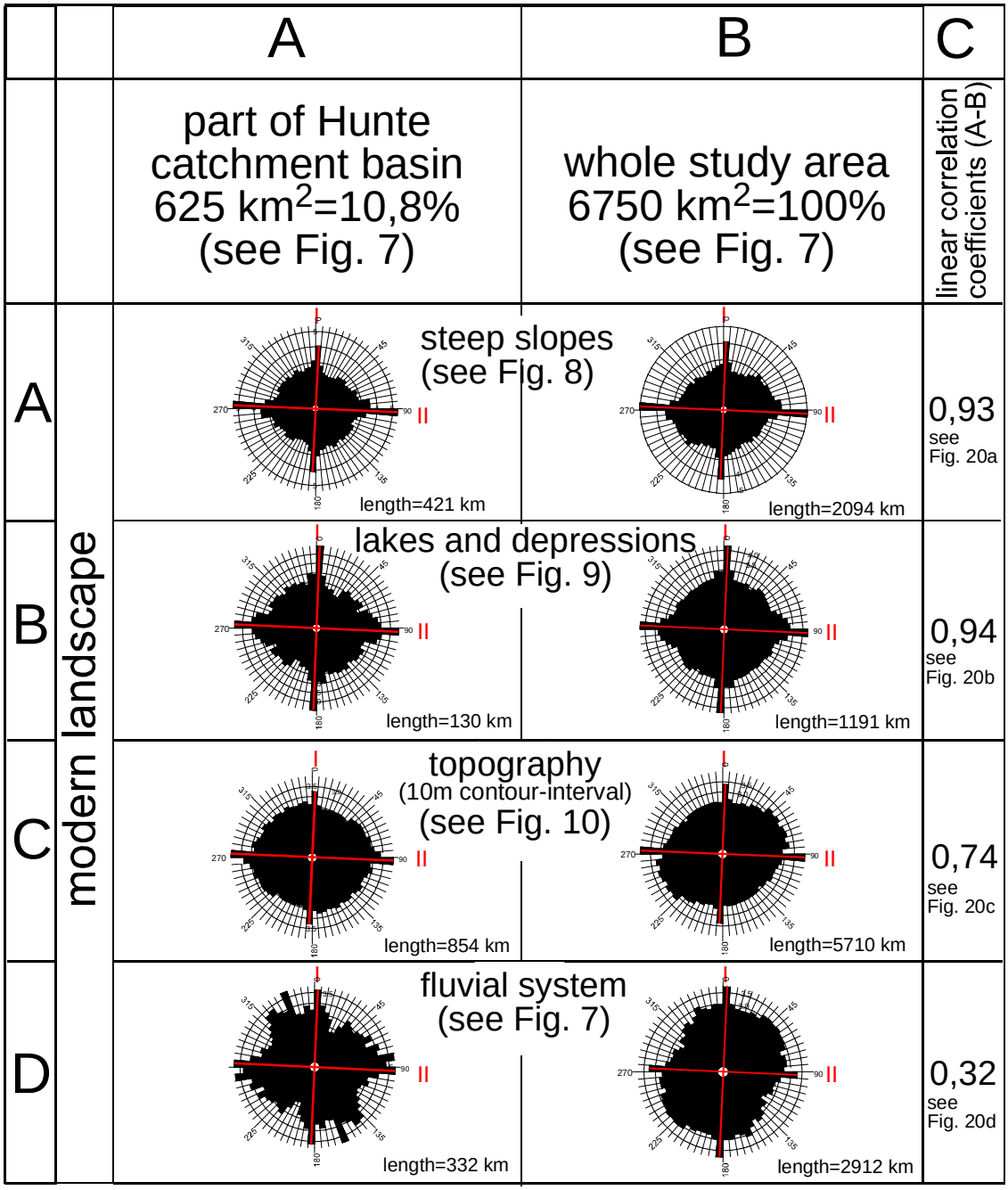

Fig. 19: Comparison between orientation analyses made on elements of the modern landscape for a part of the Hunte catchment basin (column A), (Fig. 7, [red field]) and the whole study area (column B), (Fig. 7, area of all 54 topographical maps). Rose diagrams were plotted by length [%] with a pedal width of 5°. Row (A) shows the rose diagrams for the steep slopes after the historical topographical maps (LGN, 1898), row (B) the lakes and depressions after the historical and modern topographical maps (LGN, 1898; LGN, 1994), row (C) the topography (10 m contour interval) after the historical and modern topographical maps (LGN, 1898; LGN, 1994) and row (D) the fluvial system after the historical topographical maps (LGN, 1898). The total vector length is given in [km] for each rose diagram. The red cross shows the 0-5° (I) and the 90-95° (II) direction, common in all rose diagrams. Linear correlation coefficients calculated between identical morphological elements are shown in column (C). The procedure for linear correlation coefficient calculation is explained in Chapter C.1.1.4.. The XY-plots are presented in Fig. 20.

The area of the whole study is, with 6750 km^2, about 10 times bigger than the part of the Hunte catchment basin with 625 km^2. Column A shows the rose diagrams for the part of the Hunte river and column B for the whole study area. Row A shows the rose diagrams for the steep slopes, row B for the lakes and depressions, row C for the topography (10 m contour interval) and row D for the fluvial system. Column C shows the calculated linear correlation coefficients between the two investigated areas. The corresponding XY-plots are shown in Fig. 20 a-d.

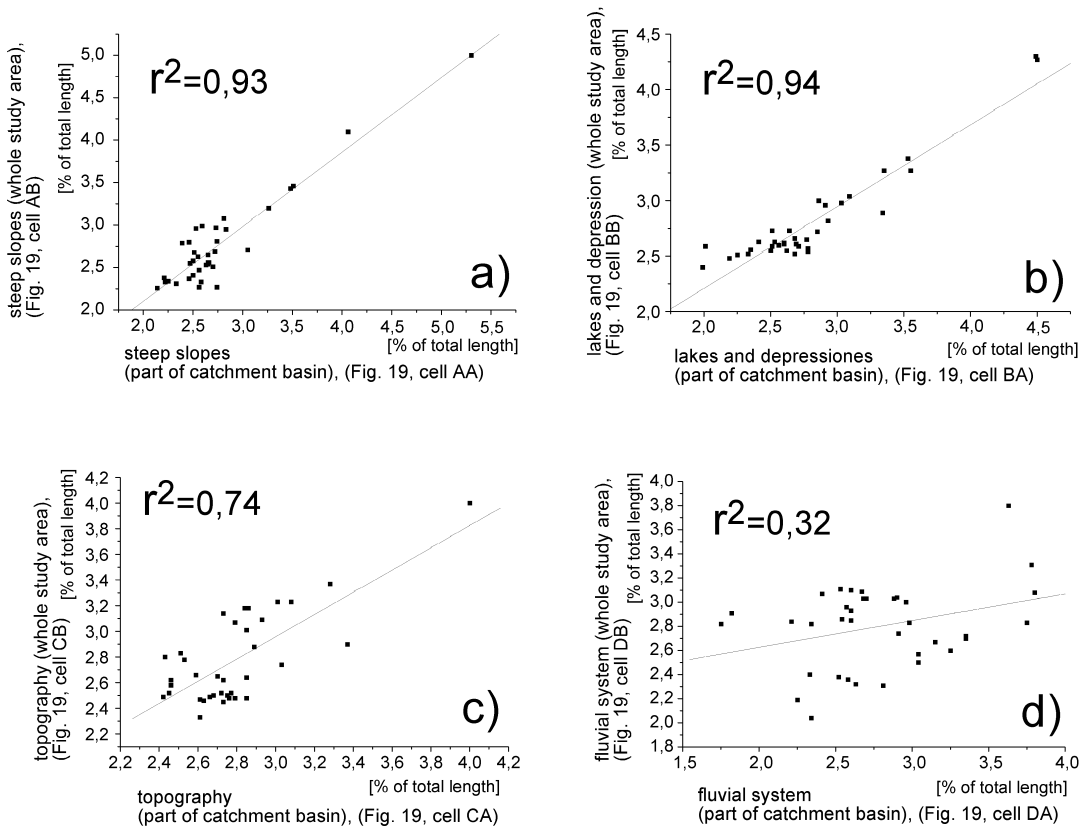

Fig. 20: XY-plots based on the rose diagrams shown in Fig. 19. The percentages for each pedal (0-5°, 5-10°,..., 175-180°) of the rose diagrams were determined. Afterwards the pedal percentages were used for the production of the XY-plots with a) steep slopes of Fig. 19, cell AA against the steep slopes of Fig. 19, cell AB, b) lakes and depressions of Fig. 19, cell BA against the lakes and depressions of Fig. 19, cell BB, c) topography (10 m contour interval) of Fig. 19, cell CA against the topography (10 m contour interval) of Fig. 19, cell CB, d) fluvial system of Fig. 19, cell DA against the fluvial system of Fig. 19, cell DB. The linear regression line and the linear correlation coefficient (r^2) is presented for all XY-plots.

The steep slopes show a linear correlation coefficient of r^2=0,93 (Fig. 19 cell AC, Fig. 20 a), the lakes and depressions of r^2=0,94 (Fig. 19 cell BC, Fig. 20 b), the topography of r^2=0,74 (Fig. 19 cell CC, Fig. 20 c) and the fluvial system of r^2=0,32 (Fig. 19 cell DC, Fig. 20 d). Consequently, the high linear correlation coefficients between morphological elements of the modern landscape is a general pattern and not only restricted to the local scale.

Summary of Chapter 1.1.4.

The iso-contour lines of the Base of Tertiary show two preferred orientations I=E-W (0-5°) and II=N-S (90-95°). The same preferred orientations can be found in the investigated elements of the modern landscape (steep slopes, lakes and depressions, topography and the fluvial system), (Fig. 17, Fig. 19; red cross inside rose diagrams). The orientation of the modern landscape correlates with the orientation at the Base of Tertiary basin geometry. Lakes and depressions show the highest correlation with the Base of Tertiary (Tab. 7 cell "AC" and Fig. 18 b). There is a high correlation between the orientation of the different elements of the modern landscape. The highest correlation can be found between the steep slopes and the lakes and depressions (Tab. 7 cell "BC" and Fig. 18 e) whereas lakes and depressions are independent of the fluvial system. There is a high correlation between spatial different investigated areas regarding the orientation of morphological elements of the modern landscape (Fig. 19, Fig. 20).

1.1.5. Watershed of the river Hunte

Topographical- and geological profiles have been constructed for the west and eastside of the watershed (Fig. 21 a, b and Fig. 22 a, b). The geographical position of the watershed profiles are shown in Fig. 4 (profile AB, Fig. 21 and profile CD, Fig. 22).

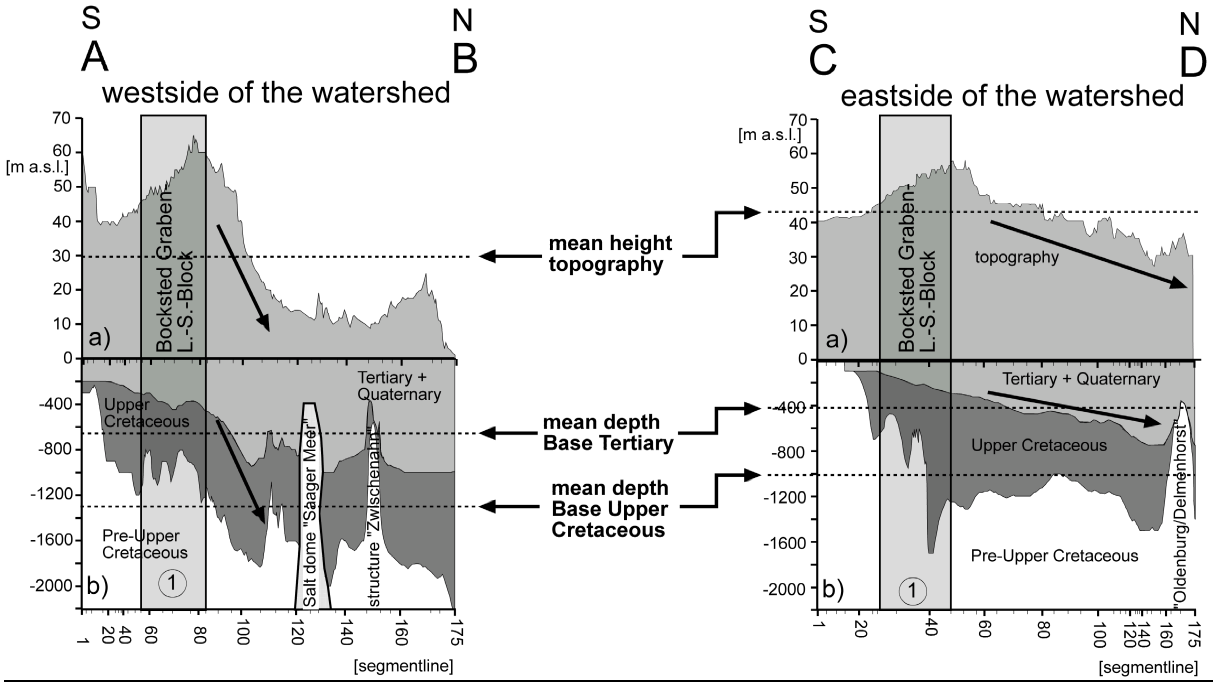

Fig. 21 (left): Longitudinal profile (AB) for the westside watershed of the river Hunte from south to north with a) topography, based on historical and topographical maps (LGN, 1898; LGN, 1994), b) depth at the Base of Tertiary and the Base Upper Cretaceous after Geotectonic Atlas of NW-Germany (Baldschuhn et al., 1996) and 3D Seismic contour map of the Base Tertiary (BEB, 2002). Gray marker 1 shows the position of the Bockstedt Graben Lessen-Staffhorst-Block. The geographical position of this Block is given in Fig. 3, letter E. The geographical position of the profile is presented in Fig. 4.

Fig. 22 (right): Longitudinal profile (CD) for the eastside watershed of the river Hunte from south to north with a) topography, based on historical and topographical maps (LGN, 1898; LGN, 1994), b) depth at the Base of Tertiary and the Base Upper Cretaceous after Geotectonic Atlas of NW-Germany (Baldschuhn et al., 1996) and 3D Seismic contour map of the Base Tertiary (BEB, 2002). Gray marker 1 shows the position of the Bockstedt Graben Lessen-Staffhorst-Block. The geographical position of this Block is given in Fig. 3, letter E. The geographical position of the profile is presented in Fig. 4.

1.1.5.1. Correlations between the depth of the geological subsurface and the watershed topography

Linear correlation coefficients have been calculated between the westside watershed topography and the depth of the geological subground (Base Tertiary and the Base of Upper Cretaceous). The profile for the westward watershed is shown in Fig. 21 a, b. The calculated linear correlation coefficients are summarized in Tab. 8. The linear correlation coefficient between the topography and the depth at the Base Tertiary is 0,71 (Tab. 8, cell “AB”), between the depth at the Base Tertiary and the depth at the depth at the Base of Upper Cretaceous 0,91 (Tab. 8 cell “BC”) and between the depth at the Base of Upper Cretaceous and the topography 0,63 (Tab. 8 cell “AC”). Consequently, there is a positive correlation for the westside watershed between the depth of the geological subsurface and the topography.

The linear correlation coefficients for the eastside watershed are shown in Tab. 9. The profile is shown in Fig. 22 a, b. The linear correlation coefficient between the topography and the depth at the Base Tertiary is 0,74 (Tab. 9, cell “AB”), between the depth at the Base Tertiary and the depth at the depth at the Base of Upper Cretaceous 0,57 (Tab. 9, cell “BC”) and between the depth at the Base of Upper Cretaceous and the

topography –0,03 (Tab. 9, cell “AC”). Thus, there is no significant correlation between the topography and the depth at the Base of Upper Cretaceous, but between the depth at the Base of Tertiary and the depth at the Base of Upper Cretaceous.

The mean topographic height of the westside watershed is 29,90 m and 42,80 m for the eastside (Fig. 21 a, 22 a bold dashed line). Thus, the mean eastside topography is 13,00 m higher than the westside. The westside shows a mean depth at the Base of Tertiary of –640 m, the eastside of –410 m. Thus, the eastside Base of Tertiary is 230 m higher elevated than the westside. A similar picture is visible at the Base of Upper Cretaceous. Here, the westside shows a mean depth of –1350 m, the eastside of –1020 m. Consequently, the eastside watershed topography and geological subsurface is higher than that of the westside.

Tab. 8: Linear correlation coefficients calculated between the westside watershed topography [yellow field, cell A], the Base of Tertiary [blue field, cell B] and the Base of Upper Cretaceous [blue field, cell C]. After the longitudinal profile (AB) for the westside watershed of the river Hunte (Fig. 21). For detailed explanation see Chapter C. 1.1.5.1..

westside watershed

		A	B	C
		Topography	Base Tertiary	B. U. Cretaceous
A	Topography		0,71	0,63
B	Base Tertiary			0,91
C	B. U. Cretaceous			

Tab. 9: Linear correlation coefficients calculated between the eastside watershed topography [yellow field, cell A], the Base of Tertiary [blue field, cell B] and the Base of Upper Cretaceous [blue field, cell C]. After the longitudinal profile (CD) for the westside watershed of the river Hunte (Fig. 22). For detailed explanation see Chapter C. 1.1.5.1..

eastside watershed

		A	B	C
		Topography	Base Tertiary	B. U. Cretaceous
A	Topography		0,74	-0,03
B	Base Tertiary			0,57
C	B. U. Cretaceous			

Summary of Chapter 1.1.5.1.

There is a positive correlation between the depth at the Base of Tertiary and the watershed topography, visible for both sides (Tab. 8, Tab. 9) and an asymmetry between the east- and westside watershed, regarding the depth of the geological subsurface and the topographical height. The topography and the geological subsurface (Base of Upper Creatceous and Base of Tertiary) is higher elevated on the east than on the westside watershed (Fig. 21, Fig. 22).

1.1.6. Ratio of valley width to valley height (V-ratio)

A ratio of valley width to valley height (V-ratio) was calculated in order to show the development of the Hunte valley geometry by means of a longitudinal profile. The calculation of the V-ratio is based on topographic profiles through the Hunte valley (catchment basin)**.** These profiles have been constructed from the Digital Elevation Model of Fig. 5. The cross profiles are shown in Fig. 23, presented from the west to the eastside and are sorted from south (Fig. 23 j) to north (Fig. 23 a). The position of the profiles is given by the position of the segment lines, shown in Fig. 5 and Fig. 6 by the dashed lines through the river Hunte catchment basin and numbered from 1 in the south to 175 in the north. The determination of the V-ratio will be descibed exemplary on crossprofile Fig. 23 j. A triangle was constructed, which extends from the eastward watershed (A) to the westward watershed (B) and to the position of the river Hunte C (marked by the black arrow). The height of the Hunte valley was determined by the distance CD and the width of the Hunte by the distance A`B`. The V-ratio was calculated by dividing the distance A´B´ by the distance CD. The smaller the valley width and the higher the valley the lower the V-ratio and vice versa. The V-ratio was calculated for all 36 segment lines (1, 5, 10, ..., 175). Fig. 24 d shows all V-ratios in the form of longitudinal profiles from south to north. The dashed horizontal line shows the mean of 1381, the black curve the polynom of 6^{th} order, calculated for all V-ratios. V-ratios below the mean are visible between segment line 30-110. The river Hunte catchment basin is smallest at segment line 60 (Fig. 24 d, black arrow; Fig. 23 g, Fig. 5+6). This is exactly above the " Goldenstedt Blenhorst Lineament" (Fig. 3, lineament number 3). This lineament separates the Lower Saxony Basin in the south from the Pompeckj Block in the north (Fig. 24 f, gray marker 3). The highest V-ratio is visible above the Upper Cretaceous trough "Donstorf" at segment line 15, between gray marker 1 and gray marker 2, (see Fig. 4 for position of the Upper Cretaceous trough "Donstorf").

Summary of Chapter 1.1.6.

The analyses of the river Hunte Basin geometry by constructing ratios of valley width to valley height (V-ratios) show that the Hunte valley is smallest above the transition zone between two major tectonic blocks (Lower Saxony Basin - Pompeckj Block), (Fig. 23 g+24 d, black arrow).

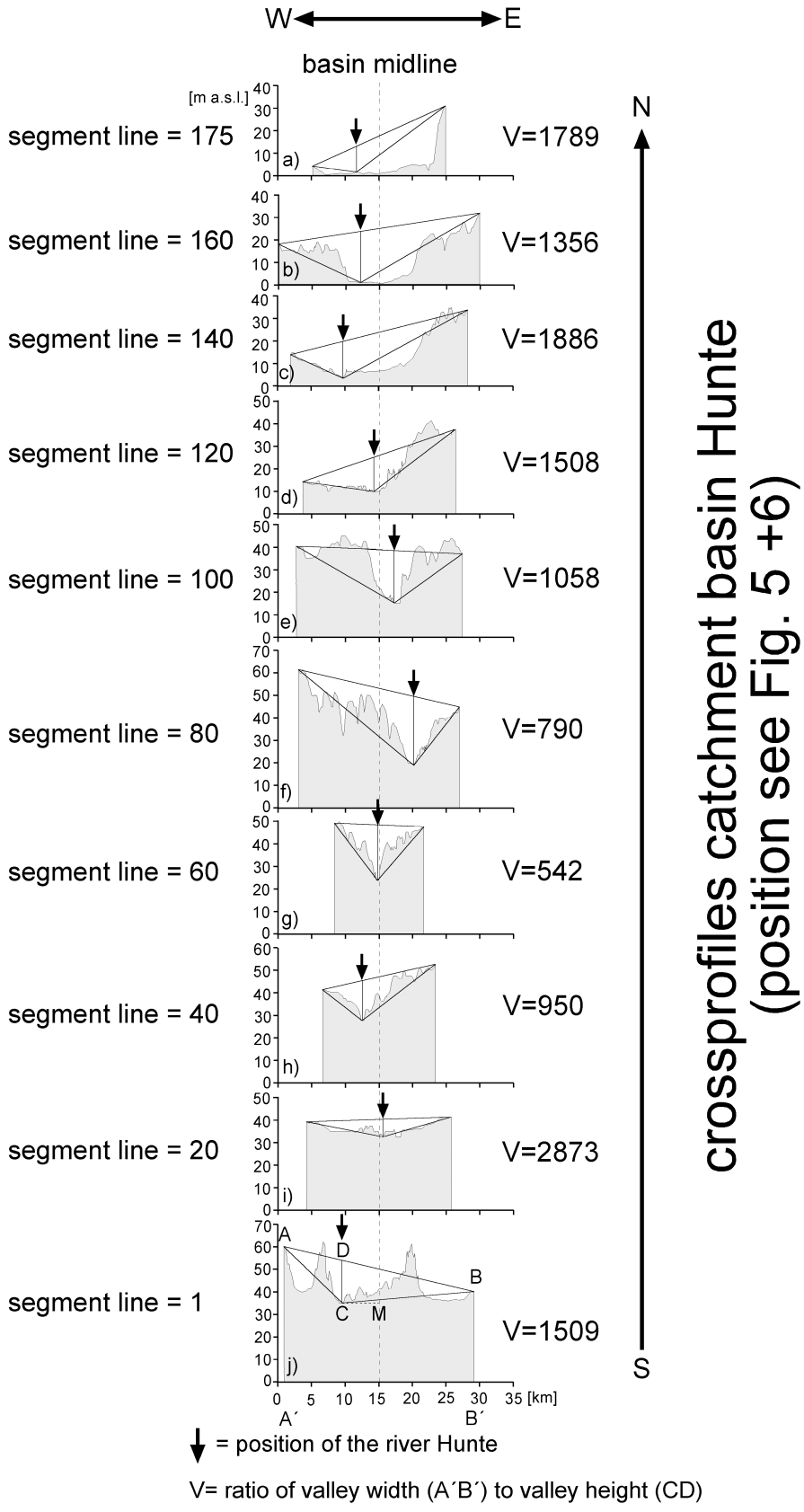

Fig. 23 a-j: Topographical W-E crossprofiles through the catchment basin of the river Hunte. The dashed line marks the basin midline of the Hunte catchment basin, the black arrows the position of the river Hunte. The geographical position of the crossprofiles is shown in Fig. 5+6 by the position of the segment lines.

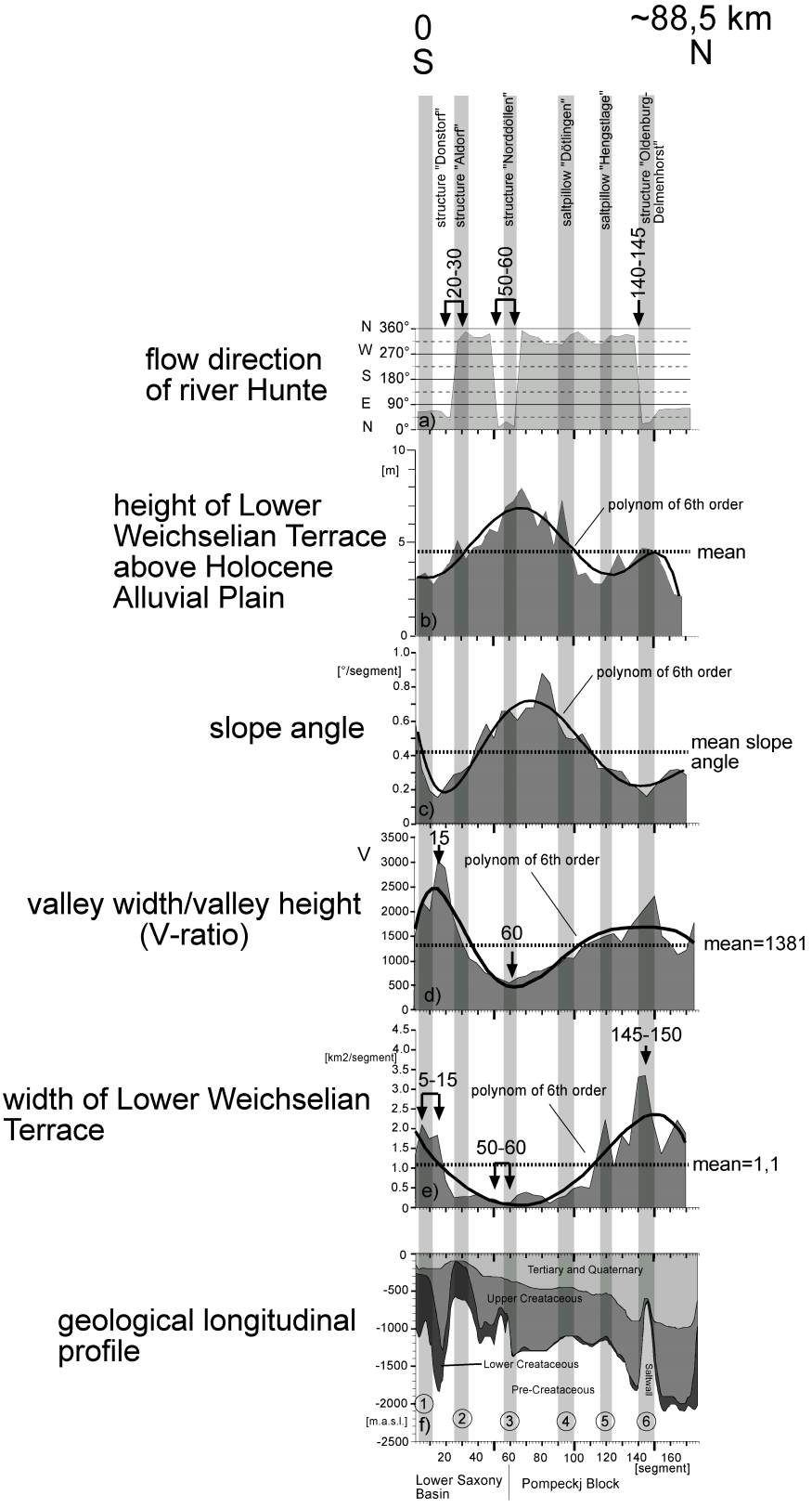

Fig. 24: Longitudinal profile of the river Hunte catchment basin from south to north, with a) general flow direction of the river Hunte, b) height of the Lower Weichselian Terrace above the Holocene Alluvial Plain in [m], c) slope of the catchment basin in [degree per segment], d) ratio of valley width to valley height (V-ratio), e) area of the Lower Weichselian Terrace in [km^2/segment], e) geological situation at the depth of the Base Lower marine Cretaceous, Base Upper Cretaceous and Base of Tertiary in [m a.s.l.], after Geotectonic Atlas of NW-Germany (Baldschuhn et al., 1996) and 3D Seismic contour map of the Base Tertiary (BEB, 2002). Gray markers 1 to 6 show the position of anticlines crossed by the river Hunte with the names of the geological structures, presented in Fig. 4.

1.1.7. Slope of the catchment basin

Slope angles of the river catchment basin have been determined to provide information about the development of the valley geometry along the course of the river Hunte. Slope angles were derived from the DEM (Fig. 5) by GIS calculated for each segment of the catchment basin. The slope angles are presented as a longitudinal profile from south to north in Fig. 24 c. The dashed line marks the mean slope angle for the whole longitudinal profile, the black line the polynom of 6^{th} order (smoothed data). Slope angles below the mean can be found above the Upper Cretaceous syncline "Donstorf"(between gray marker 1 and 2) and above the structure "Oldenburg-Delmenhorst" (gray marker 6). Maximum slope angles are visible between gray marker 3 and 4. Accordingly, the river slope angle is minimal above the centre of halocinetic uplift.

1.1.8. Drainage Basin Asymmetry

Topographic Symmetry Factors (TSF) were calculated from the topographic cross profiles of the catchment basin (Fig. 23). The procedure for the calculation of TSF follows the work of (Cox, 1994). The author used this method for the detection of possible Quaternary tilt-block tectonics in the Mississippi embayment. An example of calculation of a TSF is illustrated on the profile of segment line 1 (Fig. 23 j). The TSF was calculated by dividing distance MC (distance between the basin midline and the river Hunte) by the distance A´M (distance of half basin width). A ratio of one would mean the river is positioned near the watershed and a ratio of zero that it is positioned in the basin centre. Consequently, the TSFs are an indicator for the deflection of the river Hunte from the centre of catchment basin (basin midline). The basin midline of the river Hunte catchment basin is shown in Fig. 6 (thick black line). The calculated TSFs were used for the construction of a longitudinal profile as shown in Fig. 25 d. Eastward deflections of the river are shown by negative TSF-values (light gray) and westward deflections by positive TSF-values (dark gray). There is a westward deflection of the river Hunte between segment line 1 and 20. Between segment line 20 and 30 the river Hunte flows in the basin centre with a small eastward deflection (above the anticline structure "Aldorf", Fig. 25 e, gray marker 1). A westward deflection of the river Hunte is visible between segment line 30 and 60. The Hunte crosses the basin midline between segment line 60 and 65. This is exactly above the " Goldenstedt Blenhorst Lineament" (Fig. 3, lineament number 3). This lineament separates the Lower Saxony Basin in the south from the Pompeckj Block in the north (Fig. 25 e, gray marker 2). The river flows between segment line 60 and 120 in the eastward section of the catchment basin. The Hunte crosses the basin midline again between segment line 115-120, near the saltpillow "Hengstlage", (Fig. 25, gray maker 3). Between segment line 115 and 120 and segment line 175 the river flows in the westward section of the catchment basin.

Fig. 25 a, b show the maximum topographic altitudes calculated for each segment east and westward of the basin midline. The height differences between the maximum altitudes for the westward (Fig. 25 a) and the eastward side (Fig. 25 b) were calculated and presented in Fig. 25 c. Fig. 25 c shows which side of the catchment basin is higher or lower elevated. By comparing Fig. 25 c with Fig. 25 d it is striking that north of segment line 30 the river Hunte is deflected to the eastward side of the catchment basin (Fig. 25 d) in the situation where the westward side is higher elevated (Fig. 25 c) and vice versa. An XY-Plot (Fig. 25 f) was constructed based on the data of Fig. 25 c (X-axis) and Fig. 25 d (Y-axis). The linear correlation coefficient of –0,72 emphasize the already graphically obvious connection between the topography and the deflection of the Hunte.

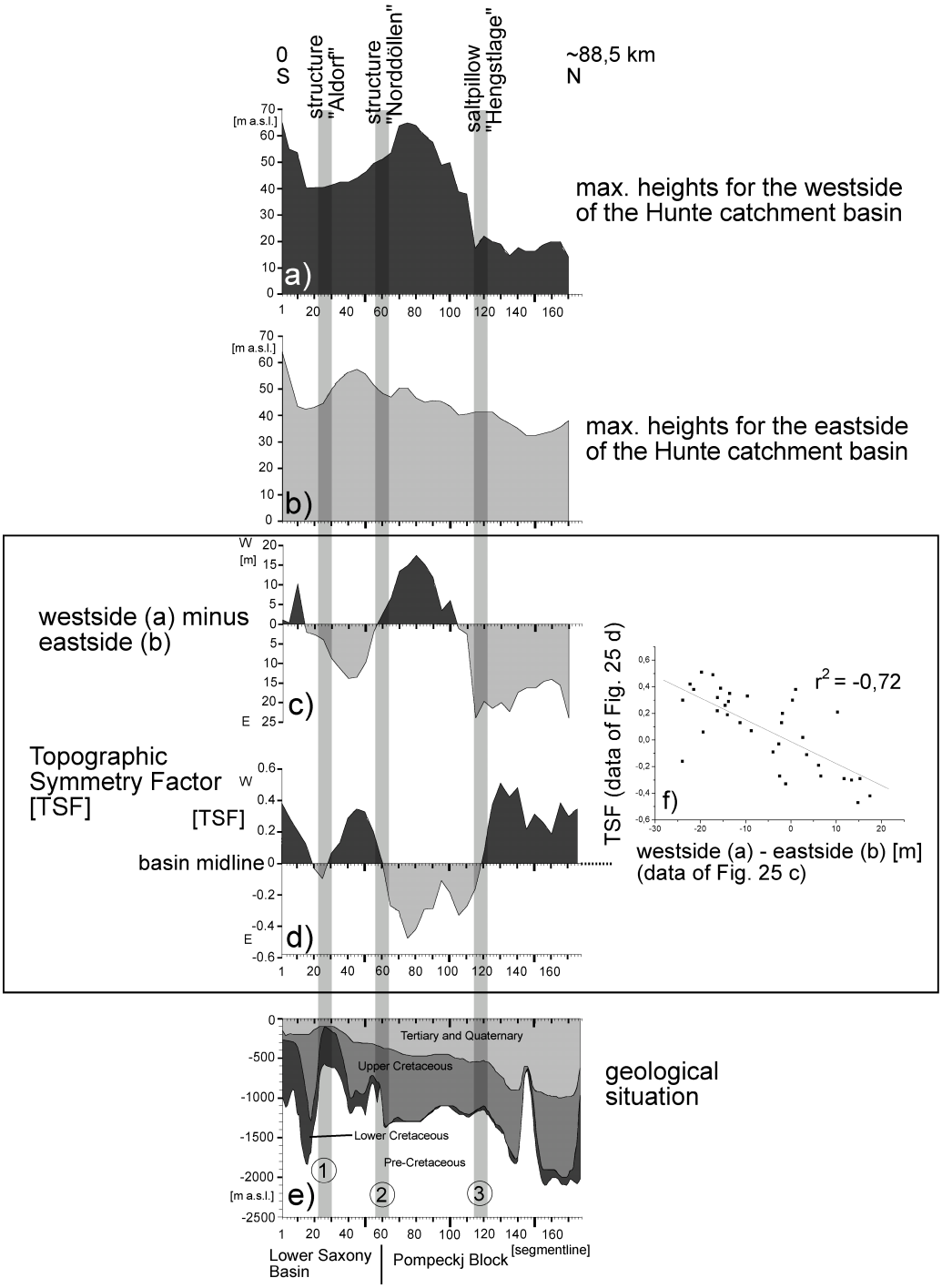

Fig. 25: Maximum topographical heights east (a) and westward (b) of the Hunte basin midline (basin midline is shown in Fig. 6), c) height differences between maximum altitudes of the westward [a] and the eastward side [b] of the Hunte catchment basin, d) topographic symmetry factor, e) geological situation for the depth at the Base of Lower marine Cretaceous, Base Upper Cretaceous and the Base of Tertiary in [m a.s.l.], after Geotectonic Atlas of NW-Germany (Baldschuhn et al., 1996) and 3D Seismic contour map of the Base Tertiary (BEB, 2002), f) XY-plot with data of [c] against data of [d] with linear regression line and linear correlation coefficient.

Summary of Chapter 1.1.8.

The river Hunte is deflected to the eastward side of the catchment basin where the westward side is higher elevated and vice versa (Fig. 25 c, d, f). The cross points of the river Hunte with the basin midline are positioned above structural highs of the geological basement (Fig. 25 e, d).

1.1.9. Orientation of drainage network and drainage pattern

Fig. 6 shows the drainage of the catchment basin of the Hunte. The tributaries of the river Hunte are marked by numbers, separated by east and west side. Fig. 26 b shows the position of confluences of the tributaries. The total length of each tributary is given by the y-axis in [km]. Fig. 26 a shows the number of confluences with the river Hunte, each calculated for a length of 10 segments. The mean number of confluences is 2,5 (Fig. 26 a, black line). Between segment line 20 and 90 the number of confluences is above the mean with a maximum between segment line 60 and 70 (6 confluences/10 segments). This is above/north of the transition zone between the Lower Saxony Basin and the Pompeckj Block (gray marker).

Between segment 25-30 tributaries 1E, 2E and 4W flow into the river Hunte (Fig, 26 b, Fig. 6). These confluences are positioned above the anticline structure "Aldorf" (Fig. 4) near the town of Barnstorf. Fig. 27 a shows the area of crustal doming in more detail. The background reproduces the depth of the base of the Upper Cretaceous, which is found up to 2000 m below the surface and reaches a local maximum of –100 m a. s. l. at segment 30. The Base of Tertiary is displaced over the doming (-100 m a. s. l., Fig. 13 c, gray marker 2). 3-Dimensional-Seismic-Data (kindly provided by the Wintershall-AG), show a graben structure on top of the dome (Fig. 27 b). The position of the profile is shown in Fig. 27 a (XY). The Hunte flows in the centre of this graben structure. It is unknown as yet if deep faults reach the surface because the resolution of the 3-D seismic data is inadequate for the uppermost 300 m.

It is visible in Fig. 1 that most of the Zechstein faults inside the Lower Saxony Basin strike with 110-120° (rose-diagram [b]). This direction is dominant for most of the river Hunte tributaries positioned above the Lower Saxony Basin (Fig. 3). Tributaries 2W, 3W, 2E (Fig. 6) show clear spatial relationships to the strike direction of the basement fault pattern (Fig. 3, block G, F). The orientation of tributary 6E fits well with the ~110° orientation of block E (Fig. 3, Fig. 27 a). Most of the Zechstein faults of the Pompeckj Block strike with NNW (Fig. 1, rose diagram [a]). This direction is also dominant in the fluvial system. Parts of tributary 12E and 17W show a clear NNW pattern. Fig. 3 shows that the „Berdum-Jaderberg-Sagermeer-Fault" (number 3) strikes with NNW. The tributary 22W which is positioned between the watershed and the „Berdum-Jaderberg-Sagermeer-Fault" shows partly the same NNW orientation. Fig. 3 shows that there is a strong correlation between the NW-SE striking part of tributary 23W and the orientation of the „Leer-Bremen-Lineament" at this position. This deep seated fault at the basement can be traced from the Base Zechstein up to the Base Lower Miocene to Pliocene (Appendix, Fig. 3 to Fig. 15).

Summary of Chapter 1.1.9.

The number of the tributary confluences with the river Hunte is highest above and north of the transition zone from the Lower Saxony Basin to the Pompeckj Block (Fig. 26 a, b). A large number of confluences with the Hunte are parallel to faults and domings of the geological basement (e.g. Fig. 27 a, b). The strike direction of some tributaries is identical to faults which can be traced from the deeper basement up to the Tertiary strata.

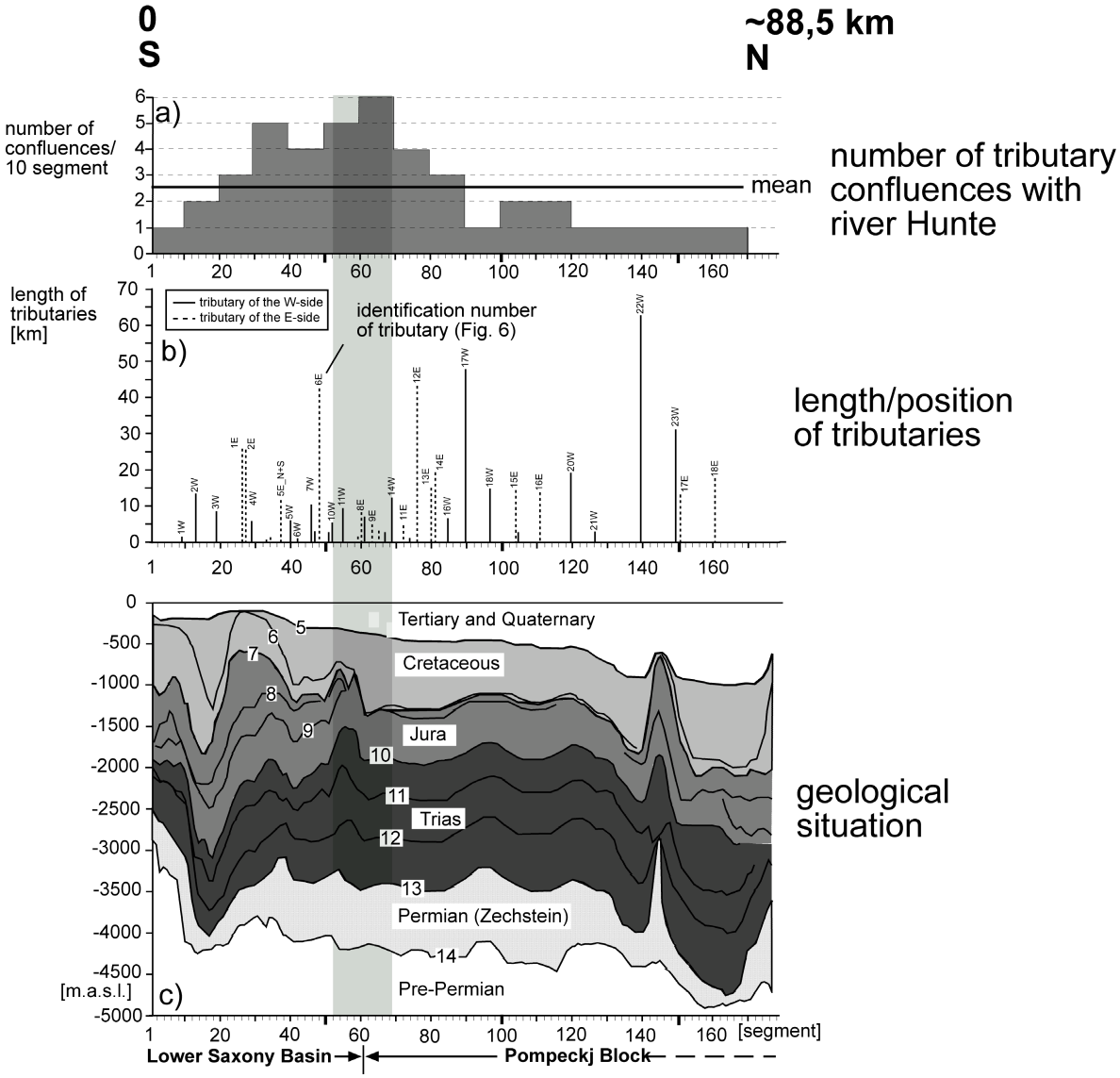

Fig. 26: Longitudinal profile of the Hunte from south to north with a) number of tributary confluences with the Hunte, calculated for an interval of 10 segments, b) position of tributary confluences with the Hunte, the length of the tributaries is given in [km], dashed lines show the east side tributaries, the solid line the westside Hunte tributaries, c) geological situation, depth at the Base of Zechstein (number 14) to the Base of Tertiary (number 5), after Geotectonic Atlas of NW-Germany (Baldschuhn et al., 1996). The depth at the Base of Tertiary is based between segment 58-129 and 158-177 on the 3D-seismic data contour map (BEB, 2002).

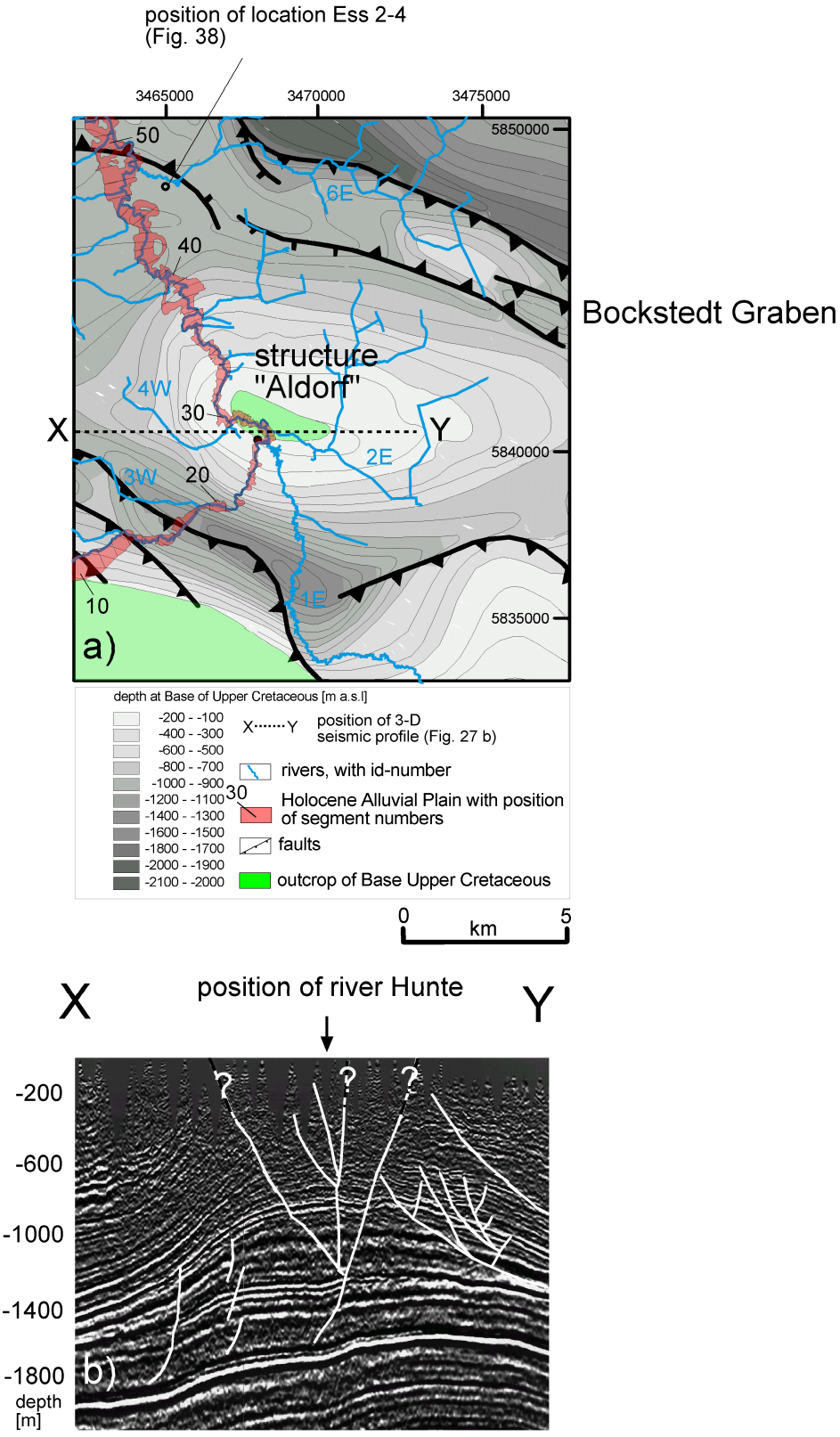

Fig. 27 a) Structural contour map, depth at the Base of Upper Cretaceous after Geotectonic atlas of NW-Germany (Baldschuhn et al., 1996). The Holocene Alluvial Plain of the river Hunte is shown in red with the position of the segment numbers, rivers are shown in blue with the position of the identification number. The position of the 3-Dimensional-Seismic-Data profile is given by the letters XY. The profile is shown in Fig. 27 b,
b) Cross section from 3-Dimensional-Seismic-Data with a graben structure on top of the updoming, faults (white). The question marks symbolize the lack of seismic information of the uppermost 300 m b. s. l.. The arrow marks the position of the river Hunte (kindly provided by the Wintershall AG).

1.1.10. Holocene Alluvial Plain

1.1.10.1. General flow direction

Fig. 24 a) shows the flow direction of the Hunte. The strike direction for each segment of the Holocene Alluvial Plain was measured from south to north in [°] and plotted against the segment number. The first stronger change in flow direction occurs between segment 20 and 30 above the anticline, inversial structure “Aldorf” (Fig. 24 f, gray marker 2). Here, the Hunte turns from NE to NW. The second stronger change is visible between segment 50 and 60 above the inverse structure “Norddöllen”, (Fig. 24 f, gray marker 3). The last stronger change in direction occurs between segment 140 and 145, directly positioned above the structure “Oldenburg-Delmenhorst” (Fig. 24 f, gray marker 6).

Summary of Chapter 1.1.10.1.

All major shifts in the flow direction of the Hunte are positioned above structural highs of the geological underground (Fig. 24 a, f).

1.1.10.2. Width of the Holocene Alluvial Plain

Fig. 28 a) shows the area of the Holocene Alluvial Plain calculated for each segment in [km^2] plotted against the segment number. The Holocene Alluvial Plain was cut into equal segments with a fixed length of 500 m. Changes in area of a single segment are therefore an indicator for the width of the Holocene Alluvial Plain. Five pronounced local minima are recognizable. The minimum at segment 21 is located at the southern flank of the structure “Aldorf” (Fig. 28 d, gray marker 2). The minimum at segment 68 is positioned ~5 km north of the frontier between the Lower Saxony Basin and the Pompeckj Block (Fig. 28 d gray marker 3). The minimum around segment 95 is located above the saltpillow “Dötlingen”. The minimum around segment 106-110 is positioned between the salt pillow “Dötlingen” and “Hengstlage” (Fig. 28 d, between gray marker 4 and 5). The width of the alluvial plain rises rapidly approximately north of segment 120. A minimum (segment 147-157) is visible above the structure “Oldenburg-Delmenhorst” (Fig. 28 d, gray marker 6).

Summary of Chapter 1.1.10.2.

The Holocene Alluvial Plain of the Hunte is smaller above most of the anticline structures (Fig. 28 a, d).

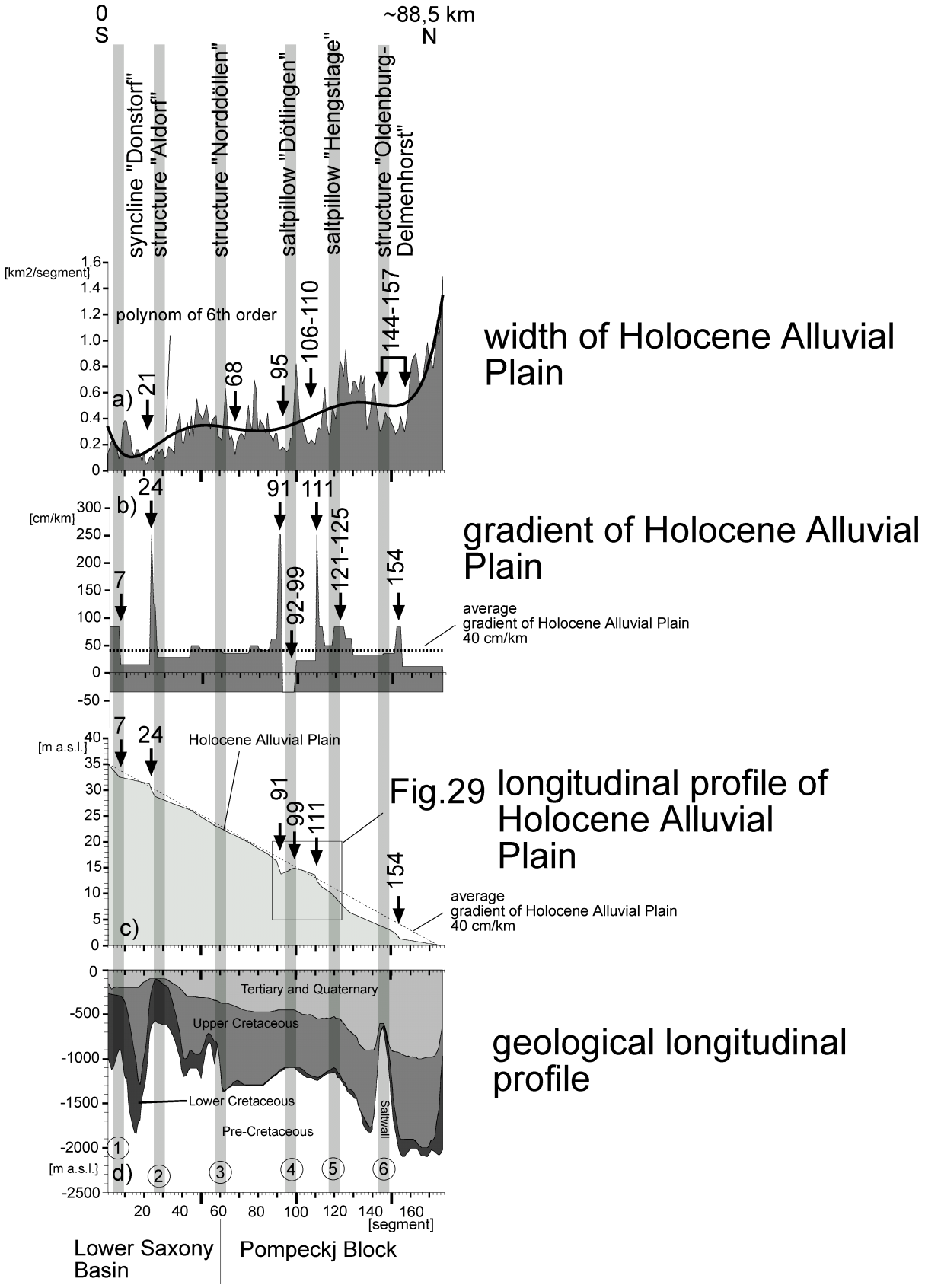

Fig. 28: Longitudinal profile of the Hunte from south to north with a) area of the Holocene Alluvial Plain in [km^2/segment], (indicator for the width of the Holocene Alluvial Plain), b) gradient of the Holocene Alluvial Plain in [cm/km], c) height of the Holocene Alluvial Plain in [m a.s.l.], d) geological situation at the depth of the Base Lower marine Cretaceous, Base Upper Cretaceous and Base of Tertiary in [m a.s.l.], after Geotectonic Atlas of NW-Germany (Baldschuhn et al., 1996) and 3D Seismic contour map of the Base Tertiary (BEB, 2002). Gray markers 1 to 6 show the position of anticlines crossed by the river Hunte with the names of the geological structures, presented in Fig. 4.

1.1.10.3. Gradient line of the Holocene Alluvial Plain

Fig. 28 c) shows also the gradient line for the Holocene Alluvial Plain of the Hunte. The gradient line was constructed from topographical maps (LGN, 1994). The height was determined from contour lines crossing the Holocene Alluvial Plain segments. No benchmarks (point-data) were used for the construction of the longitudinal profile. Fig. 28 b) shows the gradient of the Holocene Alluvial Plain in cm/km based on the data shown in Fig. 28 c). The dashed line shows that the average gradient for the investigated section of the river is 40 cm/km (a height difference of 35 m over a distance of ~88,5 km). Seven abnormal sections with pronounced discrepancies from this average are visible. The first anomaly is positioned at segment 7 (arrow 7) above a syncline visible at gray marker 1 (Fig. 28 d). Above the syncline “Donstorf” (segment 8-23) the gradient is reduced with ~16 cm/km. This is 2,5 times smaller than the average gradient. Above the anticline structure “Aldorf” (gray marker 2), the first stronger knickpoint (arrow/segment 24) is visible. The knickpoint gradient is 6,3 times greater than the average gradient. The second stronger knickpoint can be found at segment/arrow 91, which shows the identical gradient as the knickpoint before. A rise of the Holocene Alluvial Plain is visible between segment 92 and 99, which results in a negative gradient of -36 cm/km. Fig. 29 a, b shows this section (between segment 88 and 124) in more detail. The rise of the Holocene Alluvial Plain is exactly above the salt pillow of “Dötlingen” (Fig. 28 d, gray marker 4). Segment 111 is the position of the next stronger knickpoint with a gradient of 250 cm/km (Fig. 28 b). Between segment 111 and 129 the gradient is above and between segment 131-152 below average. North of the structure “Oldenburg/Delmenhorst” (Fig. 28 d, gray marker 6) at segment 154 the last stronger knickpoint is visible.

Summary of 1.1.10.3.

Most knickpoints in the gradient line of the Hunte are positioned near domings of the geological strata (Fig. 28 b, c, d). The Holocene Alluvial Plain of the Hunte rises exactly above the salt pillow of “Dötlingen” (Fig. 28 b, c, d, gray marker 4).

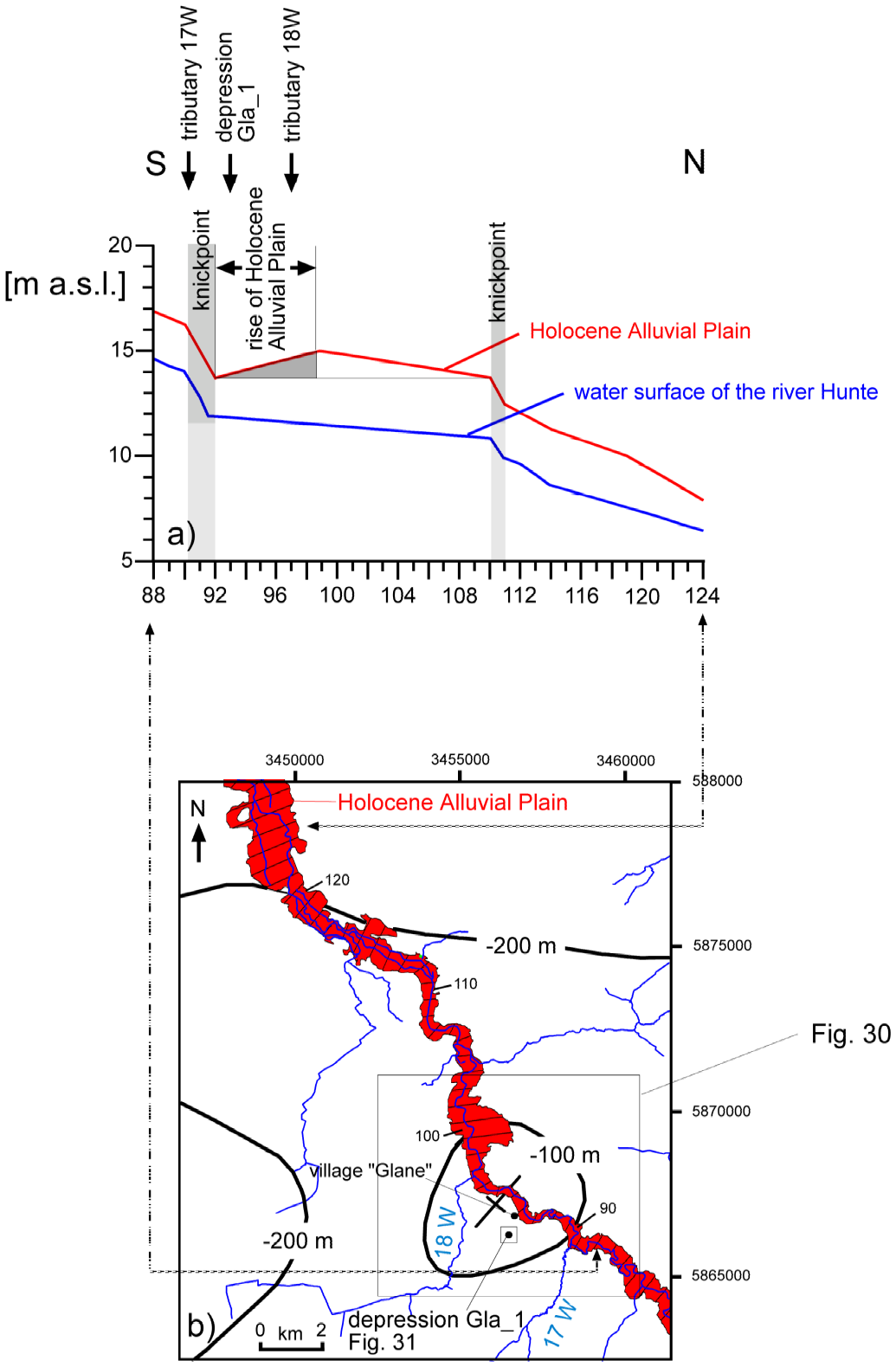

Fig. 29 a) Longitudinal profile for a section of the Hunte (segment 88-124) with height of the Holocene Alluvial Plain (red) and the water surface (blue); b) map view of the longitudinal profile shown in [b] with Holocene Alluvial Plain, shown in red and the position of the segment numbers. The rivers are shown in blue with the position of identification numbers. The contour line represents the depth at the Base Middle Oligocene to Upper Oligocene with the position of the anticlinal axis, after the Geotectonic Atlas of NW-Germany (Baldschuhn et al., 1996).

1.1.11. Height position and width of the Lower Weichselian Terrace (LWT)

The LWT is visible as a planar surface. The height level of the LWT could be post-depositionally lowered by fluvial erosional processes of the tributaries or elevated by Holocene dune sands. These post-depositional/erosional processes complicate a reliable height determination of the LWT. For this reason, areas of tributary catchment basins and dune fields which are positioned on the Lower Weichselian Terrace were not taken into account for later height calculation by GIS. The LWT was separated into segments of nearly equal length (~2,5 km length), (Fig. 6). Afterwards, the average altitude for each of the LWT-segments was calculated. The resulting segment height was subtracted from the height of the corresponding/adjacent Holocene Alluvial Plain. By this process, the gradient of the Holocene Alluvial Plain was calculative removed and all heights along the LWT longitudinal profile are comparable. Fig. 13 a) shows the resulting longitudinal profile. The height of the Lower Weichselian Terrace above the Holocene Alluvial Plain changes along the course of the river Hunte. The maximum height difference is 5,9 m. The maximum offset is visible at the transition zone from the Lower Saxony Basin to the Pompeckj Block (Fig. 13 a, c, gray marker 3). Fig. 24 e shows the area of the LWT, calculated per segment along the course of the Hunte, using the same technique as already explained in Chapter 1.1.10.2. “Width of the Holocene Alluvial Plain”. Thus, the area of the LWT is an indicator for its width. Between segment line 20 and 102 the width of the LWT is below its mean of 1,1 km^2/segment. The LWT is smallest between segment line 50-60, above the transition zone from the Lower Saxony Basin to the Pompeckj Block (Fig. 24 f, gray marker 3).

Summary of Chapter 1.1.11.

The height of the Lower Weichselian Terrace above the Holocene Alluvial Plain changes along the course of the Hunte. The maximum offset is visible at the transition zone from the Lower Saxony Basin to the Pompeckj Block (Fig. 13 a, c). Here the Lower Weichselian Terrace is smallest (Fig. 24 e, f).

1.1.12. Depression (Location Gla_1) on the Lower Weichselian Terrace

This chapter describes the morphological situation, geological and structural framework of a small scaled depression. The investigated depression Gla_1 can be found near the village Glane (Fig. 30).

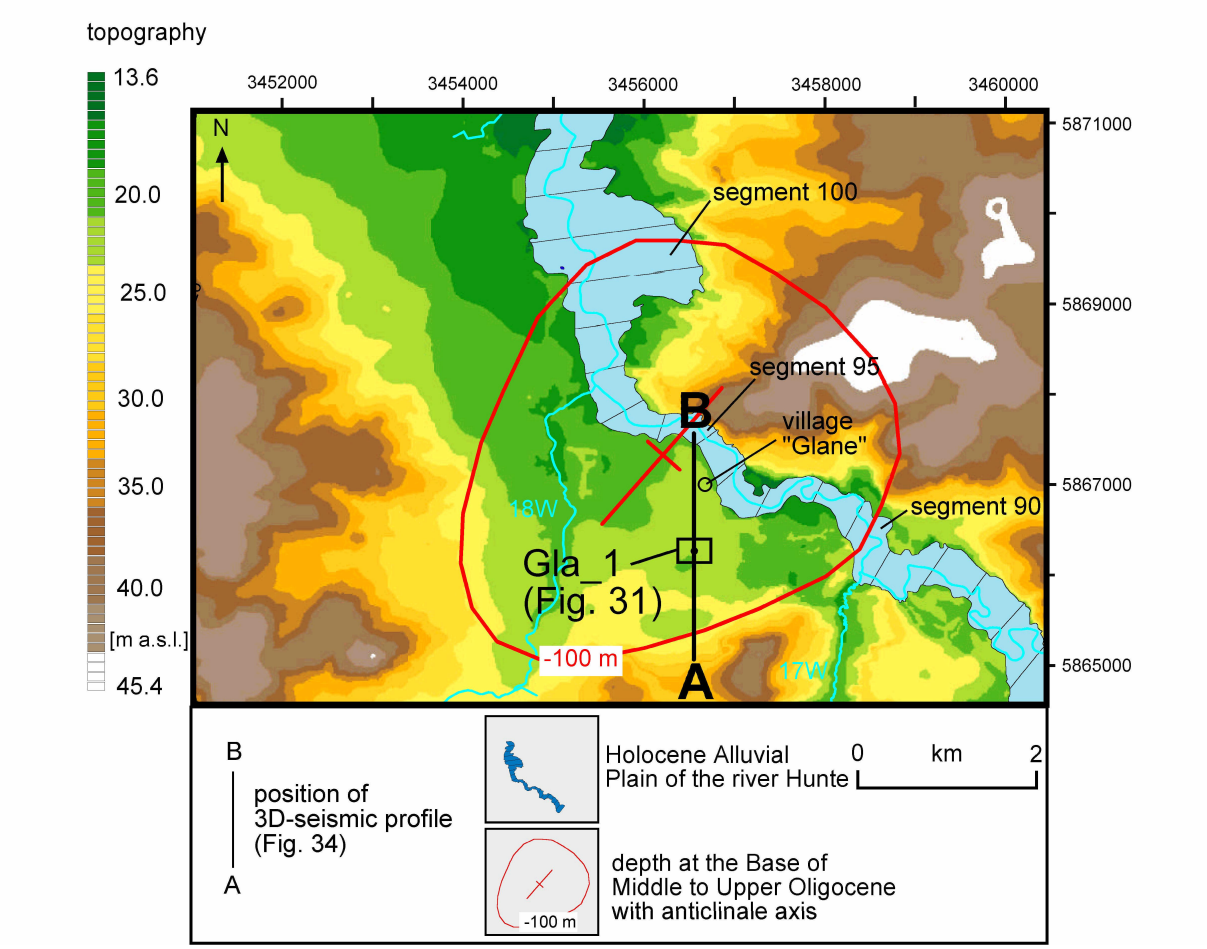

Fig. 30: Topography for a section of the Hunte catchment basin (segment 85-103), with position of depression Gla_1. Range of altitude is 13,6 (dark green) to 45,4 m a.s.l. (white), the red line shows the depth at the Base of Middle to Upper Oligocene with the position of the anticlinal axis after the Geotectonic Atlas of NW-Germany (Baldschuhn et al., 1996), rivers are shown in dark-blue (with identification number of tributaries), Holocene Alluvial Plain of the river Hunte in light blue with position of segment numbers and the position of 3D-seismic profile (AB). The profile is presented in Fig. 34.

The depression is on the level of the Lower Weichselian Terrace of the river Hunte at 21,25 m a.s.l.. The photo Fig. 11 b shows the depression. A Digital Elevation Model was constructed based on topographic field levelling (Fig. 31 a). The depression is about 120 m long and 100 m wide with a maximum depth of ~2,0 m and strikes with ~160°. The slopes of the west and south side are steeper than those of the east and and north side (W-side: ~2,6°, E-side: ~1,5°, N-side: ~1,0°, S-side: ~1,8°).

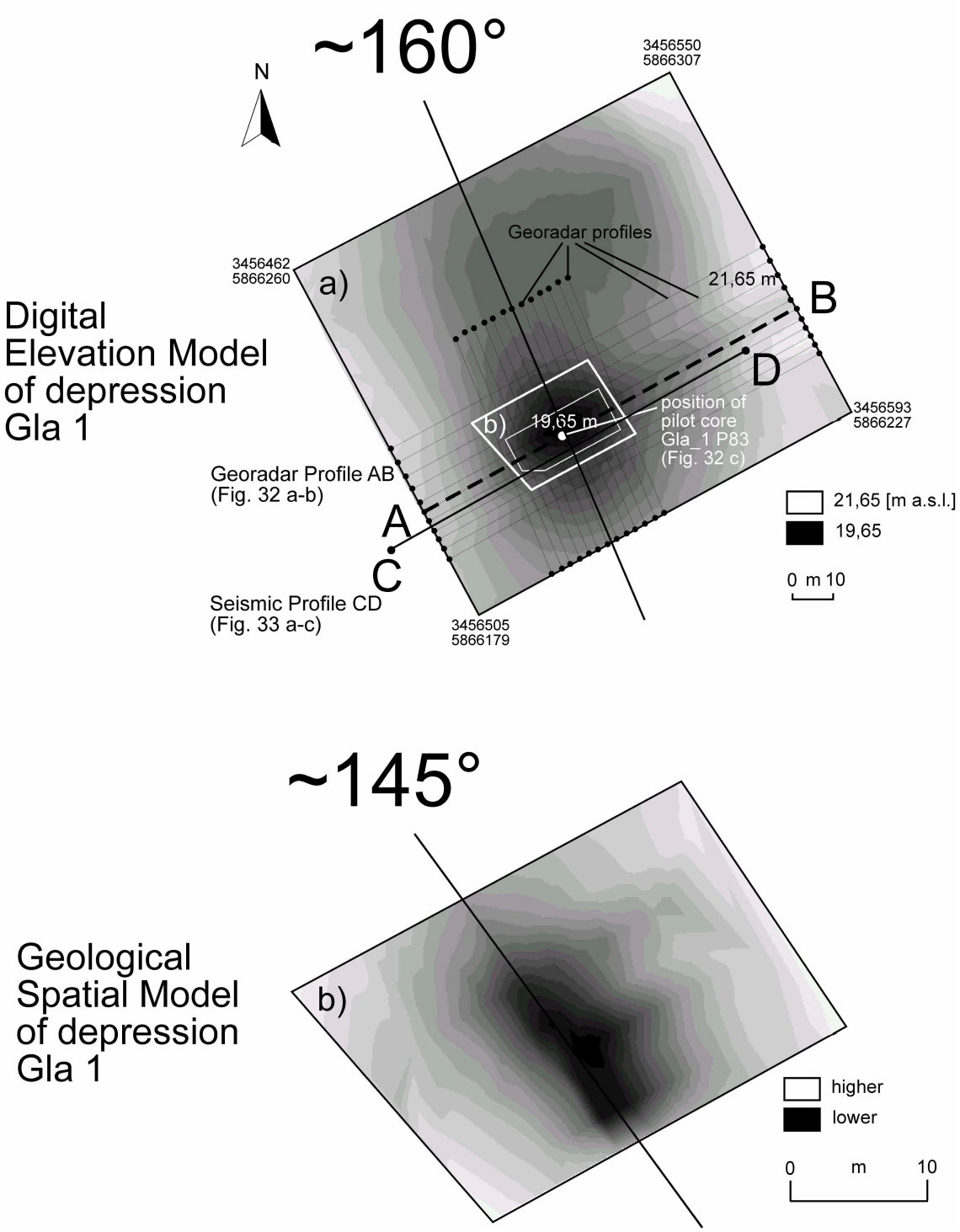

Fig. 31 a) Digital Elevation Model of depression Gla_1 after field levelling, highest elevation of depression is 21,65 and deepest point 19,65 m a.s.l.. The depression strikes with 160° (black line). The position of georadar profiles is given by the black lines, georadar profile AB (dashed line) is shown in Fig. 32 a, b. The seismic profile CD is shown in Fig. 33 a-c.
b) Geological Spatial Model (position shown in [a]), constructed by georadar profiles. The strike direction of the depression is ~145°, shown by the black line along the synclinal axis.

Georadar was used to record the uppermost geological strata. The Georadar system is shown in Fig. 11 a). A total of 24 Georadar profiles (with a total length of 1180 m) were recorded. The position of the georadar profiles are shown in Fig. 31 a. Eleven profiles are orientated ~NE-SW and thirteen ~NW-SE. A single measurement was taken every 0,2 m along the profiles. In order to achieve the optimal signal coupling from the georadar, the antenna was placed on the ground at each measuring point. A refraction hyperbola, caused by a gas pipeline, was

used for the time-depth transfer (Fig. 32 b). Based on this, the maximum radar penetration depth is about 15-20 m below surface. The NE-SW orientated profiles were chosen for the construction of a geological spatial model, shown in Fig. 31 b. The position of the spatial model is visible in Fig. 31 a. The NW-SE profiles were used to check the spatial model. The spatial model is based on unprocessed raw data. Fig. 32 a is an example of a radargram used for the construction of the spatial model.

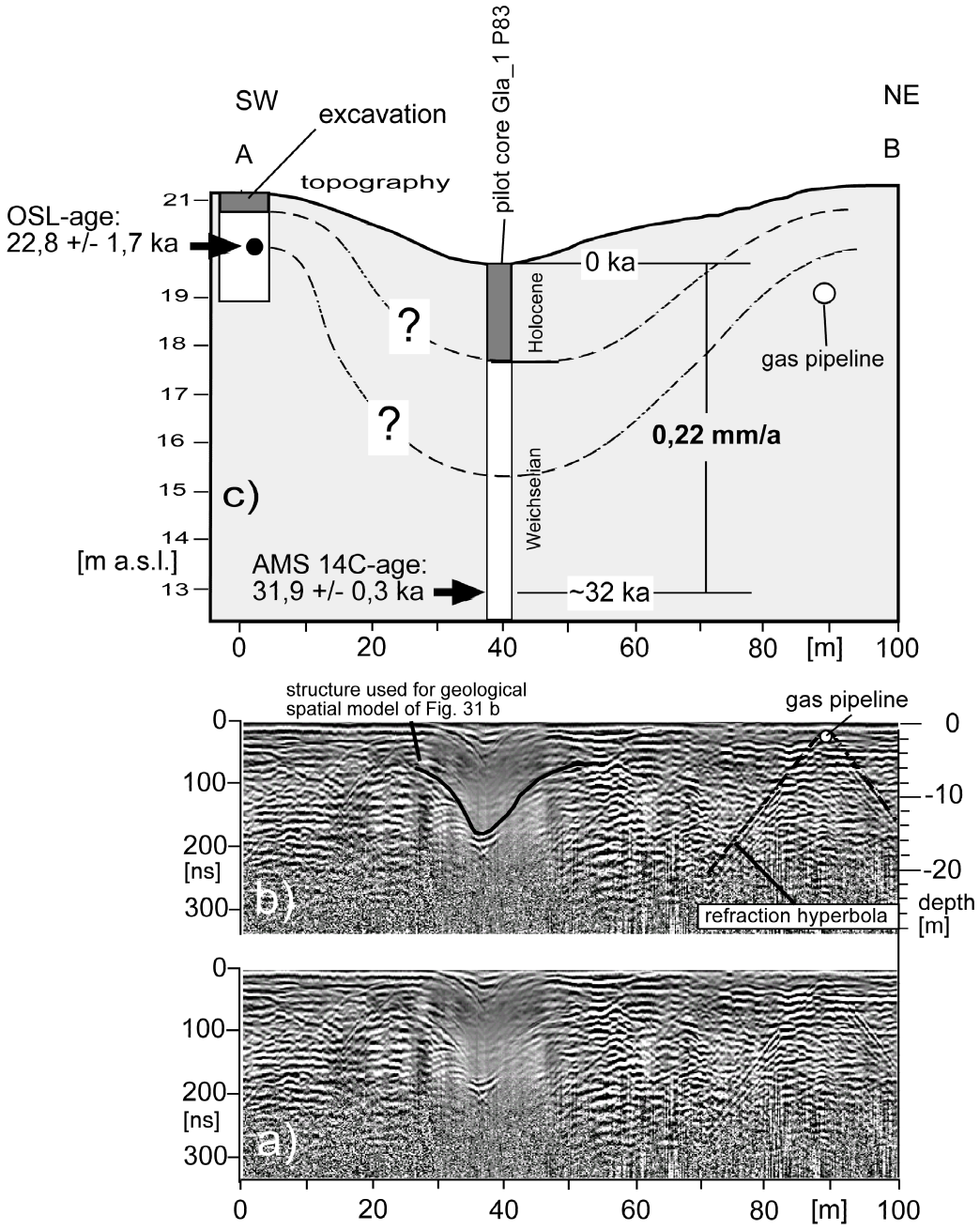

Fig. 32 a) Georadar profile AB through depression Gla_1 (position is shown in [Fig. 31 a]). The profile is 100 m long, the depth is given in TWT [ns],
b) the position of the depressional-like structure between profile meter 25-45 is marked by the black line. The depth of this structure was used for the construction of the Geological Spatial Model shown in [Fig. 31 b]. The refraction hyperbola (dashed line) is caused by a gas pipeline. This refraction hyperbola was used for the time/depth transfer (the depth in [m] is shown by the right-hand Y-axis),
c) topographical cross profile AB. The profile was constructed on the basis of the DEM shown in Fig. 31 a), with position of the pilot core Gla_1 P83 and AMS ^{14}C -dating and the position of the excavation with OSL-age.

The position of the radargram is given in Fig. 31 a, profile AB (dashed line). A depression-like structure is visible between profile-meter 25-50. The black line in Fig. 32 b marks the depression. The depression is traceable in the adjacent profiles. The spatial model of the depression was calculated by GIS from the spatial development of this structure (Fig. 31 b). Data processing of the raw data has shown that refraction hyperbolica superimpose the useable signals (K.J. Sandmeier, [company Sandmeier Scientific Software]). Nevertheless, the structure seen in the radargrams must be of geological origin since the shape and position of the structure is almost identical in both the NE-SW and NW-SE profiles. For this reason depths and slopes are not reconstructable from the spatial model. However, the spatial position of the depression itself is. The structure is ~22 m long, ~20 m wide and strikes with ~145° (Fig. 31 b). The depression as reconstructed by Georadar is about 27 times smaller in area than its morphological counterpart.

A 14 m long core was taken from the centre of the depression (Fig. 31 a). The drilling is shown in Fig. 32 c). Organic rich silty sands were drilled at a depth of 12,25-13,15 m a.s.l. An AMS ^{14}C dating on plant debris at 12,70-12,80 m a.s.l. resulted in an age of 31,9 +0,33/-0,32 cal. ka BP. Consequently, the filling of the depression at and above this dating is of Weichselian to Holocene age. The Holocene age is evident by the recent soil on top (0-1 m) and peat layers between 1-2 m. The mean sedimentation rate inside the depression is ~0,22 mm/a as calculated between the time interval of ~32 ka and today.

An area outside the depression was excavated. The position of the excavation is shown in Fig. 32 c). An OSL sample was taken at a depth of 1,0 m, which resulted in a Weichselian age of 22,8 +/-1,7 ka. Thus, the depression is positioned on the Lower Weichselian Terrace, but started to subside already in OIS 3.

A seismic reflection profile was shot to achieve geological informations deeper than 15-20 m (which was the maximum penetration depth of the Georadar at site Gla_1). The position of this profile is shown in Fig. 31 a (profile CD) and the resulting seismogram in Fig. 33 a.

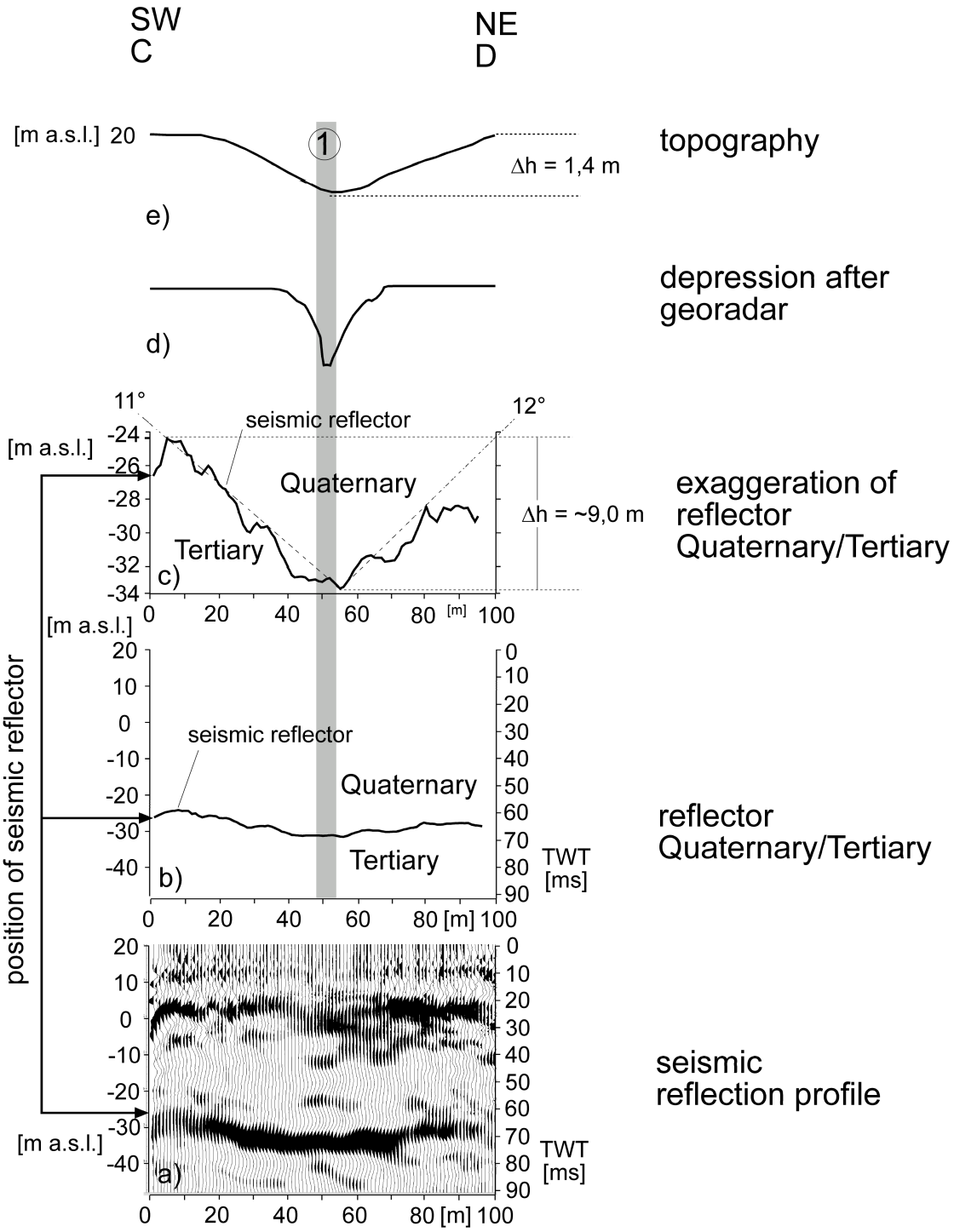

Fig. 33: a) Seismic reflection profile CD through depression Gla_1 (position of profile is shown in [Fig. 31 a], TWT in [ms], depth in m a.s.l..;
b) interpreted seismic reflector of [a]
c) the same seismic reflector as shown in [a, b] for the depth interval of -34 to -24 m a.s.l..
The dashed lines show the dip angles of the seismic reflector for the SW and NE-flank.
d) Depression, constructed from the Georadar Spatial Model of Fig. 31 b.
e) Topography, constructed from Digital Elevation Model of Fig. 31 a.

The profile is 100 m long. The midpoint of the profile is positioned above the centre of the syncline axis of the depression. A seismic reflector is visible at a Two Way Travel Time (TWT) of about 70-80 ms. The propagation velocity of the seismic waves at this depth is 1500 m/s. Taking this velocity into account, a depth of about 50 m results for this reflector. This reflector depth is in a good agreement with the depth of the Base Quaternary shown by the Map of the Base of Quaternary (depth of 45 m), (NLfB, 1993) and a drilling by the oil industry positioned about 2 km NW of depression GLA_1 (depth of 40 m), (Brink, H.J., [BEB, Hannover] personal communication). Therefore, it is assumed that this seismic reflector represents the Quaternary to Tertiary boundery. Fig. 33 b) shows the depth for the top of the reflector visible in Fig. 33 a. An exaggeration for the depth interval of -24 to -34 m a.s.l. is presented in Fig. 33 c. The deepest point is visible at profile meter 50 (gray marker 1) with a maximum offset of about 9 m. The dip angle of the SW-flank is ~11° and ~12° for the NE-flank. Fig. 33 d shows the depression constructed from the georadar spatial model of Fig. 31 b and Fig. 33 e the topography constructed from the Digital Elevation Model of Fig. 31 a. Gray marker 1 (Fig. 33) illustrates that the deepest part of the trough at the Base Quaternary/Top Tertiary (Fig. 33 c) coincides with the “georadar depression” (Fig. 33 d) and the topographical depression (Fig. 33 e). Consequently, the depression Gla_1 is not only a morphological phenomenon. The geological subground is also deflected, as shown by georadar and reflection seismic investigations.

Structural situation of depression Gla_1

The depression Gla_1 is positioned above a doming at depth. This doming is caused by the saltpillow “Dötlingen” (Fig. 4). Fig. 13 c, (gray marker 4) shows that this doming can be traced from the Base Zechstein (-4100 m a.s.l.) up to the Base Tertiary (-450 m a.s.l.). It is evident in Fig. 30 that this doming is traceable in the uppermost Tertiary strata. The red circle in Fig. 30 shows the depth at the Base of Middle to Upper Oligocene (-100 m a.s.l.) with the position of the anticline axis. Consequently, the doming is traceable over a vertical distance of about 4000 m from the Basin´s deepest part up to the uppermost Tertiary strata. The anticline axis of the Base Middle to Upper Oligocene is positioned near the river Hunte at segment number 95. Anomalies of the Hunte´s morphology focus above this doming. It is visible in Fig. 28 d), (gray marker 4) that the Holocene Alluvial Plain of the river Hunte shows a negative gradient ([Fig. 28 b, c and Fig. 29 a, b] between segment number 92-99), and the width of the Holocene Alluvial Plain is smallest (Fig. 28 a, arrow 95). The Lower Weichselian Terrace of the Hunte shows local high of 7 m above the Holocene Alluvial Plain (Fig. 13 a, c; gray marker 4) and the flow direction of the river Hunte changes from SE-NW to N (Fig. 24 a, gray marker 4; Fig. 29 b + Fig. 30).

Fig. 30 shows the position of profile AB. The profile is shown in Fig. 34. This profile is based on 3-D Seismic Data (kindly provided by the oil company BEB, Hannover). The profile is NS orientated with a length of 2,5 km and crosses the depression Gla_1 at a profile distance of 1,2 km. The original seismic data cannot be shown. The Base Upper Cretaceous and the Base Tertiary reflectors have been mapped from the original seismic data. The Base Tertiary reflector shows two height levels. Level one at ~ -450 and level two at ~ -440 m a.s.l.. The centre of the depression Gla_1 is directly positioned above the southern border of this transition zone from level one to level two (gray marker 1). At this transition zone the gradient of the Base Upper Cretaceous steepens from 0,6° to 0,8° (shown by the dashed gradient lines).

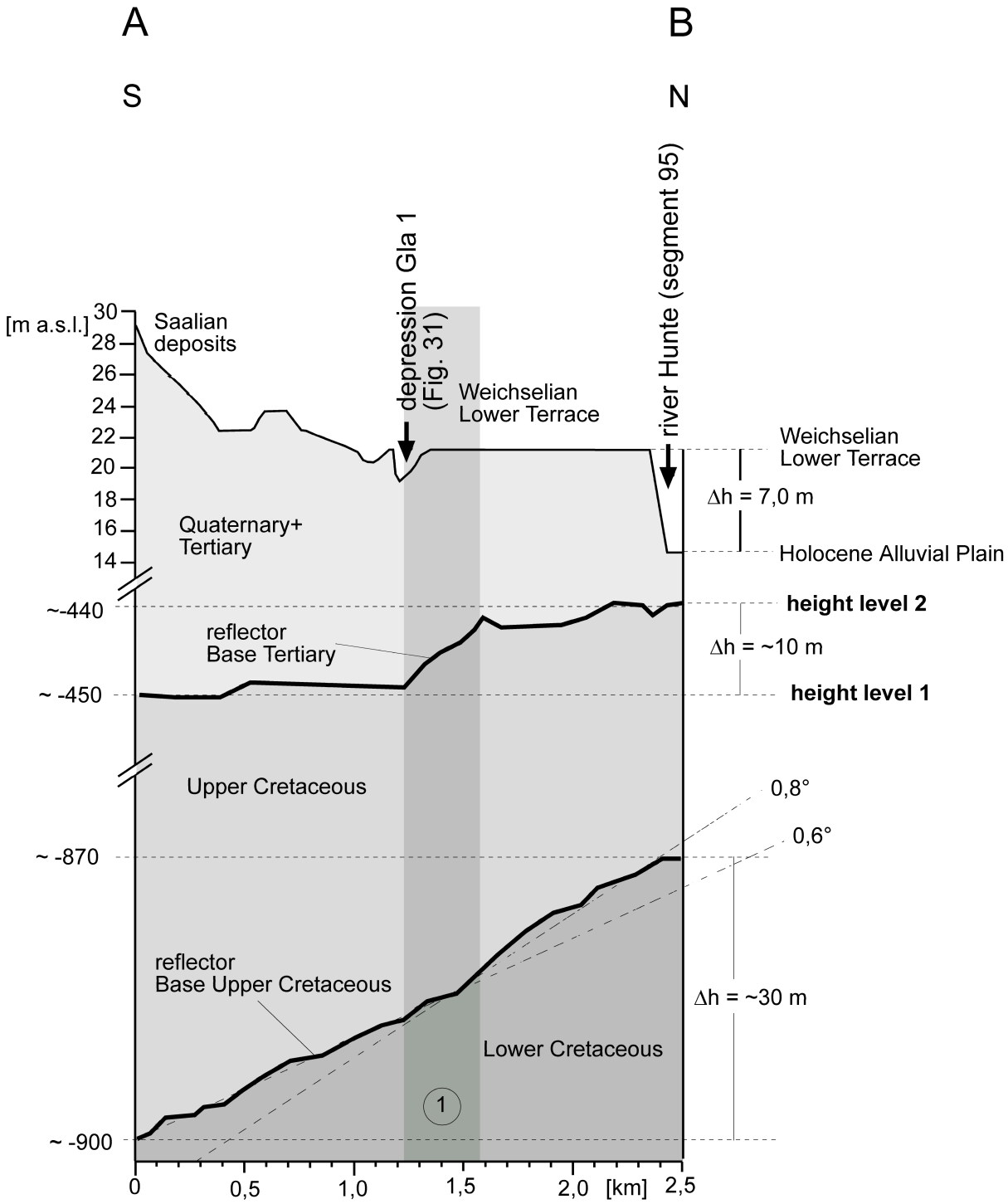

Fig. 34: Profile AB [geographical position shown in Fig. 30] with topography, depth of the Base Tertiary and Base Upper Cretaceous. The black arrows show the position of depression Gla_1 and the Holocene Alluvial Plain of the river Hunte. The river Hunte incised about 7,0 m into the Lower Weichselian Terrace at segment number 95.
Depth of the Base Tertiary and Base Upper Cretaceous after seismic reflectors of 3D Seismic profile (kindly provided by the BEB, Hannover; original seismic profiles are not shown). Topography after topographical maps (LGN, 1898; LGN, 1994).

Summary of Chapter 1.1.12.

The depression Gla_1 is of geological origin and not an anthropogenic feature as shown by Georadar, drilling and dating of sediments (Fig. 31, 32). The morphological expression of the depression is about 27 times greater in area than the geological one (as reconstructed by Georadar), (Fig. 31). The geological syncline axis strikes with 145°, the morphological one with 160° (Fig. 31 a, b). The depression is positioned on the Lower Weichselian Terrace as shown by the OSL dating (Fig. 32 c). The fill of the depression is of Weichselian to Holocene age with a mean sedimentation rate of about 0,22 mm/a (Fig. 32c). The Base of Quaternary shows a trough which is evident by reflection seismic data. The deepest point of this trough coincides with the deepest part of the depression as reconstructed by Georadar and the morphological one (Fig. 33 a-e, gray marker 1). It is evident by 3D seismic data profile that anomalies regarding the dip angle of Upper Cretaceous and the depth at the Base of Tertiary coincide with the position of the depression (Fig. 34, gray marker 1).

The depression is positioned on the flank of a doming of the geological subground, caused by a salt pillow at a depth of about –4100 m a.s.l.. The doming can be traced over a vertical distance of about 4000 m from the Base of Zechstein at a depth of –4100 m a.s.l. up to the uppermost Tertiary (Base of Middle- to Upper Oligocene [-100 m a.s.l.], (Fig. 13, gray marker 4; Fig. 30).

The following fluvial anomalies of the river Hunte focus above this doming, about 1 km far from depression Gla_1:

(1) the Lower Weichselian Terrace is positioned higher above the Holocene Alluvial Plain than north and south of the doming (Fig. 13 a, gray marker 4),

(2) the Holocene Alluvial Plain is smallest (Fig. 28 a, arrow 95),

(3) the Holocene Alluvial Plain of the river Hunte shows a negative gradient (Fig. 28 b, c and Fig. 29 a, b; between segment number 92-99),

(4) the flow direction of the river Hunte changes from ~SE-NW to ~N above the centre of doming (Fig. 24 a, gray marker 4; Fig. 29 b, Fig. 30).

1.2. Repeated Geodetic fine-levelling (Norddeutsches Küsten Nivellement (NKN), between NKN 1 = 1928-1931 and NKN 3 = 1980

Two levelling campaigns, the first between 1928-1931 (NKN 1) and the second in 1980 (NKN 3), were carried out in Lower Saxony and the northerly adjacent Schleswig-Holstein within the scope of the "Norddeutsches Küsten Nivellement (NKN)", (data kindly provided by the LGN [Landesvermessung + Geobasisinformation Niedersachsen]), (LGN, 2002). During both campaigns, identical benchmarks were absolutely levelled in m a.s.l.. Velocities of vertical motions were calculated by dividing the height differences for identical benchmarks between the two levelling campaigns by the time differences. The first levelling campaign (NKN 1 1928-1931) was set to 1929 and half year. This results in a time span of 50,5 years ([NKN3=1980] - [NKN1=1929 and half year]). The velocities were calculated for a total of 1544 benchmarks. The data range for all measurements is between -12,51 and +3,70 mm/a with a mean of -0,57 mm/a and a standard deviation of 0,76. The histogram (Fig. 35) shows the percentage of the benchmarks in relation to the vertical velocity.

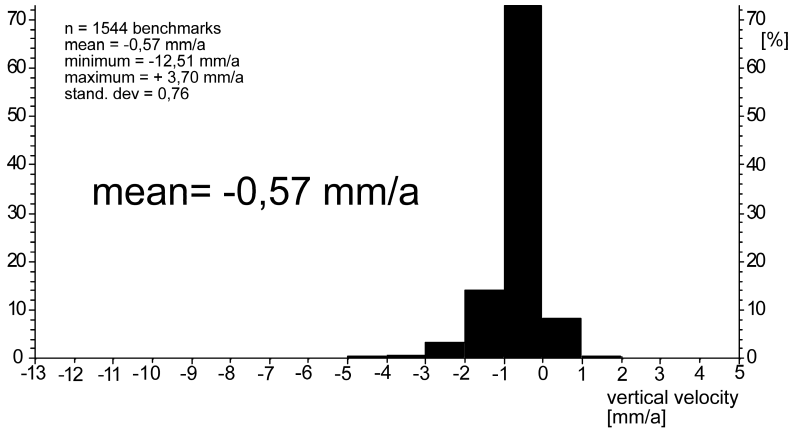

Fig. 35: The histogram shows the percentage of the benchmarks (n=1544) against the vertical velocity in [mm/a] with a class interval of one mm/a. After repeated geodetic fine-levelling (Norddeutsches Küsten Nivellement [NKN], between NKN 1 = 1928-1931 and NKN 3 = 1980). Data kindly provided by the LGN (Landesvermessung + Geobasisinformation Niedersachsen), (LGN, 2002).

The mean, nearly three-quarters (~73%), of the data points can be found in the class interval of 0 to -1 mm/a, about 14% in the interval of -1 to -2 mm/a , ~3% in the interval of -2 to -3 mm/a and less than 1% in the range of greater than –4 mm/a. About 8% are in the range of 0 to +1 mm/a and less than 1% in the range of greater than +1 mm/a. Consequently, subsidence is the dominating recent movement in the NW-German Basin. Fig. 36 shows the geographical position of the benchmarks. The black points present the position of benchmarks with a negative vertical velocity (the bigger the symbol size, the higher the negative velocity) and the yellow rectangles the position of benchmarks with a vertical velocity of ≥0 mm/a. The mean rate of vertical velocity for the coastal zone (green area) is –0,80 mm/a, which is nearly three times greater than those of the non-coastal zones (-0,24 mm/a). The study area (gray rectangle) shows with -0,21 mm/a a similar mean vertical motion as the non-coastal zone.

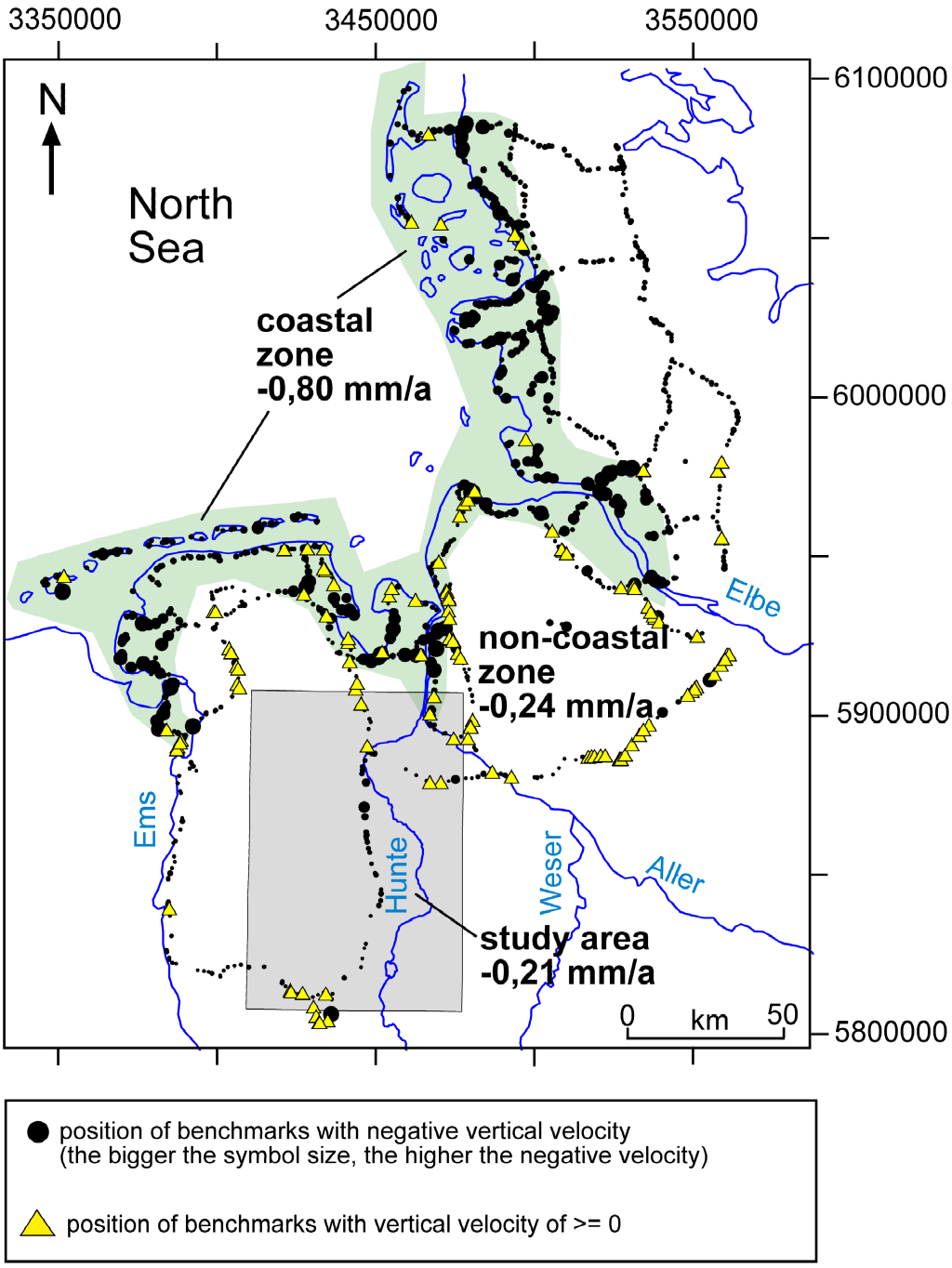

Fig. 36: The map of NW-Germany shows velocities of vertical motion, calculated from repeated geodetic fine-levelling. Database: Norddeutsches Küsten Nivellement (NKN 1 = 1928-1931) and (NKN 3 = 1980), data kindly provided by the LGN (Landesvermessung + Geobasisinformationen Niedersachsen), (LGN, 2002). The black points present the position of benchmarks with a negative vertical velocity (the bigger the symbol size, the higher the negative velocity) and the yellow triangles the position of benchmarks with a vertical velocity of ≥0 mm/a. The mean rate of vertical velocity for the coastal zone (green area) is –0,80 mm/a, for the non-coastal zones -0,24 mm/a and the study area (gray rectangle) -0,21 mm/a.

Summary of Chapter 1.2.

A mean recent vertical motion of –0,57 mm/ a was calculated from a repeated geodetic fine levelling of Northern Germany over a time span of 50,5 years (Fig. 35). With –0,80 mm/a the mean negative velocity of the coastal zones is clearly above the mean for Northern Germany (Fig. 36). The study area shows a recent movement of -0,21 mm/a (Fig. 35).

C.2. Sedimentation rates calculated from dated corings and outcrops

Absolute datings by OSL on clastic sequences and AMS ^{14}C on organic carbon rich sediments were obtained on outcrops and corings of the study area. Tab. 2 summarizes the AMS ^{14}C datings, Tab. 3 the OSL datings. A total of nine AMS ^{14}C samples have been measured ranging in age from >51 ka ^{14}C radiocarbon years BP to ~12,9 ka BP and a total of five OSL-datings in the range of 23-32 ka BP. The radiocarbon age conversion program (CALPAL, 2001) was used for the calibration of the ^{14}C ages into calendar years by using the data set CALPAL 2001 which is incooperated into the program. There are great uncertainties converting ^{14}C ages of older ~25 ka into into calendar years, because of geomagnetic field excursions during the Laschamp (~40-43 [cal] ka BP) and the Mono Lake event (~30-32 [cal] ka BP), (e.g. Voelker et al., 1998).

2.1. Outcrop Essemühle 1

The outcrop Essemühle 1 is positioned 850 m northwest of location Essemühle 2-4 (Fig. 12). The outcrop is of natural genesis, caused by a undercut slope of tributary 6E (Fig. 27). It is obvious in Fig. 37 a that the outcrop is about 5,5 m high.

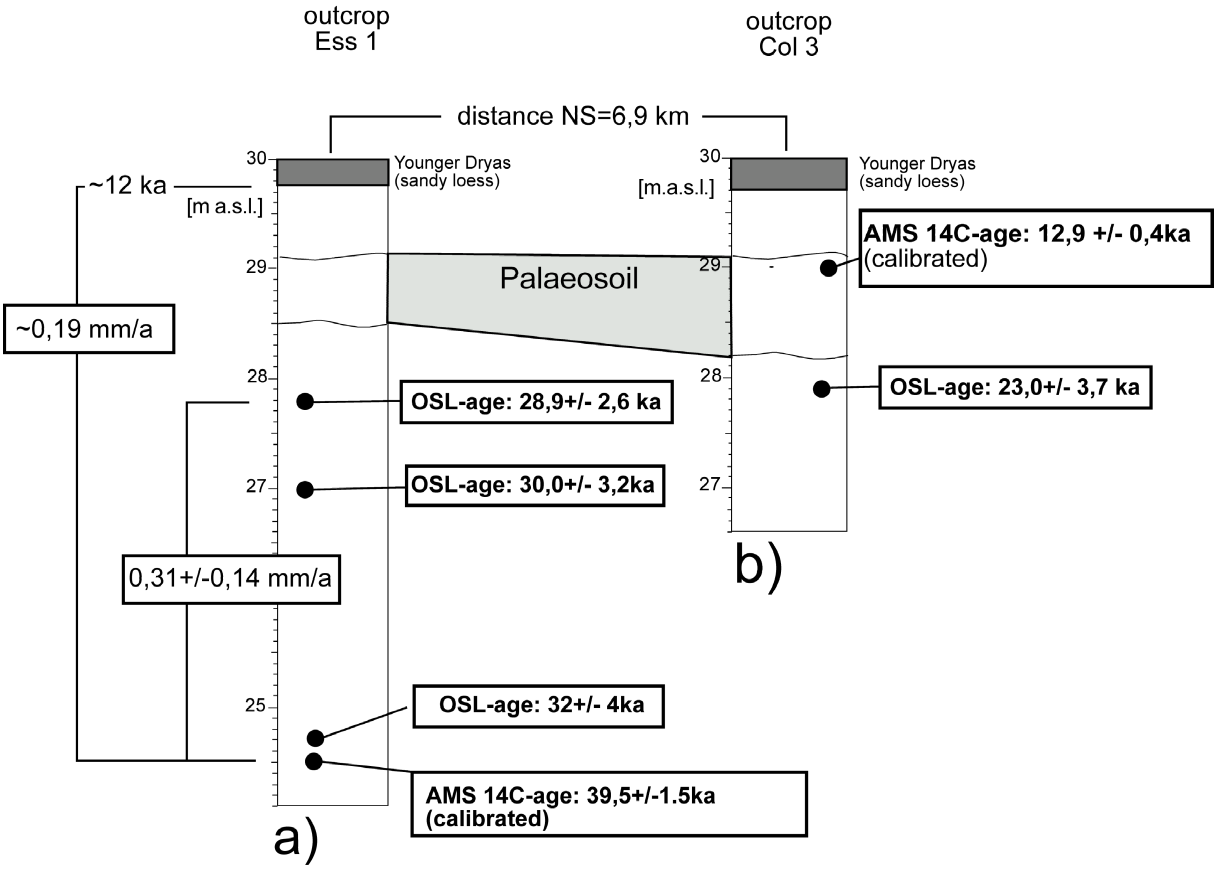

Fig. 37 a) Outcrop Essemühle 1 [Ess 1] on the Lower Weichselian Terrace of the river Hunte with position of AMS 14 C and OSL datings and calculated sedimentation rates,
b) outcrop Colnrade 3 [Col_3] with position of AMS 14 C and OSL datings. The geographical position of the outcrops is shown in Fig. 12.

Three OSL samples and one AMS ^{14}C sample have been measured. The AMS ^{14}C age of 39,5 +/-1,5 ka at 24,5 m a.s.l. was determined on seeds of the plant crowfoot (Tab. 2, lab code KIA 2945). A second age on the same sample was carried out on plant detritus (Tab. 2, lab code 2944). Both datings show nearly the same radiocarbon ages. Therefore, dating on plant detritus leads to reliable results. An OSL sample positioned at 24,70 m a.s.l.

(directly above the AMS ^{14}C sample) led to an age of 32,0 +/- 4 ka. Two OSL samples at 27,0 and 27,8 m a.s.l. were measured. The lower one shows an age of 30,0 +/- 3,2 ka, the upper one of 28,9 +/- 2,6 ka. A palaeosoil can be found on top of the outcrop (28,5- 29,1 m a.s.l.). The same palaeosoil is visible at the outrcop Colnrade 3 (Col_3), (Fig. 37 b). An AMS ^{14}C dating on a fossil single root led to a calibrated age of 12,9 +/- 0,4 ka (29,05 m a.s.l.), (Fig. 37 b). The carbon content of the AMS ^{14}C measurement was with 0,17 mg clearly lower than the minimum amount of 1 mg required for accurate dating (Tab. 2, lab code KIA 372). For this reason the presented age could be seen only as a value for orientation (P. Grootes, personal communication). The 1,15 m deeper positioned OSL-sample at 27,90 m shows an age of 23,0 +/- 3,7 ka., (Fig. 37 b). Based on the dating results and the sandy loess cover on top there is evidence for a Late Glacial age (Bölling, Alleröd) of the palaeosoil found at outcrop Colnrade 3 and Essemühle 1. Consequently, the base of sandy loess cover was set to an age of about 12 ka for the calculation of sedimentation rates. The sedimentation rate between the AMS ^{14}C age at the base of the outcrop (24,5 m) and the uppermost OSL age at 27,8 m is 0,31 +/-0,14 mm/a (Fig. 37 a). The error is relatively high because of the high error bars shown by OSL and AMS ^{14}C datings. The sedimentation rate between the outcrop base at 24,5 m and outcrop top at 29,8 m is about 0,19 mm/a.

2.2. Location Essemühle 2-4

The location Essemühle 2-4 can be found on the east side of the Lower Weichselian Terrace of the river Hunte, near tributary 6E (Fig. 27 a). The terrace surface is at 31,25 m a.s.l.. Fig. 38 shows the position of corings and the outcrop at this location. The pilot core Ess_3 with 10 m (Fig. 38 b) and the sediment core Ess_4 (Fig. 38 c) of 38 m depth were drilled on the footwall of outcrop Ess_2 (Fig. 38 a, 0 - +4 m). Sandy loess forms the top of this outcrop, probably of Younger Dryas age (~11 ka BP), (Meier, 1996). Frost fissures were detected inside horizontal bedded fluvial overbank deposits at a depth of about + 3 m, indicating a High Glacial age (24,0 - 14,5 ka BP). Bioturbation traces are visible on top of the outcrop immediately under the sandy loess layer, most likely formed under the warmer climatic conditions of the Late Glacial (Bölling, Alleröd). Based on the palaeoclimatic/lithological indicators and the absolute datings of the cores (Fig. 38 b, c) the top of the outcrop was set to a Late Glacial age of around 12 ka.

Four organic rich layers (containing plant detritus) were drilled by the pilot core Ess_3 (Fig. 38 b). Two AMS ^{14}C dates (black arrows) show a calibrated age of ~42,8 ka BP at a depth of 8,64-9,00 m and ~32,0 ka BP at a depth of 4,50-4,80 m. The sedimentation rate between the two layers is about 0,40 mm/a. The sedimentation rate between the dating at 8,64-9,00 m and the top of outcrop is with ~0,41 mm/a similar to those between the both AMS ^{14}C datings shown before.

The sediment core Ess_4 (Fig. 38 c, 0-38 m) which was drilled only a few meters from the pilot core Ess_3 contains four organic rich layers (1-4). Layer 1-3 were dated by AMS ^{14}C. Dating of layer 1 at a depth of 4,21-4,24 m resulted in a calibrated age of 32,8 +0,27/-0,26 ka BP, layer 2 at 8,52-8,58 m in a calibrated age of 47,0 +1,8/-1,5 ka. Dating of layer 3 at 9,74-9,75 m resulted in a ^{14}C age of >51 ka. This age is beyond the detection limit of the radiocarbon method. Two OSL samples, the first at a depth of 37,60-37,70 m and the second at 13,85-13,95 m were undatable, because of inadequate bleached sediments (M. Krebetschek, personal communication, 2002). Therefore, the absolute depositional age of the sediments below organic layer 2 is still unknown. Four further OSL samples (positioned below organic layer 2) are already prepared and ready for future dating. The sedimentation rate calculated between layer 1 and 2 is ~0,3 mm/a, between layer 2 and the top of outcrop Ess_2 ~0,35 mm/a.

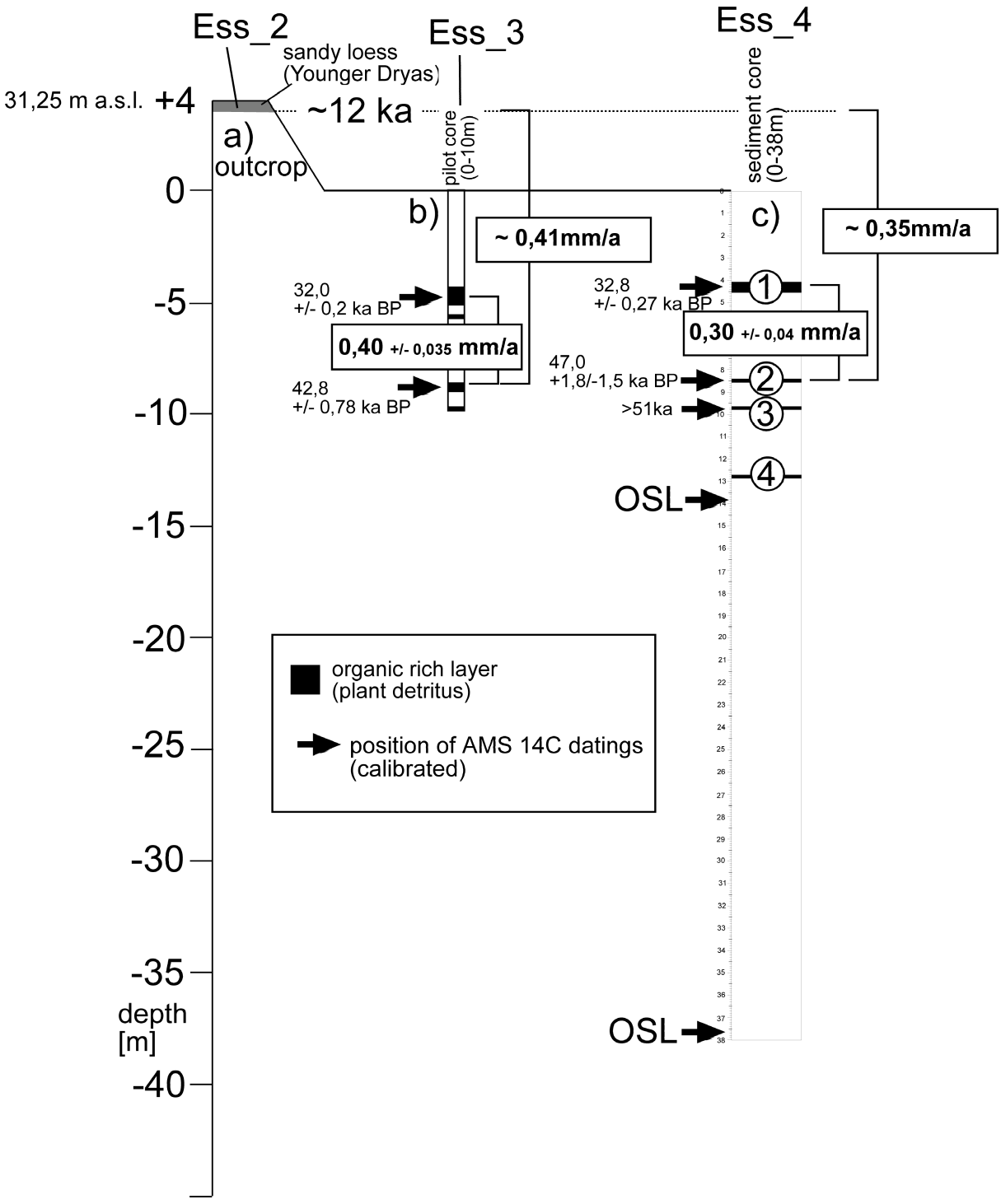

Fig. 38: Location Essemühle 2-4 on the Lower Weichselian Terrace of the river Hunte with position of a) outcrop Ess 2, b) pilot core Ess 3 (0-10 m) and c) sedimentcore Ess 4 (0-38 m). The positions of drilled organic rich layers are given in black, AMS ^{14}C and OSL dates by arrows. Sedimentation rates were calculated on basis of the dates. The geographical position of the outcrop and cores are shown in Fig. 12.

Summary of Chapter C.2.

All calculated sedimentation rates are in the range of about 0,2 – 0,4 mm/a.

D) Discussion

D.1. Evidence for tectonic geomorphology in the NW-German Basin: Correlations between modern landscape and geological subground

Potential driving mechanism for active tectonics in the NW-German Basin

It is evident from the distribution of the global seismicity that the majority of earthquakes is concentrated in the narrow belts of currently active plate boundaries. However, crustal deformation also occurs in the interior of the plates as evident by intraplate seismicity and geodetic measurements of vertical and horizontal crustal movements caused by crustal loading and epeirogeny processes (Brown and Reilinger, 1986; Harrison et al., 1999; Nelson et al., 1999; Talwani, 1999). Two endogenic forces, (1) crustal rebound (glacial unloading of the Weichselian ice cap) and (2) plate tectonic processes caused by [a] convergence of Africa-Eurasia, [b] North Atlantic sea-floor spreading (ridge-push), have the most potential to cause active crustal movements inside the NW-German Basin.

Glacial isostatic rebound

It is evident by repeated precise levelling data from Fennoscandia that the region is still subject to vertical uplift, caused by post glacial rebound of the earth crust (Bakkelid, 1986; Sharma, 1984), (Fig. 39, yellow isolines). Recent geodetic measurements (Global Positioning system [GPS], Very Long Baseline Interferometry [VLBI]) confirm the results of these earlier works on crustal uplift (James and Lambert, 1993; Milne et al., 2001). GPS measurements show a maximum uplift rate of 11,2 +/- 0,2 mm/a at the centre of doming at the site Umea (Sweden) and even a tangential (horizontal) divergence away from the centre of uplift in the order of ~1,0 mm/a (Milne et al., 2001). The glacio-isostatic adjustment of Fennoscandia enables modelling of the elastic flexing of the lithosphere, the viscous flow of the mantle and the study of processes associated with this crustal uplift like fracture formation, fault instability, seismicity and changes of the stress field inside and outside the formerly glaciated areas (Grollimund and Zoback, 2000; Gudmundsson, 1999; Johnston et al., 1998; Klemann and Wolf, 1998; Lagerbäck, 1990; Steward et al., 2000; Wahlström, 1993; Wolf, 1986; Wolf, 1987; Wolf, 1993; Wolf, 1996; Wu et al., 1999; Zoback and Grollimund, 2001). The recent generation of rebound models show that horizontal stresses can be transmitted over several hundred kilometers outside the formerly glaciated regions (i.e. well into northern Germany) and that these stresses are able to cause crustal deformation, fault instability and seismicity (James and Lambert, 1993; Johnston et al., 1998; Klemann and Wolf, 1998; Mitrovica et al., 1994; Wu et al., 1999). Fig. 39 shows that the study area (red rectangle) is ~150 km away from the maximum extent of the Weichselian ice sheet during the Last Glacial Maximum (LGM) about 20 ka BP. Consequently, the study area could be influenced by processes of glacio isostasy during both the glaciated Weichselian and the deglaciated Holocene time. During glacial times upper-crustal flexural upwarping occurs in the area of the ice-free foreland within the surrounding forebulge rim due to in-migration of sub-crustal material exuded from below the ice sheet (Steward et al., 2000). During deglaciation, the formerly glaciated area shows crustal uplift caused by the removal of the ice load which leads to elastic rebound, faulting and seismicity (Steward et al., 2000). Ductile flow of mantle material inside the formerly glaciated region must lead to a mass deficit in the area outside and possibly to a downwarping of the crust. It is evident by geodetic measurements (Fig. 39) that the process of crustal uplift of Fennoscandia is still going on and that NW-Germany is subsiding at about

-0,57 mm/a (Fig. 35, 36), probably caused by migration of mantel material into the area of recent Fennoscandian uplift.

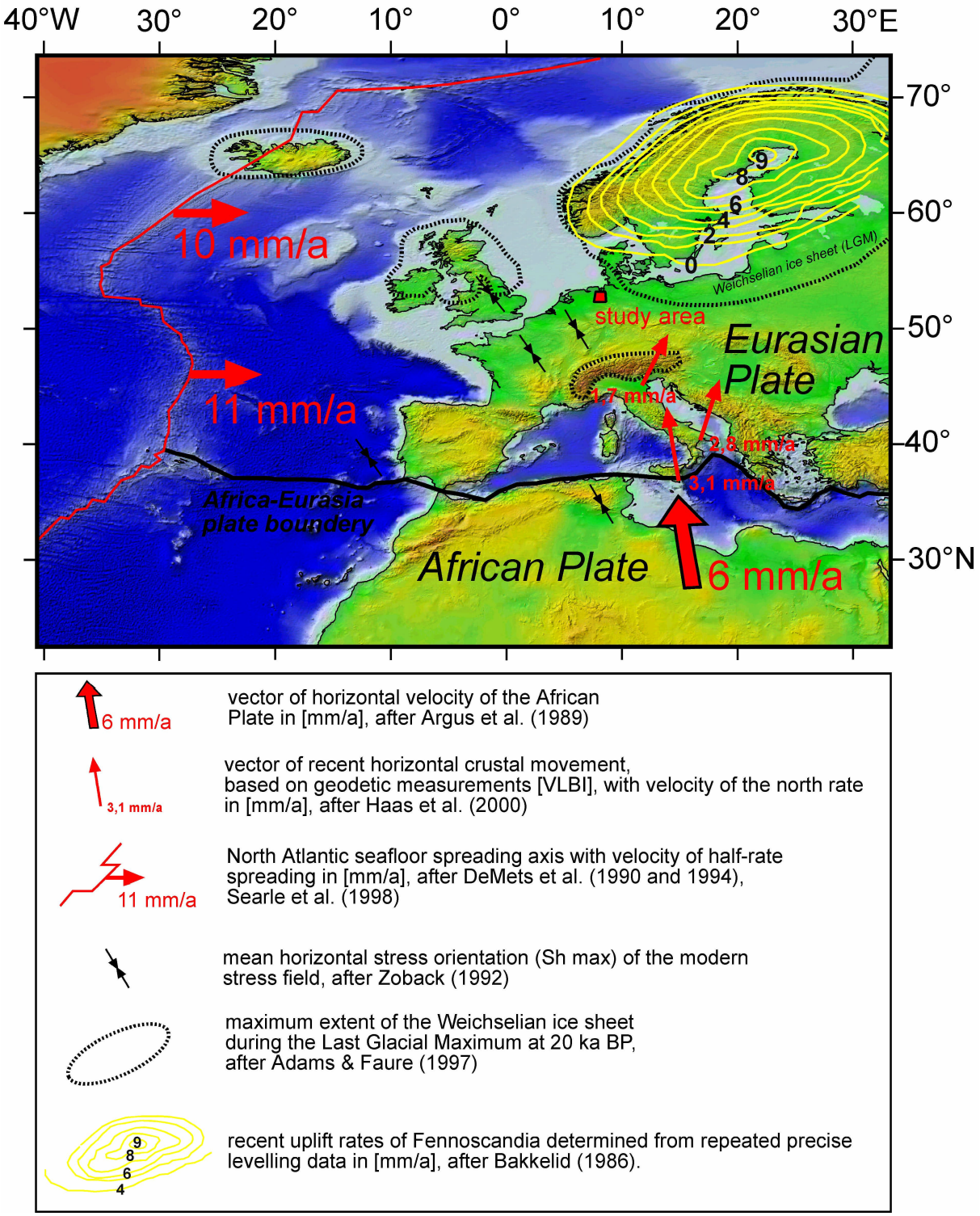

Fig. 39: Topographical and bathymetrical overview over northern Africa, Europe and the Atlantic ocean. The red motion vector shows the recent horizontal velocity of 6 mm/a of the African Plate relative to the Eurasian Plate (convergence) based on rotations around the Euler pole, (after Argus et al., 1989). The red line gives the position of the active Atlantic spreading ridge and transform faults with the total spreading rate of between 18-23 mm/a after the NUVEL-1A model (DeMets et al., 1990; DeMets et al., 1994; Searle et al., 1998). The red arrows give the recent horizontal crustal movement, based on geodetic measurements (VLBI), with velocity of the north rate in [mm/a], (after Haas et al., 2000). The doubled black arrows give the mean horizontal stress orientation (Sh max) of the modern stress field (after Zoback, 1992). The yellow iso-lines show the recent uplift pattern of Fennoscandia of maximal 9 mm/a, derived from precise relevelling campaigns, (after Bakkelid, 1986). The dashed line shows the maximum extend of the Weichselian ice sheet during the Last Glacial Maximum (LGM), (after Adams and Faure, 1997). The position of the study area is given by the red rectangle.

Plate tectonic processes, plate velocities and stresses in the lithosphere

Africa and Eurasia are still subject to convergence as evident from plate velocities which were derived from magnetic seafloor-spreading anomalies over a time span of the last 3 Ma and earthquake slip vectors (DeMets et al., 1990; DeMets et al., 1994; Minister, 1978). The counterclockwise rotation of Africa which results in a north to northwestward-directed push against Eurasia is caused by the higher spreading rate of the South Atlantic (~40 mm/a) compared with the lower one of the North Atlantic (~20 mm/a) which leads to a recent lithospheric shortening of about 5-6 mm/a in the area of the Mediterranean (Fig. 39, big red arrow). Beneath the evidence from the seafloor-spreading rates, present day seismicity of the Mediterranean region clearly outlines the collision zone between Africa and Eurasia (USGS, 2002). Current geodetic measurements of horizontal crustal movements based on space techniques ([VLBI], [GPS], Satellite Laser Ranging Measurements [SLR]) are in a good agreement with the present understanding of the geodynamic situation of the Mediterranean and central Europe (Anzidei et al., 2001; Bastos et al., 1998; Devoti et al., 2002; Kahle et al., 1998; Reilinger and McClusky, 1997). VLBI data shows that southern Italy moves at maximal ~3 mm/a northward (Fig. 39, small red arrows) which results in a northward orientated compressional strain between the VLBI-station Medicina (Italy) and Wetzell (Germany), (Campell and Nothnagel, 2000; Haas et al., 2000). This general compressive stress field postulated by the VLBI-data is consistent with local GPS-measurements from the region of the southern and western Alps which indicate a north-south shortening at rates of about 1-2 mm/a (Ferhat et al., 1998; Sue et al., 2000).

The World Stress Map Project has shown that these compressive lithospheric stresses can be transmitted from the plate boundaries over great distances into the continental and oceanic domains (Zoback, 1992; Zoback et al., 1989). The observed European broad-scale stress field could be simulated by modelling the North Atlantic seafloor-spreading in combination with the northward directed motion of the African Plate (Gölke and Coblentz, 1996; Grünthal and Stromeyer, 1992) and Richardson (1992) has shown for North America, western Europe and South America that the ridge torque correlates strongly with the absolute velocity of the plates and the intraplate stresses. Consequently, there is great accordance between the direction of recent horizontal crustal movements (based on geodetic observations [VLBI, GPS]), the estimates of current plate motions (based on global plate motion models [NUVEL 1A]) and the orientation of the modern stress field (World Stress Map Project). Nevertheless, there is still a debate as to which way the compressional stress field influences sedimentary basins (Cloetingh et al., 1995; Cloetingh et al., 1996; Cloetingh et al., 1994; Cloetingh et al., 1997; Cloetingh et al., 1993; Kooi and Cloetingh, 1989; Marshak et al., 1999; Ziegler et al., 1995; Zoback et al., 1993). One scenario which is still under discussion is lithospheric folding which causes broad-scale negative and positive deflections of the lithosphere and leads to upwarping of broad arches and basin subsidence (Bird and Gratz, 1990; Burov et al., 1993; Cloetingh and Kooi, 1992; Kooi et al., 1989; Kooi et al., 1991; Nikishin et al., 1993; van Wees and Cloetingh, 1996). The modern stress field of NW-Europe which was established during the Pliocene (Bergerat, 1987; Letouzey, 1986; Müller et al., 1992) led to broad scale negative deflection of the lithosphere in the area of the North Sea Basin (Cloetingh and Kooi, 1992) and to uplift of the Fennoscandian Shield (Ziegler, 1990) and it is suggested by (Ziegler, 1994) that the uplift of the Massif Central, Vosges-Black Forest, Bohemian Massif and Rhenish shield is connected with the development of the modern stress field. Fig. 40 shows a geological profile (EF) through the southern part of the study area, after Geotectonic Atlas of NW-Germany (Baldschuhn et al., 2001).

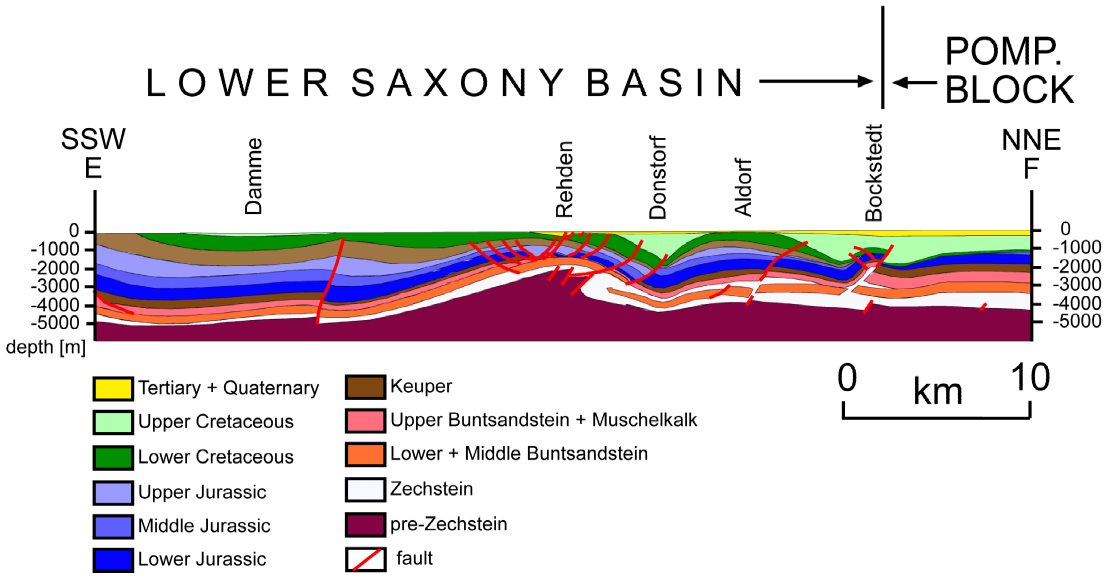

Fig. 40: Geological profile (EF), through a part of the NW-German Basin (Lower Saxony Basin, Pompeckj Block) from the pre-Zechstein (brown) to the Tertiary + Quaternary (yellow). The position of the profile is shown in Fig. 4. Faults are given in red, after Geotectonic Atlas of NW-Germany (Baldschuhn et al. 2001).

The position of the profile is given in Fig. 4. The profile crosses the inversional anticline structures Rehden, Aldorf and Bockstedt which show mostly gentle northward dipping overthrust faults. It is clearly visible that even the pre-Zechstein (brown) which can be found at a depth of between -5000 to -2000 m was affected by the Upper Cretaceous inversional phase. A relatively thin Zechstein layer (salts) of between ~100 and ~500 m is evident in the southern part of the profile which becomes thicker in the northern part of the profile. This Zechstein layer separates the pre-Zechstein (brown) from the upper tectonic story (Lower + Middle Buntsandstein to Quaternary). It is mentioned by (Faccenna et al., 1995; Kossow et al., 2000; Nalpas et al., 1995; Poblet et al., 1997) that Zechstein salts can act as a detachment layer by a process of decoupling. The modern horizontal compressional stress field which is orientated in the study area with 150° (Fig. 1) is probably able to cause fault reactivation or flexural doming of the already present anticlinal structures. There is evidence for tectonic geomorphology in the NW-German Basin as shown in this study by correlations between the modern landscape and the geological subground which will be discussed in following in more detail.

Correlations between the depth of the geological strata and the height of the modern topography

To investigate the depth/height relationship between the geological subground and the modern topography linear correlation coefficients have been calculated (Tab. 5, 6, 8, 9). A connection between the modern landscape and the geological subground is proven by the high linear correlation coefficients. What causes these high correlations? A non-tectonic and a tectonic mechanism is thinkable. The depth at the Base of Tertiary increases from about –200 in the south to –1000 m a.s.l in the north. The same northward orientated gradient is shown by the Hunte (Fig. 28 c, d). Potentially the sedimentary fill of the basin deeper parts in the north is still not finished. Thus, the S-N gradient could be caused by a non-compensated paleorelief which forces the Hunte to flow in a northerly direction. After this non-tectonic model the correlation between the depth at the Tertiary strata and the height of the Holocene Alluvial Plain is caused by a pure exogenic process of sedimentary fill of the given paleorelief without any tectonic influx on sedimentation.

Unlike the exogenic scenario (see above) one could also interpret that active tilting of the basin forces the Hunte to flow northward. There is evidence for Cenozoic tectonic subsidence in the North Sea Basin and uplift of the

adjacent mainland. Fig. 41 shows that the Central Graben of the North Sea is a depocentre for Cenozoic sediments (Ziegler, 1990).

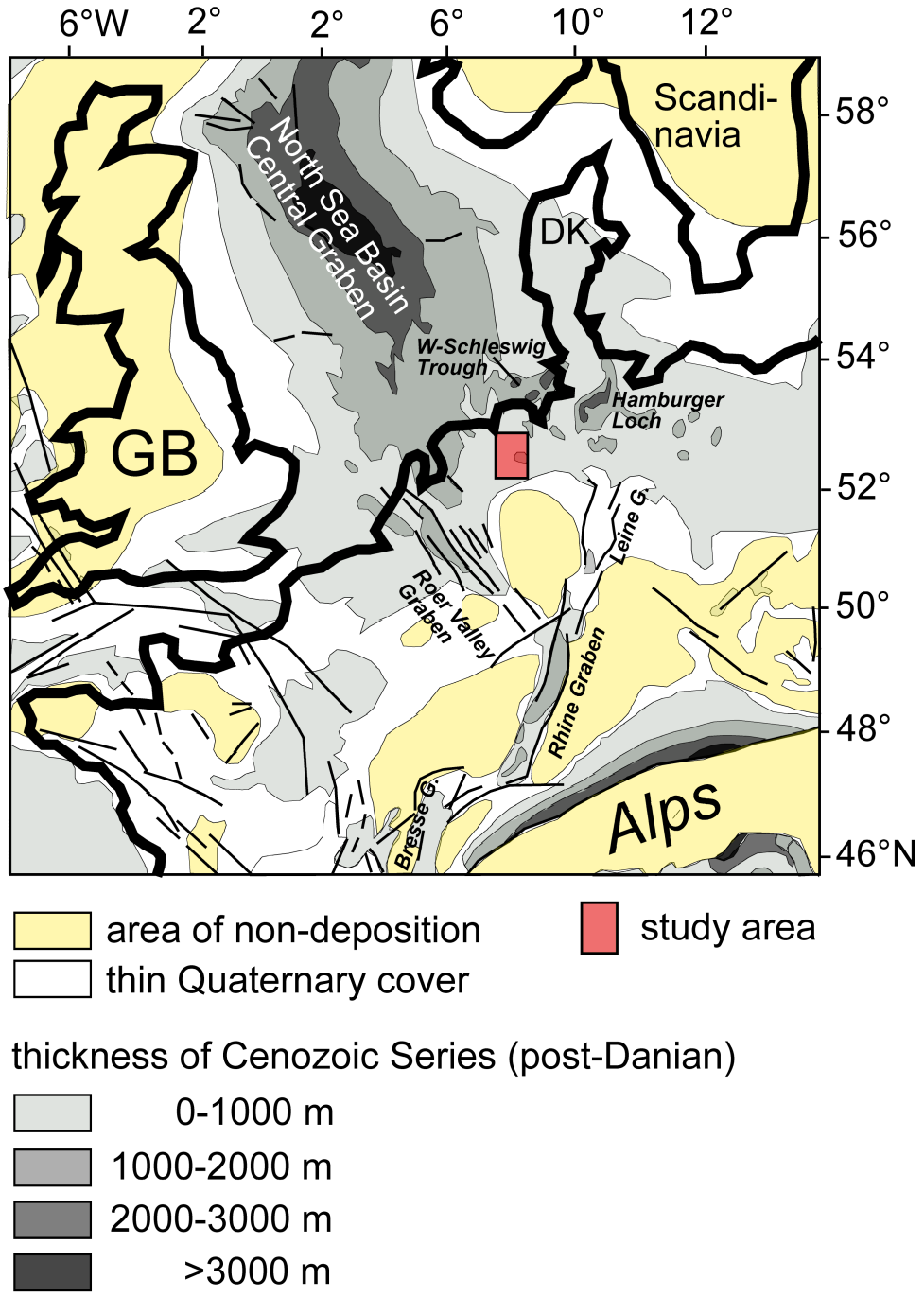

Fig. 41: Thickness of Cenozoic sediments (post Danian) from 0 to >3000 m, after Geological Atlas of Western and Central Europe, (Ziegler 1990). The position of the study area is given by the red rectangle.

The thickness of all Tertiary sediments increases towards the Central Graben and more than 3600 m of compacted sediments have been deposited in this axial zone, 1600 m alone during the time span Middle Miocene to Quaternary (Kockel, 1988), (Fig. 42).

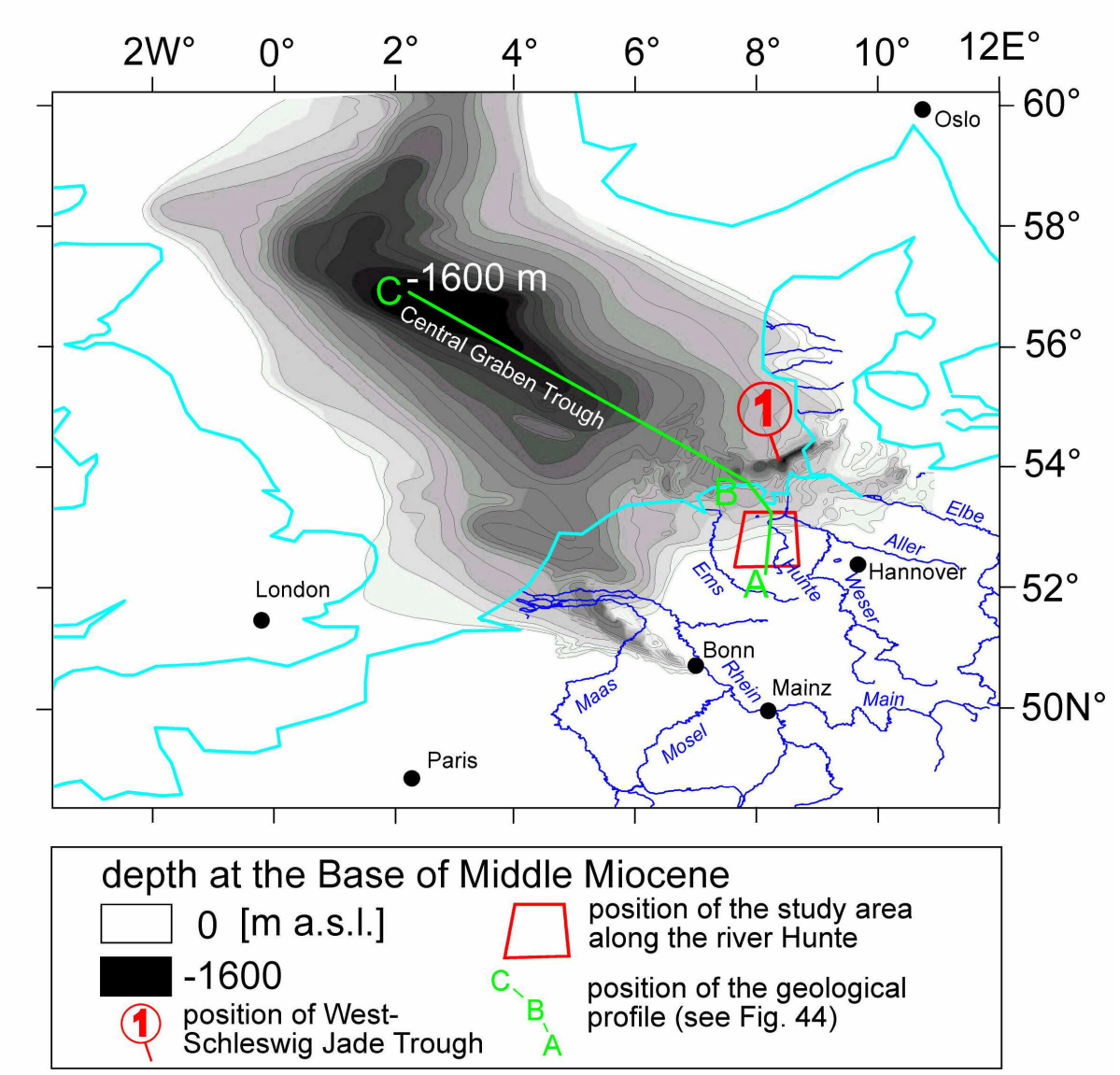

Fig. 42: Depth of the Base Middle Miocene from 0 (white) to -1600 m a.s.l. (black) after Kockel (1988). The position of the study area is given by the red rectangle and the position of the profile ABC by the green line (see Fig. 44).

Up to 1000 m of Quaternary sediments have been deposited at the southern tongue of the Central graben with a mean subsidence rate of about 0,5 mm/a (deposition of about 1000 m of Quaternary sediments over a time span of 1,8 Ma), (Caston, 1977), (Fig. 43).

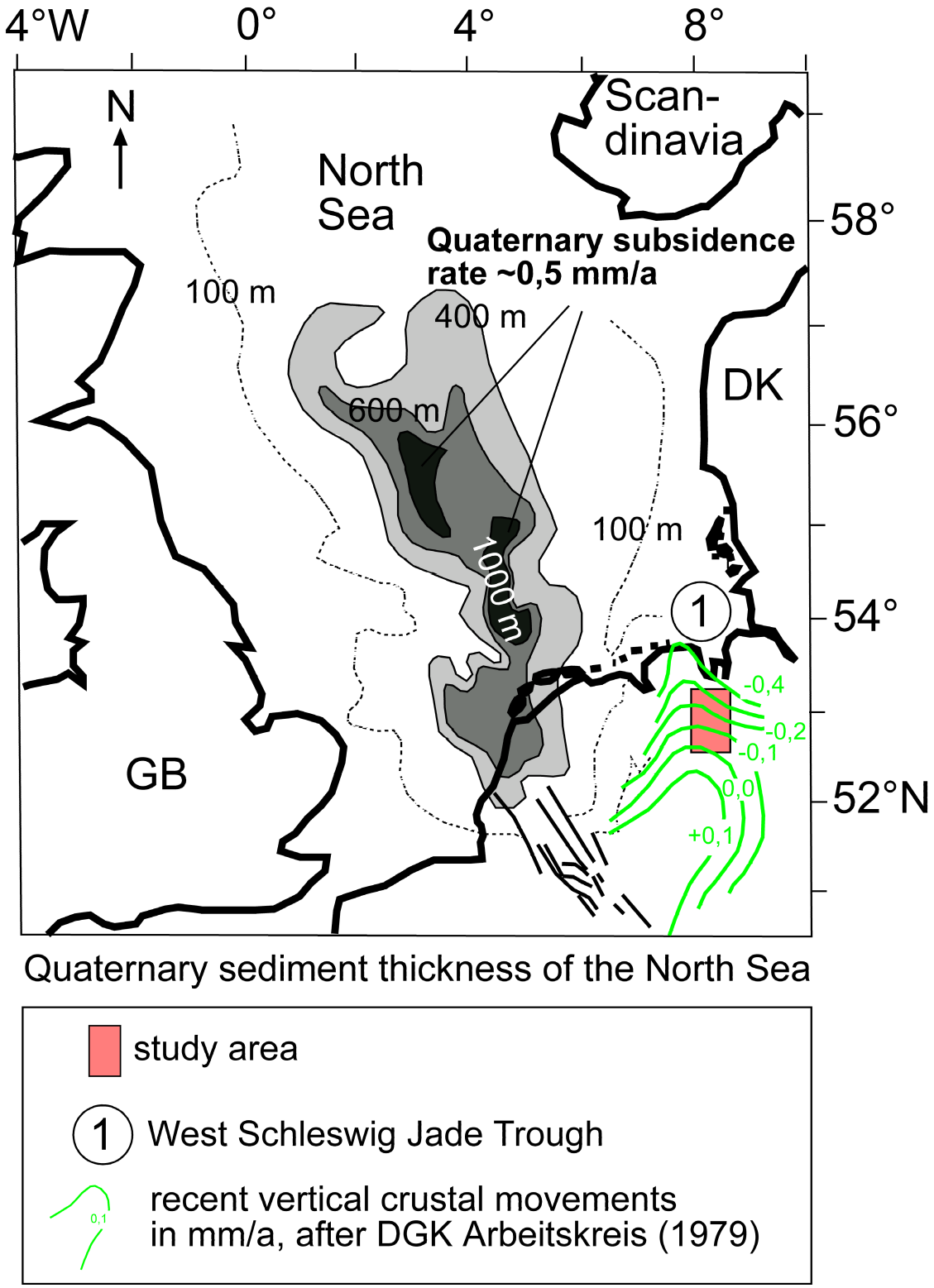

Fig. 43: Thickness of Quaternary sediments of the Southern North Sea from 100 m (dashed line) to 1000 m (black), (after Caston, 1977); the circled number 1 gives the position of the West-Schleswig-Jade Trough, position of the study area is given by the red rectangle, the green isolines show the rate of recent vertical movements from +0,1 to -0,4 mm/a (after DGK-Arbeitskreis, 1979).

The subsidence rate in the southern part of the North Sea area shows an acceleration during the Late Pliocene and Quaternary (Kooi et al., 1989; Kooi et al., 1991; Thorne and Watts, 1989; Zagwijn, 1989). This acceleration of subsidence in the North Sea Central Graben occurred well before the onset of the Quaternary with a ten-fold increase during the Late Pliocene relative to previous Tertiary rates (Kooi et al., 1991). The large Pliocene-Quaternary sediment thickness in the southern North Sea Basin is not caused by sediment infill of a Pliocene deep-water basin as suggested by (Sclater and Christie, 1980), because sediment infill is shallow marin (littoral and epineretic) or of continental facies (Kooi et al., 1991). Subsidence and sedimentation rates were nearly in equilibrum whereas subsidence never became so rapid to cause water depths of considerably more than 100 meters (Zagwijn, 1989).

Fig. 44 shows a longitudinal profile from the Osnabrücker Bergland (A) in the south over the North Sea coastal zone in the north (B) to the centre of Cenozoic subsidence at the North Sea Central Graben in the NW (C). The position of the profile which crosses the study area between profile point AB is shown in Fig. 42.

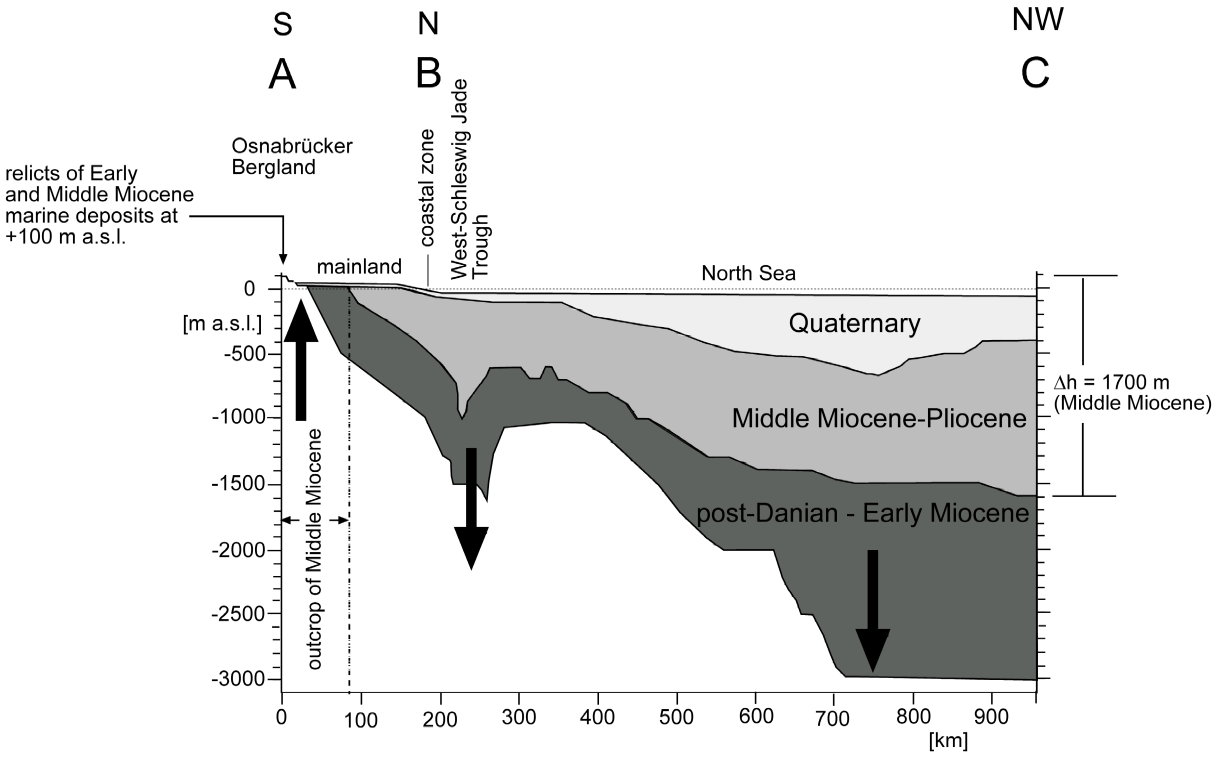

Fig. 44: Geological profile from A (Osnabrücker Bergland) over B (North Sea coast) to C (depocentre of Cenozoic sediments of the Central Graben). The depth of the Base Quaternary after Caston (1977), the depth of the Base Middle Miocene and the Base post-Danian after Kockel (1988). The geographical position of the profile is shown in Fig. 42.

Relicts of Early to Middle Miocene marine deposits can be found in the area of the Osnabrücker Bergland (Wiehengebirge) at a height of about +100 m a.s.l. (Anderson and Indans, 1969; Haack, 1932; Hiltermann, 1984; Hinsch et al., 1978; Hinze, 1979; Thiermann, 1970). At the West-Schleswig Jade Trough the depth of the Base Middle Miocene is about -1000 m (Fig. 42, red circle 1 and Fig. 44) and at the centre of the North Sea Central Graben about -1600 m (Fig. 42). The geological profile of Fig. 44 shows that the height difference of the Base Middle Miocene between the Osnabrücker Bergland in the south and the Central Graben in the north is about 1700 m and between the Osnabrücker Bergland and the West-Schleswig Trough about 1100 m. This increase of depth in a northerly direction can not be explained by changes of the paleo-bathymetry alone, because Middle Miocene sediments were deposited under shallower marine conditions (Hinsch and Ortlam, 1974). The relicts of

Early to Middle Miocene sediments which can be found in the area of the Osnabrücker Bergland prove that the Middle Miocene sea extended to the area of the Osnabrücker Bergland and probably even connected the North Sea with the Upper Rhine valley (Hinsch et al., 1978). Post-Middle Miocene uplift of the hinterland led to erosion of the formerly deposited marine sediments (Fig. 44, between profile distance 0-80 km), (Hinsch and Ortlam, 1974). This uplift continued during the Pliocene which led to sculpturing of the formerly low relief land surfaces (Gramann and Kockel, 1988). Whilst the hinterland was uplifted, the West-Schleswig-Jade Trough which can be found north of the estuary mouth of the river Weser and Elbe (Fig. 42, 43, 44) subsided strongly during the Miocene and continued to subside during the Pliocene (Gramann and Kockel, 1988). The West-Schleswig-Jade Trough was strongly affected by halocinetic movements as evident by the formation of deep rim synclines (Baldschuhn et al., 2001). However, these diapiric movements alone are unable to explain the total amount of subsidence, because most of the salt movements occurred already during the pre-Oligocene as evident by the rim syncline formation (Ludwig and Schwab, 1995).

There is evidence for neotectonic movement in the area of the North Sea and the coastal zone of the Baltic sea from height changes of marine Holsteinian and Eemian deposits during the Quaternary. Height differences of the top of marine Holsteinian are about 100 m between the North Sea and the Baltic Sea coast which results in a mean velocity of about 0,1 mm/a since the End of the Holsteinian Interglacial (Ludwig and Schwab, 1995). Post-Eemian crustal movements are proven by dislocations of Eemian marine terraces and deposits in the area of the marginal southern North Sea. A mean deformation rate of about 0,17 mm/a is evident by a maximal height difference of 20,5 m since the end of the Eemian (Streif, 1991). This rate is very similar to that of the long term subsidence rate of The Netherlands which is about 0,14 mm/a since the Eemain (Zagwijn, 1983). Streif (1991) suggests that a process of glacial rebound is responsible for the observable post-Eemian crustal movements in the North Sea area. Whilst the southern North Sea area subsided with maximal 0,50 mm/a over the past 1800 ka (Fig. 43, 45 a), the Rhenish Shield was uplifted over the last 800 ka with a mean vertical velocity rate of about 0,25 mm/a as evident by a maximum uplift of about 200 m of the Younger Main Terrace (Meyer and Stets, 1998), (Fig. 45 j). The magnitude of recent subsidence rates shown for the North Sea coastal zone (determined from repeated precise levelling data) is with 0,70 – 0,80 mm/a (Fig. 45 b, c) similar to those shown by the long term Quaternary subsidence or rate of –0,50 mm/a (Fig. 45 a). Fig. 43 shows contour isolines of recent crustal movements (green) which are crossing the study area (red rectangle), (determined from repeated precise levelling data), (after DGK-Arbeitskreis, 1979). A northward oriented gradient of increasing subsidence is visible from about 0 mm/a at the southern border of the study area near the Osnabrücker Bergland to –0,4 mm/a at the northern part near the coastal line of the North Sea. This northward oriented gradient of modern crustal movements fits well with the long term observed post-Miocene northward tilting (Fig. 44).

The examples given above demonstrate that crustal movement in the North Sea and marginal regions persisted over the entire Cenozoic period until today. Consequently, there is no evidence for tectonic quiescence during the Tertiary and Quaternary. Thus, it seems unlikely that the high correlations between the depth of the Tertiary strata and the modern topography were caused by a pure exogenic process of sedimentary fill of the given paleorelief without any tectonic influx on sedimentation. More likely, a process of northward tilting caused by uplift of the hinterland (Wiehengebirge [Osnabrücker Bergland]/Rhenish Massif) and subsidence of the North Sea area persists until today and forces the river Hunte to flow in a northerly direction.

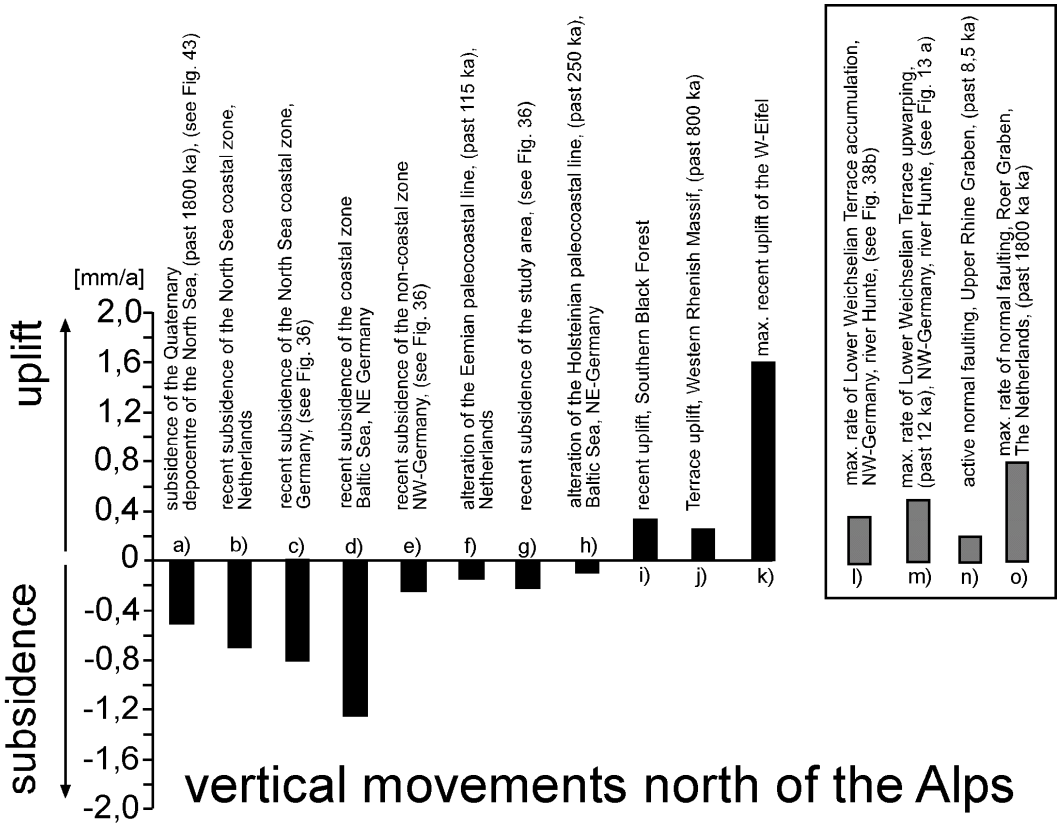

Fig. 45 a-k) velocity rates of vertical movements (subsidence/uplift) north of the Alpine deformation front during the Quaternary,
a) subsidence rate of the North Sea Quaternary depocentre [-0,50 mm/a] during the past past 1800 ka , database: (Caston, 1977), (see Fig. 41);
b) recent subsidence rate of the North Sea coastal zone, The Netherlands, [-0,70 mm/a], determined from repeated precise levelling data, (after Kooi et al., 1998);
c) recent subsidence rate of the North Sea coastal zone, Germany [-0,80 mm/a], determined from repeated precise levelling data, database: (LGN, 2002), (see Fig. 36);
d) recent subsidence rate of the coastal zone, Baltic Sea, NE-Germany, [-1,25 mm/a], determined from repeated precise levelling data, (after Ihde et al., 1987);
e) recent subsidence rate of the non-coastal zone, NW-Germany, [-0,24 mm/a], determined from repeated precise levelling data, database: (LGN, 2002), (see Fig. 36);
f) post-Eemian subsidence rate of North Sea coastal-zone, The Netherlands, [-0,14 mm/a], determined from alterations of the Eemian paleocoastal line, (after Zagwijn, 1983);
g) post-Holsteinian coastal subsidence rate of the Baltic Sea, NE Germany, [-0,10 mm/a], determined from alterations of the Holsteinian paleocoastal line, (after Ludwig and Schwab, 1995);
h) recent maximum uplift rate of the Southern Black Forest [+0,33 mm/a], determined from repeated precise levelling data, (after Demoulin et al., 1998);
i) uplift of the Western Rhenish Massif at Cochem during the past 800 ka [+0,25 mm/a] , determined from Terrace uplift, (after Meyer and Stets, 1998);
j) maximum recent uplift rate of the West-Eifel [+1,60 mm/a], determined from repeated precise levelling data, (after Mälzer et al., 1983);
k) recent subsidence rate of the study area [-0,21 mm/a], determined from repeated precise levelling data, database: (LGN, 2002), (see Fig. 36);
l) max. rate of Lower Weichselian Terrace accumulation, river Hunte, Lower Saxony, [0,40 mm/a], (see Fig. 38 b);
m) max. rate of Lower Weichselian terrace warping during the past 12 ka, river Hunte, Lower Saxony, [0,50 mm/a], (see Fig. 13 a);
n) rate of active normal faulting in the Upper Rhein area [0,21 mm/a] during the past 8,5 ka, (after Meghraoui et al., 2001);
o) max. rate of active normal faulting in the Roer Valley Graben [0,80 mm/a] during the Quaternary (~1,8 Ma), (after Geluk et al., 1994).

Correlations between orientations in the modern landscape and the orientation of the Base Tertiary

The Base of Tertiary shows two preferred orientations I=E-W (0-5°) and II=N-S (90-95°). The same preferred orientations can be found in the investigated elements of the modern landscape (steep slopes, lakes and depressions, topography and the fluvial system), (Fig. 17, Fig. 19; red cross inside rose diagrams). The orientation of the modern landscape correlates with the orientation of the Base of Tertiary basin geometry. Lakes and depressions show with r^2=0,78 the highest correlation with the Base of Tertiary (Tab. 7 cell "AC" and Fig. 18 b). There is a high correlation between the orientation of the different elements of the modern landscape.

The highest correlation can be found between the steep slopes and the lakes and depressions (r^2=0,90, Tab. 7 cell “BC” and Fig. 18 e). There is also a high correlation between spatially different investigated areas regarding the orientation of morphological elements of the modern landscape (Fig. 19, Fig. 20).

Which process(es) is (are) able to cause similarities in orientation between (1) the Base Tertiary and the modern landscape, (2) different elements of the modern landscape and (3) spatially different areas regarding morphological elements of the modern landscape? It seems unlikely that they were caused by the glacial processes of Saalian times, because 130000 years have passed since the last ice coverage and the relief was strongly modified during that time. Most depressions (e.g. dead ice holes) should have already filled with sediment during the Weichselian or their shape must be strongly modified. Because the investigated morphological structures are still influenced by exogenic processes, their orientation must be regarded as recent/subrecent.

Subrosion as a controlling factor can be excluded. Subrosional processes (visible at the earth surface) are only possible above salt structures with a position near the earth surface (Lehne, 2001; Ortlam and Schnier, 1981; Seelos, 2000). The salt dome "Saager Meer” can be found with a depth of about 125 m near the earth surface, but covers only 2% of the investigated area (Fig. 4). Thus, the surface area which is potentially influenced by subrosion is too small to cause the correlations and preferred orientations of the modern landscape.

The Base of Tertiary was clearly affected by halokinetic processes as evident by the rise of salt structures and the formation of peripherial rim synclines (Appendix, Fig. 6: Base Tertiary). Thus, halokinetic processes have the potential to cause the correlations between the orientation of the Base Tertiary and the modern landscape.

The fluvial system shows with r^2 = 0,55 the lowest linear correlation with the Base of Tertiary (Tab. 7 cell “AE” and Fig. 18 d). The fluvial system is permanently changing its course by meandering. Most likely this random process is responsible for the low correlation. Steep slopes are connected with the fluvial system, because they mark the transition zone between the Holocene Alluvial Plain and the Lower Weichselian Terrace/Saalian deposits (compare Fig. 7 with Fig. 8). The steep slopes show in contrast to the fluvial system with r^2=0,72 a high correlation with the Base of Tertiary (Tab. 7 cell “AB” and Fig. 18 a). Thus, the orientation of the steep slopes [based on historical topographical map (LGN, 1898)] shows indirectly that the fluvial system is also connected with the orientation of the Base of Tertiary.

There is a high correlation between spatially different investigated areas regarding the orientation of morphological elements of the modern landscape (Fig. 19, Fig. 20). The area of the whole study is, with 6750 km^2, about 10 times bigger than the part of the Hunte catchment basin with 625 km^2. The steep slopes show a linear correlation coefficient of r^2=0,93 between the whole study area and the part of the Hunte catchment basin (Fig. 19 cell AC, Fig. 20 a), the lakes and depressions of r^2=0,94 (Fig. 19 cell BC, Fig. 20 b), the topography of r^2=0,74 (Fig. 19 cell CC, Fig. 20 c) and the fluvial system of r^2=0,32 (Fig. 19 cell DC, Fig. 20 d). Consequently, the high linear correlation coefficients between morphological elements of the modern landscape is a general pattern and not only restricted to the local scale, indicating that a higher ranking process is acting. These similarities are unlikely to be caused by fluvial erosion, because the same high correlations are shown by the lakes and depressions which are closed structures and independent of fluvial erosion.

Based on the results of this study, tectonics have most likely caused the correlations and preferred orientations found in the modern landscape. Exogenic processes like glacial processes and fluvial erosion could be excluded, because ice did not reach the investigated area since ~135 ka. Tectonic processes have the potential to cause

nearly identical orientations on local and regional scale and to influence modern topography in the Hunte area [see similar results of (Eyles et al., 1997; Scheidegger, 2001; Scheidegger, 1981; Scheidegger, 2002)].

Warping of the Lower Weichselian Terrace and Holocene Alluvial Plain

Several studies of fluvial behaviour have shown that crustal movements are able to cause uplift/upwarping of fluvial terraces (e.g. Antoine et al., 2000; Burbank and Anderson, 2001; Burnett and Schumm, 1983; Holbrook and Schumm, 1999; Houtgast et al., 2002; Keller and Pinter, 1996; Krzyszkowski and Stachura, 1998; Maddy et al., 2000; Marple and Pradeep, 2000; Marple and Talwani, 1993; Molnar et al., 1994; Ouchi, 1985; Schumm, 1986; Schumm and Spitz, 1996; Zuchiewicz, 1998). The height of the Lower Weichselian Terrace above the Holocene Alluvial Plain changes along the course of the Hunte. A maximum offset of 5,9 m is visible at the transition zone from the Lower Saxony Basin to the Pompeckj Block (Fig. 13 a, c). Knowing the age of the terrace surface or a geological marker horizont inside the terrace body and the amount of terrace offset, mean rates of terrace upwarping can be calculated between the time the terrace became inactive and the present. The Lower Weichselian Terrace of the Hunte was dated by OSL and AMS ^{14}C (Fig. 32 c, 37, 38). Based on these datings and lithostratigraphic correlations the surface of the Lower Weichselian Terrace was set at an age of about 12 ka (Fig. 13 a). This results in an average vertical warping velocity of about 0,5 mm/a since about 12 ka BP (5900 mm/12.000 a = 0,5 mm/a) at the position of maximum terrace offset (Fig. 13 a, segment 60-70). This post Late Glacial terrace warping velocity is in the magnitude of vertical crustal movements north of the Alps as shown by repeated precise levelling data (Bankwitz, 1976; Demoulin et al., 1998; Demoulin et al., 1995; DGK-Arbeitskreis, 1979; Ihde et al., 1987; Kooi et al., 1998; Leonhard, 1988; Mälzer et al., 1983; Schwab, 1981; Schwab et al., 1973; Van den Berg et al., 1994; Wübbelmann, 1993), active normal faulting in the Upper Rhine Graben and the Roer Graben System (Geluk et al., 1994; Meghraoui et al., 2001), alterations of paleocoastal lines (Ludwig, 1995; Ludwig and Schwab, 1995; Streif, 1991; Zagwijn, 1983) and Quaternary subsidence of the North Sea (after Caston, 1977) which are mostly in the range of < 1,0 mm/a, (Fig. 45). The zone of Lower Weichselian Terrace uplift is covered by aeolian sandy loess of Younger Dryas age (Fig. 2). It is unlikely that this additional sediment cover has caused the offset, because the thickness of the sandy loess cover is between 0,5-1,0 m and is seldom above 1,0 m (Meier, 1996). Consequently, the offset of the Lower Weichselian Terrace is caused by endogenic forces.

A further argument in this direction comes from the observation that the Holocene Alluvial Plain of the Hunte shows a negative gradient near the village "Glane" (Fig. 29 a, b) which is most likely not caused by an additional sediment input of a Hunte tributary. Tributary 17W is the first tributary south of the rise and flows at segment number 90 into the Hunte (Fig. 29 a). Thus, the rise of the Holocene Alluvial Plain must start at this point, because sand-sized clastic material transported by tributary 17W would be deposited at the estuary. Finer material (clay, silt) is transported as suspension load longer distances before deposition. Also the existence of the knickpoint at the position of confluence contradicts the assumption that aggradation causes the rise of the Holocene Alluvail Plain, because a negative gradient should be visible north of segment 90 (Fig. 29 a). It is evident by field work that the negative gradient is not caused by a lithological change from a sandy river bed to a bed formed by more resistent morainic deposits.

Active uplift could be the reason for the rise, because the Hunte crosses a doming caused by the salt pillow "Dötlingen". This dome can be traced over a vertical distance of about 4000 m from the Base of Zechstein at a depth of –4100 m a.s.l. to the Base of Middle to Upper Oligocene [-100 m a.s.l.], indicating that this structure

was demonstrably active until the Upper Tertiary, (Fig. 13, gray marker 4; Fig. 30, red circle). Ongoing doming forces the river to incise deeper into the uplifting Holocene Alluvial Plain. The fact that above the dome the Holocene Alluvial Plain is smallest (Fig. 28 a, arrow 95) and the Lower Weichselian Terrace is warped up speaks for this process (Fig. 13 a, c gray marker 4). If halokinetic processes caused the uplift, movements at the depth of the Zechstein must be able to transform to the earth´s surface over a vertical distance of about 4000 m. The observation that the Lower Weichselian Terrace and the Holocene Alluvial Plain of the Hunte is upwarped indicates that endogenic forces still influence the modern topography.

Connection between terrace formation and vertical crustal movements

Laboratory studies and field work show that fluvial systems react with accumulation and widening of the alluvial plain by crossing an area of relative subsidence and start to incise on the other hand above zones of uplift whereas terraces are formed (Ouchi, 1985). A Lower Weichselian accumulation terrace is evident along the course of the river Hunte. Is there a connection between vertical crustal movement and the formation of this terrace? It could be shown by repeated geodetic fine levelling that mean recent vertical movements for NW-Germany are in the order of -0,57 mm/a (Fig. 35, 36). With -0,24 mm/a the non-coastal zones show a subsiding tendency. It is unlikely that this general subsidence pattern is primarily caused by consolidation of alluvial sediments/peats, because the non-coastal zones were formed predominantly by Quaternary deposits with low values of settlement (morainic deposits, meltwater sands, Lower Terrace sediments [sands]). Extraction of oil, gas and groundwater is able to cause an increase of subsidence on a local scale but is unlikely to cause the general pattern of subsidence on a regional scale (Prinz, 1997). Theoretical predicted rates of present land subsidence due to compaction of Cenozoic sediments are in the order of 0,1 mm/a as calculated for the Netherland region (Kooi et al., 1998). Provided that this rate is comparable with the region of the NW-German Basin a residual of about -0,14 mm/a would remain even for the non-coastal zone, most likely caused by endogenic processes. For these reasons it appears likely that the vertical velocities are an expression of recent crustal movements. This assumption is supported by the observation that velocity rates, calculated by repeated geodetic fine levelling in the northern area of the former German Democratic Republic and the Netherlands are in the same order as shown in this work (Bankwitz, 1976; Ihde et al., 1987; Kooi et al., 1998; Schwab, 1981; Schwab et al., 1973; Van den Berg et al., 1994) and that subsidence rates, calculated on the basis of different data and time spans but for the same area show similar results as presented in this study (DGK-Arbeitskreis, 1979; Leonhard, 1988), (Fig. 45).

The mean recent vertical movement of the study area is with -0,21 mm/a (Fig. 36) in the order of the sedimentation rate calculated for the Lower Weichselian Terrace (0,2 - 0,4 mm/a), (Fig. 37+38). This similarity indicates a connection between the recent subsidence rate calculated from the repeated precise levelling data and the velocity of Lower Weichselian Terrace aggradation. The general subsidence pattern could be a precondition for terrace accumulation, provided that the recent subsidence rate is nearly equivalent to the long term pattern of Quaternary subsidence. That means, terrace formation could be caused by subsidence. The Roer Valley Rift System (The Netherlands) is an example for the interfingering of long term subsidence pattern and fluvial deposition. Here, subsidence of the Roer Valley Graben led to deposition of thick Pleistocene fluvial deposits of the Maas and Rhine (Geluk et al., 1994; Houtgast and van Balen, 2000). Beside tectonism, fluvial systems react to climatic fluctuations like Glacial/Interglacial cycles by aggradation/incision (Vandenberghe, 1995b), but these climatic circles influencing fluvial behaviour could be overlayed by a long term tectonic signal (e.g. Antoine et

al., 2000; Houtgast et al., 2002; Maddy et al., 2000). Fig. 38 b (core Ess_3) shows that the sedimentation rate of the Lower Weichselian Terrace of the Hunte is about 0,40 mm/a between 42,8 and 32 ka BP (Δt=~13,0 ka). Nearly the same sedimentation rate of 0,41 mm/a is shown between 42,8 and about 12,0 ka BP (Δt=~30,0 ka). A similar picture is given by the core Ess_4 (Fig. 38 c). Here the sedimentation rate between 47,0 ka and 32, 8 ka is about 0,30 mm/a (Δt=~14,0 ka) and about 0,35 mm/a between 47,0 and 12 ka BP (Δt= ~35,0 ka). Consequently, fluvial sedimentation rates are nearly constant over different time spans. During these investigated intervals climate has changed rapidly over Northern Europe (Bond et al., 1997; Bond et al., 1992; Bond and Lotti, 1995; Dansgaard et al., 1993; Grootes et al., 1993; Grousset et al., 1993; Huijzer and Vandenberghe, 1998). These climate changes have affected river hydrology, morphology and sediment supply (Mol et al., 2000; Van Huissteden and Vandenberghe, 1988; Vandenberghe, 1992a; Vandenberghe, 1993; Vandenberghe, 1995b) and should therefore influence the sedimentation rate of the Lower Weichselian Terrace sediments. The fact that no change of the mean sedimentation rate is observable during times with a highly variable climate in northern Europe (Dansgaard-Oeschger Cycles) speaks for a long term subsiding tendency at the location Essemühle 2-4. This hypothesis is confirmed by the observation that the location Essemühle 2-4 is positioned at the southern border of the Bockstedt Graben (Fig. 27 a). Immediately north of location Essemühle 2-4 the Lower Weichselian terrace of the Hunte rises in respect to the Holocene Alluvial Plain, the valley gets smaller and the Hunte changes its flow direction (Fig. 24 a, b, d, e, f, gray marker 3). All these anomalies focus above the inversional structure Norddöllen (Fig. 4) which is part of the Bockstedt Graben Lessen-Staffhorst Block (Fig. 3, letter E). This inverted block, which separates the Lower Saxony Basin from the northerly adjacent Pompeckj Block, shows the highest topography of all investigated basement blocks (Fig. 15 letter E). Even the topography of the east and westward watershed is highest by crossing this block (Fig. 21+22, gray marker 1). This suggests that active uplift led to upwarping of the terrace, incision of the river and narrowing of the terrace width. Whilst the inversional structure Norddöllen was relatively uplifted, the area south of it subsided continuously which led to a permanent accumulation of fluvial sediments independent of short time climatic perturbations.

Depression on the Lower Weichselian Terrace

A small scaled depression with a maximum depth of about 2 m was investigated by Georadar, Reflection Seismic, drilling and dating of sediments (OSL and AMS ^{14}C), (Fig. 11 b). It is evident by field work that the structure is of geological origin (Fig. 31-34). The depression is positioned above the southern flank of the salt structure "Dötlingen" near the village "Glane" (Fig. 30). Which process caused this depression?

The depression is not a Saalian dead ice hole, because it is positioned on the Lower Weichselian Terrace of the river Hunte as evident by an OSL dating from outside the structure (Fig. 32 c). Small scaled depressions which can be found in Northern and Middle Europe in formerly periglacial areas are interpreted as remnants of Pingos (Bijlsma and De Lange, 1983; De Gans, 1982; De Gans and Sohl, 1981; Garleff, 1968; Lade, 1980; van der Meulen, 1988; Wiegand, 1965). It is known from recent permafrost areas that pingos occur mainly in areas of continuous permafrost, and, to a lesser extent, in areas of discontinous permafrost (Gurney, 1998; Mackay, 1988). However, fine laminated organic rich sediments of a Pleniglacial age were drilled from the centre of the depression (dated by AMS ^{14}C, ~32 ka BP), (Fig. 32 c), showing that the Pleniglacial and Late High Glacial could be excluded as a formation time, because the lamination would be destroyed by the growing ice body of the Pingo. Consequently, only the Early High Glacial (OIS 4, 72-62 ka) remains as a formation time. Even if a Pingo of Early High Glacial age has caused the structure, the question remains why the depression was not

completely filled with sediment by the aggrading Paleo-Hunte during later stages and is still visible in the modern landscape after ~60.000 years. A criteria for the identification of a pingo remnant is the presence of a rampart outside the depression, built up by unsorted material, derived from outward transport of material from the higher elevated ice body (Mackay, 1988). However, no rampart is morphologically visible. Well sorted medium sands were drilled in the periphery of the depression showing that no buried rampart is present which was possibly covered by younger sediments (Fig. 31 a, 32 c). Consequently, there is no morphological and geological indication that the depression Gla_1 represents a pingo remnant.

Solution processes are most likely not responsible for the formation of the depression, because Tertiary sandy sediments have a low solutional capacity (Ortlam, D., personal communication 2002). The calcerous and solvable sediments of the Upper Cretaceous can be found at a depth of about -450 m a.s.l., most likely too deep to cause a small scaled depressions at the earth surface (Fig. 34). Settlement of a peat layer is able to cause a depression at the earth surface, but no thicker peat layer was drilled (pilot core Gla_1, 0-14m). If a peat layer exists at a depth of >14 m it must be of Eemain age (115-130 ka), because only during this interglacial period climatic conditions were favourable for the formation of a thicker peat layer. Lade (1980) investigated twelve-small scale depressions in the area of the Bremervörder-Wesermünder Geest (north of Bremen): five of them were filled with Eemian peat. The basal depth of these Eemian peat layers can be found between 5 and 9 m below the surface and the thickness varies between 1 and 3 m. The organic rich layer of core Gla_1 P83, which is of a Pleniglacial age (about 32 ka), can be found at a depth of 7 m below the surface (Fig. 32 c). In view of these discrepancies between the depth of the Eemian peat layers proven by Lade (1980) and the depth of the organic rich layer of Pleniglacial age evident in this study, it seems unlikely that an Eemian peat layer exists at a depth greater than 14 m. However, even if such an Eemian peat body exists at a depth greater than 14 m, settlement should have already been closed up during the Pleniglacial, because a minimum column of 7 m of sediments covered this hypothetical Eemian peat over a minimum time span of a about 32 ka. Consequently, the depression is most likely not caused by settlement and/or solution processes.

The fact that the morphological expression is in area about 27 times greater than the geological one as reconstructed by georadar (Fig. 31 a, b) and that the depocentre of the depression coincides with the morphological deepest point as shown by georadar and refelection seismic data speaks for an active subsiding structure (Fig. 33 a-e). Maximum subsidence at the centre of the depression leads to a permanent lowering of the erosional base level and an enlarging of the depression by retrogressive erosion. The following geodynamical process is thought to have caused the depression. Active doming of the structure "Dötlingen" leads to movements inside the unconsolidated Tertiary and Quaternary sediments, whereas uplift is higher at the centre than at the marginal parts of the dome. These differences in uplift-velocity focus on a weakness zone below the depression which then causes sinking tendencies and the formation of the depression at the earth surface (Fig. 34, gray marker 1).

E) Conclusion

λActive tectonic movements in the upper crust led to the formation of distinct orientations which are visible in both the Base Tertiary and the orientation of the land surface.

λActive northward tilting of the NW-German Basin forces the river Hunte to flow in a northerly direction as shown by high linear correlation coefficient between the Base Tertiary and the modern topography.

λThe tilting process is caused by relative uplift of the hinterland and subsidence of the North Sea area.

λCrustal movements led to (1) warping of the Lower Weichselian Terrace with a maximum vertical velocity of about 0,5 mm/a at the border from the Lower Saxony Basin to the Pompeckj Block and to (2) the formation of a negative gradient of the Holocene Alluvial Plain above a deep seated salt pillow at the Zechstein layer.

λThe local structural geological setting plays an important role for the morphological characteristic of the Lower Weichselian Terrace (width and height above the Holocene Alluvial Plain).

λBasin subsidence has primarily triggered the aggradation of the Lower Weichselian Terrace as shown by (1) the accordance between the mean recent velocity of basin subsidence (~-0,21 mm/a) and the mean sedimentation rate of the Lower Weichselian Terrace (~0,2 - 0,4 mm/a) and (2) nearly constant fluvial sedimentation rates over different time spans. Short time climatic fluctuations took control of Lower Weichselian Terrace aggradation but these short time climatic fluctuations were superimposed by a long term tectonic subsidence signal which supported a continuous sedimentation of fluvial deposits during the Middle and Late Weichselian (47-12 ka).

λPlate tectonic processes (convergence of Africa-Eurasia, North Atlantic sea-floor spreading [ridge-push]) and crustal rebound (glacial unloading of the Weichselian ice cap) or ongoing basin subsidence have the potential to cause recent and subrecent crustal movements inside the NW-German Basin. Which of the processes (or a combination of them) causes the active movements remains to be discovered.

F) References

Adams, J.M. and Faure, H., 1997. Preliminary Vegetation Maps of the World since the Last Glacial Maximum: An Aid to Archaeological Understanding. Journal of Archaeological Science, **24**, 623-647.

Ahorner, L., 1975. Present-Day Stress Field And Seismotectonic Block Movements Along Major Fault Zones In Central Europe. Tectonophysics, **29**, 233-249.

Aitken, M.J., 1998. An introduction to Optical Dating. Oxford University Press, Oxford, 263 pp.

Anderson, H.-J. and Indans, J., 1969. Fossilien aus dem Miocän vom "Tiefen Schafberger Stollen" bei Ibbenbühren/Westfalen. Fortschr. Geol. Rheinld. u. Westf., **17**, 55-68.

Antoine, P., Lautridou, J.P. and Laurent, M., 2000. Long-term fluvial archives in NW France: response of the Seine and Somme rivers to tectonic movements, climatic variations and sea-level changes. Geomorphology, **33**, 183-207.

Anzidei, M. et al., 2001. Insights into present-day crustal motion in the central Mediterranean area from GPS surveys. Geophy. J. Int., **146**, 98-110.

Argus, D.F., Gordon, R.G., DeMets, C. and Stein, S., 1989. Closure of the Africa-Eurasia-North America Plate Motion Circuit and Tectonics of the Gloria Fault. Journal Of Geophysical Research, **94**(B5), 5585-5602.

Bachmann, G.H. and Grosse, S., 1989. Struktur und Entstehung des Norddeutschen Beckens - geologische und geophysikalische Interpretation einer verbesserten Bouguer-Schwerekarte. Niedersächsische Akademie der Geowissenschaften Veröffentlichungen, **2**, 24-46.

Bakkelid, S., 1986. The Determination Of Rates Of Land Uplift In Norway. Tectonophysics, **130**, 307-326.

Baldschuhn, R., Binot, F., Fleig, S. and Kockel, F., 2001. Geotektonischer Atlas von Nordwest-Deutschland und dem deutschen Nordsee-Sektor - Strukturen, Strukturentwicklung, Paläogeographie -. Geol. Jb., **A153**, 1-44.

Baldschuhn, R., Frisch, U. and Kockel, F., 1985. Inversionsstrukturen in NW-Deutschland und ihre Genese. Z. dt. geol. Ges., **136**, 129-139.

Baldschuhn, R., Frisch, U. and Kockel, F., 1996. Geotektonischer Atlas von Nordwestdeutschland 1:300 000. BGR, Hannover.

Baldschuhn, R., Frisch, U. and Kockel, F., 1998. Der Salzkeil, ein strukturelles Requisit der saxonischen Tektonik. Z. dt. geol. Ges., **149**(1), 59-69.

Bankwitz, P., 1976. Rezente vertikale Erdkrustenbewegungen -Materialien zum tektonischen Bau von Europa-, scale 1:600.000. Zentralinstitut für Physik der Erde, Potsdam, Akademie der Wissenschaften der DDR, 47(Karte 8).

Bastos, L., Osorio, J., Barbeito, A. and Hein, G., 1998. Results from geodetic measurements in the western part of the African-Eurasian plate boundary. Tectonophysics, **294**, 261-269.

BEB, 2002. Contour map of Base Tertiary, contour intervall of 25 m. BEB, unpublished 3D Seismic Data from the German Oil Industry, Hannover.

Becker, A., 1993. An attempt to define a "neotectonic period" for central and northern Europe. Geol. Rundschau, **82**, 67-83.

Behre, K.-E. and Lade, U., 1986. Eine Folge von Eem und 4 Weichsel-Interstadialen in Oerel/Niedersachsen und ihr Vegetationsablauf. Eiszeitalter und Gegenwart, **36**, 11-36.

Bergerat, F., 1987. Stress Fields In The European Platform At The Time Of Africa-Eurasia Collision. Tectonics, **6**(2), 99-132.

Betz, D., Führer, F., Greiner, G. and Plein, E., 1987. Evolution of the Lower Saxony Basin. Tectonophysics, **137**, 127-170.

BGR, 1982. Geologische Übersichtskarten CC3110 + CC3910, 1:200 000. Bundesanstalt für Geowissenschaften und Rohstoffe (BGR), Hannover.

Bijlsma, S. and De Lange, G.W., 1983. Geology, Palynology And Age Of A Pingo Remnant Near Daarle, Province Of Overijssel, The Netherlands. Geologie en Mijnbouw, **62**, 563-568.

Bird, P. and Gratz, A.J., 1990. A theory for buckling of the mantle lithosphere and Moho during compressive detachments in continents. Tectonophysics, **177**, 325-336.

Boigk, H., 1968. Gedanken zur Entwicklung des Niedersächsischen Tektogens. Geol. Jb, **85**, 861-900.

Boigk, H., 1981. Erdöl und Erdgas in der Bundesrepublik Deutschland. Ferdinant Enke Verlag, Stuttgart, 330 pp.

Bond, G. et al., 1997. A pervasive millennial-scale cycle in North Atlantic Holocene and glacial climates. Science, **278**, 1257-1266.

Bond, G.C. et al., 1992. Evidence for massive discharges of icebergs into the North Atlantic ocean during the last glacial period. Nature, **360**, 245-249.

Bond, G.C. and Lotti, R., 1995. Iceberg discharges into the North Atlantic on millennial time scales during the last glaciation. Science, **267**, 1005-1010.

Böse, 1995. Problems Of Dead Ice And Ground Ice In The Central Part Of The North European Plain. Quaternary International, **28**, 123-125.

Brink, H.J., Dürschner, H. and Trappe, H., 1992. Some aspects of the late and post-Variscian development of the Northwestern German Basin. Tectonophysics, **207**, 65-95.

Brown, L.D. and Reilinger, R.E., 1986. Epirogenic and Intraplate Movements, Active Tectonics - Stud. in Geophys. National Academy Press, Washington, D.C., 30-45.

Buness, A.H.B., Druivenga, G. and Wiederhold, H., 2000. SISSY - eine tragbare und leistungsstarke seismische Energiequelle. Geol. Jb., **E52**, 63-88.

Burbank, D. and Anderson, R.S., 2001. Tectonic Geomorphology. Blackwell Science, Malden, Massachusetts, 274 pp.

Burnett, A.W. and Schumm, S.A., 1983. Alluvial-River Response to Neotectonic Deformation in Louisiana and Mississippi. Science, **222**, 49-50.

Burov, E.B., Lobkovsky, L.I., Cloething, S. and Nikishin, A.M., 1993. Continental folding in Central Asia (Part II): constraints from geological observations. Tectonophysics, **226**, 73-87.

CALPAL, 2001. Cologne Radiocarbon Calibration & Palaeoclimate Resarch Package. Universität zu Köln, Institut für Ur- und Frühgeschichte, Radiocarbon Laboratory, Köln.

Camelbeeck, T. and Meghraoui, M., 1996. Large Earthquakes in Northern Europe More Likely Than Once Thought. Eos, **77**(42), 405-409.

Campell, J. and Nothnagel, A., 2000. European VLBI for crustal dynamics. Journal of Geodynamics, 30, 321-326.

Caspers, G. and Freund, H., 2001. Vegetation and climate in the Early- and Pleni-Weichselian in northern central Europe. Journal of Quaternary Science, **16**(1), 31-48.

Caspers, G. et al., 1995. Niedersachsen. In: L. Benda (Editor), Das Quartär Deutschlands. Gebrüder Borntraeger, Stuttgart, page 23-58.

Caston, V.N.D., 1977. A new isopachyte map of the Quaternary of the North Sea, Quaternary Deposits of the Central North Sea. 1. Report - Institute of Geological Sciences (United Kingdom), page 1-8.

Cloetingh, S., Argenio, B.D., Catalano, R., Horvath, F. and Sassi, W., 1995. Interplay of extension and compression in basin formation: introduction. Tectonophysics, **252**, 1-5.

Cloetingh, S., Ben-Avraham, Z., Sassi, W. and Horvath, F., 1996. Dynamics of basin formation and strike-slip tectonics. Tectonophysics, **266**, 1-10.

Cloetingh, S., Eldholm, O., Larsen, B.T., Gabrielsen, R.H. and Sassi, W., 1994. Dynamics and extensional basin formation and inversion: introduction. Tectonophysics, **240**, 1-9.

Cloetingh, S., Fernandez, M., Munoz, J.A., Sassi, W. and Horvath, F., 1997. Structural controls on sedimentary basin evolution: introduction. Tectonophysics, **282**, xi-xviii.

Cloetingh, S., Gradstein, F.M., Kooi, H., Grant, A.C. and Kaminski, M., 1990. Plate reorganization: a cause of rapid late Neogene subsidence and sedimentation around the North Atlantic? Journal of Geological Society, London, **147**, 495-506.

Cloetingh, S. and Kooi, H., 1992. Intraplate stresses and dynamical aspects of rifted basins. Tectonophysics, **215**, 167-185.

Cloetingh, S., Sassi, W. and Horvath, F., 1993. The origin of sedimentary basins: state of the art and first results of the task force. Tectonophysics, **225**, vii-x.

Cox, R.T., 1994. Analysis of drainage-basin symmetrie as a rapid technique to identify areas of possible Quaternary tilt-block tectonics: An example from the Mississippi Embayment. Geological Society of America Bulletin, **106**, 571-581.

Dahms, E., 1974. Geologische und limnologische Untersuchungen zur Entstehungs- und Entwicklungsgeschichte des Dümmer. Berichte Naturhistorische Gesellschaft, **118**, 7-67.

Dansgaard, W. et al., 1993. Evidence for general instability of past climate from a 250-kyr ice record. Nature, **364**, 218-220.

Daudre, B. and Cloetingh, S., 1994. Numerical modelling of salt diapirism: influence of the tectonic regime. Tectonophysics, **240**, 59-79.

De Gans, W., 1982. Location, Age And Origin Of Pingo Remnants In The Drentsche AA Valley Area (The Netherlands). Geologie en Mijnbouw, **61**, 147-158.

De Gans, W. and Sohl, H., 1981. Weichselian Pingo Remnants And Permafrost On The Drente Plateau (The Netherlands). Geologie en Mijnbouw, **60**, 447-452.

DeMets, C., Gordon, R.G., Argus, D.F. and Stein, S., 1990. Current plate motions. Geophys. J. Int., **101**, 425-478.

DeMets, C., Gordon, R.G., Argus, D.F. and Stein, S., 1994. Effect of recent revision to the geomagnetic reversal time scale on estimates of current plate motions. Geophysical Research Letters, **21**(20), 2191-2194.

Demoulin, A., Launoy, T. and Zippelt, K., 1998. Recent crustal movements in the southern Black Forest (western Germany). Geol. Rundsch., **87**, 43-52.

Demoulin, A., Pissart, A. and Zippelt, K., 1995. Neotectonic activity in and around the southwestern Rhenish shield (West Germany): indications of a levelling comparison. Tectonophysics, **249**, 203-216.

Devoti, R. et al., 2002. Geodetic control on recent tectonic movements in the central Mediterranean area. Tectonophysics, **346**, 151-167.

DGK-Arbeitskreis, 1979. On the "map of height changes in the Federal Republic of Germany - status 1979" 1:1000 000. Allg. Vermessungsnachr., **86**, 362-363.

Diehl, M., 2002. Georadar, Grundlagen und Einsatzmöglichkeiten zur Erkundung des geologischen Untergrundes. Diploma Thesis, Johannes Gutenberg Universität Mainz, 159 pp.

Dohr, G., 1989. Ergebnisse geophysikalischer Arbeiten zur Untersuchung des tieferen Untergrundes in Norddeutschland. Niedersächsische Akademie der Geowissenschaften Veröffentlichungen, **2**, 4-22.

Dulce, J.-C. and Gronemeier, K., 1982. Linearanalysen auf Satelliten- und Luftbildern in verschiedenen geologischen Einheiten - Anwendbarkeit in der Hydrogeologie. Z. dt. geol. Ges., **133**, 535-549.

Eyles, N., Arnaud, E., Scheidegger, A.E. and Eyles, C.H., 1997. Bedrock jointing and geomorphology in southwestern Ontario, Canada: an example of tectonic predesign. Geomorphology, **19**, 17-34.

Faccenna, C., Nalpas, T., Brun, J.-B. and Davy, P., 1995. The influence of pre-existing thrust faults on normal fault geometry in nature and in experiments. Journal of Structural Geology, **17**(8), 1139-1149.

Ferhat, G., Feigl, K.L., Ritz, J.-F. and Souriau, A., 1998. Geodetic measurement of tectonic deformation in the southern Alps and Provence, France, 1947-1994. Earth and Planetary Science Letters, **159**, 35-46.

Franke, D., 1990. Der präpermische Untergrund der Mitteleuropäischen Senke - Fakten und Hypothesen. Niedersächsische Akademie der Geowissenschaften Veröffentlichungen, **4**, 19-71.

Garleff, K., 1968. Geomorphologische Untersuchungen an geschlossenen Hohlformen (Kaven) des Niedersächsischen Tieflandes. Göttinger Geographische Abhandlungen, **44**, 142 pp.

Gast, R., 1988. Rifting im Rotliegenden Niedersachsens. Geowissenschaften, **4**, 115-122.

Geluk, M.C. et al., 1994. Stratigraphy and tectonics of the Roer Valley Graben. Geologie en Mijnbouw, **73**, 129-141.

Gölke, M. and Coblentz, D., 1996. Origins of the European regional stress field. Tectonophysics, **266**, 11-24.

Grahle, H.-O., 1968. Limnologische Probleme in Nordwestdeutschland (Geologische Untersuchungen an Niedersächsischen Binnengewässern IV). Z. deutsch. geol. Ges., **117**, 727-737.

Grahle, H.-O. and Müller, H., 1967. Das Zwischenahner Meer. Oldenburger Jahrbuch, **66**, 83-121.

Gramann, F., 1966. Das Oligozän der Hessischen Senke als Bindeglied zwischen Nordseebecken und Rheintalgraben. Z. deutsch. geol. Ges., **115**, 497-514.

Gramann, F. and Kockel, F., 1988. Palaeogeographical, lithological, palaeoecological and palaeoclimatic development of the Northwest European Tertiary Basin. In: R. Vinken (Editor), The Northwest European Tertiary Basin. - Results of the International Geological Correlation Programme Project No 124. Geol. Jb., **A100**, 428-441.

Grollimund, B. and Zoback, M.D., 2000. Post glacial lithospheric flexure and induced stresses and pore pressure changes in the northern North Sea. Tectonophysics, **327**, 61-81.

Grootes, P.M., Stuiver, M.W., White, J.W.C., Johnsen, S. and Jouzel, J., 1993. Comparison of oxygen isotope records from the GISP2 and GRIP Greenland ice cores. Nature, **366**, 552-554.

Grousset, F.E. et al., 1993. Patterns of ice-rafted detritus in the glacial North Atlantic (40-55 degrees N). Paleoceanography, **8**(2), 175-192.

Grünthal, G. and Stromeyer, D., 1992. The Recent Crustal Stress Field in Central Europe: Trajectories and Finite Element Modeling. Journal Of Geophysical Research, **97**(B8), 11.805-11.820.

Gudmundsson, A., 1999. Postglacial crustal doming, stresses and fracture formation with application to Norway. Tectonophysics, **307**, 407-419.

Gurney, S.D., 1998. Aspects of the genesis and geomorphology of pingos: perennial permafrost mounds. Progress in Physical Geography, **22**(3), 307-324.

Haack, W., 1932. Über das marine Mittelmiozän von Lechtingen bei Osnabrück und die Umwandlung des Keupermergels in seinem Liegenden. Jahrbuch der Preußischen Geologischen Landesanstalt zu Berlin, **53**, 553-576.

Haas, R., Guguen, E., Scherneck, H.-G., Nothnagel, A. and Campell, J., 2000. Crustal motion results derived from observations in the European geodetic VLBI network. Earth Planets Space, **52**, 759-764.

Hahne, J., Mengeling, H., Merkt, J. and Gramann, F., 1994. Die Hunteburg-Warmzeit ("Cromer Complex") und Ablagerungen der Elster-, Saale-, und Weichsel-Kaltzeit in der Forschungsbohrung Hunteburg GE58 bei Osnabrück. Geologische Jahrbuch, **A134**, 117-166.

Harrison, R.W., Hoffman, D., Vaughn, J.D. and Palmer, J.R., 1999. An example of neotectonism in a continental interior - Thebes Gap, Midcontinent, United States. Tectonophysics, **305**, 399-417.

Hiltermann, H., 1984. Tertiär. In: H. Klassen (Editor), Geologie des Osnabrücker Berglandes. Naturwissenschaftliches Museum Osnabrück, Osnabrück, page 463-497.

Hinsch, W., Kaever, M. and Martini, E., 1978. Die Fossilführung des Erdfalls von Nieheim (SE-Westfalen) und seine Bedeutung für die Paläogeographie im Campan und Miozän. Paläont. Z., **52**(3/4), 219-245.

Hinsch, W. and Ortlam, D., 1974. Stand und Probleme der Gliederung des Tertiärs in Nordwestdeutschland. Geol. Jb., **A16**, 3-25.

Hinze, C., 1979. Erläuterungen zu Blatt Nr. 3614 Wallenhorst -Geologische Karte von Niedersachsen 1 : 25000-. Niedersächsisches Landesamt für Bodenforschung, Hannover, 154 pp.

Höfle, C., Merkt, J. and Müller, H., 1985. Die Ausbreitung des Eem-Meeres in Nordwestdeutschland. Eiszeitalter u. Gegenwart, **35**, 49-59.

Holbrook, J. and Schumm, S.A., 1999. Geomorphic and sedimentary response of rivers to tectonic deformation: a brief review and critique of a tool for recognizing subtle epeirogenic deformation in modern and ancient settings. Tectonophysics, **305**, 287-306.

Houtgast, R.F. and van Balen, R.T., 2000. Neotectonics of the Roer Valley Rift System, the Netherlands. Global and Planetary Change, **27**, 131-146.

Houtgast, R.F., Van Balen, R.T., Bouwer, L.M., Brand, G.B.M. and Brijker, J.M., 2002. Late Quaternary activity of the Feldbiss Fault Zone, Roer Valley Rift System, the Netherlands, based on displaced fluvial terraces. Tectonophysics, **352**, 295-315.

Huijzer, B. and Vandenberghe, J., 1998. Climatic reconstruction of the Weichselian Pleniglacial in northwestern and central Europe. Journal of Quaternary Science, **13**(5), 391-417.

Huisink, M., 1998. Changing river styles in response to climate change. Examples from the Maas and Vecht during the Weichselian Pleni- and Lateglacial, Vrije Universteit Amsterdam, Wageningen, 127 pp.

ICS, 2000. International Startigraphic Chart. International Union of Geological Sciences.

Ihde, J., Steinberg, J., Ellenberg, J. and Bankwitz, E., 1987. On recent vertical crustal movements derived from relevellings within the terretory of the G.D.R.. Gerlands Beitr. Geophysik, **96**, 206-217.

Illies, J.H. and Greiner, G., 1979. Holocene Movements And State Of Stresses In The Rhingraben Rift System. Tectonophysics, **52**, 349-359.

James, T.S. and Lambert, A., 1993. A Comparison Of VLBI Data With The Ice-3G Glacial Rebound Model. Geophysical Research Letters, **20**(9), 871-874.

Jaritz, W., 1973. Zur Entstehung der Salzstrukturen Nordwestdeutschlands. Geol. Jb, **A10**, 3-77.

Jaritz, W., 1980. Einige Aspekte der Entwicklungsgeschichte der nordwestdeutschen Salzstöcke. Z. dt. geol. Ges., **131**, 387-408.

Jaritz, W., 1992. Fortschritte und offene Fragen zur Entstehung der Salzstrukturen NW-Deutschlands. Nds. Akad. Geowiss. Veröfftl., **8**, 16-24.

Johnston, P., Wu, P. and Lambeck, K., 1998. Dependence of horizontal stress magnitude on load dimension in glacial rebound models. Geophys. J. Int., **132**, 41-60.

Kahle, H.-G. et al., 1998. The strain rate field in the eastern Mediterranean region, estimated by repeated GPS measurements. Tectonophysics, **294**, 237-252.

Kaltwang, J., 1992. Die pleistozäne Vereisungsgrenze im südlichen Niedersachsen und im östlichen Westfalen. Mitt. geol. Inst. Univ. Hannover, **33**, 1-161.

Keller, A.K. and Pinter, N., 1996. Active Tectonics. Prentice Hall, New Jersey, 338 pp.

Klemann, V. and Wolf, D., 1998. Modelling of stresses in the Fennoscandian lithosphere induced by Pleistocene glacations. Tectonophysics, **294**, 291-303.

Kockel, F., 1988. The paleogeographic maps, The Northwest European Tertiary Basin. - Results of the International Geological Correlation Programme Project No 124. Geol. Jb, **A100**, 428-441.

Kooi, H. and Cloetingh, S., 1989. Some consequences of compressional tectonics for extensional models of basin subsidence. Geologische Rundschau, **78**(1), 183-195.

Kooi, H., Cloetingh, S. and Remmelts, G., 1989. Intraplate stresses and the stratigraphic evolution of the North Sea Central Graben. Geologie en Mijnbouw, **68**, 49-72.

Kooi, H., Hettema, M. and Cloetingh, S., 1991. Lithospheric dynamics and the rapid Pliocene-Quaternary susidence phase in the southern North Sea basin. Tectonophysics, **192**, 245-259.

Kooi, H., Johnston, P., Lambeck, K., Smither, C. and Molendijk, R., 1998. Geological causes of recent (~100 yr) vertical land movement in the Netherland. Tectonophysics, **299**, 297-316.

Kossow, D., Krawczyk, C., McCann, T., Strecker, M. and Negendank, J.F.W., 2000. Style and evolution of salt pillows and related structures in the northern part of the Northeast German Basin. Int. J. Earth Sciences, **89**, 652-664.

Kronberg, P., 1991. Crustal fracturing and intraplate tectonics in the area between the North Sea and the Alps: A comparison of Landsat-derived fractures with existing map data. Tectonophysics, **195**, 261-269.

Krull, P., Langer, M., Trembich, G. and Wegner, T., 1985. Methodische Beiträge zur Interpretation von Fernerkundungsdaten im Nordteil der DDR. Zeitschrift für angewandte Geologie, **31**(12), 295-300.

Krull, P. and Wegner, T., 1988. Einsatz der Fernerkundung in der Kohlenwasserstoff-Forschung im Nordteil der DDR. Zeitschrift für angewandte Geologie, **34**(8), 235-239.

Krzyszkowski, D. and Stachura, R., 1998. Neotectonically controlled fluvial features, Walbrzych Upland, Middle Sudeten Mts, southwestern Poland. Geomorphology, **22**, 73-91.

Kuster, H. and Meyer, K.-D., 1979. Glaziäre Rinnen im mittleren und nordöstlichen Niedersachsen. Eiszeitalter und Gegenwart, **29**, 135-156.

Lade, U., 1980. Quartärmorphologische und geologische Untersuchungen in der Bremervörder-Wesermünder Geest. Würzburger Geographische Arbeiten, **50**, 175 pp.

Lagerbäck, R., 1990. Late Quaternary faulting and paleoseismicity in northern Fennoscandia, with particular reference to the Lansjärv area, northern Sweden. Geologiska Föreningens i Stockholm Förhandlingar, **112**(4), 333-354.

Lehne, R., 2001. Subrosion und jüngste Hebungsraten des Wedehof-Diapirs im Projektgebiet Posthausen-Völkersen. Diploma Thesis, Johannes Gutenberg-Universität Mainz, 96 pp.

Leonhard, T., 1988. Zur Berechnung von Höhenänderungen in Norddeutschland -Modelldiskussion, Lösbarkeitsanalyse und numerische Ergebnisse-. doctoral thesis, Universität Hannover, 158 pp.

Letouzey, J., 1986. Cenozoic paleo-stress pattern in the Alpine Foreland and structural interpretation in a platform basin. Tectonophysics, **132**, 215-231.

Leydecker, G., 2002a. Das Erdbeben vom 11. Juli 2002 in Weyhe südlich Bremen im Norddeutschen Tiefland. Bundesanstalt für Geowissenschaften und Rohstoffe (BGR), Tagebuch Nr. 12 106/02, 1-6.

Leydecker, G., 2002b. Erdbebenkatalog für die Bundesrepublik Deutschland mit Randgebieten für die Jahre 800-2001. -Datenfile http://www.bgr.de/quakecat. Bundesanstalt für Geowissenschaften und Rohstoffe (BGR).

Leydecker, G. and Kopera, J.R., 1999. Seismological hazard assessment for a site in Northern Germany, an area of low seismicity. Engineering Geology, **52**, 293-304.

Leydecker, G. et al., 1980. Das Beben vom 2. Juni 1977 in der norddeutschen Tiefebene bei Soltau. Geol. Jb., **E18**, 3-18.

LGN, 1898. Preussische Landesaufnahme 1:25000. LGN -Landesvermessung + Geobasisinformation Niedersachsen-, Hannover.

LGN, 1994. Topografische Karte 1:25000. LGN -Landesvermessung + Geobasisinformation Niedersachsen-, Hannover.

LGN, 2002. Norddeutsches Küstennivellement (NKN 1 = 1928-1931) and (NKN 3 = 1980) - unpublished data of the LGN (Landesvermessung + Geobasisinformationen Niedersachsen), Hannover.

Liedke, H., 1980. Führer für die Exkursion in das Gebiet des Dümmers, Symposium des Arbeitskreises für Geomorphologie, Bochum.

Liedtke, H., 1981. Die nordischen Vereisungen in Mitteleuropa. Forschungen zur Deutschen Landeskunde, Trier, 307 pp.

Ludwig, A.O., 1995. The surface of the Holsteinian interglacial sediments as a base level for reconstruction of vertical neotectonic movements in northern Germany. Technika Poszukiwan Geologicznych, Geosynoptika i Geotermia, **3**(172), 31-36.

Ludwig, A.O. and Schwab, G., 1995. Neogeodynamica Baltica - ein internationales Kartenprojekt (IGCP-Projekt Nr. 346). Deutsche Beiträge zur Charakterisierung der vertikalen Bewegungen seit Beginn des Rupelian (Unteroligozän) bzw. seit Ende der Holstein-Zeit. Brandenburgische Geowiss. Beitr., **2**(2), 47-57.

Mackay, J.R., 1988. Pingo collapse and paleoclimatic reconstruction. Can. J. Earth Sci., **25**, 495-511.

Maddy, D., Bridgland, D.R. and Green, C.P., 2000. Crustal uplift in southern England: evidence from the river terrace records. Geomorphology, **33**, 167-181.

Mälzer, H., Hein, G. and Zippelt, K., 1983. Height Changes in the Rhenish Massif: Determination and Analysis. In: K. Fuchs, K. von Gehlen, H. Mälzer, H. Murawski and A. Semmel (Editors), Plateau Uplift - The Rhenish Shield- A Case History. Springer-Verlag, Berlin, page. 164-177.

Marple, R.T. and Pradeep, T., 2000. Evidence for a buried fault system in the Coastal Plain of the Carolinas and Virginia - Implications for neotectonics in the southeastern United States. GSA Bulletin, **112**(2), 200-220.

Marple, R.T. and Talwani, P., 1993. Evidence of possible tectonic upwarping along the South Carolina coastal plain from an examination of river morphology and elevation data. Geology, **21**, 651-654.

Marshak, S., Van der Pluijm, B.A. and Hamburger, M., 1999. -Preface- The tectonics of continental interiors. Tectonophysics, **305**, VII-X.

Meghraoui, M. et al., 2001. Active Normal Faulting in the Upper Rhine Graben and Paleoseismic Identification of the 1356 Basel Earthquake. Science, **293**, 2070-2073.

Meier, T., 1996. Früh- und spätweichselzeitliche Flugsand- und Sandlößvorkommen im Huntetal (Niedersachsen). Diploma Thesis, Universität Kiel, 58 pp.

Meissner, R., 1996. Faults and folds, fact and fiction. Tectonophysics, **264**, 279-293.

Meissner, R., 1999. Terrane accumulation and collapse in central Europe: seismic and rheological constraints. Tectonophysics, **305**, 93-107.

Meissner, R. and Strehlau, J., 1982. Limits Of Stresses In Continental Crusts And Their Relation To Depth-Frequency Distribution Of Shallow Earthquakes. Tectonics, **1**(1), 73-89.

Merkt, J., 1979. Zur Limnologie des Steinhuder Meeres. Cour. Forsch.-Inst. Senckenberg, **37**, 59-62.

Meyer, K.D., 1974. Pollenanalytische Untersuchungen und Jahresschichtenzählungen an der holsteinzeitlichen Kieselgur von Hetendorf. Geol. Jb., **A21**, 87-105.

Meyer, W. and Stets, J., 1998. Junge Tektonik im Rheinischen Schiefergebirge und ihre Quantifizierung. Z. dt. geol. Ges., **149**(3), 359-379.

Milne, G.A. et al., 2001. Space-Geodetic Constraints on Glacial Isostatic Adjustment in Fennoscandia. Science, **291**, 2381-2385.

Minister, J.B., 1978. Present-Day Plate Motions. Journal Of Geophysical Research, **83**(B11), 5331-5354.

Mitrovica, J.X., Davis, J.L. and Shapiro, I.I., 1994. A spectral formalism for computing three-dimensional deformations due to surface loads 2. Present-day glacial isostatic adjustment. Journal of Geophysical Research, **99**(B4), 7075-7101.

Mol, J., Vandenberghe, J. and Kasse, C., 2000. River response to variations of periglacial climate in mid-latitude Europe. Geomorphology, **33**, 131-148.

Molnar, P., Brown, T. and Burchfiel, C., 1994. Quaternary Climate Change and the Formation of River Terraces across Growing Anticlines on the North Flank of the Tien Shan, China. The Journal of Geology, **102**, 583-602.

Müller, B., Reinecker, J., Heidbach, O. and Fuchs, K., 2000. The 2000 release of the World Stress Map (available online at www.world-stress-map.org).

Müller, B., Wehrle, V., Zeyen, H. and Fuchs, K., 1997. Short-scale variations of tectonic regimes in the western European stress province north of the Alps and Pyrenees. Tectonophysics, **275**, 199-219.

Müller, B. et al., 1992. Regional Patterns of Tectonic Stress in Europe. Journal of Geophysical Research, **97**(B8), 11.783-11.803.

Müller, H., 1974. Pollenanalytische Untersuchungen und Jahresschichtenzählungen an der eem-zeitlichen Kieselgur von Bispingen/Luhe. Geol. Jb., **A21**, 149-169.

Müller, H., 1986. Altquartäre Sedimente im Deckgebirge des Salzstockes Gorleben. Z. dt. geol. Ges., **137**, 85-95.

Nalpas, T., Le Douaran, S., Brun, J.-P., Unternehr, P. and Richert, J.-P., 1995. Inversion of the Broad Fourteens Basin (offshore Netherlands), a small-scale model inverstigation. Sedimentary Geology, **95**, 237-250.

Nelson, W.J., Denny, F.B.D., Follmer, L.R. and Masters, J.M., 1999. Quaternary grabens in southernmost Illinois: deformation near an active intraplate seismic zone. Tectonophysics, **305**, 381-397.

Ness, D., 1994. Gewässerkundliche Beschreibung der Hunte. In: R. Ackermann (Editor), Die Hunte -Porträt eines nordwestdeutschen Flusses-. Isensee Verlag, Oldenburg, page 27-42.

Nikishin, A.M., Cloething, S., Lobkovsky, L.I., Burov, E.B. and Lankreijer, A.C., 1993. Continental folding in Central Asia (Part I): constraints from geological observations. Tectonophysics, **226**, 59-72.

NLfB, 1993. Quartärgeologische Übersichtskarte von Niedersachsen und Bremen 1:500.000. Niedersächsisches Landesamt für Bodenforschung (NLfB), Hannover.

Ortlam, D. and Schnier, H., 1981. Erdfälle und Salzwasseraufstieg in Bremen; Typbeispiel für Süsswasserdepressionsgebiete. Neues Jahrbuch fuer Geologie und Palaeontologie. Monatshefte., **4**, 236-256.

Ortlam, D. and Vierhuff, H., 1978. Aspekte zur Geologie des höheren Känozoikums zwischen Elbe und Weser-Aller. N. Jb. Geol. Paläont. Mh., **7**, 408-426.

Ouchi, S., 1985. Response of alluvial rivers to slow active tectonic movement. Geological Society of America Bulletin, **96**, 504-515.

Pfaffenberg, K., 1939. Pollenanalytische Auswertung von Bohrungen und Grabungen am Dümmer. Niersächsisches Landesamt für Bodenforschung, Archivnummer: 68620.

Pfaffenberg, K. and Dienemann, W., 1964. Das Dümmerbecken. Forschungen zur Landes- und Volkskunde, Reihe A, I. Natur, Wirtschaft, Siedlung und Planung. Veröffentlichungen des Niedersächsischen Instituts für Landeskunde und Landesentwicklung an der Universität Göttingen, **78**, 112 pp.

Poblet, J., McClay, K., Storti, F. and Munoz, J.A., 1997. Geometries of syntectonic sediments associated with single-layer detachment folds. Journal of Structural Geology, **19**(3-4), 369-381.

Prinz, H., 1997. Abriß der Ingenieurgeologie, 3. Auflage. Ferdinand Enke Verlag, Stuttgart, 536 pp.

Pyritz, E., 1972. Binnendünen und Flugsandebenen im Niedersächsischen Tiefland. Göttinger Geographische Abhandlungen, **61**: 1-153.

Reilinger, R.E., McClusky, S.C., Oral, M.B., King, R.W. and Toksoz, M.N., 1997. Global Positioning System measurements of present-day crustal movements in the Arabian-Africa-Eurasia plate collision zone. Journal of Geophysical Research, **102**(B5), 9983-9999.

Richardson, R.M., 1992. Ridge Forces, Absolute Motions, and the Intraplate Stress Field. Journal of Geophysical Research, **97**(B8), 11739-11748.

Sassi, W., Colletta, B., Bale, P. and Paquerau, T., 1993. Modelling of structural complexity in sedimentary basins: the role of pre-existing faults in thrust tectonics. Tectonophysics, **226**, 97-112.

Scheidegger, A., 2001. Surface joint systems, tectonic stresses and geomorphology: a reconciliation of conflicting observations. Geomorphology, **38**, 213-219.

Scheidegger, A.E., 1981. The Geotectonic Stress Field And Crustal Movements. Tectonophysics, **71**, 217-226.

Scheidegger, A.E., 2002. Morphometric analyses and its relation to tectonics in Macaronesia. Geomorphology, **46**, 95-115.

Schumm, S.A., 1986. Alluvial River Response to Active Tectonics, Active Tectonics -Stud. in Geophys. National Academy Press, Washington, D.C., page 80-94.

Schumm, S.A. and Spitz, W.J., 1996. Geological influences on the Lower Mississippi River and its alluvial valley. Engineering Geology, **45**, 245-261.

Schwab, G., 1996. Zum Relief der Quartärbasis in Norddeutschland. Bemerkungen zu einer neuen Karte. Z. geol. Wiss., **24**: 343-349.

Schwab, G., 1981. Paläotektonische, neotektonische und rezente Krustenbewegung in Gebiet der DDR. Z. geol. Wiss., **9**(11), 1223-1236.

Schwab, G., Tetschke, H.-J. and Jubitz, K.H., 1973. Zur Raum-Zeit-Beziehung zwischen rezenten Krustenbewegungen und Paläotektonik im Breich der Norddeutsch-Polnischen Senke. Zeitschrift für angewandte Geologie, **19**(11), 579-586.

Schwan, J., 1988. The Structure and Genesis of Weichselian to Early Holocene Aeolian Sand Sheets in Western Europe. Sedimentary Geology, **55**, 197-232.

Sclater, J.G. and Christie, P.A.F., 1980. Continental Stretching Of The Post-Mid-Cretaceous Subsidence Of The Central North Sea. Journal of Geophysical Research, **85**(B7), 3711-3739.

Searle, R.C. et al., 1998. The Reykjanes Ridge: structure and tectonics of a hot-spot-influenced, slow-spreading ridge, from multibeam bathymetry, gravity and magnetic investigations. Earth and Planetary Science Letters, **160**, 463-478.

Seelos, K., 2000. Einfluß halokinetischer Prozesse auf die Landschaftsformung im Projektgebiet Völkersen-Verden, Niedersachsen. Diploma Thesis, Johannes Gutenberg-Universität Mainz, 122 pp.

Sesören, A., 1976. Lineament Analyses From ERTS (Landsat) Images Of The Netherlands. Geologie En Mijnbouw, **55**(1-2), 61-67.

Sharma, P.V., 1984. The Fennoscandian Uplift And Glacial Isostasy. Tectonophysics, **105**, 249-262.

Sirocko, F. et al., in press. Young tectonic and halokinetic movements in the North-German-Basin: is´s effect on formation of rivers and surface morphology. Geologie en Mijnbouw/Netherlands Journal of Geosciences.

Steward, I.S., Sauber, J. and Rose, J., 2000. Glacio-seismotectonics: ice sheets, crustal deformation and seismicity. Quaternary Science Reviews, **19**, 1367-1389.

Streif, H.J., 1991. Zum Ausmaß und Ablauf eustatischer Meeresspiegelschwankungen im südlichen Nordseegebiet seit Beginn des Letzten Interglazials. In: B. Frenzel (Editor), Klimageschichte der letzten 130 000 Jahre. Gustav Fischer Verlag, Stuttgart/New York, page 231-249.

Sue, C. et al., 2000. Active deformation in the inner western Alps inferred from comparison between 1972-classical and 1996-GPS geodetic surveys. Tectonophysics, **320**, 17-29.

Talwani, P., 1999. Fault geometry and earthquakes in continental interiors. Tectonophysics, **305**, 371-379.

Thiermann, A., 1970. Erläuterungen zu Blatt 3712 -Geologische Karte von Nordrhein-Westfalen 1:25 000-. Geologisches Landesamt Nordrhein-Westfalen, Krefeld, 243 pp.

Thorne, J.A. and Watts, A.B., 1989. Quantitative Analyses of North Sea Subsidence. The American Association of Petroleum Geologists Bulletin, **73**(1), 88-116.

Trusheim, F., 1957. Über Halokinese und ihre Bedeutung für die strukturelle Entwicklung Norddeutschlands. Z. deutsch. geol. Ges., **109**, 111-147.

USGS, 2002. Earthquake Hazards Program -National Earthquake Information Center, World Data Center for Seismology, Denver. http://www.neic.cr.usgs.gov.

Vaikmäe, R., Böse, M., Michel, F.A. and Moormann, B.J., 1995. Changes In Permafrost Conditions. Quaternary International, **28**, 113-118.

Van den Berg, M.W. et al., 1994. Patterns and velocities of recent crustal movements in the Dutch part of the Roer Valley rift system. Geologie en Mijnbouw, **73**, 157-168.

van der Meulen, S., 1988. The spatial facies of pingo remnants on the southeast Frisian till plateau (the Netherlands). Geologie en Mijnbouw, **67**, 61-74.

Van Huissteden, J. and Vandenberghe, J., 1988. Changing fluvial style of periglacial lowland rivers during the Weichselian Pleniglacial in the eastern Netherlands. Z. Geomorph. N. F., **71**, 131-146.

van Wees, J.D. and Cloetingh, S., 1996. 3D Flexure and intraplate compression in the North Sea Basin. Tectonophysics, **266**, 343-359.

Vandenberghe, J., 1992a. Geomorphology and climate of the cool oxygen isotope stage 3 in comparison with the cold stages 2 and 4 in The Netherlands. Z. Geomorph. N. F., **86**, 65-75.

Vandenberghe, J., 1992b. River terrace development and its relation to climate: the Saalian Caberg terrace of the Maas river near Maastricht (The Netherlands). Meded. Rijks Geol. Dienst, **4**, 19-42.

Vandenberghe, J., 1993. Changing fluvial processes under changing periglacial conditions. Zeitschrift für Geomorphologie, **88**, 17-28.

Vandenberghe, J., 1995a. The role of rivers in palaeoclimate reconstruction. In: B. Frenzel (Editor), European river activity and climate change during the Lateglacial and Early Holocene. Gustav Fischer Verlag, Stuttgart, Jena, New York, page 11-19.

Vandenberghe, J., 1995b. Timescale, Climate And River Development. Quaternary Science Reviews, **14**, 631-638.

Vandenberghe, J., Kasse, C., Bohncke, S. and Korzarski, S., 1994. Climate-related river activity at the Weichselian-Holocene transition: a comparative study of the Warta and Maas rivers. Terra Nova, **6**, 476-485.

Vandenberghe, J. and Pissart, A., 1993. Permafrost Changes in Europe During the Last Glacial. Permafrost and Periglacial Processes, **4**, 121-135.

Vanneste, K., Meghraoui, M. and Camelbeek, T., 1999. Late Quaternary earthquake-related soft-sediment deformation along the Belgian portion of the Feldbiss Fault, Lower Rhine Graben system. Tectonophysics, **309**, 57-79.

Vierhuff, H., 1967. Untersuchungen zur Stratigraphie und Genese der Sandlössvorkommen in Niedersachsen. Mittteilungen aus dem Geologischen Institut der Technischen Hochschule Hannover, **5**, 1-99.

Vitek, J.D., Giardino, J.R. and Fitzgerald, J.W., 1996. Mapping geomorphology: A journey from paper maps through computer mapping to GIS and Virtual Reality. Geomorphology, **16**, 223-249.

Voelker, A.H.L. et al., 1998. Correlation Of Marine ^{14}C Ages From The Nordic Seas With The GISP2 Isotope Record: Implications For ^{14}C Calibration Beyond 25 ka BP. Radiocarbon, **40**(1), 517-534.

Wahlström, R., 1993. Fennoscandian seismicity and its relation to the isostatic rebound. Global and Planetary Change, **8**, 107-112.

Walter, R., 1995. Geologie von Mitteleuropa. E. Schweizerbartsche Verlagsbuchhandlung, Stuttgart, 561 pp.

Wiederhold, H., Buness, H.A. and Bram, K., 1998. Glacial structures in northern Germany revealed by a high-resolution reflection seismic survey. Geophysics, **63**(4), 1265-1272.

Wiegand, G., 1965. Fossile Pingos in Mitteleuropa. Würzburger Geographische Arbeiten, **16**, 152 pp.

Wolf, D., 1986. Glacio-isostatic adjustment in Fennoscandia revisited. J. Geophysics, **59**, 42-48.

Wolf, D., 1987. An upper bound on lithosphere thickness from glacio-isostatic adjustment in Fennoscandia. J. Geophysics, **61**, 141-149.

Wolf, D., 1993. The changing role of the lithosphere in models of glacial isostasy: a historical review. Global and Planetary Change, **8**, 95-106.

Wolf, D., 1996. Note on estimates of the glacial-isostatic decay spectrum for Fennoscandia. Geophysical J. Int., **127**, 801-805.

Wu, P., Johnston, P. and Lambeck, K., 1999. Postglacial rebound and fault instability in Fennoscandia. Geophs. J. Int., **139**, 657-670.

Wübbelmann, H., 1993. Vergleich zwischen Höhen im DHHN 85 und im Nivellementnetz 1960. Die Wiederhohlungsmessungen 1980 bis 1985 im Deutschen Haupthöhennetz und das Haupthöhennetz 1985 der Bundesrepublik Deutschland. Arbeitsgemeinschaft der Vermessungsverwaltungen der Länder der Bundesrepublik (ADV) - Arbeitskreis Höhenfestpunktfeld und Schwerefestpunktfeld (AK Niv), Bayrisches Landesvermessungsamt, München, page 155-165.

Zagwijn, W.H., 1983. Sea-Level Changes In The Netherland During The Eemian. Geologie en Mijnbouw, **62**, 437-450.

Zagwijn, W.H., 1989. The Netherlands during the Tertiary and the Quaternary: A case history of Coastal Lowland evolution. Geologie en Mijnbouw, **68**, 107-120.

Ziegler, P., Cloetingh, S. and van Wees, J.-D., 1995. Dynamics of intra-plate compressional deformation: the Alpine foreland and other examples. Tectonophysics, **252**, 7-59.

Ziegler, P.A., 1990. Geological Atlas of Western and Central Europe, 2nd Ed. Shell Internationale Petroleum Maatschappij B.V. and Geol. Soc. London, Elsevier, Amsterdam, 239 pp.

Ziegler, P.A., 1994. Cenozoic rift systems of western and central Europe: an overview. Geologie en Mijnbouw, **73**, 99-127.

Zoback, M.D. and Grollimund, B., 2001. Impact of deglaciation on present-day intraplate seismicity in eastern North America and western Europe. Earth and Planetary Sciences, **333**, 23-33.

Zoback, M.D. et al., 1993. Stresses in the lithosphere and sedimentary basin formation. Tectonophysics, **226**, 1-13.

Zoback, M.L., 1992. First- and Second-Order Patterns of Stress in the Lithosphere: The World Stress Map Project. Journal Of Geophysical Research, **97**(B8), 11703-11728.

Zoback, M.L., Zoback, M.D., Adams, J., Assumpca, M. and Bell, S., 1989. Global patterns of tectonic stress. Nature, **341**, 291-298.

Zuchiewicz, W., 1998. Quaternary tectonics of the Outer West Carpathians, Poland. Tectonophysics, **297**, 121-132.

Danksagung

An dieser Stelle möchte ich einer Reihe von Personen meinen Dank für ihre Unterstützung aussprechen:

Prof. Dr. F. Sirocko für die Vergabe der Arbeit, die Diskussionsbereitschaft und Anstöße, die für den Fortgang der Arbeit sehr wichtig waren.

Dr. B. Rein für die zahlreichen und wertvollen Diskussionen.

M. Diehl, R. Lehne, B. Lene, K. Seelos, C. Glaab, M. Hirsch, T. Fritz, R. Kilian für ihre Hilfe bei den Geländearbeiten.

Dr. F. Enzmann für seinen fachlichen Rat bei EDV/GIS Fragen und K. Jäger für die Arbeiten am GIS.

F. Dreher für die Aufbereitung und Zählung der Pollenproben.

Dr. M. Krebetschek und den Mitarbeitern seiner Arbeitsgruppe (TU Freiberg, Institut für Angewandte Physik) für die Messung der OSL-Proben und die freundliche Aufnahme in die Arbeitsgruppe.

Prof. Dr. P. M. Grootes vom Leibniz-Labor für Alters- und Isotopenforschung, Kiel für die Radiokarbondatierungen.

Dr. F. Kockel (BGR, Hannover, i.R.) für die wertvollen Hinweise zu strukturgeologischen Fragen und die anregende Diskussion.

Dr. H.-J. Brink und Dr. G. Babbel (BEB, Hannover) für die Unterstützung und Hilfe bei der Interpretation der 3D-Seismik Daten.

Dr. K. J. Sandmeier (Sandmeier Scientific Software, Karlsruhe) für die Hilfe bei der Auswertung der Georadar- und reflektionsseismischen Daten.

W. Seiferter (LGN, Hannover) für die Rechereche und Bereitstellung der Nivellemendaten.

J. Tanger, der uns auf seinem Privatgrund die Bohrungen Essemühle 2-4 niederbringen ließ und uns jederzeit bei Bohrproblemen unterstützte.

Familie Berentsen, die uns die umfangreichen Arbeiten auf ihrem Feld durchführen ließ.

G. Weller und L. Seelos für das Korrekturlesen der Arbeit.

Meiner Mutter möchte ich für ihre Unterstütztung danken, insbesondere für die angenehmen Geländeaufenthalte.

Mein allergrößter Dank gilt meiner Frau Susanne und meinem Sohn Jannis.

Der Deutschen Forschungsgemeinschaft (DFG) möchte ich für die zweieinhalbjährige finanzielle Förderung des Projekts danken. Dem Landesvermessungsamt Niedersachsen (LGN) sei für die Freigabe der Feinnivellement-Daten und die Vervielfältigungserlaubnis der topographischen Karten gedankt. Der BEB und der Wintershall AG danke ich für die Freigabe der seismischen Daten. Der Firma Stölben möchte ich für die Bohrung Essemühle 4 danken. Mein Dank gilt auch den Landwirten der Region, ohne deren Unterstützung die Geländearbeiten nicht durchführbar gewesen wären.

Appendix

Structural geological situation of the study area from the Base of Quaternary (Fig. 1) to the Base of Zechstein (Fig. 15). The position of salt walls and salt domes is given in blue, thrust faults (red) and normal faults (red with a dashed line), outcrop (pink), the depth of the presented geological horizons are given from white (highest position) to black (lowest position), after Geotectonic Atlas of NW-Germany (Baldschuhn et al., 1996) and Map of the Base Quaternary of Lower Saxony and Bremen, 1:500000 (NLfB, 1993).

The Holocene Alluvial Plain of the river Hunte and tributaries (yellow), watershed of the river Hunte (green) with the position of the segment lines, after topographical maps (LGN, 1898; LGN, 1994). The dashed squares show the position of the topographical maps with map number.

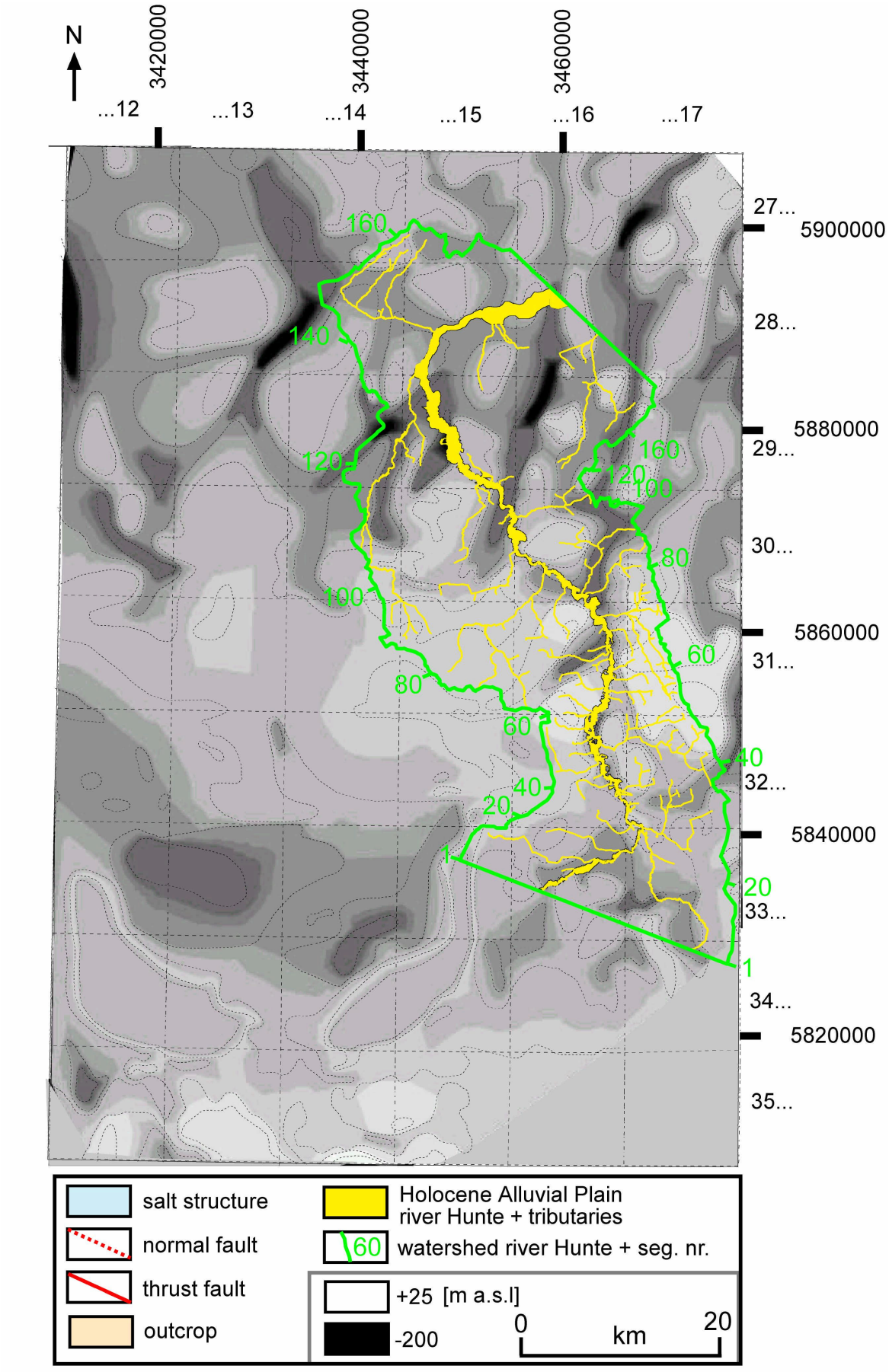

Fig. 1: Base of Quaternary

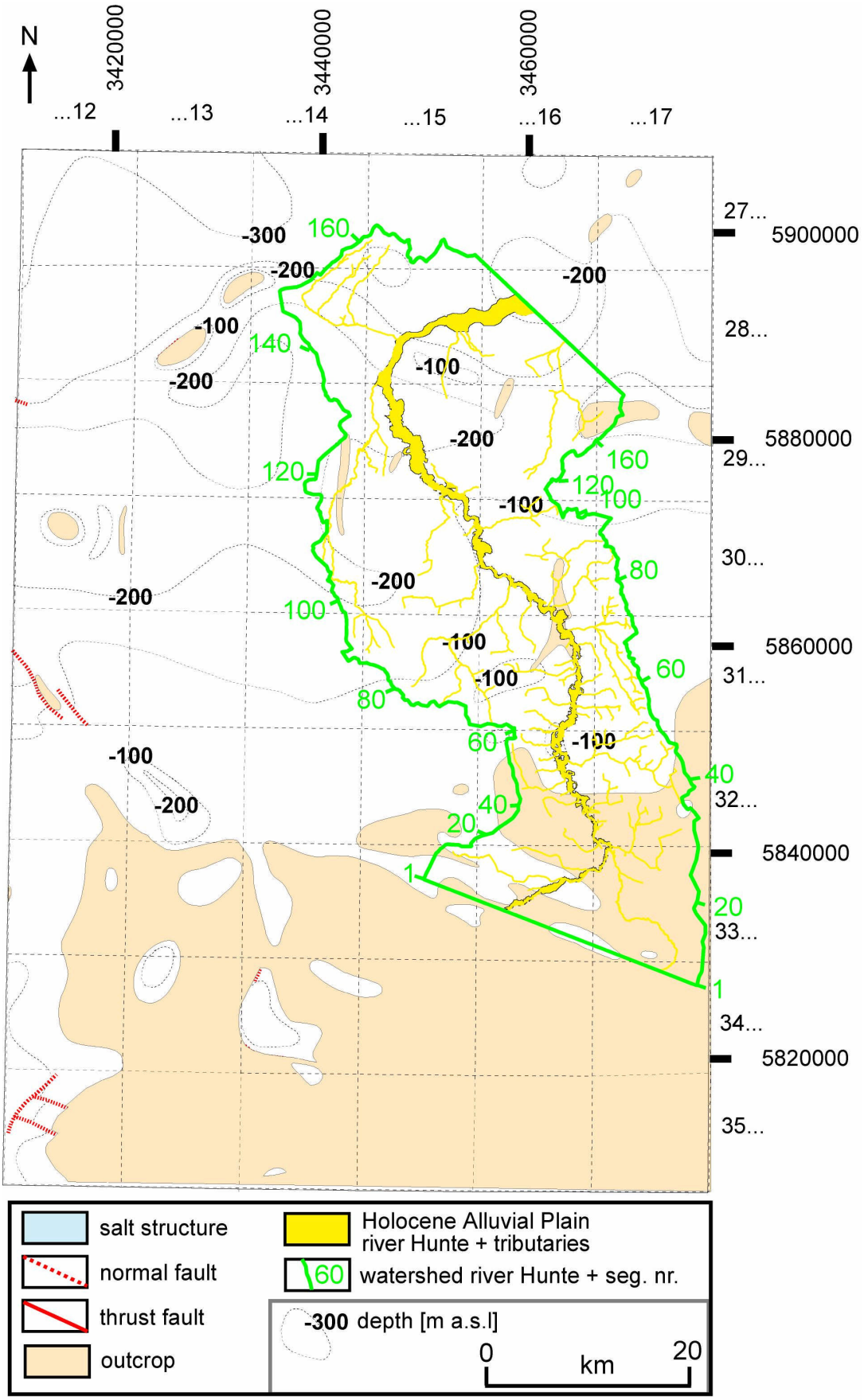

Fig. 2: Base Middle Miocene to Pliocene

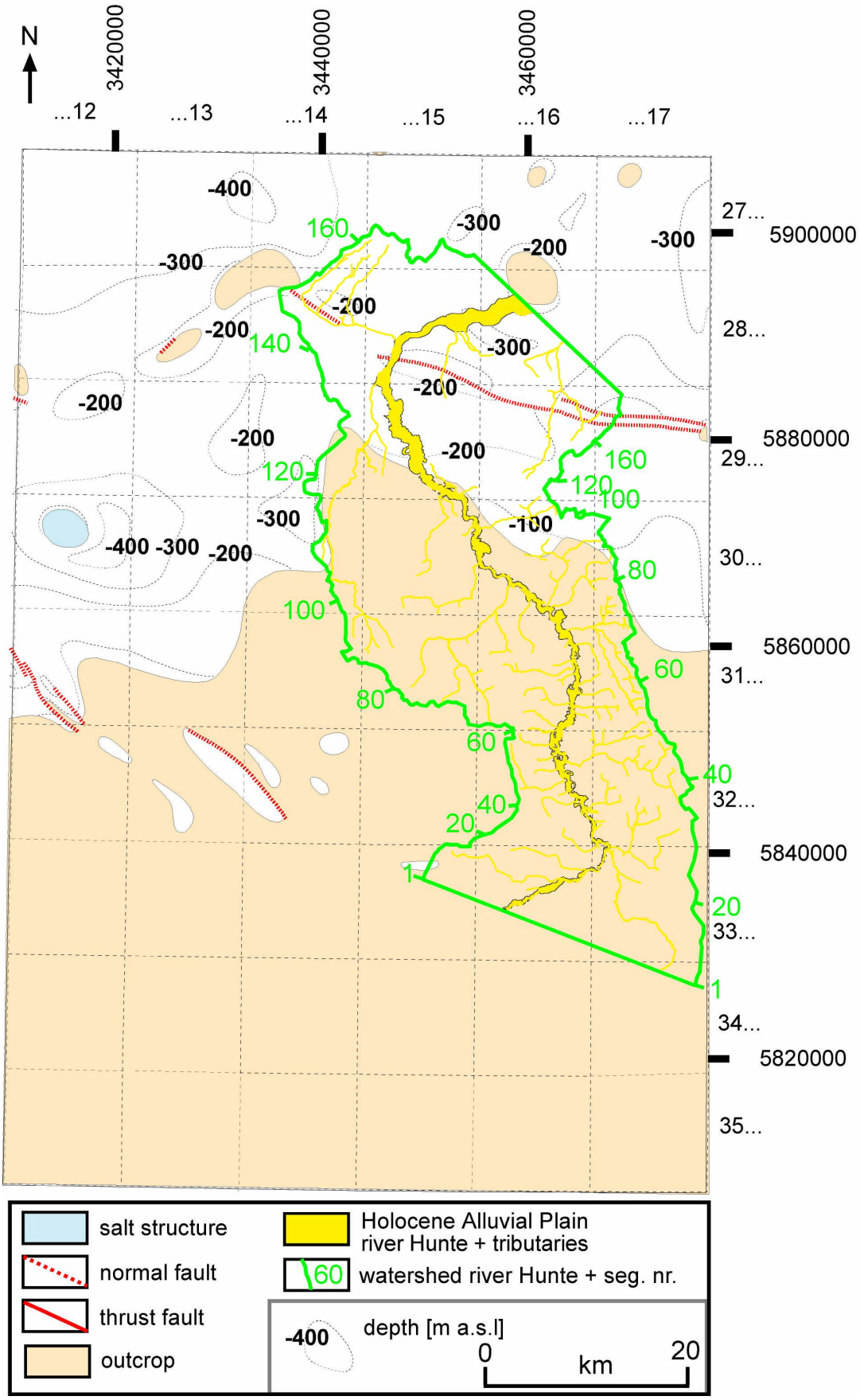

Fig. 3: Base Lower Miocene to Pliocene

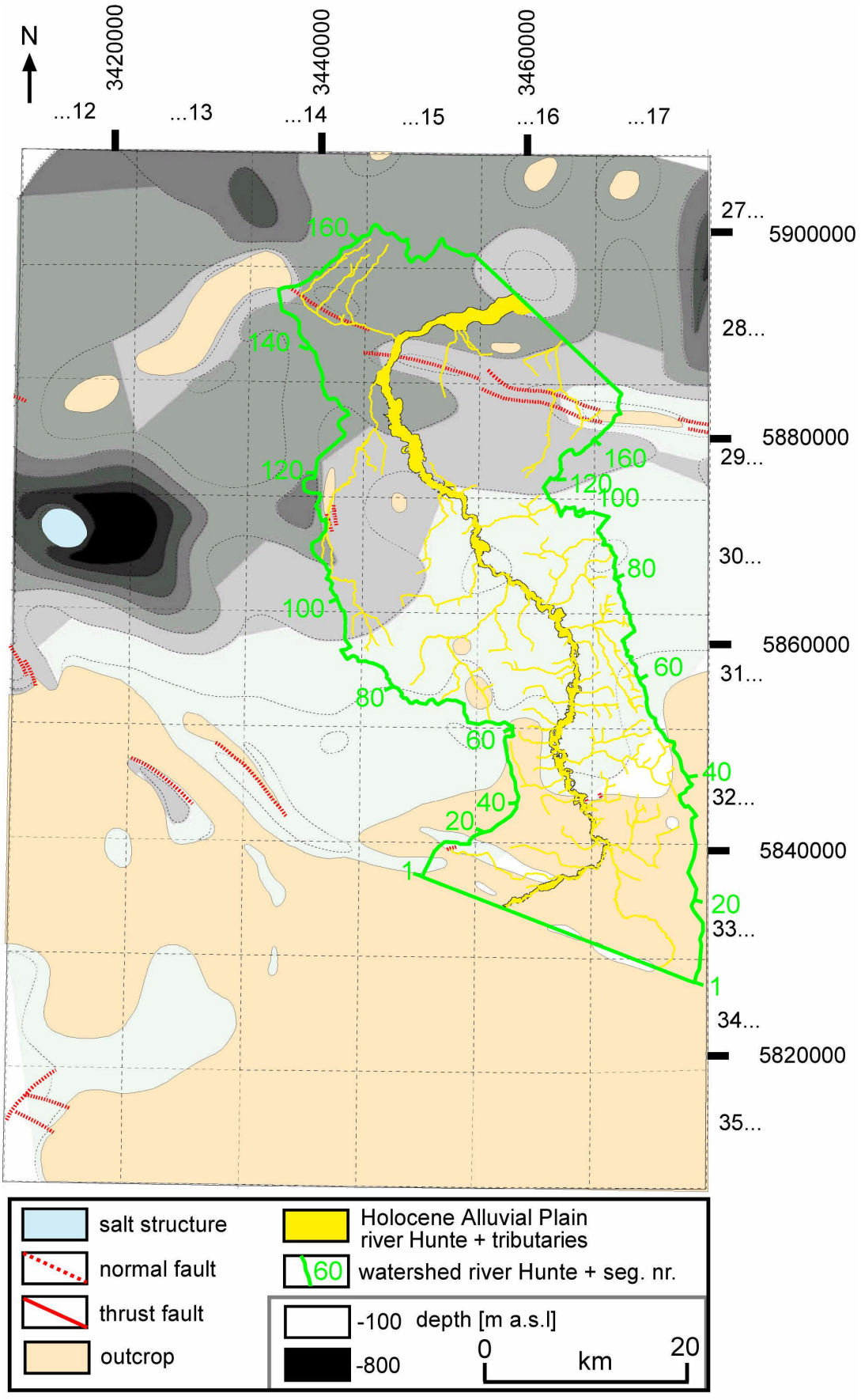

Fig. 4: Base Middle Oligocene to Upper Oligocene

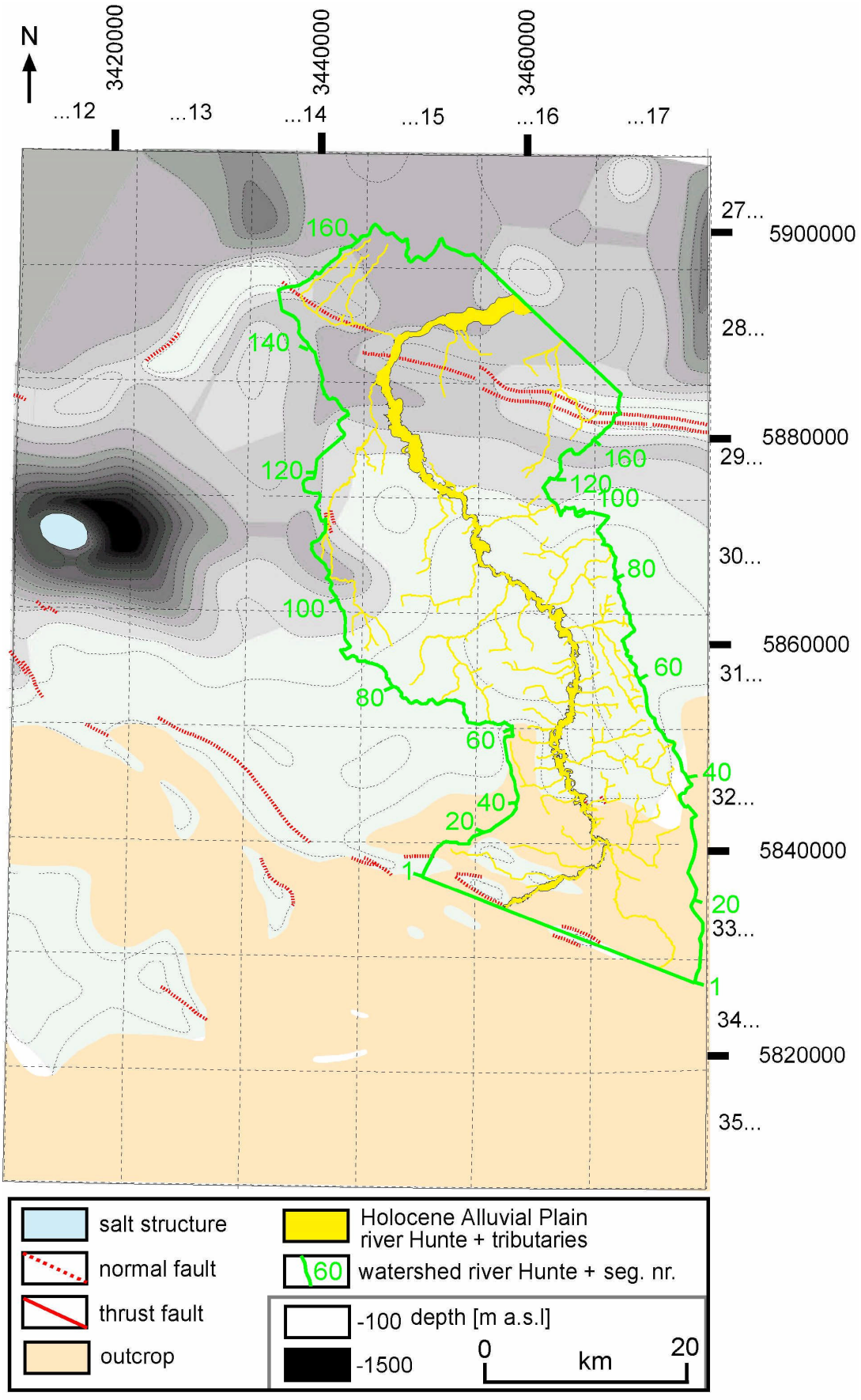

Fig. 5: Base Middle Eocene to Lower Oligocene

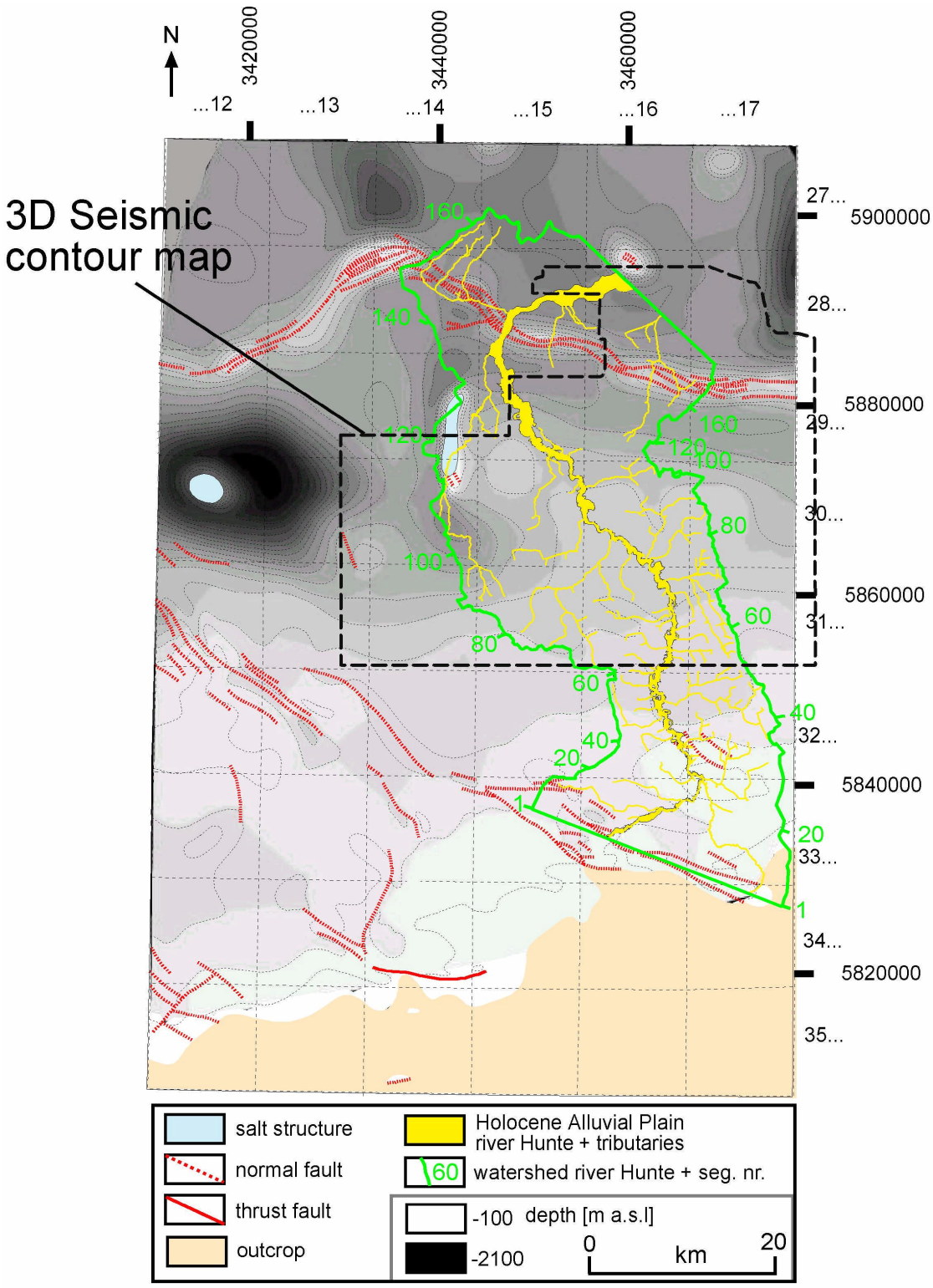

Fig. 6: Base Tertiary

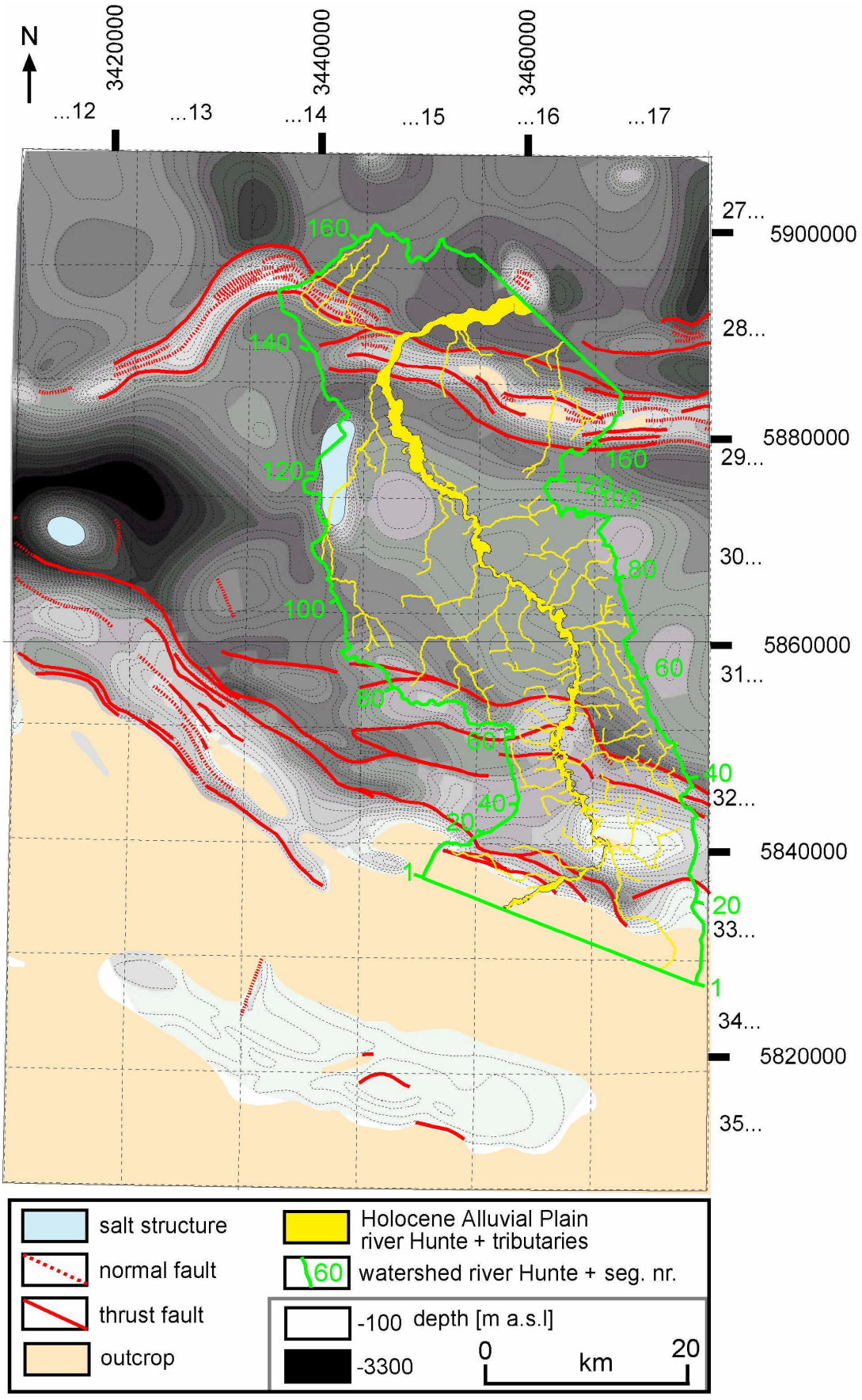

Fig. 7: Base Upper Cretaceous

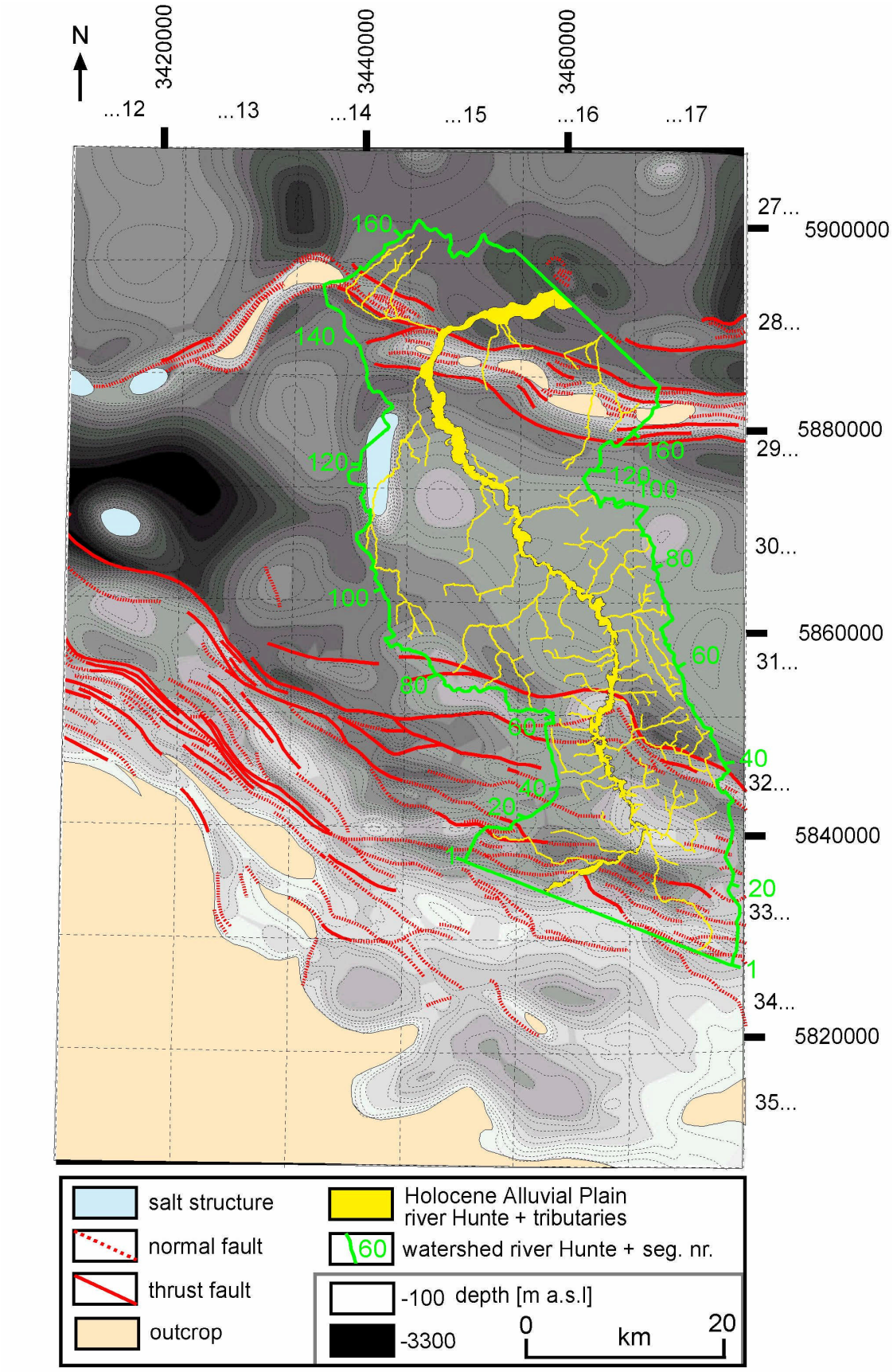

Fig. 8: Base marine Lower Cretaceous

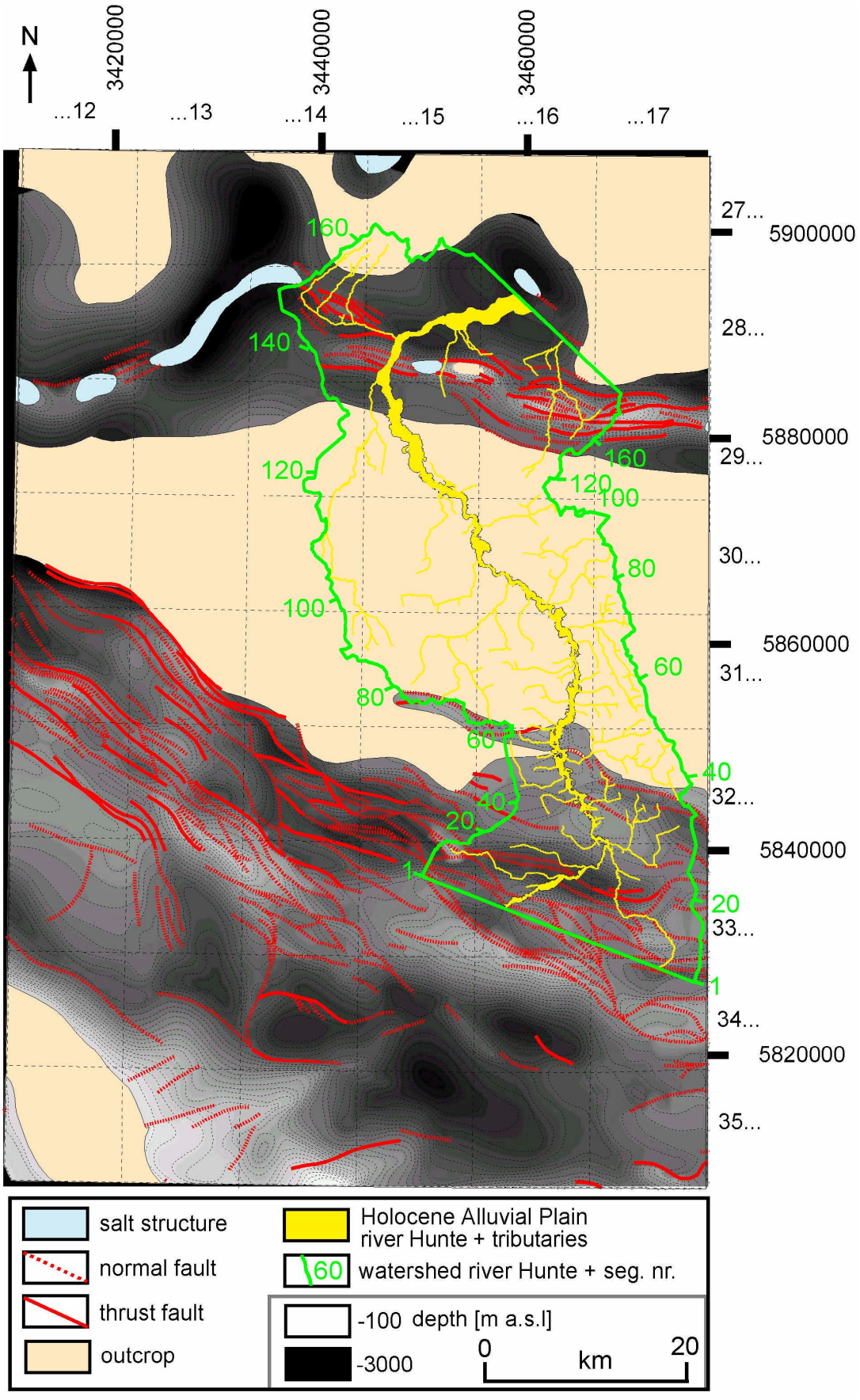

Fig. 9: Base Upper Jurassic and "Wealden"

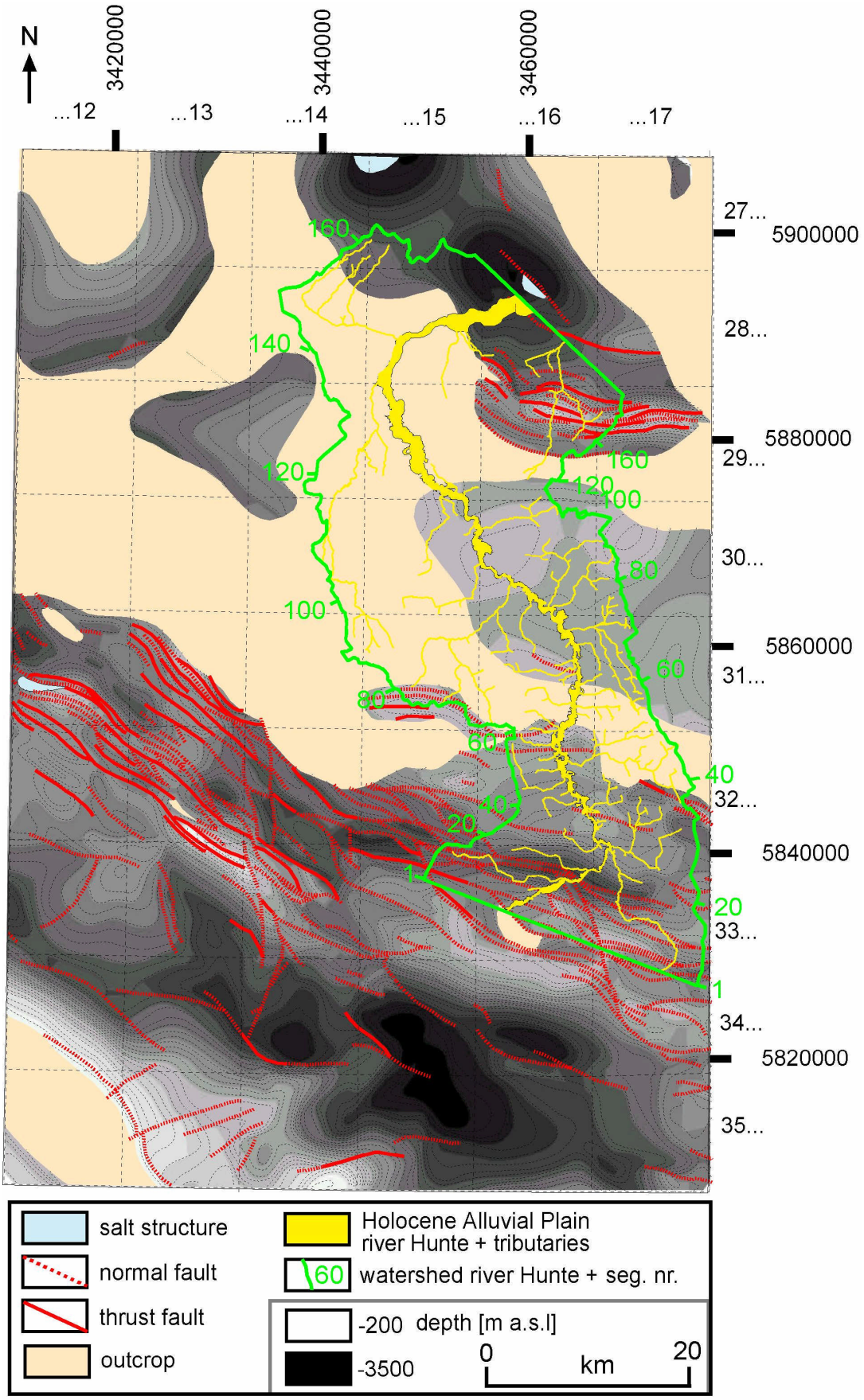

Fig. 10:Base Middle Jurassic (Dogger)

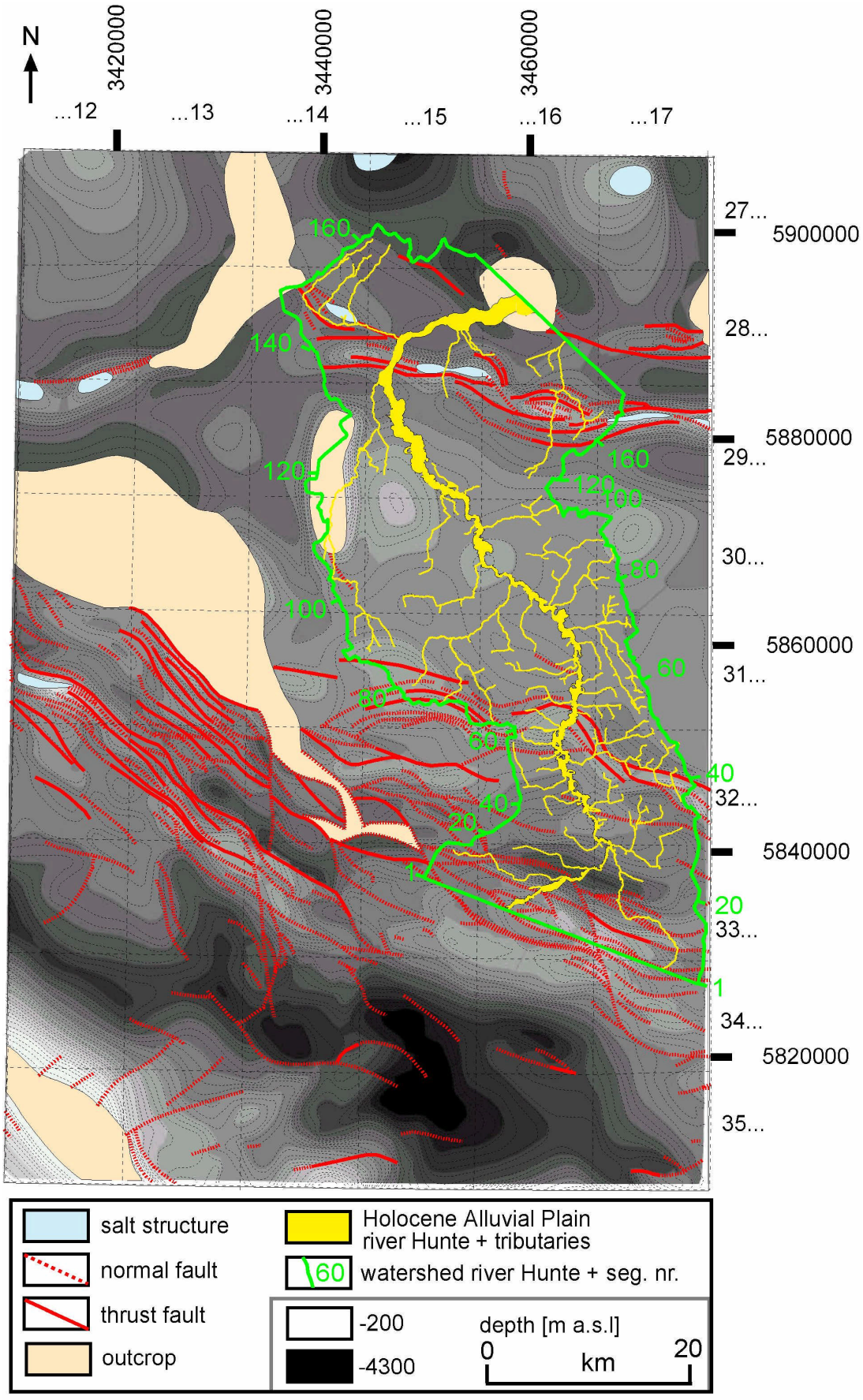

Fig. 11: Base Lower Jurassic (Lias)

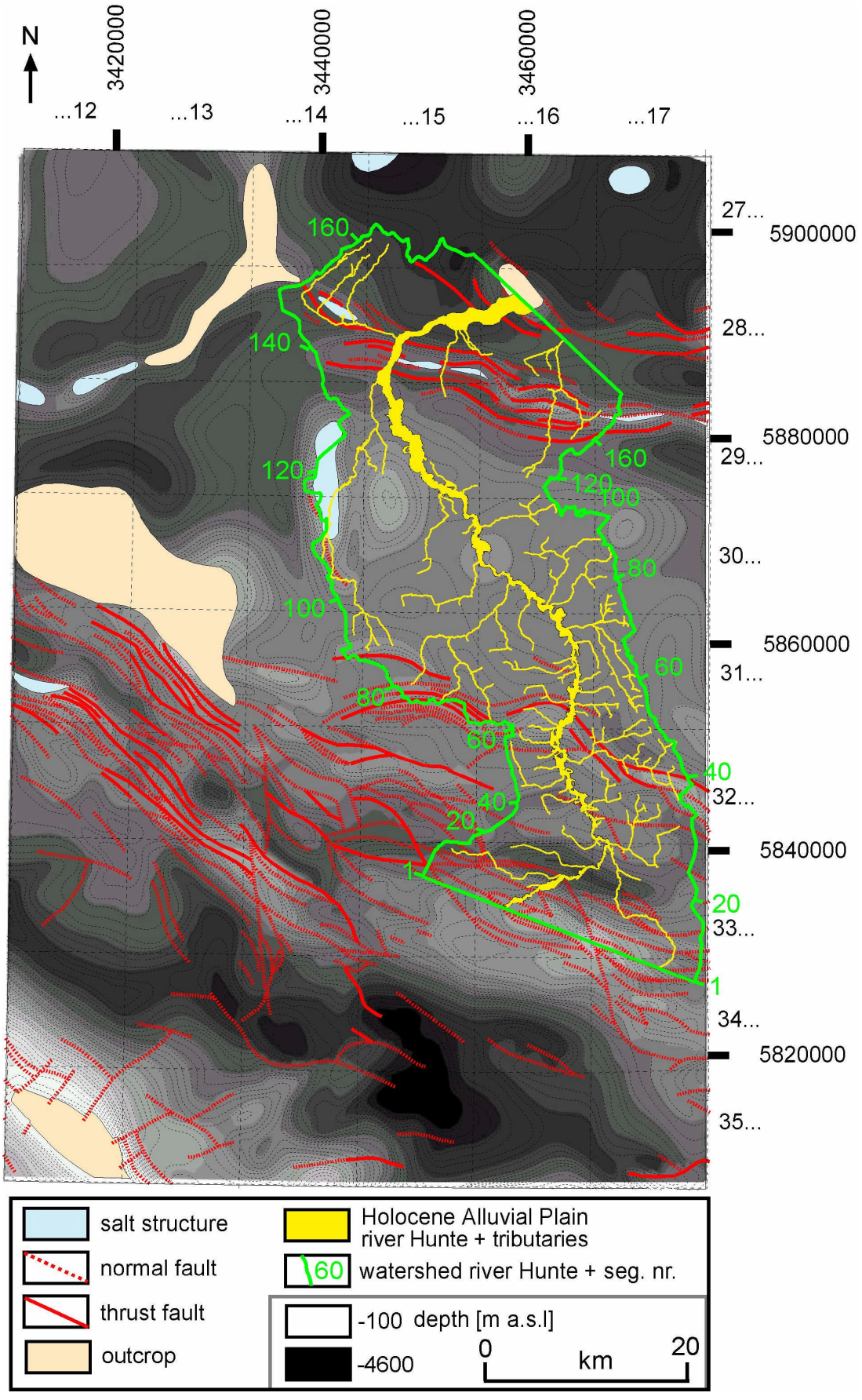

Fig. 12: Base Keuper

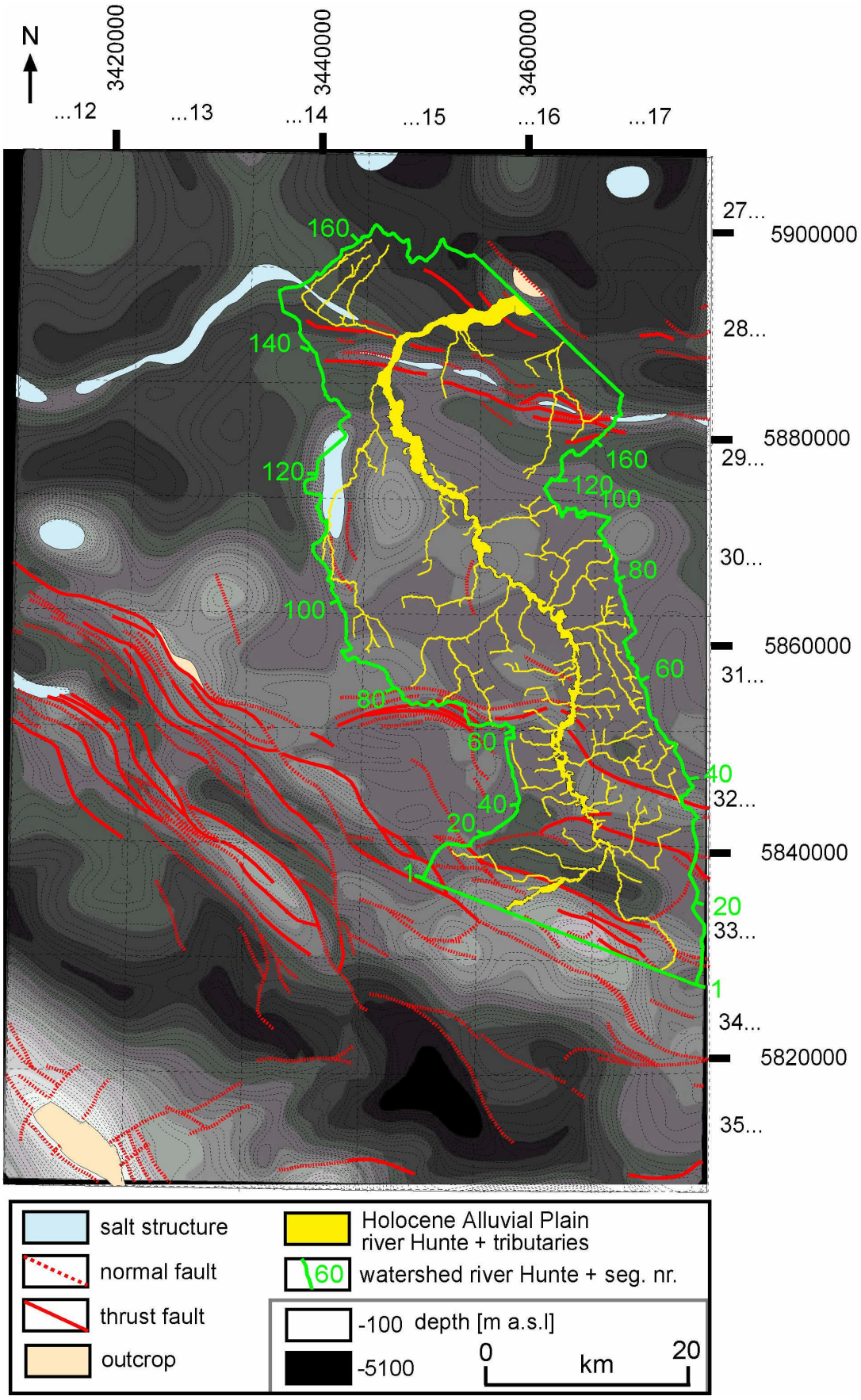

Fig. 13: Base Upper Buntsandstein and Muschelkalk

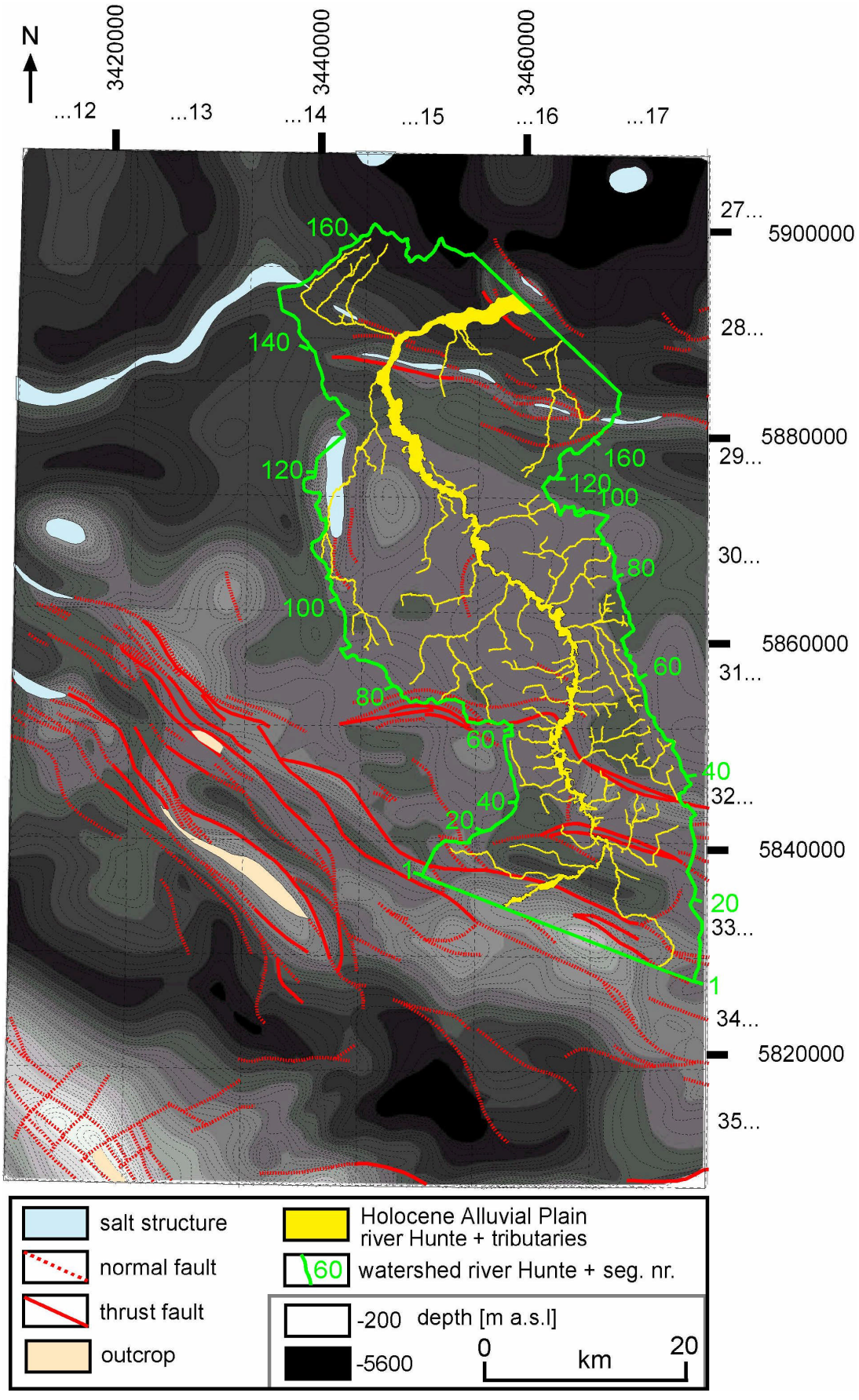

Fig. 14: Base Lower and Middle Buntsandstein

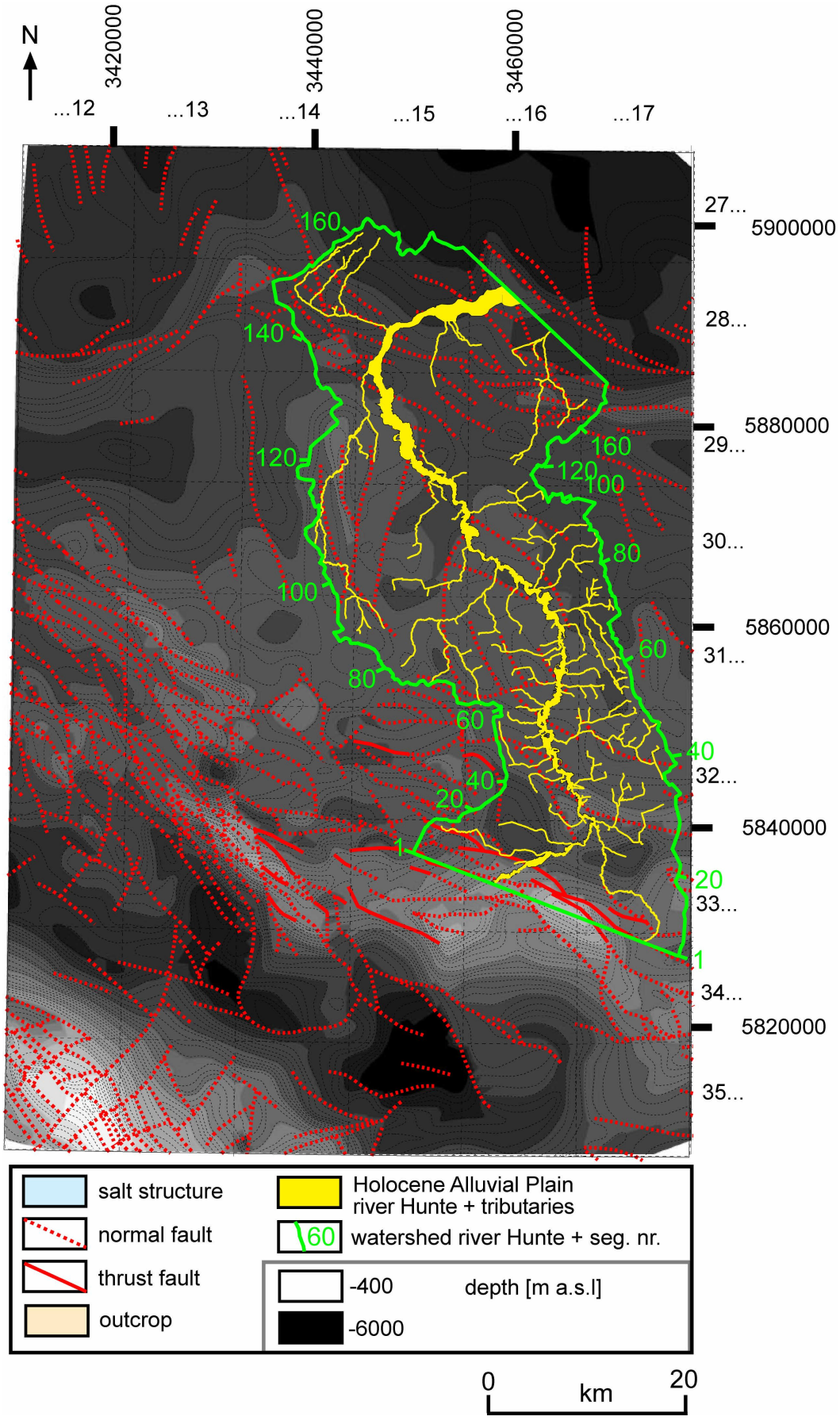

Fig. 15: Base Zechstein